

DEVELOPMENT OF COMPUTER PROGRAM
FOR FIRE SUPPRESSANT FLUID FLOW

FINAL TECHNICAL REPORT

VOLUME I
MAIN REPORT

By

Kemal Tuzla, Thomas Palmer and John C. Chen
Lehigh University

And

Ramu K. Sundaram and Woon-Shing Yeung
Duke Engineering and Services, Inc.

September, 2000

Contractor:
Institute of Thermo-Fluid Engineering & Science
Lehigh University
Bethlehem, PA 18015 USA

Subcontractor:
Duke Engineering and Services, Inc.
Marlborough, MA

DISCLAIMER

This report was prepared as a partial account of work performed for the National Institute of Standards and Technology by Lehigh University and Duke Engineering & Services, Inc. Neither Lehigh University nor Duke Engineering & Services, Inc., nor any of their employees, makes any warranty, expressed or implied, or assumes any legal liability or responsibility for any third party's use, or the results of such use, of any information, apparatus, product, or process disclosed in this report, or represents that its use by such third party would not infringe privately owned rights.

TABLE OF CONTENTS

DISCLAIMER	2
TABLE OF CONTENTS	3
ACKNOWLEDGEMENTS	6
ABSTRACT	7
NOMENCLATURE	8
FIGURE CAPTIONS	11
TABLE CAPTIONS	14
1. DESCRIPTION OF PROJECT AND OBJECTIVES	15
2. PREVIOUS WORKS AND SELECTION OF THE BASE CODE	17
2.1. Experimental Data with Fire Suppressants	17
2.2. Physical Property Data for Fire Suppressant Fluids	18
2.3. Desired Feature of the New Code	18
2.4. Two-Phase Codes Considered for this Work	19
2.5. Selection of the Base Code	20
3. EXPERIMENTAL WORK	21
3.1. Experimental Test Facility	21
3.1.1. Pressure Sensors	24
3.1.2. Flow Rate Sensor	25
3.1.3. Temperature Measurement Sensors	26
3.1.4. Void Fraction Sensor	28
3.2. Test Matrix Performed In Study	29
3.3. A Typical Experimental Run	32
3.4. Observations and Conclusions	33
4. CODE DEVELOPMENT WORK	63
4.1. INTRODUCTION	63
4.1.1. SCOPE OF PROGRAM	63
4.1.2. BACKGROUND	64
4.2. CODE THEORY	66
4.2.1. GOVERNING EQUATIONS	67
4.2.2. NUMERICAL SOLUTION	70
4.2.3. STATE RELATIONSHIPS AND FLUID PROPERTIES	71

4.2.3.1.	Basic Thermodynamic Property Tables	71
4.2.3.2.	Generation of Thermodynamic Property Tables	73
4.2.3.3.	Implementation Of Thermodynamic Property Tables	73
4.2.3.4.	Sample Binary Data File Generation for Halon 1301	74
4.2.3.5.	Critical Region Properties	77
4.2.3.6.	Transport Properties	78
4.2.4.	CONSTITUTIVE MODELS	80
4.2.4.1.	Wall Friction	81
4.2.4.2.	Interphase Friction	82
4.2.4.3.	Interphase Heat and Mass Transfer	83
4.2.4.4.	Wall Heat Transfer	83
4.2.4.5.	Coefficient of Virtual Mass	85
4.2.4.6.	Release of Dissolved Gas	85
4.2.5.	SPECIAL PROCESS MODELS	89
4.2.5.1.	Choked Flow	89
4.2.5.2.	Horizontal Stratification and Entrainment	89
4.2.5.3.	Abrupt Area Change	90
4.2.5.4.	User-Specified Form Losses	90
4.2.5.5.	Cross Flow Junction	91
4.2.6.	COMPONENT MODELS AND SYSTEMS	91
4.2.6.1.	Branch	91
4.2.6.2.	Valves	92
4.2.6.3.	Trip Systems	93
4.2.6.4.	Control Systems	93
4.3.	CODE ARCHITECTURE	102
4.3.1.	COMPUTER ADAPTIBILITY	102
4.3.2.	TOP LEVEL ORGANIZATION	102
4.3.3.	INPUT PROCESSING	103
4.3.4.	TRANSIENT PROCESSING	104
4.4.	CODE INSTALLATION AND EXECUTION	109
4.4.1.	SYSTEM REQUIREMENTS	110
4.4.2.	INSTALLATION	110

4.4.3.	FSP VERSION 1.0 FILES	112
4.4.4.	CODE EXECUTION	113
4.4.4.1.	Editing a File	113
4.4.4.2.	FSP Execution	114
4.4.4.3.	Rstrip Execution	115
4.4.4.4.	Ace Execution	116
4.5.	INPUT PREPARATION AND SAMPLE PROBLEM	119
4.5.1.	System Configuration	119
4.5.2.	Development of FSP Model	119
4.5.3.	Input File Listing	125
4.5.4.	Results & Data Comparison	130
4.6.	ASSESSMENT AGAINST EXPERIMENTS	135
4.6.1.	FSP ASSESSMENT AGAINST NIST EXPERIMENTS	135
4.6.1.1.	NIST Experimental Apparatus	135
4.6.1.2.	FSP Simulations of NIST Experiments	136
5.	Comparison of Code Predictions to Lehigh Experimental Data	145
5.1.	Comparison with Experimental Data Collected at Lehigh Test Facility	145
6.	SUMMARY	168
7.	REFERENCES	172

ACKNOWLEDGEMENTS

This research was supported in part by the U.S. Department of Defense, through the Strategic Environmental Research and Development Program (SERDP). Dr. Richard Gann, Director of Next Generation Fire Suppression Technology Program (NGP) and Dr. William Grosshandler, Program Director, provided valuable guidance throughout the duration of the project. Dr. Jiann Yang of NIST provided technical expertise in the experimental work and also needed information on fluid properties. Their support is gratefully acknowledged.

It is noted that the present computer program was developed from a base computer program, RELAPS/MOD3, developed originally at the Idaho National Engineering Laboratory for nuclear reactor safety analysis under the sponsorship of the U.S. Nuclear Regulatory Commission.

ABSTRACT

A computer program has been developed for predicting the hydraulic performance of delivery systems of fire-suppressant fluids. The program was developed under the Next Generation Fire Suppression Technology Program being managed by the National Institute of Standards and Technology.

The program is based on a one-dimensional, two-fluid model of two-phase flow. In this model, separate conservation equations are written for the liquid and gas phases for mass, momentum and energy. Constitutive relationships are specified for interphase transport of mass, momentum and energy. Heat transfer between the fluid and passive structures such as pipe walls can be modeled. The program also contains built-in models for wall friction and two-phase critical flow. The transport of non-condensable gas in the system, namely the Nitrogen fill gas, as well as the Nitrogen released from solution during agent discharge, is modeled via separate mass conservation equations, with constitutive relations to specify the rate of gas release. The conservation equations are solved using a semi-implicit numerical method, with user-supplied boundary and initial conditions.

The program was deliberately made flexible in terms of types of fluids and piping layout. The current version of the program allows the user to select any one of five fluids – water, Halon-1301, CO₂, HFC-227ea or HFC-125. Modules are available in the program with which the user can model a delivery system, including one or more supply tanks and a combination of piping networks. The user can also model valves in the system, with specified valve opening times if needed.

The suppressant discharge is a highly transient process, generally lasting less than a second to few seconds. The program was benchmarked against transient experimental data available in the literature, as well as experiments conducted as a part of this project, on the discharge of HFC-227ea and HFC-125 in a specially prepared discharge loop. The present experiments lasted between 1.5 to 6 seconds. In addition to transient system pressure at various points, these experiments also measured critical parameters, such as the transient mass discharge history, fluid temperature and the void fraction near the exit. These are first dynamic measurements of mass flow rate, fluid temperatures and void fraction during suppression discharge. This allowed a more comprehensive assessment of the computer program than possible with previously available experimental data. The results of the assessment showed that the program is capable of predicting the performance of various delivery systems with several fluids.

This report is prepared in two volumes. First volume provides a detailed description of the experimental work and discussion of the results. It also includes a brief description of the theory and numerical solution method, instructions for installation on a personal computer with the WINDOWS operating system, and instructions on preparation of the input needed to describe the system being analyzed. Volume II of the report consists of three appendices: a) an input manual for the computer program, b) information on the experimental data, and c) comparison of the present data to predictions of the computer program.

NOMENCLATURE

A	area, cross-sectional area (m^2)
A_t	throat area (m^2)
a	interfacial area per unit volume (m^{-1})
B	drag coefficient, momentum conductance
B_x	body force in x coordinate direction (m/s^2)
C	coefficient of virtual mass
C_p	specific heat at constant pressure (J/kg.K)
C_v	specific heat at constant volume (J/kg.K), valve flow coefficient
D	diameter (m)
DISS	energy dissipation function (W/m^3)
FIF, FIG	interphase drag coefficients (liquid, vapor) (s^{-1})
FI	interphase drag coefficient ($m^3/kg.s$)
FWF, FWG	wall drag coefficients (liquid, vapor) (s^{-1})
f_f	friction factor of pipe
G	mass flux ($kg/m^2.s$)
g	gravitational constant (m/s^2)
H	volumetric heat transfer coefficient ($W/K.m^3$)
h	specific enthalpy (J/kg), heat transfer coefficient ($W/m^2.K$), energy transfer coefficient for Γg
K	energy form loss coefficient
k	thermal conductivity ($W/m.K$)
L	length
M	molecular weight, mass (kg)
\dot{m}	instantaneous rate of mass flow (kg/s)
P	pressure (Pa), channel perimeter (m)
P_i	initial nitrogen pressure in supply vessel (Pa)
P_N	partial pressure of Nitrogen in gas phase
P_o	atmospheric pressure (Pa)
P_1, P_2, P_3	pipe position #1, #2, #3 pressure (k/Pa)
p	wetted perimeter (m)
Pr	Prandtl number
PT1, PT2. . .	pressure taps for pressure drop measurements
Q	volumetric heat addition rate (W/m^3)
q	heat transfer rate (W), heat flux (W/m^2)
R	radius (m)
R_n, R_s	gas constants (noncondensable, steam) (N.m/kg.K)
r_c	critical gas bubble radius (m)
s	specific entropy (J/kg.K)
T	temperature (K), trip
T_c	critical temperature (K)
T_R	reduced temperature (K)
T_1, T_2, T_3	pipe position #1, #2, #3 temperature
t	time (s)
U	specific internal energy (J/kg)
	volume (m^3), specific volume (m^3/kg)

v	mixture velocity (m/s), phasic velocity (m/s)
v_c	choking velocity (m/s)
X	flow quality, static quality, mass fraction
x	spatial coordinate (m)
x_N	dissolved gas concentration (mol/mol)
ΔZ	height of volume (m)
z	elevation change coordinate (m)

Symbols

α	void fraction
β	coefficient of isobaric thermal expansion (K^{-1})
Γ	volumetric mass exchange rate ($kg/m^3 \cdot s$)
ΔP	pressure drop (k/Pa)
ΔP_{NUC}	pressure difference at initiation of gas release (Pa)
Δt	increment in time variable (s)
ε	wall vapor generation/condensation flag
κ	coefficient of isothermal compressibility (Pa^{-1})
μ	viscosity ($kg/m \cdot s$)
ν	kinematic viscosity (m^2/s)
ρ	density (kg/m^3),
σ	surface tension (J/m^2)
υ	specific volume (m^3/kg)

Subscripts

CHF	value at critical heat flux condition
cr, crit	critical property or condition
cv	collection vessel
f	liquid phase
fg	phasic difference (i.e., vapor term-liquid term)
g	vapor phase
I	interface
i	interface
j, j+1, j-1	spatial noding indices for junctions
K	spatial noding index for volumes
k	numbering index for volumes
L	spatial noding index for volume
M	spatial noding index for volume
m	mixture property
min	minimum value
ref	reference value
s	steam component of vapor phase, superheated, solute
sat	saturated quality
T	turbulent
v	vapor quantity
w	wall
wall	wall

wg, wf wall to vapor, wall to liquid
 μ viscosity

Superscripts

s saturation property

FIGURE CAPTIONS

- Figure 3.1: Schematic of Test Facility: Source Vessel, Discharge Piping, and Collection Vessel.
- Figure 3.2: Schematic of Source Vessel Showing Mass Inventory Measurement.
- Figure 3.3: Pressure versus Temperature Saturation Curve for HFC-227ea & HFC-125.
- Figure 3.4: Marotta Valve.
- Figure 3.5: Top View of Test Facility, schematic of Discharge Piping System.
- Figure 3.6: Schematic of Pressure Fittings for Temperature and Pressure Ports.
- Figure 3.7: Schematic of Rack Used to Hold the Source Vessel.
- Figure 3.8: Picture of Test Facility: Source Vessel, Discharge Piping, Collection Vessel, Support Structure and Instrumentation.
- Figure 3.9: Pressure Histogram for Experimental Run #5.
- Figure 3.10: Plot of Source Vessel Pressure Showing the Repeatability of the Experimental Runs.
- Figure 3.11: Schematic of Alternate Piping Configuration #1.
- Figure 3.12: Schematic of Alternate Piping Configuration #2.
- Figure 3.13: Pressure Drop Histogram Across a 90° Elbow from Run #9.
- Figure 3.14: Diagram Transducer Setup for Mass Inventory Measurement.
- Figure 3.15: Mass Inventory Histogram of Run #5
- Figure 3.16: Schematic of Thermocouple Construction.
- Figure 3.17: Temperature Histogram from Film Thermocouples of Run #5.
- Figure 3.18: Temperature Histogram from Shielded Thermocouples of Run #5.
- Figure 3.19: Schematic of Capacitance Probe for Bench Setup.
- Figure 3.20: Bench Setup to Test Capacitance Sensor.
- Figure 3.21: Void Fraction from Bench Tests of Capacitance Sensor.
- Figure 3.22: Schematic of Capacitance Probe for Test Facility.
- Figure 3.23: Cross-Section of Capacitance Setup Showing Electrical Field.
- Figure 3.24: Void Fraction Histogram of Run #5.
- Figure 3.25: Comparison of Experimental Run Length with Straight Pipe (#1) and a Pipe with Fittings (#8).
- Figure 3.26: Comparison of Pressure Drop Across the Top and Bottom Branches of a Tee Split From Experimental Run #13.
- Figure 3.27: Comparison of Collection Vessel Temperature with HFC-227ea (#5) and HFC-125 (#16) as a Test Fluid.
- Figure 3.28: Cumulative Mass for Experimental Run #18 Using Water as a Test Fluid.
- Figure 3.29: Temperature and Void Fraction Histograms from Experimental Run #19 Using Water as a Test Fluid.
- Figure 4.2.1: Staggered mesh numerical method.
- Figure 4.2.2: Flow Chart of Generation Program.
- Figure 4.2.3: Curve Fit for Henry Constant.
- Figure 4.2.4: Effect of Release Coefficient on Calculated Pressure Response.
- Figure 4.2.5: Comparison of Calculated and Measured Bottle Pressure for Test 146.
- Figure 4.2.6: Void Fraction Responses in Lower Portion of Bottle.
- Figure 4.2.7a: 90-degree Tee model with cross flow junction.
- Figure 4.2.7b: Tee model with normal junctions.

- Figure 4.3.1: Top Level Structure.
- Figure 4.3.2: Modular Structure of Transient Calculations.
- Figure 4.3.3: Transient (Steady-State) Block Structure.
- Figure 4.5.1: Schematic of Lehigh Test Apparatus.
- Figure 4.5.2: FSP Nodalization Diagram for Lehigh Tests.
- Figure 4.5.3: Comparison of Calculated and Measured Bottle Pressure for Sample Problem.
- Figure 4.6.1: NIST Test Apparatus (adapted from Gann et al, 1995).
- Figure 4.6.2: Piping Configurations for NIST Experiments.
- Figure 4.6.3: FSP Input Model.
- Figure 4.6.4: Comparison of Calculated and Measured Bottle Pressure for B-59.
- Figure 4.6.5: Comparison of Calculated and Measured Bottle Pressure for B-68.
- Figure 4.6.6: Comparison of Calculated and Measured Bottle Pressure for B-61.
- Figure 4.6.7: Comparison of Calculated and Measured Bottle Pressure for B-60.
- Figure 5.1: Comparison of Experimental and Predictive Source Vessel Pressure Data in Sensitivity Study on Critical Radius Value for Conditions of Run #4.
- Figure 5.2: Comparison of Experimental and Predictive Source Vessel Pressure Data in Sensitivity Study on Gas Release Rate Value for Conditions of Run #4.
- Figure 5.3: Comparison of Experimental and Predictive Void Fraction Data in Sensitivity Study on Gas Release Rate Value for Conditions of Run #4.
- Figure 5.4: Comparison of Experimental and Predictive Pressure Data using Final Values for Code Operating Parameters for Conditions of Run #4.
- Figure 5.5: Comparison of Experimental and Predictive Void Fraction Data using Final Values for Code Operating Parameters for Conditions of Run #4.
- Figure 5.6: Comparison of Cumulative Mass for Experimental Run #5 and Predictive Computer Code Data.
- Figure 5.7: Comparison of Void Fraction for Experimental Run #5 and Predictive Computer Code Data.
- Figure 5.8: Comparison of Source Vessel Pressure for Experimental Run #5 and Predictive Computer Code Data.
- Figure 5.9: Comparison of Pipe Position #1 Pressure for Experimental Run #5 and Predictive Computer Code Data.
- Figure 5.10: Comparison of Pipe Position #2 Pressure for Experimental Run #5 and Predictive Computer Code Data.
- Figure 5.11: Comparison of Pipe Position #3 Pressure for Experimental Run #5 and Predictive Computer Code Data.
- Figure 5.12: Comparison of Collection Vessel Pressure for Experimental Run #5 and Predictive Computer Code Data.
- Figure 5.13: Comparison of Pressure Drop Across a Capped Tee for Experimental Run #9 and Predictive Computer Code Data.
- Figure 5.14: Comparison of Pressure Drop Across a 90° Elbow for Experimental Run #9 and Predictive Computer Code Data.
- Figure 5.15: Comparison of Pressure Drop Across a Union for Experimental Run #9 and Predictive Computer Code Data.
- Figure 5.16: Comparison of Source Vessel Fluid Temperature for Experimental Run #16 and Predictive Computer Code Data.
- Figure 5.17: Comparison of Pipe Position #1 Fluid Temperature for Experimental Run #16 and Predictive Code Data.

Figure 5.18: Comparison of Collection Vessel Gas Temperature for Experimental Run #16 and Predictive Computer Code Data.

TABLE CAPTIONS

- Table 3.2: Matrix of Experimental Runs Conducted at the Lehigh Test Facility.
Table 4.1: PROFISSY Results.
Table 4.4.1: Contents of the WinZip Archive fspv1.zip

1. DESCRIPTION OF PROJECT AND OBJECTIVES

The objective is to develop a computer program (or code) capable of predicting the delivery rates of a fire suppressant fluid to a designated location, via a piping network system.

The current delivery systems for Halon generally consist of a suppressant vessel connected to the delivery location by a piping network. The suppressant vessel is pressurized by an inert gas, usually nitrogen. The suppressant fluid is maintained in a liquid state by the pressurization of the system, usually up to several MPa. The system is activated by a quick opening valve in response to either an automatic or manual trigger. This causes the gas driver to expel the suppressant fluid through the piping system. The delivery system has to be able to begin delivering the fluid to the discharge location very quickly, generally within a few seconds. Complete discharge of the system is required to occur within 0.1 to 10 seconds.

Since Halon and its potential replacement fluids are in a vapor state at standard pressure and temperature, at the discharge location the fluid would be a two-phase mixture of superheated liquid and vapor. Thus significant thermodynamic and thermal non-equilibrium can be expected between the phases. Also, due to the large pressure difference between upstream source vessel and downstream exit, continuous flashing is anticipated as the fluid travels through the piping, and two-phase critical (choked) flow can occur at various locations.

Hence, to accurately predict performance of the delivery system, the computer code should be a transient two-phase code, which allows for phase non-equilibrium. The short delivery times require fairly high flow rates, which promote homogeneous two-phase flow, i.e. little slip. However, in imbalanced piping networks, with side tees and other fittings, some separated flow could occur (stratified flows, slug/plug flow, etc.). Hence the code should be able to predict slip between phases and the corresponding effect on pressure drop. This can be especially important when separated flow encounters directional change, such as at a side tee. The ability to predict the transport of non-condensable gas is also important. The fluid, pressurized with a driver gas, is initially saturated with the gas. During the delivery, as the system depressurizes, the driver gas comes out of solution and expands. This gas evolution phenomenon needs to be accounted for. One additional requirement is that the code should be useful for estimation of the transient hydrodynamic loads in the piping network. Thus the momentum equations need to be sufficiently detailed to estimate the unbalanced force in piping sections between locations of elbows and other fittings.

There has been some work conducted on modeling Halon 1301 flows. In a 1988 summary of the state-of-the-art, DiNenno and Budnick (1988) indicate that most of the flow calculations are performed by vendors using proprietary methods. These methods are verified against standard NFPA procedures for calculations and by discharge to testing in sealed tests. However, there are significant uncertainties in the calculations and also in extrapolation of test results to actual configurations.

Therefore, the objective of the present work was to develop a computer code capable of predicting single and two-phase hydrodynamic behavior of fire suppressant fluids during transport through delivery piping systems.

A key technical approach in the present program was utilization of advancements made in other applications that deal with multi-phase flows. In particular, the highly sophisticated computer codes that have been developed for thermal-hydraulic analysis of nuclear power systems have all the characteristics required for analysis of fire suppressant systems. These include models that account for relative slip between liquid and vapor phases, thermodynamic non-equilibrium between the phases, changes in two-phase flow regimes, critical choke flows, and transport of non-condensable gases. Such codes are also structured for numerical analysis of fast transients, well capable of the transients anticipated for suppressant systems.

Furthermore, since the fluids being considered for use in fire suppressant systems is different from the water/steam system of nuclear power systems, physical property packages need to be modified and expanded. Here again, we have leveraged existing technology by borrowing from existing property packages. Specifically the REFPROP package, developed by the National Institute of Science and Technology (NIST), covers many refrigerant fluids including those that are potential candidates for the fire suppressant systems.

The present project contained an experimental task, to obtain data needed to assess the code. The experimental program envisioned a discharge loop using new fire suppressants. In this experimental program, we successfully measured major flow parameters, which have not been measured heretofore. These include measurements of instantaneous discharge flow rate, fluid temperature, and void fraction at various locations along the discharge pipe.

This program has been carried out as a team effort; the Institute of Thermo-Fluid Engineering and Science at Lehigh University was the main contractor. Duke Engineering and Services is subcontractor to Lehigh University and responsible for code development work.

2. PREVIOUS WORKS AND SELECTION OF THE BASE CODE

2.1 Experimental Data with Fire Suppressants

To fully test the computer code developed in this research, comparisons of code predictions against experimental data will be made. A literature survey has been conducted to find possible sources for experimental data for transient two-phase flows. One widely referenced study is the "The Marviken Tests" conducted using water/steam for the nuclear reactor industry, Marviken Power Station (1982) and EPRI Report NP-2370 (1982). These tests used a liquid/vapor filled vessel under high pressure and measured the vertical discharge characteristics as this system was released to atmospheric conditions. A similar test was carried out by Edwards and O'Brien (1979), but focused on the effects of a horizontal discharge. Even though the Marviken and Edwards tests were conducted with water/steam systems, they still provide some means for assessing portions of the code, which use mechanistic models for predicting non-homogeneous, non-equilibrium two-phase flows. These mechanistic models are fluid-independent and are invoked for all fluids.

Three studies, which more closely reflect the intentions of the current study, have used fire suppressants as their test fluids, rather than water and steam. The work undertaken by Elliot et al. in 1984, include both theoretical and experimental investigations. In this work, Halon 1301 (widely used in both military and commercial applications) was used as the suppressant fluid. The tests discharged Halon under nitrogen gas pre-pressure, resulting in flow of a liquid/vapor/non-condensable-gas mixture through a configuration of piping and an end nozzle. This study provides data on pressure decay as a function of time, allowing for the estimation of discharge flow rates, which are useful for accessing code predictions. This study also provides observations of experimental phenomena as the discharge proceeded. An example is the phenomenon of evolution of the dissolved nitrogen from the liquid Halon, which causes an increase in the pressure of the discharge vessel and an increase in the driving force propelling the discharge of the fluid.

The most comprehensive tests conducted to this date were launched in the mid 1990's by the National Institute of Standards and Technology, Pitts et al. (1994) and Yang et al. (1995). Their tests not only utilized Halon 1301 as a test fluid, but also utilized HFC-125, HFC-227ea, and CF3I. They conducted several experimental runs with each fluid, providing extensive data for various pipe configurations and operating conditions. Experiments with different initial fill volumes, pressures, and temperatures were performed to determine their effects on the two-phase system. Their findings provide important information about the characteristics of the two-phase transient flow as it discharges from the source vessel and through the piping. The pressure histograms from this earlier program will be used as a benchmark in gauging the effectiveness of the code being developed in the current program.

These prior studies provide the beginning of an experimental database. However, there are no data on several key parameters important to code assessment. Primary among these is the instantaneous mass discharge rate and void fraction, at the exit of the source vessel and at the exit of the distribution pipe. Such parameters reflect the mechanisms of phase change (vaporization) and interfacial momentum transfer (slip velocity) that must be correctly modeled in the computer code. Without specific experimental measurements of such key parameters, it is impossible to fully assess the validity of any prediction. This is the

reason why the experimental program at Lehigh has been structured to obtain a number of additional measurements, above and beyond the usual measurement of pressure decay.

2.2 Physical Property Data for Fire Suppressant Fluids

Two-phase flow calculations require thermodynamic and transport properties of the fluid. These properties are required for single-phase liquid, for single-phase vapor, and for saturated vapor/liquid mixtures. The following thermodynamic properties are needed as functions of absolute pressure:

- Saturation temperature
- Specific heat for gas and liquid phases
- Thermal expansion coefficient for gas and liquid phases
- Isothermal compressibility for gas and liquid phases
- Specific volume for gas and liquid phases
- Specific entropy for gas and liquid phases

In addition, the following transport properties are also required for two-phase flow calculations:

- Dynamic viscosity for gas and liquid phases
- Thermal conductivity for gas and liquid phases
- Surface tension

Most fire suppressants are also used as refrigerants. The refrigerant property package REFPROP developed at NIST by Gallagher et al. (1993) covers most of the fire suppressants. For example, it contains properties of Halon 1301, and present fire suppressant candidate FC-227ea. After evaluation, we find that REFPROP is a suitable package for determining the properties required by the new code for two-phase flow calculations with suppressant fluids.

2.3 Desired Feature of the New Code

As discussed in the original proposal, Chen, Tuzla, Sundaram (1997), the base code should be developed with some specific features in terms of its technical ability to model the basic phenomena of two-phase flows. In addition, user convenience and ease of development are also desirable features. The present development seeks to build the following features into the new code:

Required Features

Desirable Features

1. Non-proprietary, publicly available
 2. Portable to various computer and operating systems
 3. Ease of development (well-documented, flexible architecture)
-
1. Non-homogeneous two-phase flow accounting for relative slip between phases
 2. Non-equilibrium two-phase flow, allowing for metastable conditions during flashing

3. Choking under single and two-phase conditions
4. Non-condensable (dissolved gas) transport
5. Multi-component mixtures (liquids, gases, powders)
6. Flexible system modeling capability (choice of piping components and layout)
7. Robust set of equations, for simulation of fast transient two-phase flows (for example, momentum equation to include frictional losses, energy equation to include dissipation)
8. Demonstrated ability to model representative systems (assessment against experiments)
4. Ease of application (user-friendly inputs)

There are other intangible features that have also been considered, such as the existence of an active user group, which would facilitate future modifications and developments.

2.4 Two-Phase Codes Considered for this Work

The relevant codes are those used in the nuclear industry for loss-of-coolant accident analyses (LOCA). These codes address the major phenomena of interest (non-homogeneous, non-equilibrium two-phase flows, choking conditions, fast transients). The survey was limited to codes developed and available in the United States and consisted of RELAP5, RETRAN, TRAC-P, TRAC-B and GOTHIC. Codes developed in other countries that could be used (ATHLET, CATHARE) were not considered because easy access to these codes may not be available.

All these codes have many of the required and desirable features for the present application. They are all based on a two-fluid model of two-phase flow, with constitutive equations to specify the interfacial transport terms. Although some of them have multi-dimensional modeling capability, they are predominantly used in a one-dimensional mode. A brief history of these codes is presented below, with some relevant information:

1. RELAP5

The latest version of this code is RELAP5/MOD3, version 3.2, available since 1995, RELAP5/MOD3 Code Manual (1995). This code was developed at the Idaho National Engineering and Environmental Laboratories (INEEL) under sponsorship of the U.S. Nuclear Regulatory Commission (USNRC). It is used for a variety of reactor accident analyses, including LOCA analyses, for a variety of types of reactors. It is also used in a variety of general thermal-hydraulic analyses in nuclear and non-nuclear systems. It is non-proprietary, and is publicly available, for a transmittal fee, from the USNRC. An active user group, including U.S. and international organizations, meets once a year. Information on user problems, error correction, etc. is transmitted to user group members once every three months.

2. RETRAN

The latest version of this code is RETRAN-03, RETRAN-03 (1992). This code was developed by Computer Simulations and Analysis, Inc., under sponsorship of the Electric Power Research Institute (EPRI). It is used primarily for analyses of reactor systems, with

focus on the primary cooling system, and usually for non-LOCA scenarios. It is proprietary, and can be obtained from EPRI, with license fees and user group membership fees. The user group, including U.S. and international organizations, is active and meets regularly.

3. TRAC-P

The latest version of this code is TRAC-PF1/MOD2, TRAC-PF1/MOD2 Code (1992). It was developed by the Los Alamos National Laboratory (LANL) under USNRC sponsorship. It is used primarily for LOCA analysis of pressurized water reactors. It is non-proprietary and can be obtained, for a transmittal fee, from the USNRC. There are relatively small number of users and no regular user group meetings.

4. TRAC-B

The latest version of this code is TRAC-BF1/MOD1, TRAC-BF1/MOD1 Code (1992) and TRAC-BF1/MOD1 Models (1992). It was developed by INEL under USNRC sponsorship. It is used for accident analyses of boiling water reactors. It is non-proprietary and can be obtained from the USNRC for a transmittal fee. The user group is active and meets regularly.

5. GOTHIC

The latest version of this code is GOTHIC version 5.0, GOTHIC Containment Analysis Package Version 5.0 (1995). It was developed by Numerical Applications, Inc., under EPRI sponsorship. It is used primarily for analysis of reactor containments. It was developed from the COBRA series of codes originally developed at the Pacific Northwest Laboratory under USNRC sponsorship. The original COBRA series of codes are non-proprietary, but were not maintained by the USNRC after the mid-1980's, and are now difficult to obtain. The GOTHIC code is proprietary and can be obtained from EPRI for license fees and user membership fees. The user group is active and meets regularly.

2.5 Selection of the Base Code

The documentation for each of the candidate codes was reviewed. It was concluded that all the codes listed above have many of the required and desirable features, but none have all the features. The conclusion was that the RELAP5 code (MOD3, version 3.2) has more of the required and desirable features than the other codes. In addition, the code has been adapted previously for operation with a fluid other than water, and the code architecture to accomplish this is available in the latest version of the code. This is especially helpful for insertion of new property packages for suppressant fluids. Besides, the code development team at Duke Engineering and Services has accumulated significant operating experience with RELAP5, thus providing confidence that the program objectives could be met successfully with this code. Based on these characteristics, RELAP5/MOD3 version 3.2 has been selected as the base code platform for the present development.

3. EXPERIMENTAL WORK

The objective for the experimental work was to collect experimental data using new fire suppressant agents as test fluids. This data will then be used in the assessment of the product code for simulating possible suppressant delivery systems. Descriptions of pertinent dimensions and design features of the test facility are provided below.

3.1 Experimental Test Facility

The test facility consists of a source vessel for the suppressant fluid, a quick opening discharge valve, a holding rack, a piping network, and a collection tank. This arrangement allows the system to be operated as a closed loop, with recycle of the test fluid. A simple schematic has been provided in figure 3.1, showing the layout of the facility. The dimensions of this test system adhere as closely as possible to the standard sizes used in present-day fire suppression systems.

The source vessel, one of the main components of the facility, is shown in figure 3.2. The source vessel has a total internal volume of 3.81 liters and was initially charged with liquid to about 60% of that volume. The source vessel was constructed from a 2 meter long piece of 2-inch (5.08 cm) nominal diameter stainless steel pipe with an internal diameter of 1.94 inches (4.93 cm) and a wall thickness of 0.22 inches (0.55 cm). Using a vessel of large length-diameter ratio improves the accuracy of measuring liquid inventory. This will be explained in more detail in Section 3.1.2, but simply speaking, we will use a pressure difference associated with the static head of the liquid in the vessel to measure the liquid inventory in the vessel at any time during the experimental run. The long length, or height, of the source vessel provides a greater range of static head measurements, thus increasing the accuracy of determining the transient liquid inventory. This pipe will be positioned vertically and capped at both ends by stainless steel pipe flanges approximately 1 inch (2.54 cm) thick. Two slip-on flanges with o-ring grooves for the pressure seals were welded to either end of the pipe so that the top and bottom plates could be bolted in place. The top plate has an identical outer diameter as the flanges, at 6.5 inches (16.51 cm), and was tapped to allow for a mixing line inlet and a fill/relief line. The bottom plate has a larger diameter of 11 inches (27.94 cm) for the purpose of anchoring the vessel to the holding rack minimizing any vibration or movement during operation. This plate has also been tapped to allow the discharge valve to be screwed into place and sealed with a crushable, tempered aluminum gasket. Other features incorporated into the source vessel include pressure and temperature ports, a liquid level gauge, a mixing line, and the differential pressure transducer with fluid transmission line for measurement of liquid inventory.

Since tests will require pressures up to 40-50 atmospheres in the source vessel, pressurization by a nitrogen cover gas will be employed. As shown in figure 3.3, for FC-227ea, the equilibrium vapor pressure of suppressant fluids will only reach about 5 atmospheres at room temperature, insufficient for the desired pressure without the additional partial pressure of an inert cover gas such as nitrogen. A potential problem with this method is that the total pressure in the vessel will not reach equilibrium until the liquid has become saturated with dissolved nitrogen. In order to expedite this process, a mixing system has been incorporated into the design, using a pump to recycle liquid suppressant from the

bottom of the source vessel to a spray nozzle located in the vapor/gas space. By spraying small droplets of liquid through the nitrogen gas, the surface area of liquid in contact with nitrogen will increase, therefore increasing the rate at which nitrogen can be dissolved into the liquid.

Additional ports in the source vessel include an opening near the top, which will serve as the connection to the nitrogen supply and as one leg of the transmission line for the differential pressure transducer. A liquid level gauge made of armored glass has also been attached to the middle section of the vessel to visually determine the liquid fill level in the vessel at the beginning of each experimental run. Also, there are two thermocouple ports for the vapor and liquid spaces and a pressure port in the vapor space. The last port is in the top plate, providing access for filling of the vessel and also serving as a connection for a safety pressure-relief device.

The next pertinent item in our design is the release mechanism of the source vessel, for initiating discharge of the test agent. A quick-opening plunger valve with an inlet diameter of 1.25 inches (3.18 cm) and an exit diameter of 1.75 inches (4.45 cm) was used for this purpose. This valve, shown in figure 3.4, is a Model MV121KJ-2 valve made by Marotta Scientific Controls Inc. A feature of this valve is the use of the fluid pressure to drive the plunger upon command; thereby eliminating the need for springs or motors. To set or close the valve, the plunger is pushed up into its armed position and held in place by a small locking latch. Two O-rings are attached to the plunger to form a pressure seal along the valve casing. Pressure must then be provided on the inlet side of the valve for the valve to operate properly. To open the valve, an electrical charge provided by 20-volt DC power source releases the latch, allowing the fluid pressure to rapidly drive open the plunger. This release is much faster than that of traditional solenoid valves, and is similar to that of a burst diaphragm or explosive-charge release, which is used in present-day suppression systems. The valve is connected to the 1/2-inch discharge piping in the loop by a tapered transition piece. This transition incorporates a flange connection to permit access to the O-ring seals on the plunger for lubrication.

The piping in the test facility consists of 1/2-inch nominal diameter stainless steel pipe with an internal diameter of 0.546 inches (1.39 cm) and a wall thickness of 0.15 inches (0.38 cm). There are five other pieces including the adapter piece described above, which make up the discharge piping system. Two of these pieces are approximately 12 inches (30.5 cm) in length with flanges at either end to provide for easy disassembly. All the flanges are machined with an O-ring groove to provide an adequate seal against the high pressures experienced in the tests. These 12-inch sections will be used as access points at the beginning and end of the piping system, as indicated in figure 3.5. They will also be the first and last locations of the pressure and temperature measurement ports. Ports for the pressure transducers and film thermocouples used for these measurements required special weld fittings in order to insure a complete pressure seal in the loop. These fittings were specially designed to cause minimal disturbance to the flow, while allowing for the sensor to be as close to the flow as possible. See figure 3.6 for a schematic diagram of these fittings.

The other two pieces in the piping system include a special section used for the void fraction measurement and a long middle section of pipe. The section used in the measurement of void fractions will be described in section 3.1.4. The long middle section of

pipe represents the distribution spool piece often found in fire-suppressant piping systems. Both ends are flanged and are capped by valves, allowing for the isolation of this section when dismantling. The middle piece will be tapped in the middle for temperature and pressure ports as described previously. This middle piece of long discharge piping allows for easy reconfiguration to different piping schemes (i.e. inclusion of tees or elbows). This whole piping system is then connected by a flange to the collection vessel, providing a closed flow path from the source vessel, through the piping system, to the collection vessel.

The collection vessel is designed to serve two purposes: to catch the test fluid for recycle and to enable monitoring of the transient discharge pressure during test runs. The collection vessel has an internal volume of approximately 30 liters, chosen to limit the final pressure after discharge to less than 10-12 atmospheres. This vessel is made of a 10 inches diameter stainless steel pipe with an internal diameter of 9.56 inches (24.3 cm) and a wall thickness of 0.59 inches (1.50 cm). The bottom of the collection vessel is a hemispheric cap with a 1/2-inch port, to be used for emptying the contents. At the top end is a pair of 1.75 inches thick flanges sealed by an O-ring. The outside flange has access holes to allow for a cooling coil, a vacuum line, and a temperature port. The cooling coil will carry either cold water or liquid nitrogen for the purpose of condensing the spent suppressant fluid for recycle. The vacuum line is connected to the top of the vessel for the purpose of relieving the excess pressure before the next run. The line is connected to a knock-back condenser to prevent a minimal amount of suppressant from escaping. Additional ports in the sides of the vessel provide connections for the piping system and a fast-response pressure transducer.

In anticipation of potentially large reaction forces during fluid discharge, a rugged framework was designed to support the test facility. As shown in figure 3.7, an 8 inch I-beam, 10 feet high, was chosen to give a rigid backing for the source vessel while being heavy enough to dampen any vibrations exhibited during the test runs. This rack I-beam is directly bolted to the building structure for rigidity. The rack I-beam has three welded shelves for use in supporting the source vessel. The first is positioned just below the middle of the beam and is used to hold the source vessel from the bottom. Since this area experiences most of the forces during the discharge tests, the shelf in this area is bolted to the large flange at the bottom of the source vessel. This shelf is equipped with support legs for added stability. The next shelf is located near the top of the rack and anchors the top section of the source vessel by clamping to the 2-inch pipe. The last shelf, positioned lower down on the beam, is used to hold the mixing pump. The I-beam is also equipped with boltholes along its face in order to add support structures for the level gauges and mixing lines. As for the piping system, it is supported by a metal framework, which has provisions for clamping the pipe and preventing movement in both horizontal and vertical directions. The collection vessel is attached to a movable dolly to allow for opening of the piping system when access is necessary. To account for substantial forces associated with the fluid discharging into the vessel, the collection vessel is held in place by support braces attached to a building I-beam. A picture of this entire system is shown in figure 3.8, where the source vessel, straight piping system, collection vessel, support structure and instrumentation can be seen.

3.1.1 Pressure Sensors

The test facility is equipped to measure instantaneous pressure readings in the source vessel, along the piping system, and in the collection vessel by means of fast response pressure transducers. Two types of transducers were used in the experiments conducted, the Entran Model EPX-V01 with a range of 0-1000 PSIG (0-68 atmospheres) and the Validyne Model DP15 with varying ranges from all within 0-1000 PSIG. The Entran transducers were primarily used in the early runs when temperature drop during operation was not a concern. While the Validyne transducers were used for both pressure drop measurements and absolute pressure measurements. The Validyne transducers were used with a transmission fluid for speed of transmitting the pressure wave in the pressure drop readings and also for insulation when the temperature drop was considerable as in the HFC-125 tests. The Entran transducers have a diaphragm, which deflects according to the difference of the pressures, experienced at its front and backsides and provides an output through a strain gauge bridge located on the backside of the diaphragm. While the Validyne transducers used a magnetically permeable diaphragm which when deflected caused a magnetic reluctance, which was then interpreted by the inductance value of coils in the transducers body. In order to install these transducers at measurement locations, special fittings had to be designed and fabricated. As explained previously in section 3.1, it is desirable to locate the transducers as flush to the inside surface of the pipe as possible, in order to minimize disturbances to the flow. This was accomplished with the specially designed fittings shown in figure 3.6. With this fitting welded into place on the pipe, the transducer can be screwed into the tapped hole, allowing an O-ring to seal against the high fluid pressures. Bench top experiments were conducted to determine whether the transducers had appropriate response times for the fast transient tests conducted. Both transducers were found to be at an acceptable level of 140 milliseconds for pressurization and 190 milliseconds for depressurization when operating at 20-30 atmospheres. A detailed analysis of these tests was provided in the first annual report. Although, the best test for the instrumentation would be to view their performance in actual testing situations. Figure 3.9 shows a typical output (run #5) from the pressure transducers installed in the test facility. This run used HFC-227ea as a test fluid and was initially charged to a source vessel pressure of 4.22 MPa. As one can see in the figure the pressures in the source vessel, pipe and collection vessel remained constant until the moment when the valve was actuated (time = 0 milliseconds). Then the pressure in the source vessel dropped quickly while the pressures in the rest of the facility rose. This occurred until the pipe was filled with fluid (time = ~200 msec) and then there was a steady decrease in all the pressures until all of the fluid was discharged from the source vessel (time = ~1500 msec). At this point a small pressure increase or “bump” was prevalent in the piping pressure traces due to the exit of the remainder gas contents of the source vessel. We also carried out a set of runs with similar initial conditions to check the repeatability of the measurements and the reliability of the instrumentation. The operating conditions are shown in the Table 3.1.1.1. below.

Table 3.1.1.1: Operating Condition For Repeatability Tests.

Run	Fill Volume	Ambient Temperature	Source Vessel Pressure	Downstream Pressure
#3	2358	32	4180	720
#4	2370	29	4195	525
#5	2388	31	4220	720

All the tests used HFC-227ea, as a test fluid the repeatability was very good as shown by figure 3.10, which compares the source vessel pressure histogram of the three experimental runs. The slight discrepancies are most likely caused in the differences in the initial and environmental conditions and not due to the instrumentation. With the example of the output from the entire facility and the fact that we had good repeatability we feel satisfied that the transducers did a good job of catching the pressure fluctuations during our experimental runs.

There was also a necessity to measure the pressure drop across particular sections of the piping system. While the absolute measurements at different locations allowed us to measure the variation of absolute pressure across the discharge pipe, there was also an interest to measure pressure drop across fittings in order to determine frictional losses across these piping elements. Figures 3.11 and 3.12 show the two other piping configurations we tested in this study besides the straight pipe configuration. Validyne pressure transducers were connected on either side of the fittings to measure the distinct pressure drop associated with these fittings. This can be seen by the ports specifically designated to the fittings shown on the diagrams (i.e. PT2-PT3 across a 90° elbow). A typical output from this measurement is shown in figure 3.13, where pressure drop versus time is displayed. This plot shows the pressure drop across a 90° elbow from run #9 using HFC-227ea as a test fluid and an initial pressure of 3915 kPa. There is a notable pressure drop instantly as the fluid front passes through the elbow, which deteriorates as time passes. This continues until approximately 2300 milliseconds when the last liquid is discharged and the remaining gas leaves the system, denoted by the sudden drop in pressure attributed to a reduction in the frictional component of pressure drop associated with gas flow over liquid flow. Similar plots were made for the pressure drop across capped tees, through tees and unions. Also, a comparison was done between the vertical branches of a through tee to study the effect of phasic composition on the separation of the flow. With these measurements, it was possible to successfully analyze the effects of different fittings on the pressure losses in the discharge piping.

3.1.2 Flow Rate Sensor

As mentioned previously, a key parameter that we wish to measure is the instantaneous mass flow rate of fluid during transient discharge from the source vessel. To the best of our knowledge, this has not been successfully measured in prior experiments due to its inherent difficulty. If fluid inventory in the source vessel could be measured as a function of time, then the rate of discharge would be given by the gradient of inventory versus time. Because of possible void generation in the liquid (due to gas evolution) and associated level swelling, observation of liquid level does not provide indication of fluid inventory. Our approach is to measure the static head of fluid in the source vessel, as a dynamic function of time. Since frictional and kinetic terms are negligible in the overall momentum balance for conditions in the vessel, we expect to obtain the fluid inventory in the vessel directly from static head measurements:

$$M = \frac{A}{g} \bullet \Delta P \quad (3.1.2-1)$$

where M is the fluid inventory, A is the cross-sectional area of the vessel, g is gravitational acceleration, and ΔP is the pressure difference from the bottom to the top of the vessel (static

head). The instantaneous rate of mass flow out of the vessel is then obtained from the time derivative,

$$\dot{m} = \frac{dM}{dt} = \frac{A}{g} \bullet \frac{d\Delta P}{dt} \quad (3.1.2-2)$$

To obtain the desired accuracy for the rate of mass flow, a precise measurement of ΔP is necessary. We used a Validyne Model DP15 differential pressure transducer to obtain this static head ΔP . As shown in figures 3.2 and 3.14, this transducer was connected to the vapor space and the liquid volume at top and bottom of the source vessel, respectively. The transmission line connecting the vapor space to the liquid space was filled with a Meriam Red fluid with a specific gravity of 2.95 to maximize response time. The theory behind this was that pressure signals will be transmitted to the transducer at the speed of sound in liquid, sufficiently fast to obtain dynamic data during suppressant discharge and much quicker than through a compressible gas volume. Therefore, the connections to the liquid and vapor spaces were made at the wall of the Marotta valve and the wall of the source vessel, respectively. This allowed for an almost flush-mounted differential pressure transducer with an excellent response time for measuring liquid inventory. Figure 3.14 shows a diagram of the set up for this differential pressure transducer. Notice that we attempted to fill the transmission line as close to the source vessel as possible, therefore reducing any pockets of fire suppressant vapor and making a more accurate measurement.

We were pleased to find that our thinking worked very well, as shown in figure 3.15, a plot of the cumulative mass leaving the source vessel versus time. This example shows the same experimental run described in the previous section (3.1.1). It shows that at the point when the valve was actuated a quick release of test fluid left the source vessel and continued gradually until the source vessel was empty, at approximately 3.37 kg. This corresponded with the pressure drop in the source vessel shown in figure 3.9 and with the end of the liquid flow and beginning of the gas flow at a time of ~1500 milliseconds. This is what we would expect since we did not have much fluctuation in the pressure histogram leading us to believe that there was a steady flow of fluid through the facility. Once again, we had excellent repeatability and felt that this method for measuring the instantaneous liquid inventory gave an acceptable representation.

3.1.3 Temperature Measurement Sensors

Fluid temperatures along the discharge pipe are to be measured using film thermocouples. It has been experimentally shown at Lehigh, Cokmez-Tuzla, Tuzla, Chen (1993), that this type of thermocouple can provide response times in the order of milliseconds. A schematic of the film thermocouple is shown in Figure 3.16. Since the hot junction of the thermocouple is comprised of the metallic film, it is essential to maintain a continuous electric conductive-path through that film. Two issues are involved: compatibility of the film material to the test fluid, and the erosive effects of the flow on the film. During the past experiments at Lehigh, a metallo-organic paint was used to make the film at the tip of the thermocouple. This film worked well in experiments with high temperature steam and water. After a search for alternatives, we decided once again to use this same material for the junction film. A bench setup was prepared to test the thermocouple with this film junction.

After forming the film, the thermocouple assembly was exposed to test liquids for duration of up to five minutes. Tests with the primary test fluid, HFC-227ea, indicate that the junction film holds up well to such exposure. No bench test for erosion of the film was attempted prior to the running of the test facility, due to the significant effort involved. We found that the film held up for anywhere from 5-10 experimental runs before deterioration in the film deemed it necessary to dismantle the thermocouple from the facility and reapply the metallic film. We determined the need for reapplication of the metallic film by an increased fluctuation in the output signal of the thermocouple or in some cases a loss in the signal altogether. Many of the failures in the thermocouple were not attributed to the metallic film at all, but to the disintegration of the inner wiring of the thermocouple. This was most likely due to the vibration encountered in the test facility when the experimental runs were conducted and the tight seal on the thermocouple casing needed to hold the thermocouple in place during testing.

An example of a typical output from the four film thermocouples located throughout the test facility is shown in figure 3.17. The top set of data is the signal from the film thermocouple located in the vapor space of the source vessel. The next three sets are from the film thermocouples in pipe positions #3, #2, and #1, respectively from top to bottom. This plot shows no significant temperature change in the vapor space, which is due to the fact that there was only a gas expansion involved in this region. While an adiabatic gas expansion from a volume of 1.5 L to 34 L should have resulted in a large decrease in temperature, in our case this was not an adiabatic expansion due to the availability of a large heat sink in the stainless steel walls. With the considerable warming from the facility walls and the thermocouple's location at the top most portion of the entire facility, the only temperature drop experienced would be minimal. As for the other set of thermocouple traces, we believe the most significant reason for the difference in temperature drop as we move along the pipe is also due to the warming effects.

There were also two standard, 1/32" diameter, shielded thermocouples placed at different locations in the facility, one each in the source and collection vessels. Figure 3.18 shows a standard temperature trace from these thermocouples, again from run #5. The two traces shown in this diagram are significantly different from each other. The collection vessel temperature does a quick dip and then warms back up to room temperature. This is due to the filling of the vessel with cold fluid, which is probably still going through the process of dissolution of nitrogen from liquid suppressant. Also, there is an energy loss associated with the phase change of the suppressant fluid as it goes from liquid in the pipe to gas in the collection vessel. This goes on until the collection vessel reaches the saturation pressure of the suppressant fluid and then the vessel begins to heat up due to compression of the gas in the volume. On the other hand the thermocouple located at the bottom of the source vessel initially does not change much since it is submersed in liquid suppressant. Then as the liquid in the source vessel runs out, it experiences the vaporization of the suppressant fluid on its surface and the expansion of the remaining gas in the system. To fully understand the complete picture of the changes of phase taking place in the experimental runs, we need a representation of the void in the facility, which is described below.

3.1.4 Void Fraction Sensor

One of the major flow variables for two-phase flow is the void fraction. Many flow parameters, such as thermodynamic quality, vapor and liquid mass fluxes, and transport properties of vapor and liquid affect the void fraction. In turn, the void fraction strongly affects pressure drop, holdup inventory, and flow rate for any given operating condition. Thus, it is desirable to experimentally measure the void fraction during the transient discharge of suppressant. Once again, this is a difficult measurement in two-phase flows and was not attempted in prior experiments of suppressant flow. In the present work we attempted to measure the transient void fraction at the end of the discharge pipe. The desirable features of a sensor for void fraction are:

- No disturbance on flow
- Integrate the void fraction over the cross-section
- Fast response

Based on previous experience at Lehigh University, we selected to use a capacitance sensing method for this measurement, in expectation that this method will satisfy all of the above desirable features.

A number of different capacitance probes were designed, fabricated, and bench tested. The final probe configuration is shown schematically in figure 3.19. As indicated the probe consists of a positive electrode and a ground electrode, both placed on the outside surface of the discharge pipe. The section of the discharge pipe at this location needs to be electrically nonconductive to allow capacitance measurements. For the purpose of these bench tests, a glass tube is being used as the pipe material. The positive electrode is a strip of copper in contact with the outer surface of the pipe. The electrode span is as wide as the ID of the pipe. The ground electrode is placed on the opposing side of the pipe. When powered by a high-frequency voltage, this probe would measure an overall capacitance between the two electrodes, which includes the whole cross-section of the tube. This capacitance can then be calibrated to give the void fraction of the vapor/liquid mixture in the pipe. There is a guard electrode around the positive electrode to prevent/reduce stray capacitance.

This probe was tested on a bench loop with water and HFC-134a. The schematic of the bench setup is shown in figure 3.20. The test started with the glass tube filled with water. During the test, the tube was emptied from the bottom so that the liquid level receded with a constant speed. The recorded signal from the capacitance sensor was compiled as a voltage signal from the capacitance meter and then reduced into void fraction with a calibration using the signals associated with all liquid and all vapor. An example of the output from this test is shown in figure 3.21. It is seen that initially the probe senses 100% liquid in the tube. As the liquid level approaches the top edge of the sensor, the signal slowly starts to show some void in the sensing volume (edge effect). When the liquid level is within the sensing volume, the variation of measured void fraction is linear with liquid level. Again, there is an edge effect when the liquid level is close to the bottom edge of the sensing volume. Later, when the liquid level falls clear of the sensing volume, the probe senses all air in the tube. Despite the fact that we guard the sensing area, there are some edge effects in the axial direction. The above test was repeated with HFC-134a under pressure and similar results were observed. Our biggest problem with changing this design to fit the conditions experienced in our

experimental test facility would be containing the higher pressures. In the previous bench examples we dealt with only low-pressure systems and in the present application the system pressure is as high as 1250 kPa at the location of the void probe. The other difficulty was that we must not have an electrically conductive surface between the probe and the tested medium. Due to these limitations we developed a design that would be constructed on the inner surface of the pipe as shown in figure 3.22. There were three main pieces to this design; the first was the electrical plug welded to the metal pipe, which served as a pressure seal and as an electrical connection to the capacitance meter. The next two pieces were the guard and the probe separated by a small layer of insulation. To insure that these pieces were not washed away in the flow during the runs, they were covered in a thin layer of epoxy. This capacitance probe used the pipe wall as its ground creating an electrical field similar to the one shown in figure 3.23. While the orientation of this design was horizontal as compared to vertical in the bench test setup, we believed that it would give us similar results. We conducted an insitu calibration by filling the area with all liquid suppressant and then letting it run out so that only suppressant vapor remained. An example of the final output of an actual experimental run is provided in figure 3.24 where void fraction versus time of run #5 is shown. The signal initially starts out at a void fraction of 1.0 (all vapor) and then shoots down to approximately 0.4 as the area is flooded with the transient flow of two-phase fluid. The signal jumps around as the mixture of the two phases changes depending on the speed and location of the dissolution of the nitrogen from the liquid suppressant. As the flow slows down, so does the fluctuation in the capacitance signal, until the liquid runs out (time = 1700 msec) and the remaining gas is vented into the collection vessel causing the signal to abruptly go back to the 1.0 region. Our largest problem with the capacitance signal resulted from the static charge build up of the fast moving dispersed flow. It caused the signal to jump out of range and required a significant filtering effort to be conducted. This is also the reason for the offset in the final value at the end of the run. Despite these slight problems, we feel that the capacitance probe design gave an excellent representation of the void fraction values experienced during the experimental runs.

3.2 Test Matrix Performed In Study

After the completion of the test facility, we needed to choose the appropriate initial conditions in which to conduct the experimental runs. Our main goal was to encompass a wide variety of test parameters while keeping the total number of runs at a minimum to lessen the wear on our instrumentation. Table 3.1 shows the experimental runs conducted in this study. We used HFC-227ea, also known as HFC-227ea as our primary test fluid, since it was recommended at the time as the alternative fire suppressant with the best fire retarding ability. We also used HFC-125 or R125 since it had been studied recently and there was some test data that we could use for future comparison. In the preliminary experiments, water and carbon dioxide were used to test the new instrumentation after installation. For example, run #19 used water as a test fluid and was undertaken to test the capacitance sensor and film thermocouple without exposing them to high pressure or a corrosive fluid. Run #18 also used water and had the intent of testing the mass flow sensor response and all of the thermocouples in the facility. In a similar manner, runs #20 & #21, which used CO₂, were used to measure the response of the film thermocouples to a sudden drop of temperature as low as -40° Celsius, while also allowing for us to gauge the error encountered by the pressure transducers at this temperature. These four runs utilized the straight pipe configuration in the test facility shown previously in figure 3.5. The HFC-125 runs (#14-#17) were conducted

with only one objective, to test the influence of changing the source vessel pressure. The four runs were carried out at source vessel pressures varying from 2050 to 5000 kPa. It must also be noted that any runs using source vessel pressures with initial conditions using low pressures were conducted at fill levels between 85-90%. This was done in an attempt to facilitate as much vaporization during the flow discharge as possible since the downstream pressure would remain at a lower pressure with the smaller amount of nitrogen gas available to expand.

The majority of our experimental runs used HFC-227ea as a test fluid and were broken into three main piping configuration groups. First, there were the tests using the straight pipe configuration. These tests had three different goals: (1) to test the repeatability of the instrumentation, (2) to observe the effect of changing the source vessel pressure, and (3) to determine the effect of a heat source or “hotspot” along the piping system. The repeatability runs (#3-#5) were conducted at an initial source vessel pressure of about 42 atmospheres. The result of the source vessel pressure histogram is shown in figure 3.10. While the “hotspot” run (#7), was conducted at a similar starting pressure with a foot long section at 55° Celsius between the 2nd and 3rd instrumentation ports on the pipe. Only one such run was needed since it was the conclusion of this group that a minimal effect resulted from the heat addition under such rapid transient conditions. The third goal was to observe the effect of varying the initial source vessel pressure from 2125 to 4910 kPa (#1-#6). The second main piping configuration group used the piping configuration shown in figure 3.11, where a vertical “U” turn was built into the piping system. It allowed us to measure the effect of pipe fittings on the pressure loss in the system. The pressure drops across a capped tee, 90° elbow and union were measured with varying initial source vessel pressures from 2120-4910 kPa in runs #8-#10. The third piping configuration group used a complete vertical split as shown in figure 3.12, where the tee was no longer capped but used to join two symmetric piping sections. The two sections were identical to the one used in the previous grouping although this time the pressure drop across the split was measured. A sensor was placed before the tee and after the 90° elbows on either arm of the split to test whether there was an effect from the splitting of the flow. These test were also conducted at three varying initial source vessel pressures from 2140-4910 kPa in runs #11-#13. These tests gave us a good look at the effects of changing the initial source vessel pressures, changing the test fluids, changing the piping configurations and the repeatability of our instrumentation.

Table 3.2: Matrix of Experimental Runs Conducted at the Lehigh Test Facility

Run #	Test Fluid	Piping Configuration	Fill Volume [mL]	Psvo [kPa]	Pcvo [kPa]	Temperature [°C]
1	HFC-227ea	Straight Pipe	3571	2125	10	32
2	HFC-227ea	Straight Pipe	2340	3235	635	33
3	HFC-227ea	Straight Pipe	2358	4180	720	32
4	HFC-227ea	Straight Pipe	2370	4195	525	29
5	HFC-227ea	Straight Pipe	2388	4220	720	31
6	HFC-227ea	Straight Pipe	2150	4910	715	31
7	HFC-227ea	Straight Pipe w/ Hotspot @ 55°C	2200	4230	710	27
8	HFC-227ea	Capped Tee (Config. #1)	3420	2120	125	21
9	HFC-227ea	Capped Tee (Config. #1)	2500	3915	575	24
10	HFC-227ea	Capped Tee (Config. #1)	2450	4910	615	25
11	HFC-227ea	Through Tee (Config. #2)	3507	2140	600	26
12	HFC-227ea	Through Tee (Config. #2)	2400	3935	655	24
13	HFC-227ea	Through Tee (Config. #2)	2460	4910	615	25
14	HFC-125	Straight Pipe	2900	2050	110	26
15	HFC-125	Straight Pipe	2363	3635	175	26
16	HFC-125	Straight Pipe	2400	4245	165	26
17	HFC-125	Straight Pipe	2467	5000	125	24
18	Water	Straight Pipe	3585	2875	120	28
19	Water	Straight Pipe	3100	4150	100	23
20	CO ₂	Straight Pipe	~1000	5215	100	20
21	CO ₂	Straight Pipe	~1000	5360	100	20

3.3 A Typical Experimental Run

Since we have explained our objectives behind the building and operating of the test facility, the operating procedure and output should be explained in more detail. First we set the plunger in the Marotta valve into the closed position using the arming tool. Once the valve is closed, the next task is to recycle any fluid remaining in the collection vessel back to the source vessel using a magnetically driven centrifugal pump. If there is not enough test fluid in the collection vessel to reach the desired initial fill level for the next run, then the recycle line is closed and a line to a fresh-supply tank above the test facility is opened, allowing the remaining liquid needed for the run to be pumped into the source vessel. Once this is accomplished, the supply line is closed and a circulation line is opened allowing the liquid at the bottom of the source vessel to be pumped to a spray nozzle at the top of the vessel. The spray nozzle then creates a fine mist of liquid to float through the vapor space of the vessel before joining the rest of the liquid. At this point we begin to slowly add nitrogen gas to the source vessel through a connection at the top of the vessel. We continue to run the circulation pump until the liquid is saturated with nitrogen. This is recognized by the constant pressure in the source vessel, which usually took about 120 minutes. The circulation pump is then turned off and the contents of the source vessel are allowed to settle and cool down to room temperature. The data acquisition system is initiated and run for 500 milliseconds before the Marotta valve is actuated. This allows for the collection of the initial conditions of the system. Once the valve is actuated, the contents of the source vessel discharge through the Marotta valve into the piping system and finally collect in the collection vessel. To fully understand the output from a single run, a typical experimental run (#5) will be examined in more detail. The pressure histograms can be seen in Figure 3.9 where the traces go from the source vessel at the top to the collection vessel at the bottom and the pipe ports in the middle. In specific, the black line (diamond) is the source vessel trace and the green (circle), red (square) and blue (triangle) traces are the first, second and third pipe positions, respectively, with the orange (cross) line being the collection vessel. Initially the source vessel is at 4220 kPa and the pressure downstream of the closed valve is at 720 kPa. After the valve is opened, the pressure in the source vessel quickly drops as its contents fill the piping system, explaining the sudden rise in pressure there. At the point when the pipe is completely filled, ~200 milliseconds, there is a consistent drop in pressure as the fluid empties into the collection vessel. At ~1600 milliseconds the fluid begins to run out and the flow in the system is predominately vapor. This quickly causes the entire system to equilibrate to the same ending pressure, ~1100 kPa.

Not only can we follow this discharge with pressure histograms, but we can also follow the temperature change throughout the system. Figure 3.17 shows the output of the highly sensitive film thermocouples placed at the top of the source vessel in the vapor space and along the bottom of the piping system at the three port locations. The same color and symbol scheme is used as in the pressure histogram with the source vessel being on top, followed by the third, second, and first pipe positions, respectively. There was little temperature change experienced in the fluid flow portion of the discharge since there was little flashing of the suppressant. The main temperature drop occurs at the point when the vapor discharge begins (~1600 ms). This is due to the sudden expansion of the remaining nitrogen gas and falls as low as 10° Celsius at the first pipe position. There are lesser temperature drops as it travel farther down the pipe due to the increased distance from the initial point of expansion and the warming of the vapor by the system walls. There were also

two 1/32" shielded thermocouples placed in both the source vessel and collection vessel. The outputs of these are shown in Figure 3.18, where the black (diamond) symbols are for the bottom, fluid space of the source vessel, and the orange (cross) symbols are for the top, vapor space of the collection vessel. There is a small dip in the temperature of the collection vessel as the fluid initially reaches the large volume of the vessel and then it warms back up to room temperature rather quickly. As for the source vessel temperature, this thermocouple experiences the temperature drop due to the expansion of the gas that the film thermocouple in the vapor space did not. This is most likely due to the fact that the film thermocouple at the top of the vessel is in contact with stagnant gas and did not have enough time to sense its temperature while the lower thermocouple experienced the shock of the quick expansion from the fast flowing gas.

The next insight into this study was provided by the differential pressure transducer, which measured the mass flow rate of the discharge. As seen in figure 3.15, this instrumentation allowed for the measurement of the cumulative mass of liquid leaving the system. This gives us a good idea of how much liquid has left the source vessel and might possibly land on the desired destination, in this case, into the collection vessel. Ideally, we would have liked to locate such a sensor near the desired destination, but since we could not develop an accurate, quick response method of measuring the collected fluid, this seemed the most suitable alternative. Figure 3.15 verifies what we have already observed from the previous measurements of pressure and temperature. At first there is a primarily liquid flow, starting rapidly and slowly dying out as the inventory is relinquished to the piping system, until no liquid is left at ~1600 ms. Along with this additional measurement to backup our other assessments, we also measured the void fraction leaving the pipe by use of a capacitance sensor located at the end of the pipe. This instrument obtained an electrical signal, which pertained to a capacitance measurement of the flow passing through this section. This signal was then converted into a measurement of void fraction through a previous calibration where a value of 0.0 denotes all liquid flow and a value of 1.0 denotes all vapor flow with everything in the middle being a mixture of the two. Figure 3.24 shows the output from this sensor during the experimental run. Once again we notice that the main liquid flow seems to end in the 1600-1800 millisecond range. The slight discrepancy between this measurement and the mass inventory measurement is most likely caused by the fact that they are on either ends of the pipe. This trace shows us that at the beginning there is a flow of predominately liquid, void fraction of 0.4-0.2, which slowly rises to a more consistent value of 0.5 until the liquid runs out and the value jumps back up to an all vapor level. There are many peaks in the trace due to the fact that the flow is highly turbulent at this period in the flow, with the phasic composition changing with the rate of nitrogen coming out of solution. The flow slows down a little near the end and the trace smooth out, until the end when there is no more flow. These four different methods of taking measurements allows us to believe that we have a good grasp on what is going on during the rapid transient phase of the experimental run. For the detailed output of all of the experimental runs conducted in this study see Appendix B.

3.4 Observations and Conclusions

After analyzing the full range of experiments conducted in this study we found many findings and observations. The most exciting developments in this study pertained to the previously unsuccessful measurements of mass flow rate, void fraction and local

temperature. Our transient fluid inventory method gave excellent results providing us with not only another check for the computer code developed in this work, but also an innovative technique currently unavailable in two-phase flow experiments. The void fraction measurement using a capacitance sensor has been used in other applications, but never in such a rapid-transient setting. In addition, most methods used in previous studies required the probe to extend out into the measured flow, which causes obstruction to the flow and obvious changes in the resulting flow characteristics. Our method provides a quick, accurate signal with minimal disturbance to the flow, resulting in the measurement of more realistic flow characteristics. Last, the film thermocouples used in this study also allowed for the measurements to be made without disturbing the fluid flow. In previous studies thermocouples were always extended into the middle of the pipe in order to get the most accurate representation of the local temperatures causing them to break and deflect the fluid as it flowed. These techniques had another shortcoming of not allowing a fast response due to the thermocouple sheathing. In our case, we have only a paper-thin layer shielding the thermocouple junction from the flow while having no effect on the flow due to their flush-mounted design. These techniques allowed this study to provide a more comprehensive comparison for the computer code simulations to be tested against.

The experiments in this study primarily focused on the use of HFC-227ea as a test fluid. The first set of experimental runs examined the effect of changing the initial source vessel pressure on the flow characteristics through a straight, 1/2" nominal diameter pipe, see Figure 3.5. The main difference between these runs was the speed at which the source vessel discharged its contents into the piping system and hence into the collection vessel. All the runs exhibited the same basic phenomena as seen in Figure 3.9; (1) a quick pressure drop as the pipe filled, (2) a continuous drop in the pressure as the source vessel discharged its remaining fluid, and (3) a slight pressure "bump" in the pressure measurements in the pipe due to the venting of the remaining gas and vapor in the source vessel. Similar observations can be made by examining the void fraction and mass flow measurements. The lowest void fraction can be seen at the beginning of the runs, Figure 3.24, when the liquid content in the flow is the greatest. Near the end of the run, we see a marked increase in the void fraction as more nitrogen comes out of solution causing it to rise. The corresponding mass flow measurement, Figure 3.15, shows the fastest discharge at the beginning of the run when the source vessel pressure is at its highest value providing the greatest driving force. Once the pressure begins to wane, so does the flow rate shown in the measurement, until it ends at the end of the liquid flow for the run.

The second set of experiments were conducted using an alternative piping system which contained tees, elbows, and a union as shown in Figure 3.11. The main goal for these runs were to measure the pressure drop associated by adding specific pipe fittings into the piping network. As we would have expected, the flow was significantly reduced by the pipe fittings, as shown in Figure 3.25. The comparison shows that the run (#1) with the straight pipe finishes discharging its contents at approximately 4600 milliseconds compared with the run (#8) that used the piping layout containing two capped tees, a 90° elbow, a union and two 45° elbows, which finished at about 7500 milliseconds. To study these pressure drop measurements, a comparison to the literature values for non-compressible, turbulent flow through pipe fittings using the friction loss factor method was conducted. This method is based on the procedure where pipe fittings are set equal to equivalent lengths of pipe depending on the anticipated pressure drop associated with the fitting. In our experimental

setup, the pressure ports used to measure the pressure drop across the fittings included not only the fitting but also some piping in between, see figure 3.11. In each case the additional piping plus the fitting between the pressure ports was included to remain as accurate as possible. For example the 90° elbows was made up of the pressure port then 2 inches of piping, then the elbow, then 3 more inches of piping and the final pressure port. Therefore, what we denote as the “90° elbow” is actually the elbow plus 5 inches of piping. The literature values were obtained by using the literature value for the friction loss factor, K , for the particular fitting and adding it to the calculated value for the additional piping, found by using equation 3.4-1.

$$K = 4f_f \frac{L}{D} \quad (3.4-1)$$

Where f_f is the friction factor of the pipe found by using a chart in the literature with the diameter and estimated roughness of the pipe, L and D are the length and diameter of the pipe, respectively. Once a total K is found for the fitting and additional piping it can be used in equation 3.4-2 to find the literature value for ΔP .

$$\Delta P = \frac{K \rho v^2}{2} \quad (3.4-2)$$

Where ρ is the mixture density calculated using the experimental void fraction measurements, and v is the flow mixture velocity calculated from the experimental values of mass flow through the pipe and the mixture density.

Table 3.4.1: Comparison of Experimental Pressure Drop Values to Literature Values*.

	Run #8	Run #9	Run #10
Initial Source Vessel Pressure [kPa]	2120	3915	4910
Void Fraction	0.649	0.507	0.485
Liquid Density [kg/m ³]	1403.5	1392.8	1389.0
Mixture Density [kg/m ³]	514.43	704.73	733.18
Velocity [m/sec]	3.446	9.007	7.630
90° Elbow			
Experimental ΔP [kPa]	9900	27800	36000
Literature Value ΔP (mixture ρ) [kPa]	21594 (118%)	106073 (282%)	72775 (102%)
Literature Value ΔP (liquid ρ) [kPa]	7915 (20%)	53673 (93%)	38414 (7%)
Capped Tee			
Experimental ΔP [kPa]	11300	40400	62600
Literature Value ΔP (mixture ρ) [kPa]	29778 (164%)	195398 (384%)	134059 (114%)
Literature Value ΔP (liquid ρ) [kPa]	14580 (29%)	98871 (145%)	70763 (13%)
Union			
Experimental ΔP [kPa]	11100	31500	50400
Literature Value ΔP (mixture ρ) [kPa]	17048 (54%)	83742 (166%)	57454 (14%)
Literature Value ΔP (liquid ρ) [kPa]	6248 (44%)	42373 (35%)	30327 (40%)

* From Fundamentals of Momentum, Heat, and Mass Transfer by Welty, Wicks, and Wilson.

Since our experiments took place under two-phase conditions, we used the mixture density in order to get as close to the actual conditions in the pipe as possible. The one drawback of this method is that the void fraction sensor was not located at the local position of the fitting, but at the end of the pipe so it may not be a precise representation of the void conditions at the fitting. For this reason and because the literature values for K were developed using liquid turbulent flow, we also included a comparison to values using the liquid density and liquid velocity in place of the mixture density and mixture velocity. See table 3.4.1 for the detailed values of this comparison. As the comparison shows, there are some discrepancies between the literature and the experimental values, with the calculations using liquid density being in reasonable agreement. In order to compare whether the mixture or the liquid density is best used when calculating the literature value for ΔP , the error has been provided in parentheses. This error was determined using the experimental value as the actual value. The experimental values for pressure, void fraction, density and velocity were taken in the middle of the runs, with run #8 being from 1500 to 3500 milliseconds and runs #9 & #10 being from 500 to 1500 milliseconds. Some of the possible reasons for the discrepancies in the comparison between the calculations using the liquid density and those using the mixture density may be:

- 1) Because of the phasic composition of the flow at the particular time during the run. For example, at the beginning of the run there is a large amount of liquid flowing but there is also a large quantity of nitrogen degassing, so it is hard to tell how this will effect our calculations.
- 2) The capped tee is near the beginning of the piping layout while the void sensor that we are using for the calculation of the mixture density is at the end.
- 3) The fact that the literature value for the union is actually considered as if the fitting is just a section of straight pipe. In theory this should be the case since the union when assembled should not interfere with the flow, but there are still ridges from the male and female sections connecting on the inside of the union possibly causing disturbances to the flow.
- 4) The role of the two-phase flow that we have in the experiments. An assumption made when modeling two-phase flow through pipe fittings is that the differences with single-phase liquid flow are marginal, but this may not be the case. The void fraction may play a large part in the pressure drop experienced through a pipe fitting since it will influence the flow conditions through the fitting.

Overall, the liquid density yielded a better calculation than the mixture assumption with an average error of 47.3% compared with 155.3%. These findings lead us to believe that the phasic composition of the flow through the fitting plays a major role in the pressure drop experienced at any instantaneous time during the discharge and local flow characteristics will play a large role in what magnitude of pressure drop occurs.

The third set of experiments also used an alternative-piping configuration, which included a vertical split of the flow, see Figure 3.12. The goal of these runs was to examine whether there would be any difference in pressure drop between the two legs of the split. At slower flow velocities, separation of the flow may occur based on the flow regime of the discharge. For example, if the flow were stratified then all the liquid may flow through the bottom leg of the split and the entire vapor may travel through the top leg. This would be

evident from the difference in pressure drop between the two legs since the vapor would have a much lower pressure drop than the liquid. In our experimental runs we examined no such trend, as can be seen in figure 3.26, which depicts the pressure drop across both legs after a vertical tee split. The plots for both the top and bottom branch are almost identical which was the case for the entire tested pressure range of 2140 kPa to 4910 kPa. This proves our theory that at these high velocities the flow is in the bubbly flow regime causing an even split between the two branches.

The fourth set of experiments used the same piping configuration as the first set, the straight pipe, but we changed the test fluid to HFC-125. The main difference observed in these runs over the HFC-227ea runs was the drop in temperature as the liquid vaporized. If a comparison is made between run #5 (HFC-227ea) and run #16 (HFC-125), which have initial source vessel pressure within 5 kPa of each other, there is an undeniable difference in the temperature traces in the collection vessel. As Figure 3.27 shows, the temperature in run #5 only drops about 3 degrees compared to a temperature drop of almost 35 degrees in run #16. While the other temperature traces between these runs are similar, this may be because the flow passes through the pipe at such a fast rate with a high convective heat transfer coefficient, which causes the fluid to warm up. However, in the collection vessel the volume/surface ratio is much larger and convective heat transfer to surface area is smaller. Although, it would have been beneficial to measure the temperature at the end of the pipe to justify this theory we were unable to take this measurement due to a thermocouple failure. Once the liquid reaches the collection tank it must vaporize to reach the saturation conditions in the collection vessel causing a drop in temperature. These conditions did not significantly effect the other measurements near the end of the pipe for either fluid. For instance, for either fluid the void fraction followed a similar trend as expected from the previous runs, it dropped off as the initial flow passed the sensor and then rose slowly until the liquid ran out, then it returned to the all vapor value. These plots can be examined in more detail in Appendix B as the forth graphs under runs #5 and #16. During runs with both of these fluids we did not observe a noticeable pressure recovery due to the degassing of the nitrogen, which was seen in previous studies. Although, when examined closely, we see a sudden slow down in the pressure decay after the initial pressure drop, which may indicate a slight recovery. This theory is based on the fact that in the HFC-227ea runs there was a much smoother transition shown on the source vessel pressure histogram between the initial pressure drop and the filling of the pipe. This can be seen best by once again comparing runs #5 & #16, where there is a slight “bump” in the source vessel pressure trace at about 400 milliseconds of run #16. The absence of a more pronounced pressure recovery due to the degassing of nitrogen can be accounted for by either of two reasons. The speed of the flow is too great for a noticeable increase in pressure from degassing to be observed at any one point or the degassing took place gradually over the run preventing one noticeable increase to be possible. We do know that the degassing occurred at some point since the void fraction validated that a two-phase flow existed and we are certain it was not due to vaporization since there was no temperature drop to make us believe otherwise.

The last sets of run were conducted during preliminary runs to test the instrumentation after installation in the system. The first test using water, run #18, allowed for a sampling of the mass flow rate sensor. As can be seen in figure 3.28, this test worked out very well and gave an excellent representation of the instantaneous mass inventory in the source vessel. This test also showed us that our thermocouples could pick up quick drops in

temperature, as shown in the pipe position 1, trace of the film thermocouple which picked up the nitrogen expansion at the end of the run, see Appendix B, run #18, graph 2. The second test, run #19, gave us an excellent sample of the capabilities of the capacitance probe for measuring void fraction. Since there would be no vaporization or dissolution of gas in this run, the void fraction should go from a value of 1.0 to 0.0 as the liquid flowed. This is exactly what was found at the beginning of the run until it stopped at precisely the same point as the temperature dropped signifying the start of the nitrogen expansion through the system, as can be seen in Figure 3.29. The final set of experimental runs used carbon dioxide as a test fluid and were conducted with an open collection vessel to prevent a high pressure at the end of the run. The goal of these tests was to get a grasp on the response time of the film thermocouples and what range of temperature drop they could collect. The thermocouples were able to pick up a quick drop in temperature of up to -40° Celsius. Detailed graphs of the measurements of all 21 experimental runs can be found in Appendix B.

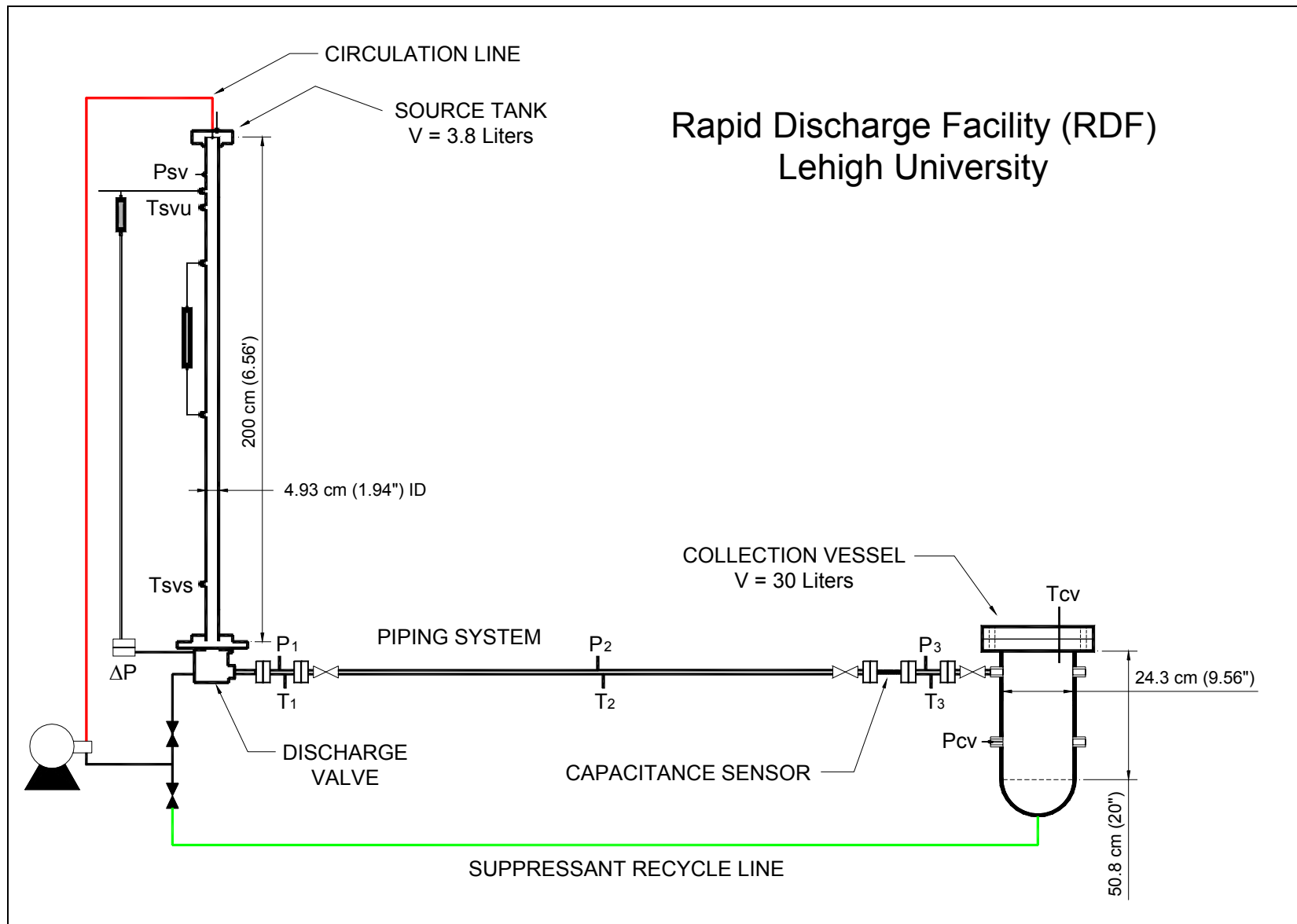


Figure 3.1: Schematic of Test Facility: Source Vessel, Discharge Piping, and Collection Vessel.

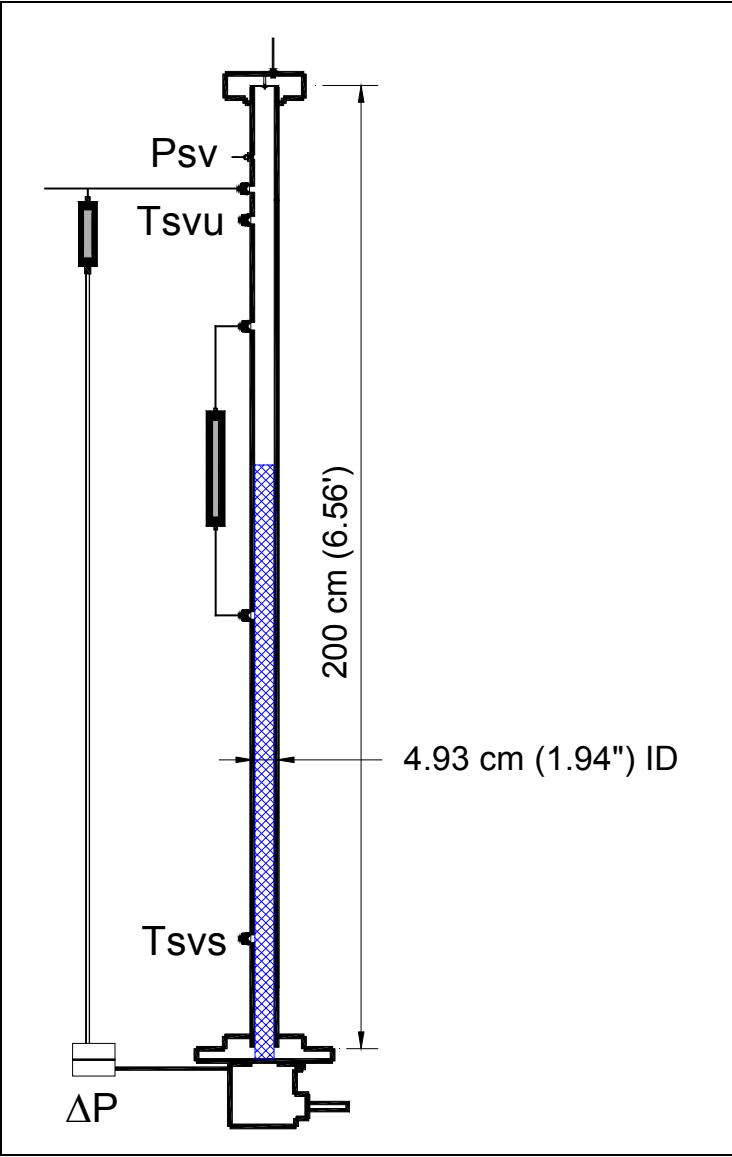


Figure 3.2: Schematic of Source Vessel Showing Mass Inventory Measurement.

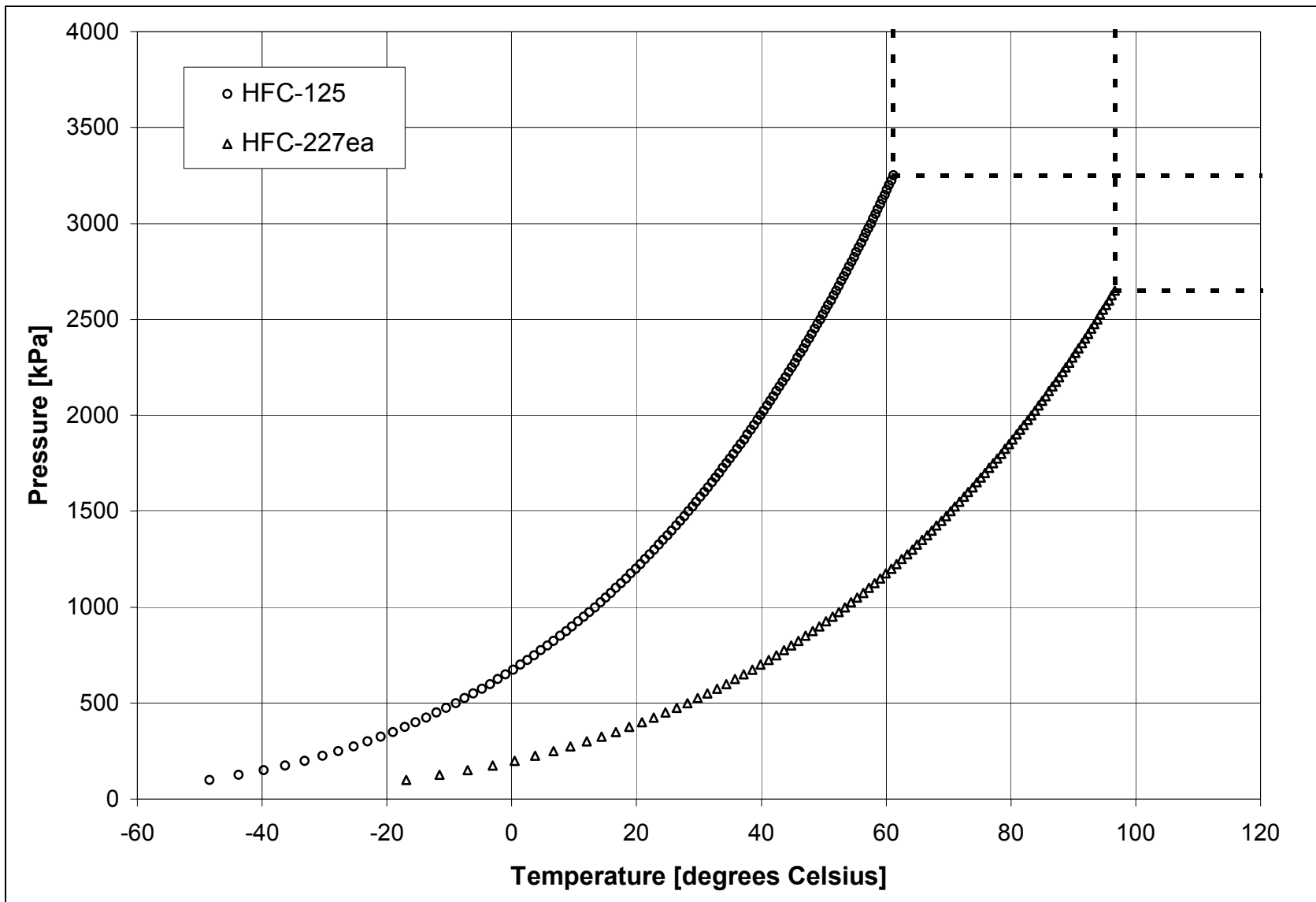


Figure 3.3: Pressure versus Temperature Saturation Curve for HFC-227ea & HFC-125.

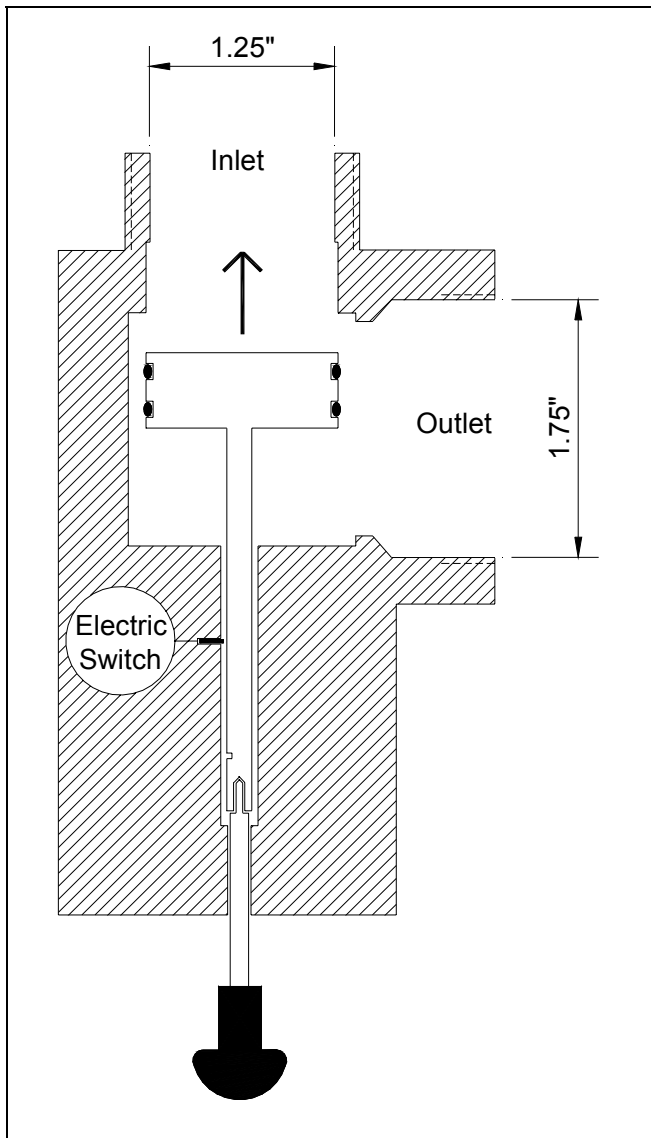


Figure 3.4: Marotta Valve.

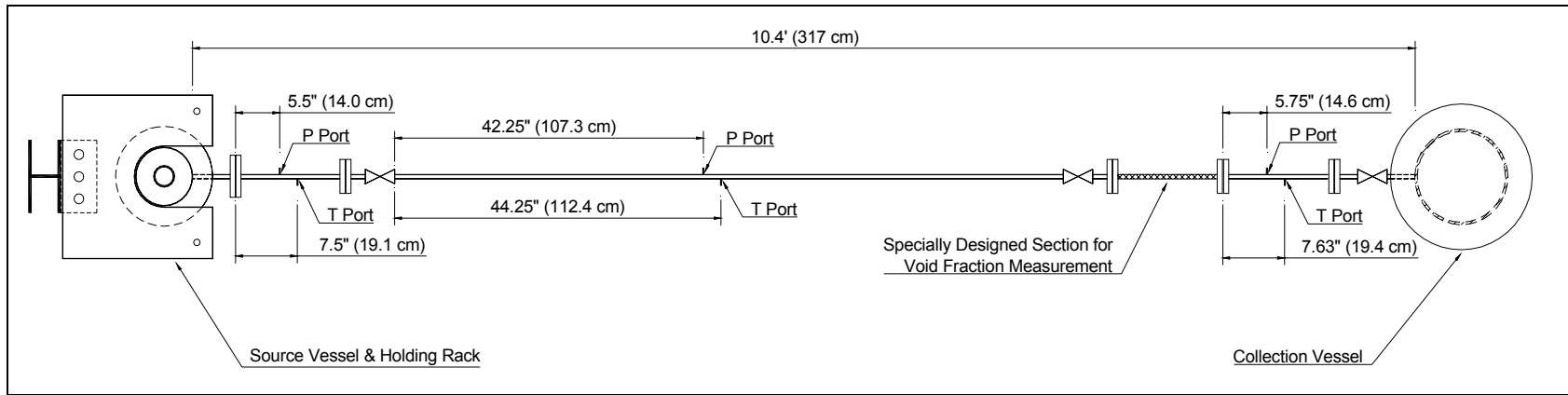


Figure 3.5: Top View of Test Facility, schematic of Discharge Piping System.

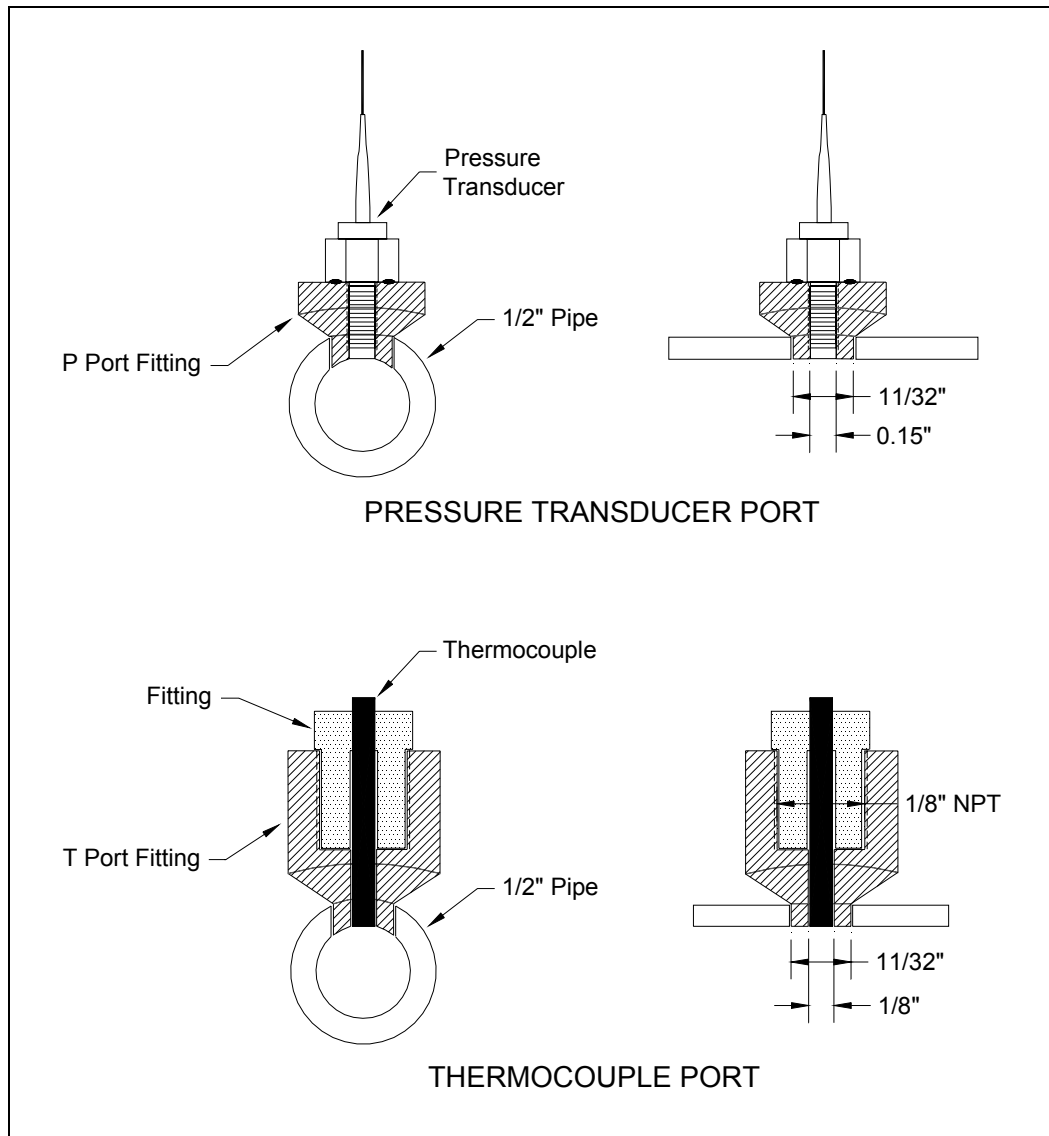


Figure 3.6: Schematic of Pressure Fittings for Temperature and Pressure Ports.

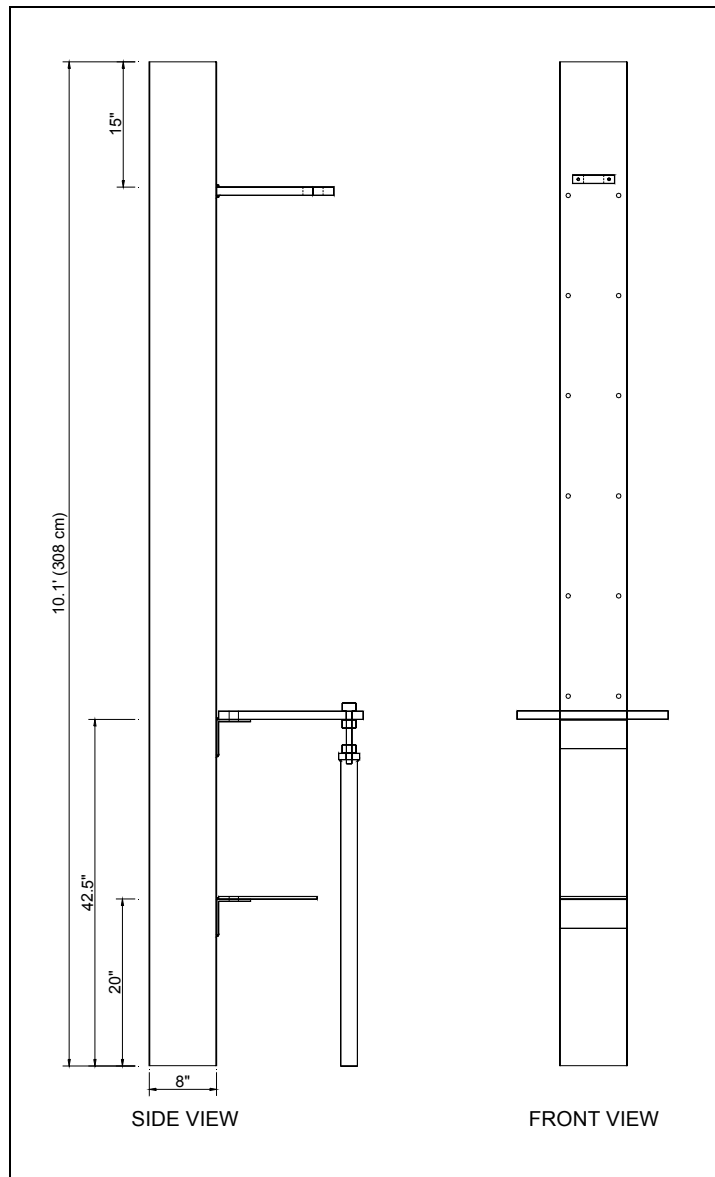


Figure 3.7: Schematic of Rack Used to Hold the Source Vessel.

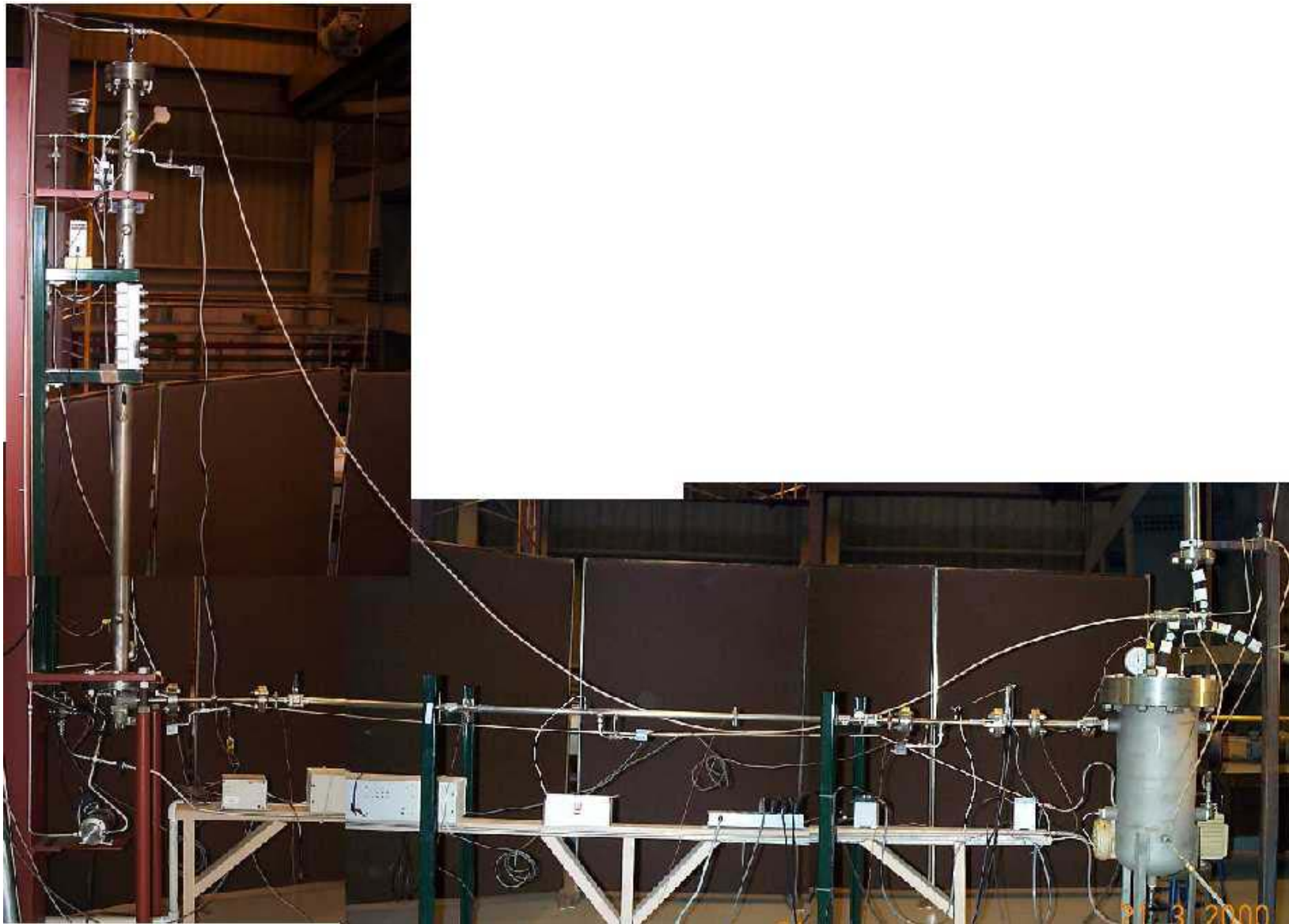


Figure 3.8: Picture of Test Facility: Source Vessel, Discharge Piping, Collection Vessel, Support Structure and Instrumentation.

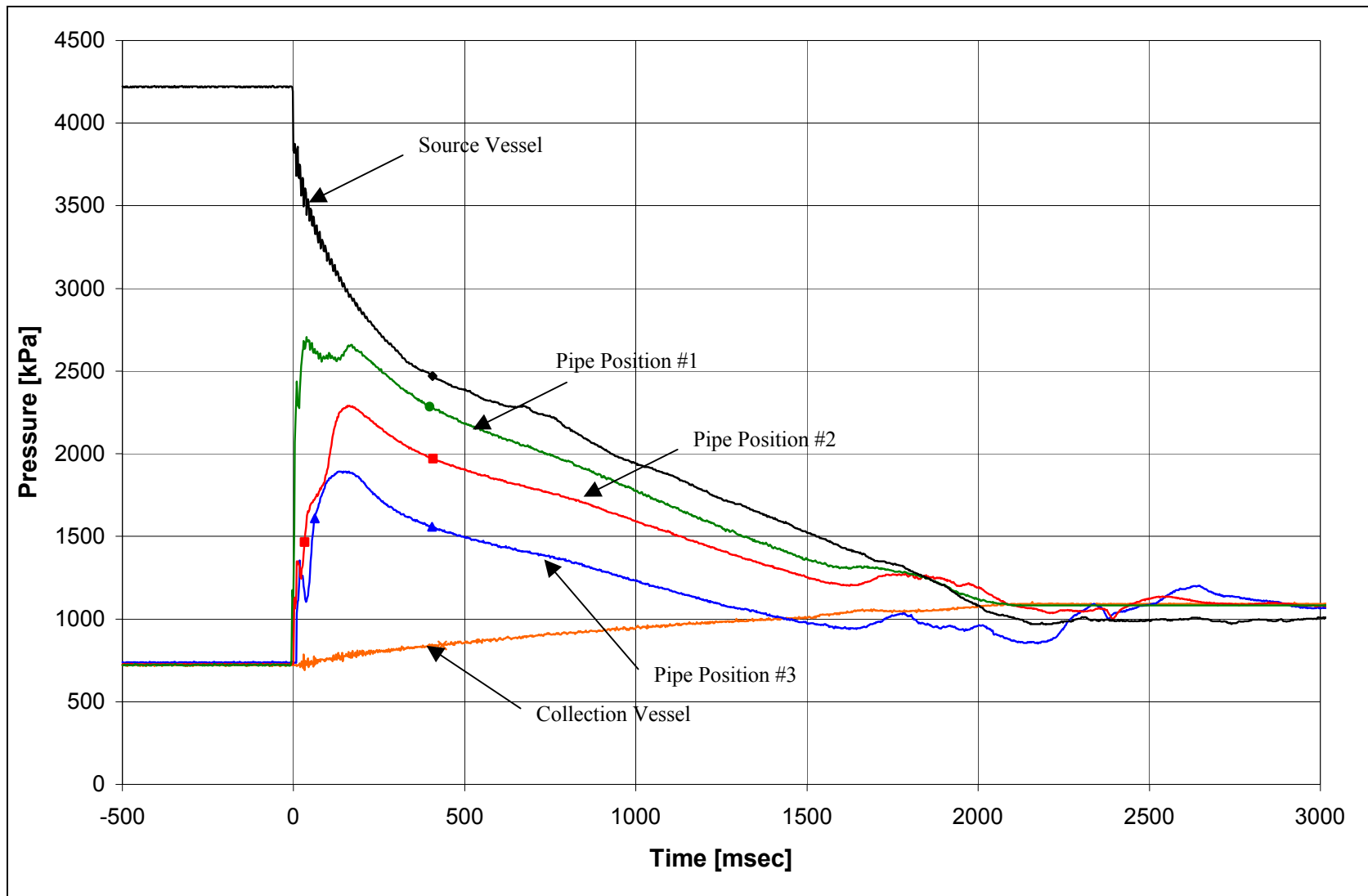


Figure 3.9: Pressure Histogram for Experimental Run #5.

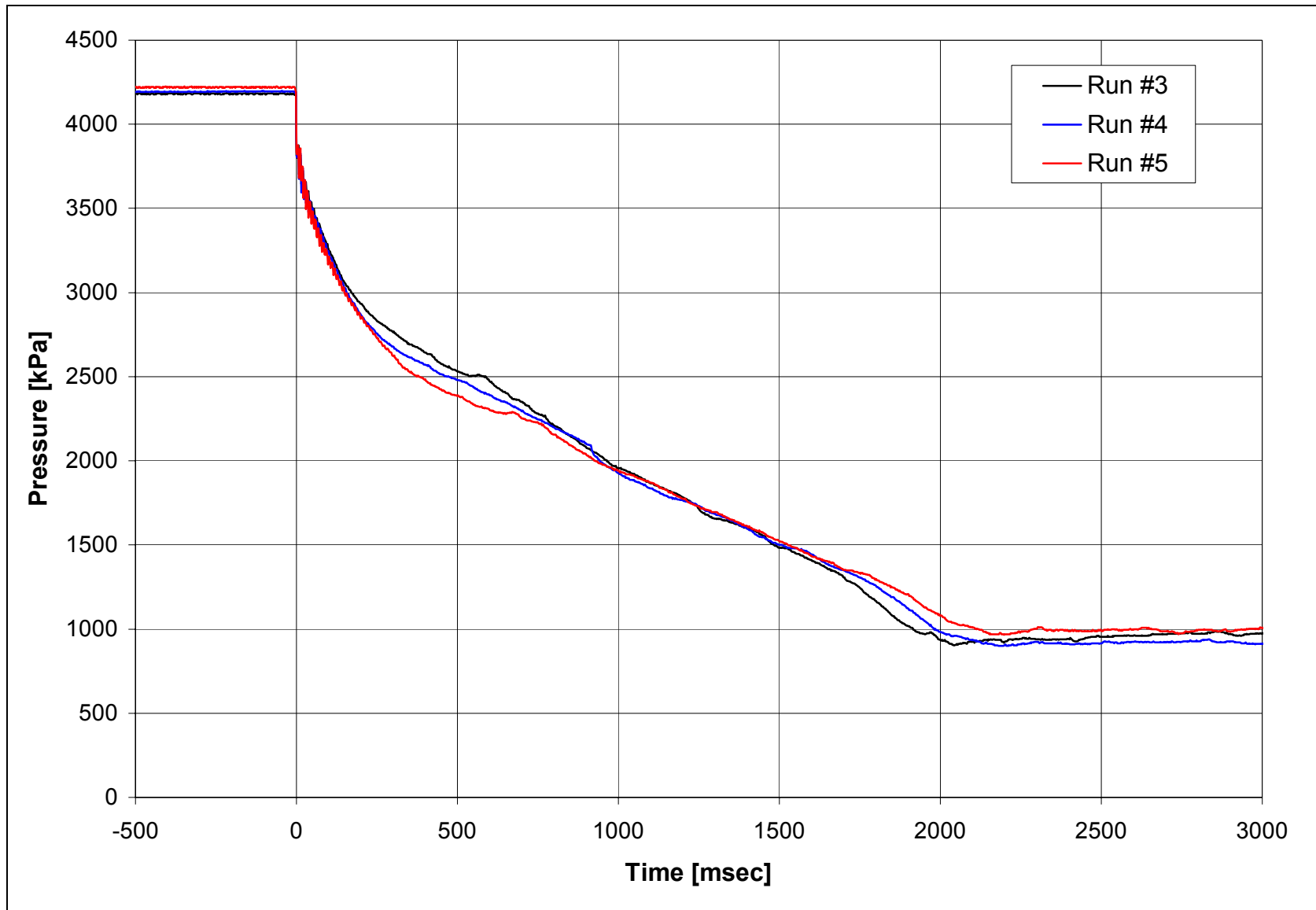


Figure 3.10: Plot of Source Vessel Pressure Showing the Repeatability of the Experimental Runs.

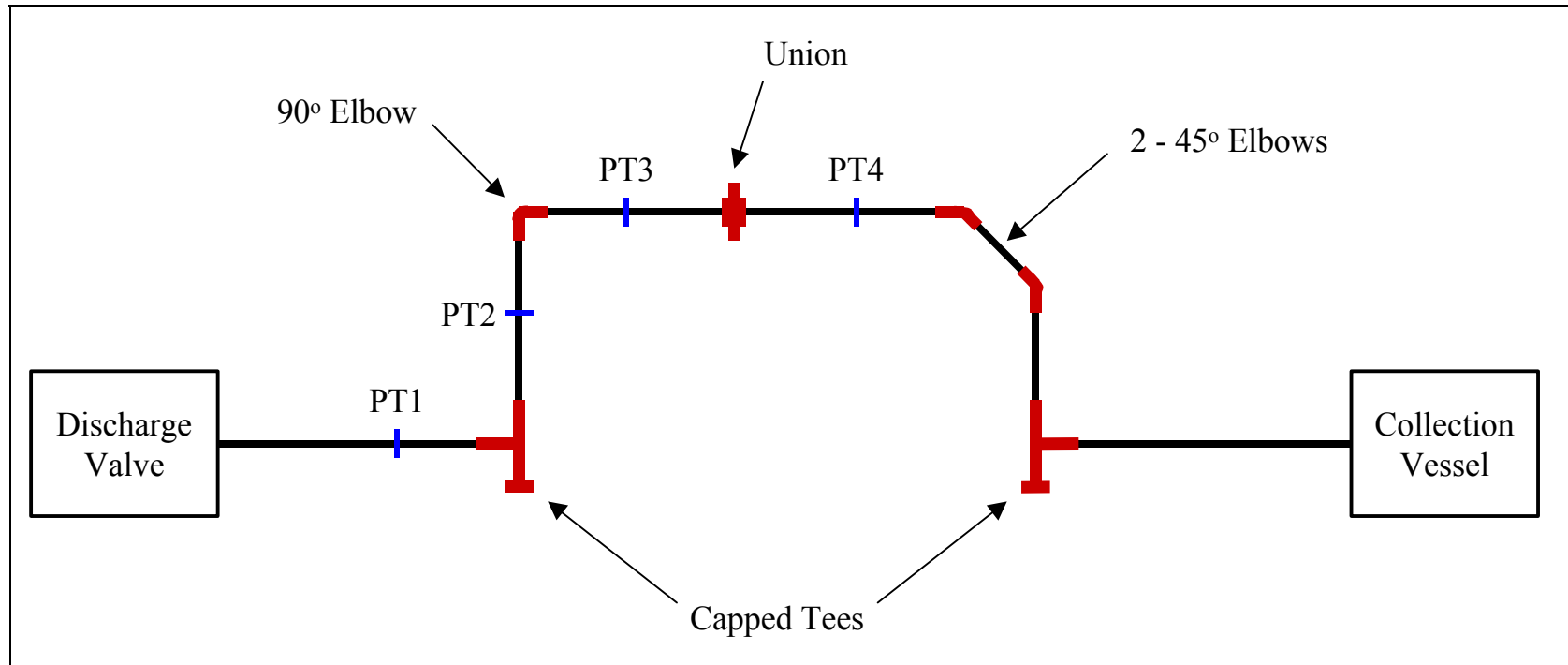


Figure 3.11: Schematic of Alternate Piping Configuration #1.

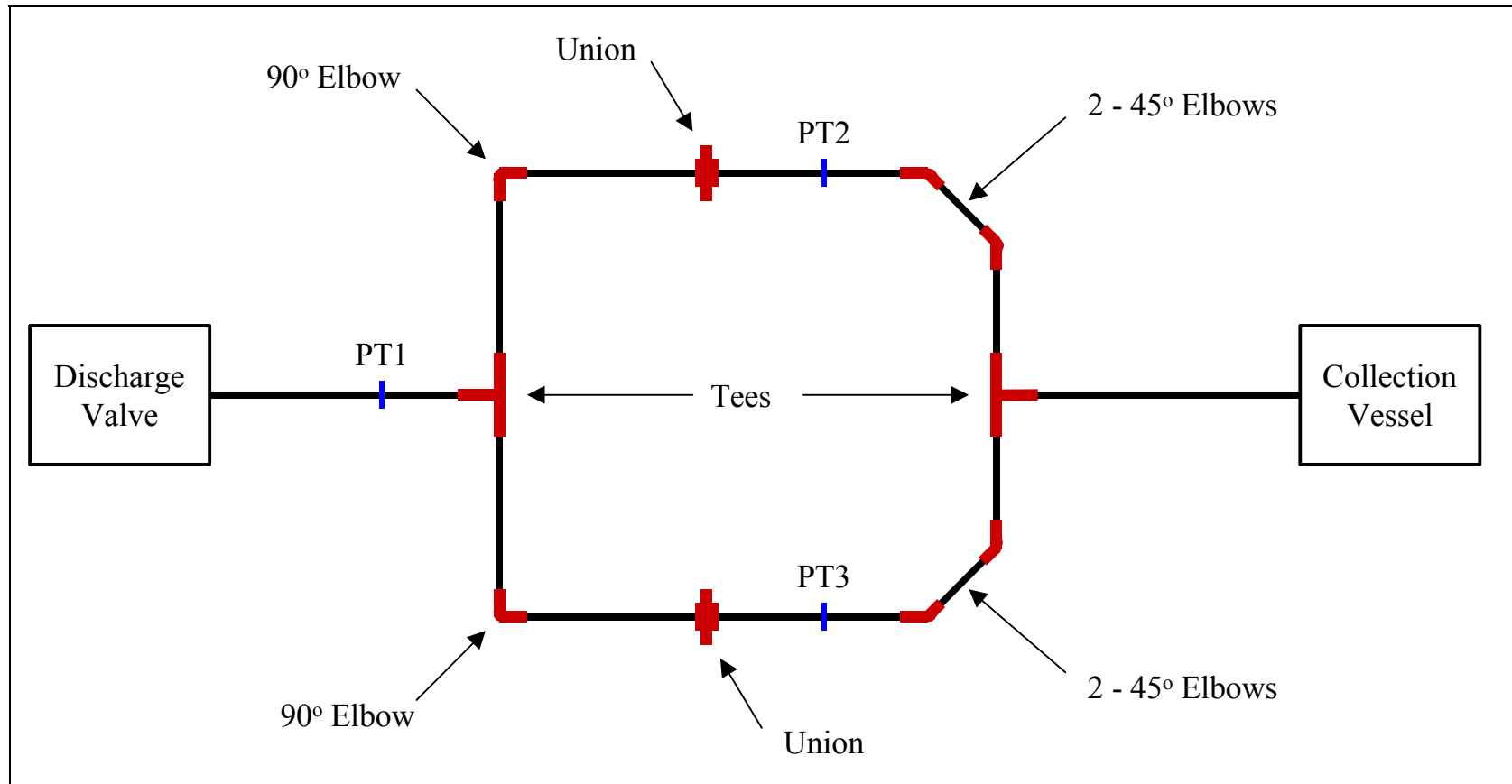


Figure 3.12: Schematic of Alternate Piping Configuration #2.

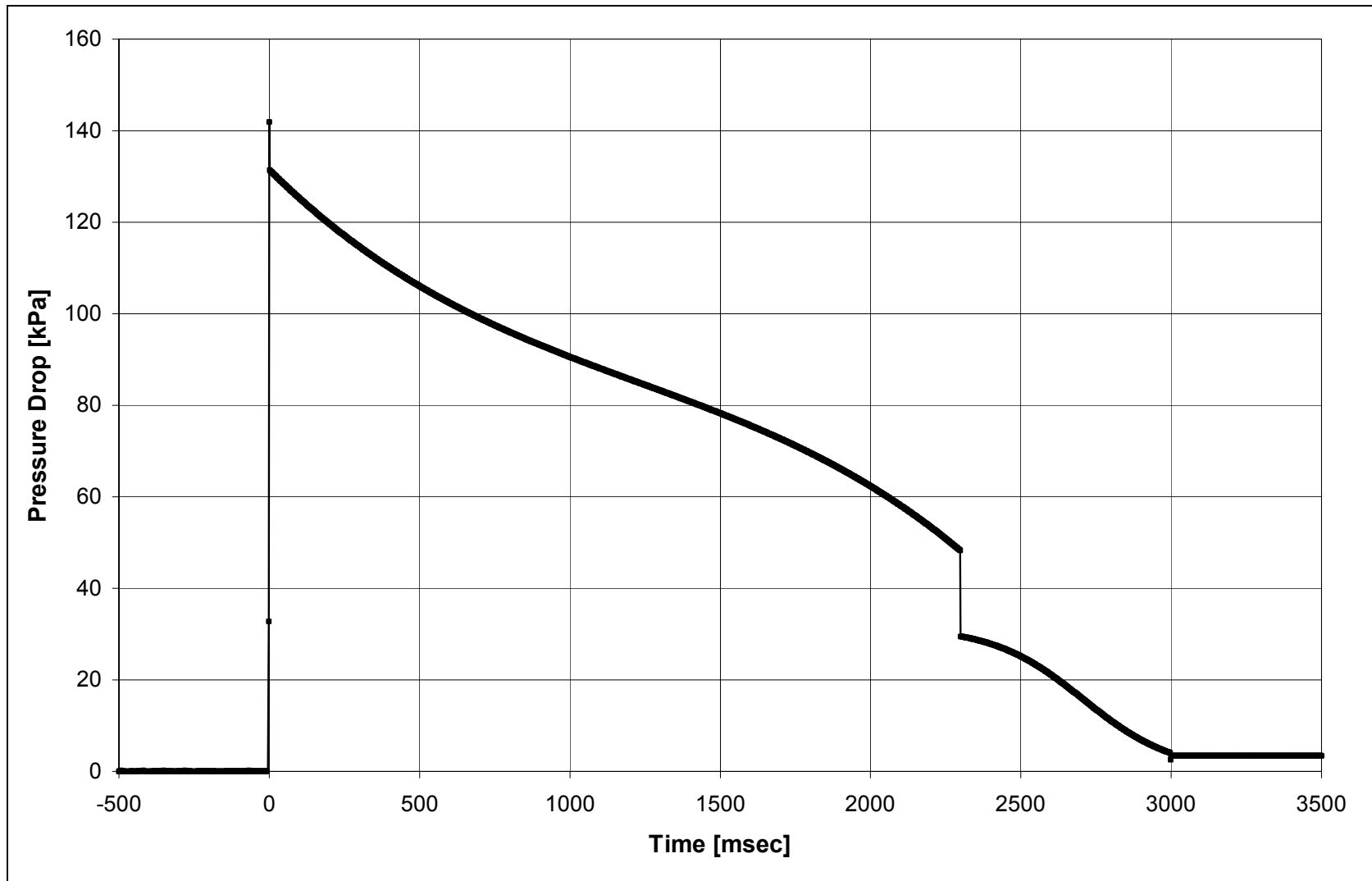


Figure 3.13: Pressure Drop Histogram Across a 90° Elbow from Run #9.

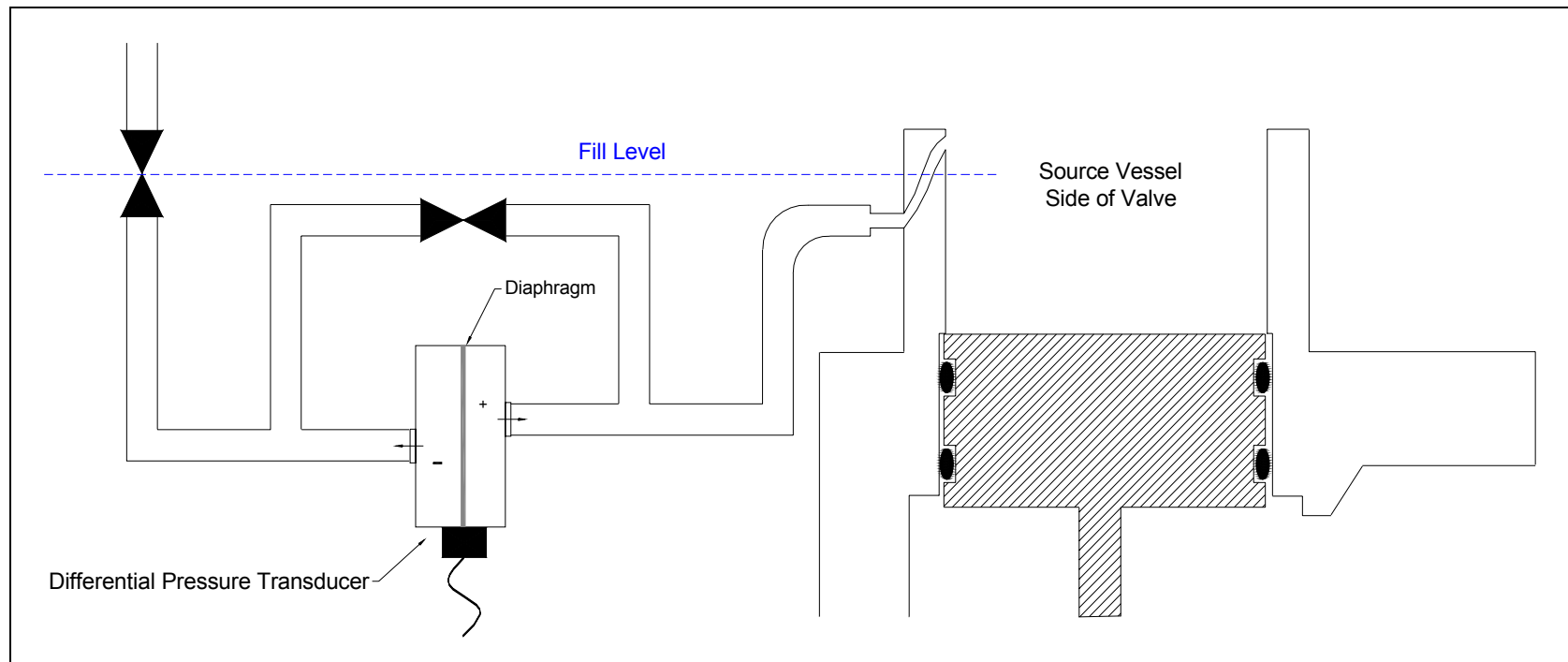


Figure 3.14: Diagram Transducer Setup for Mass Inventory Measurement.

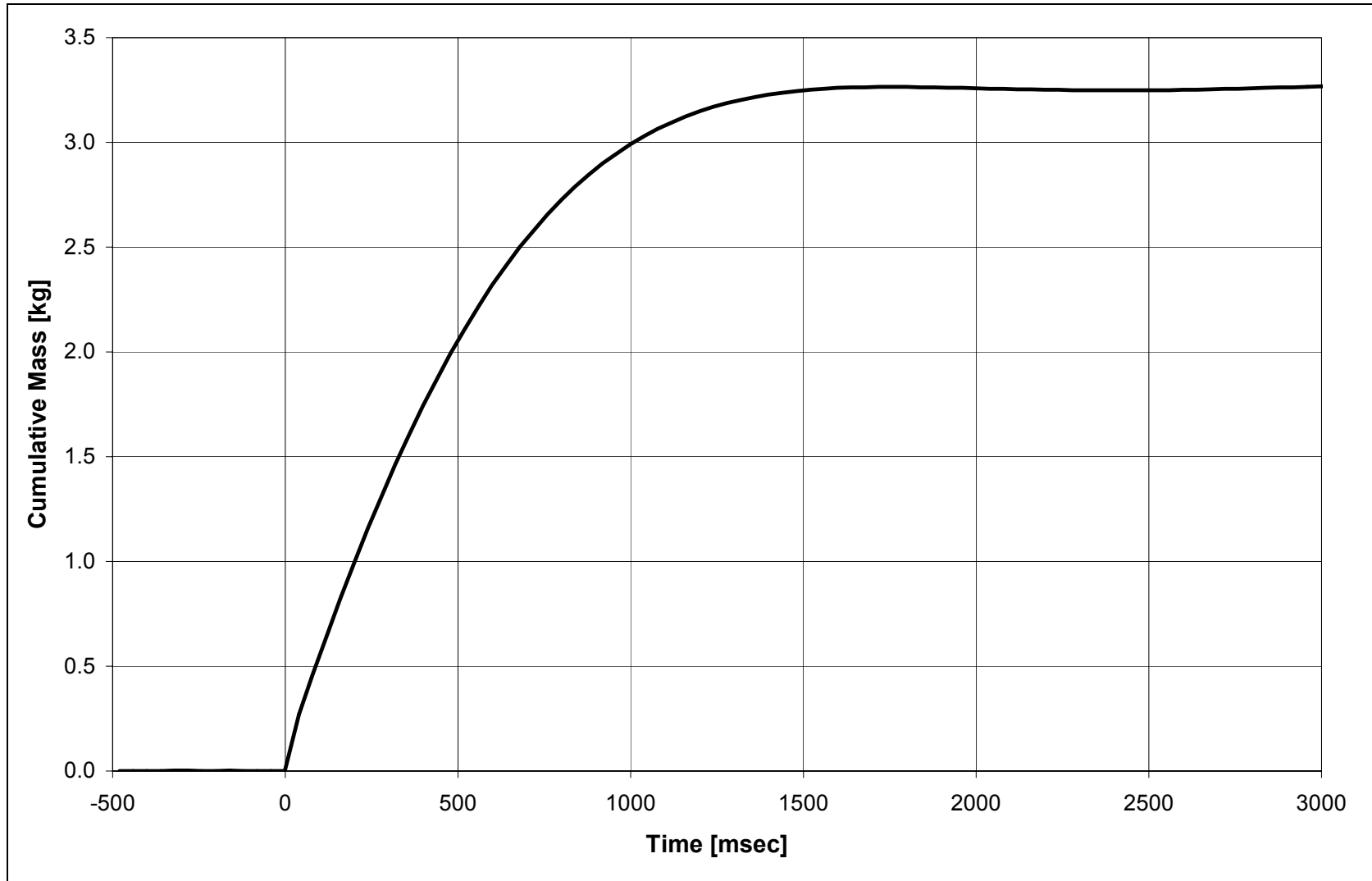


Figure 3.15: Mass Inventory Histogram of Run #5

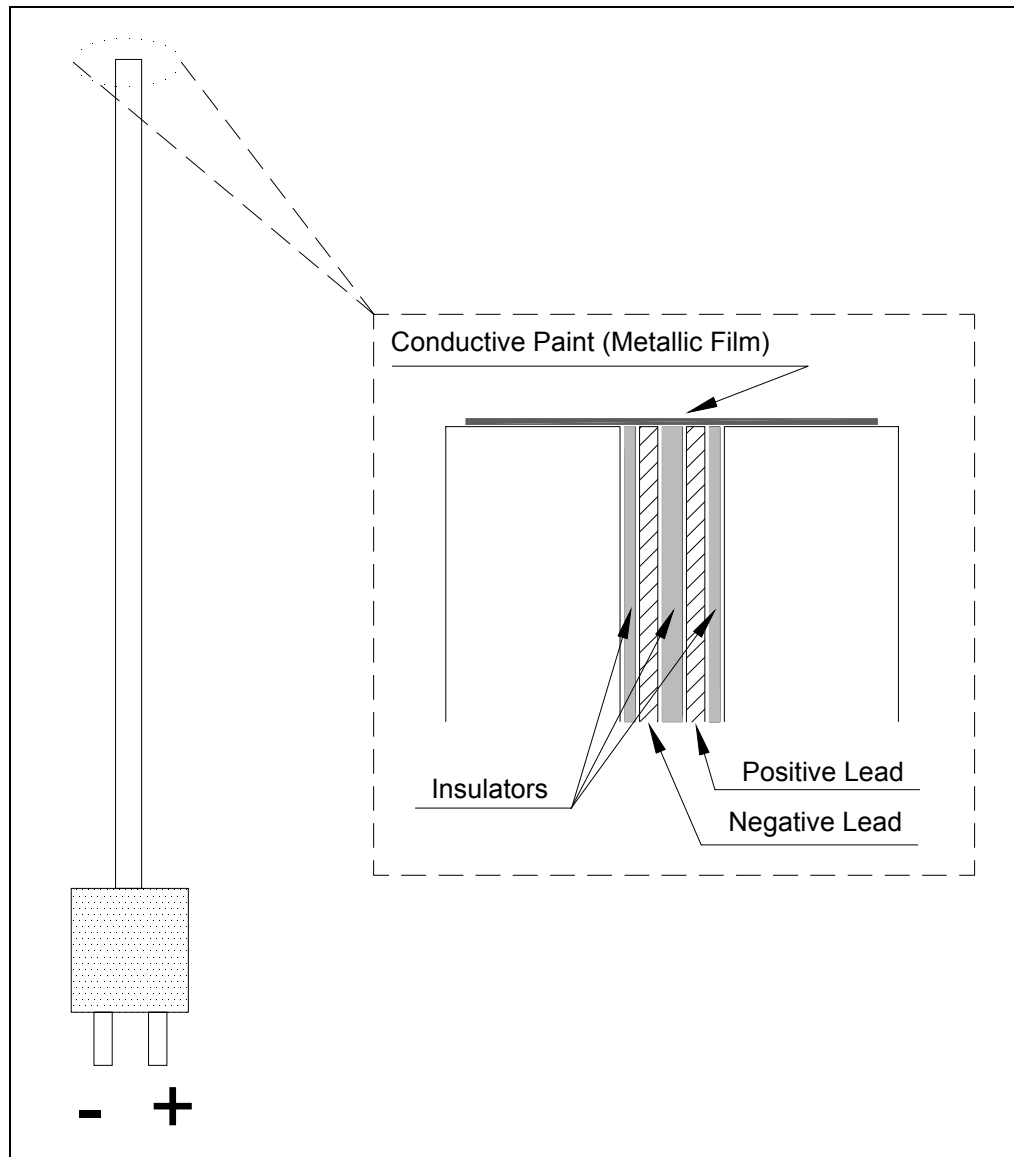


Figure 3.16: Schematic of Thermocouple Construction.

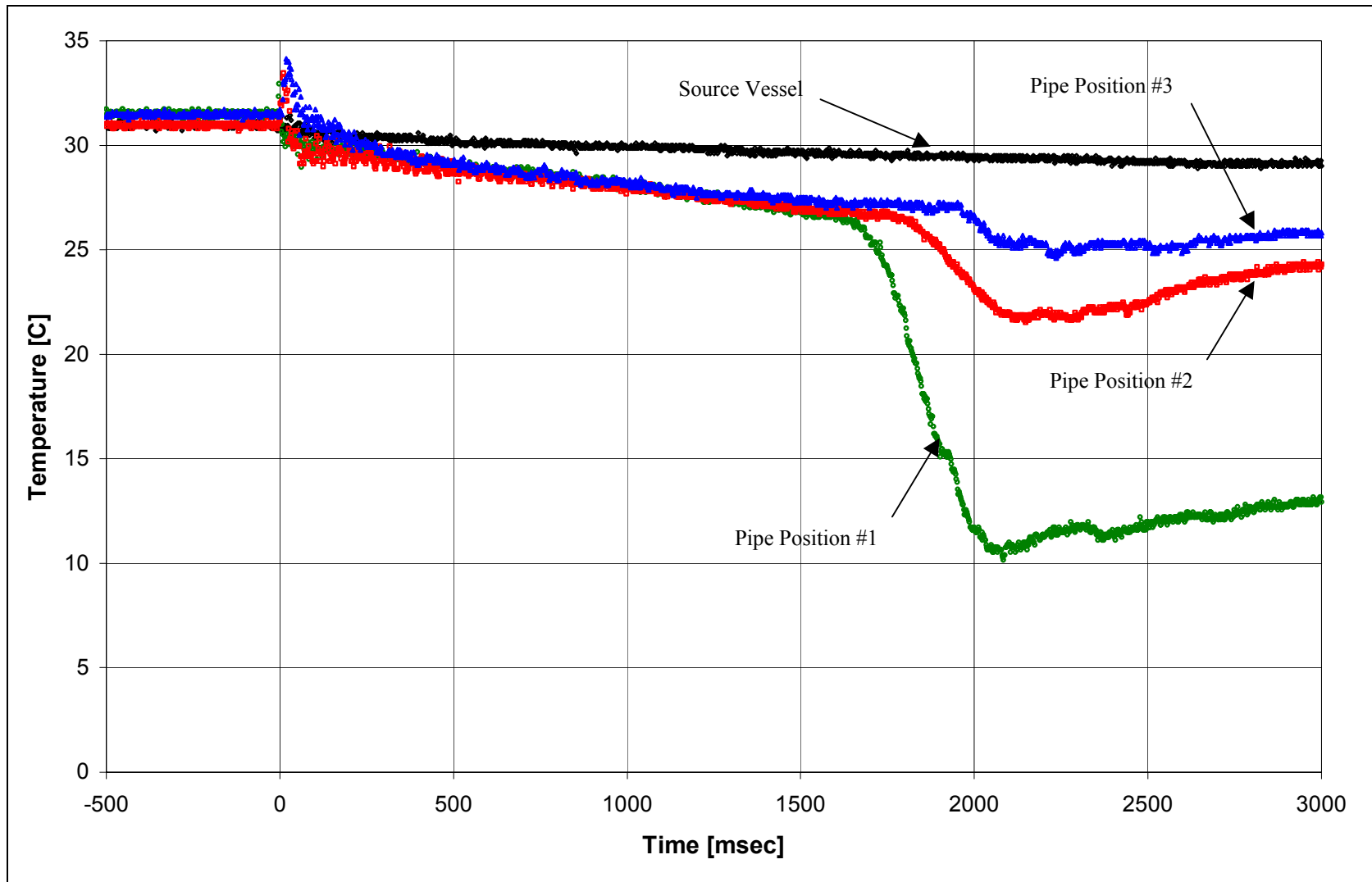


Figure 3.17: Temperature Histogram from Film Thermocouples of Run #5.

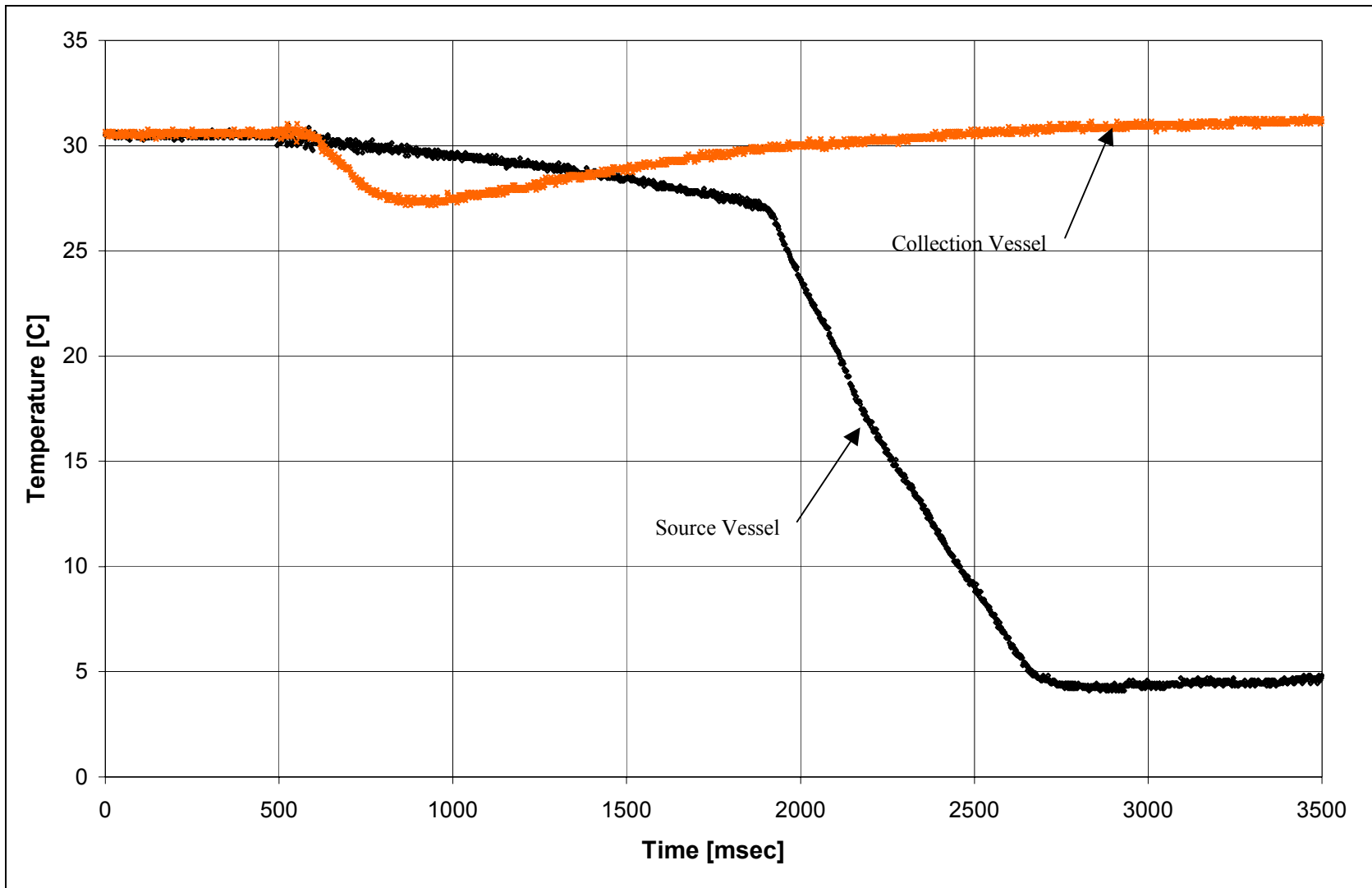


Figure 3.18: Temperature Histogram from Shielded Thermocouples of Run #5.

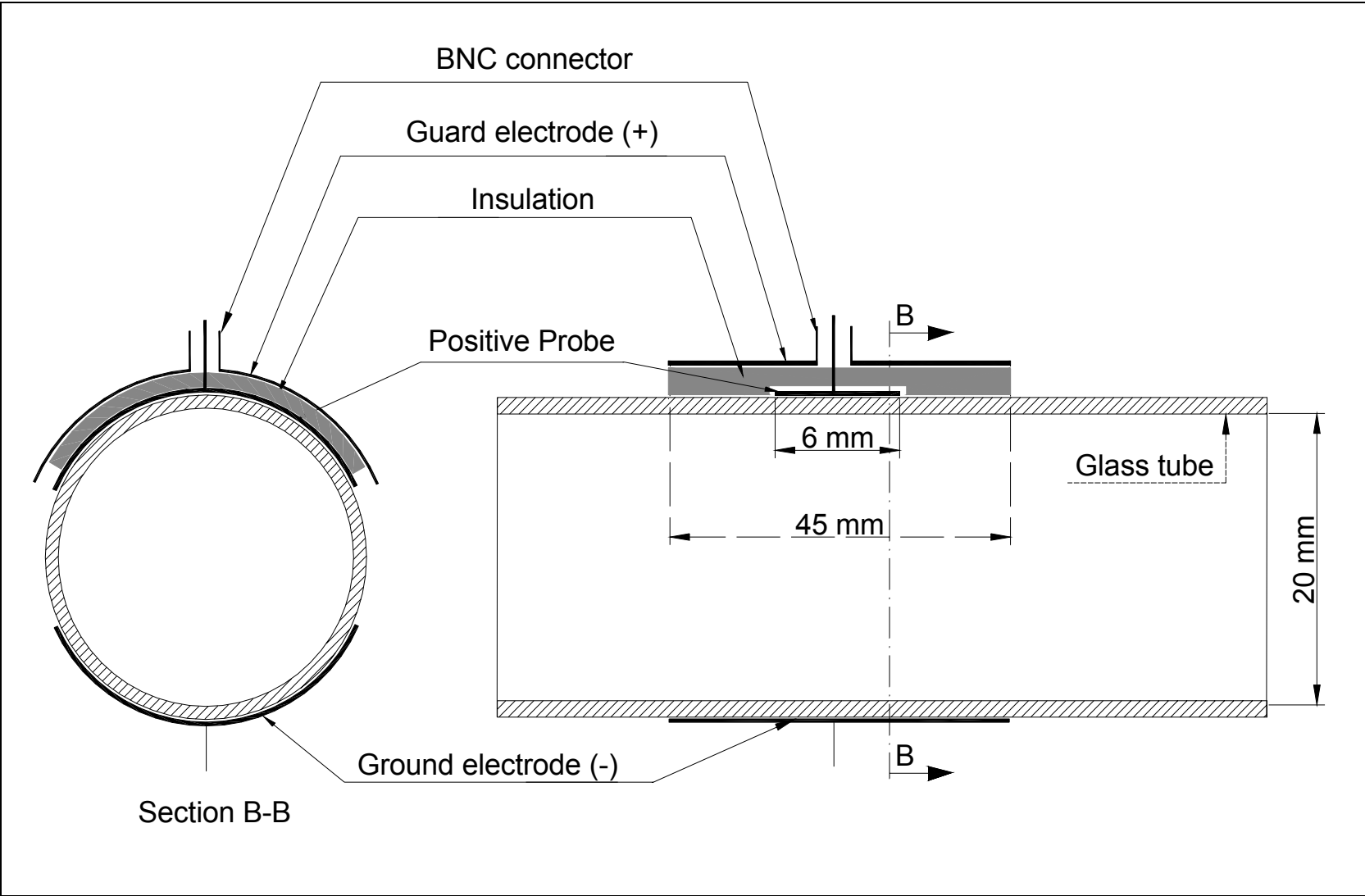


Figure 3.19: Schematic of Capacitance Probe for Bench Setup.

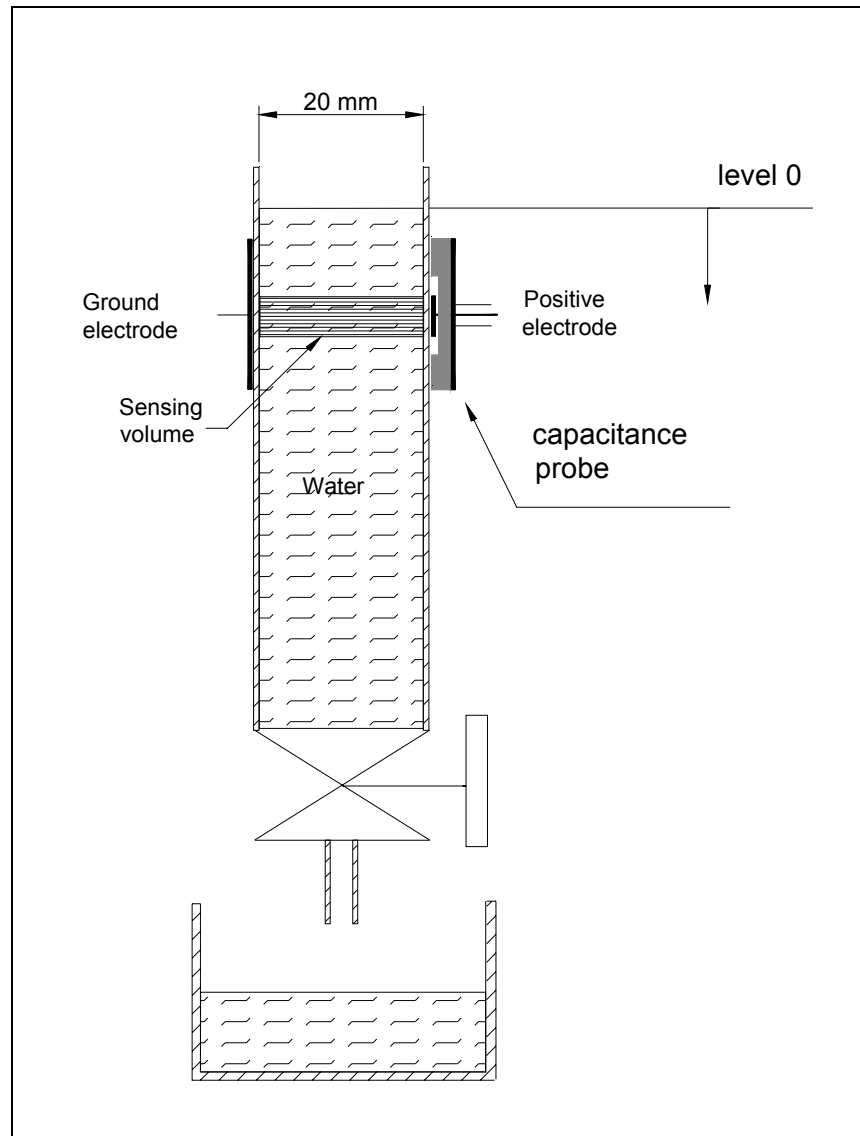


Figure 3.20: Bench Setup to Test Capacitance Sensor.

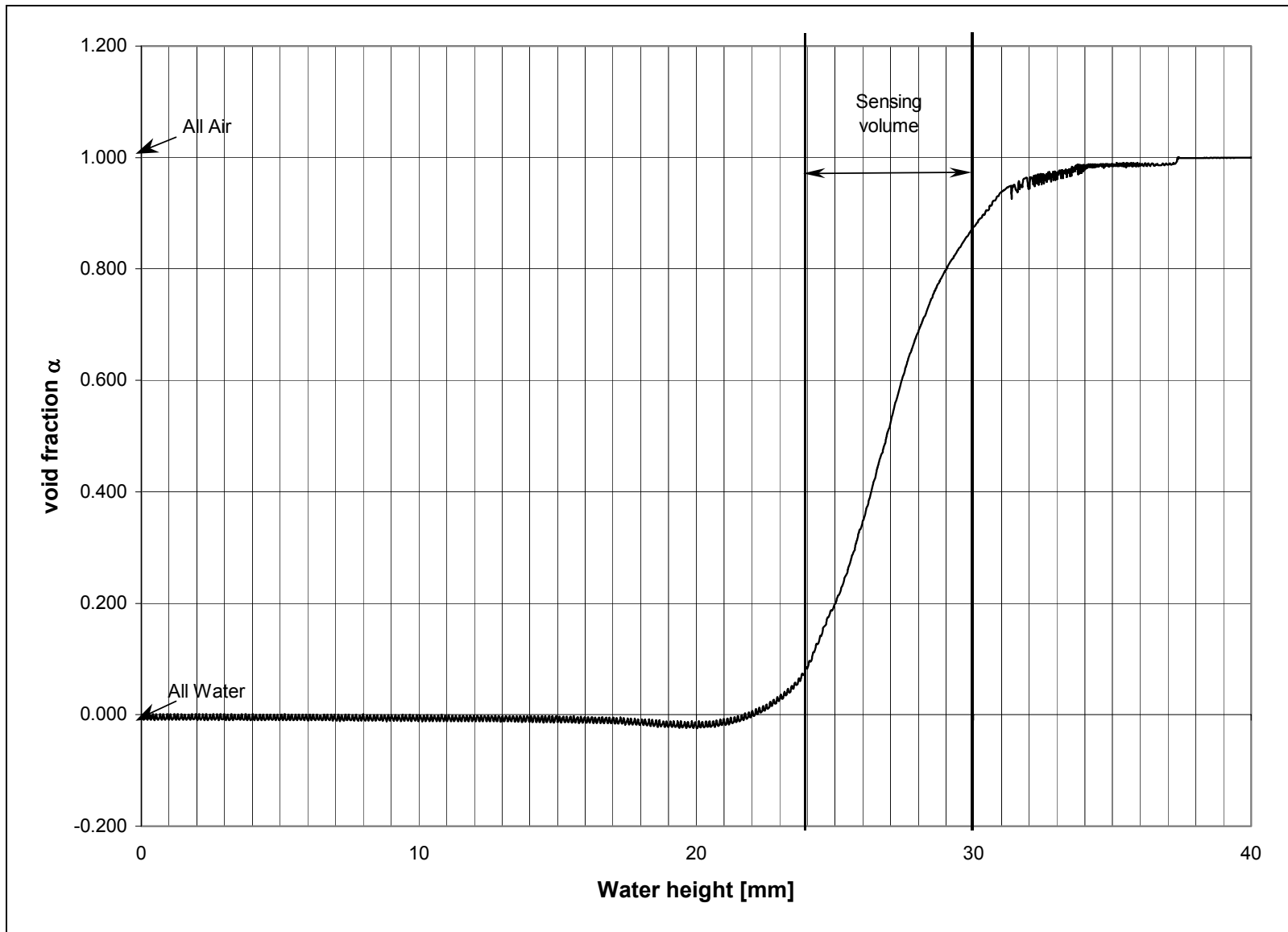


Figure 3.21: Void Fraction from Bench Tests of Capacitance Sensor.

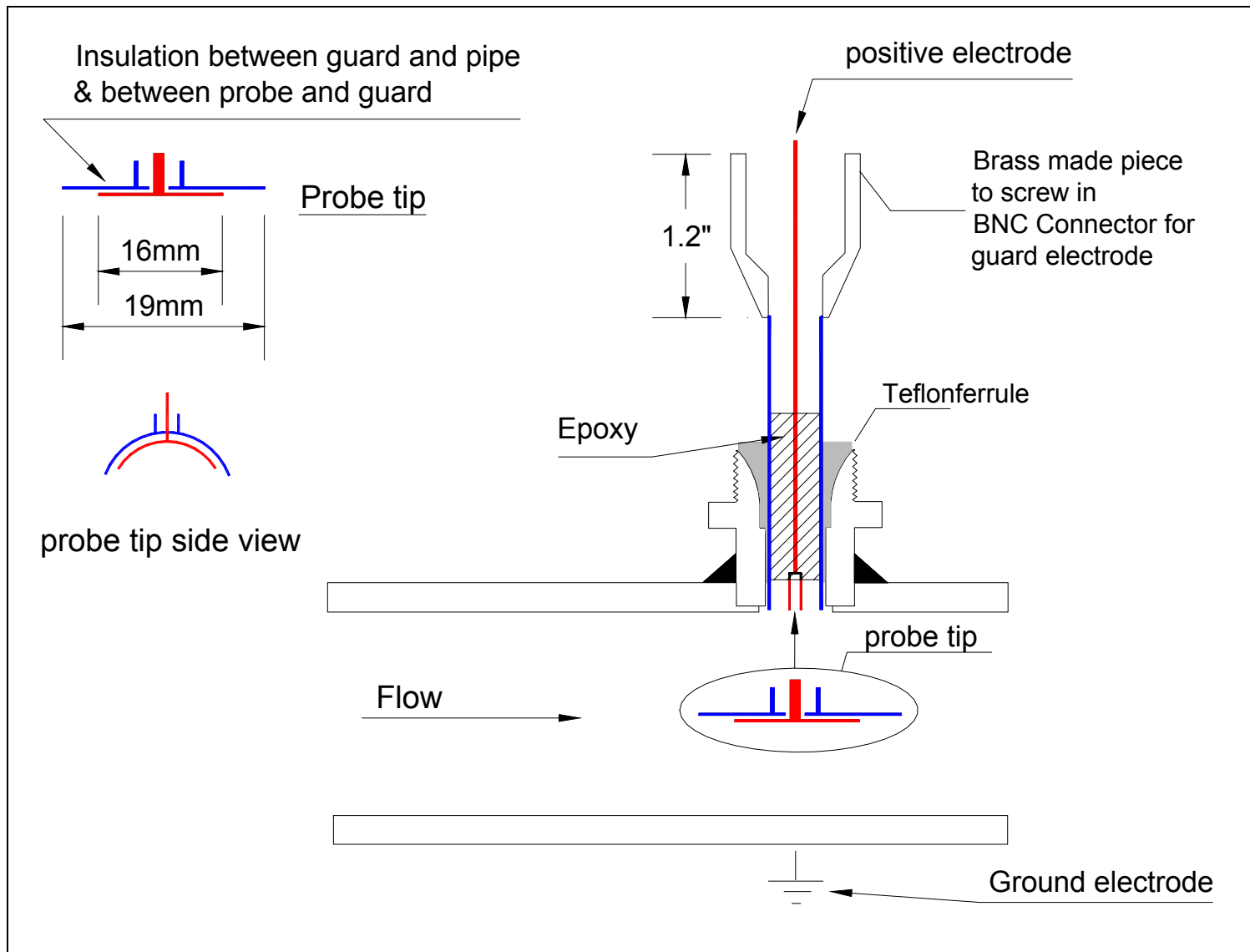


Figure 3.22: Schematic of Capacitance Probe for Test Facility.

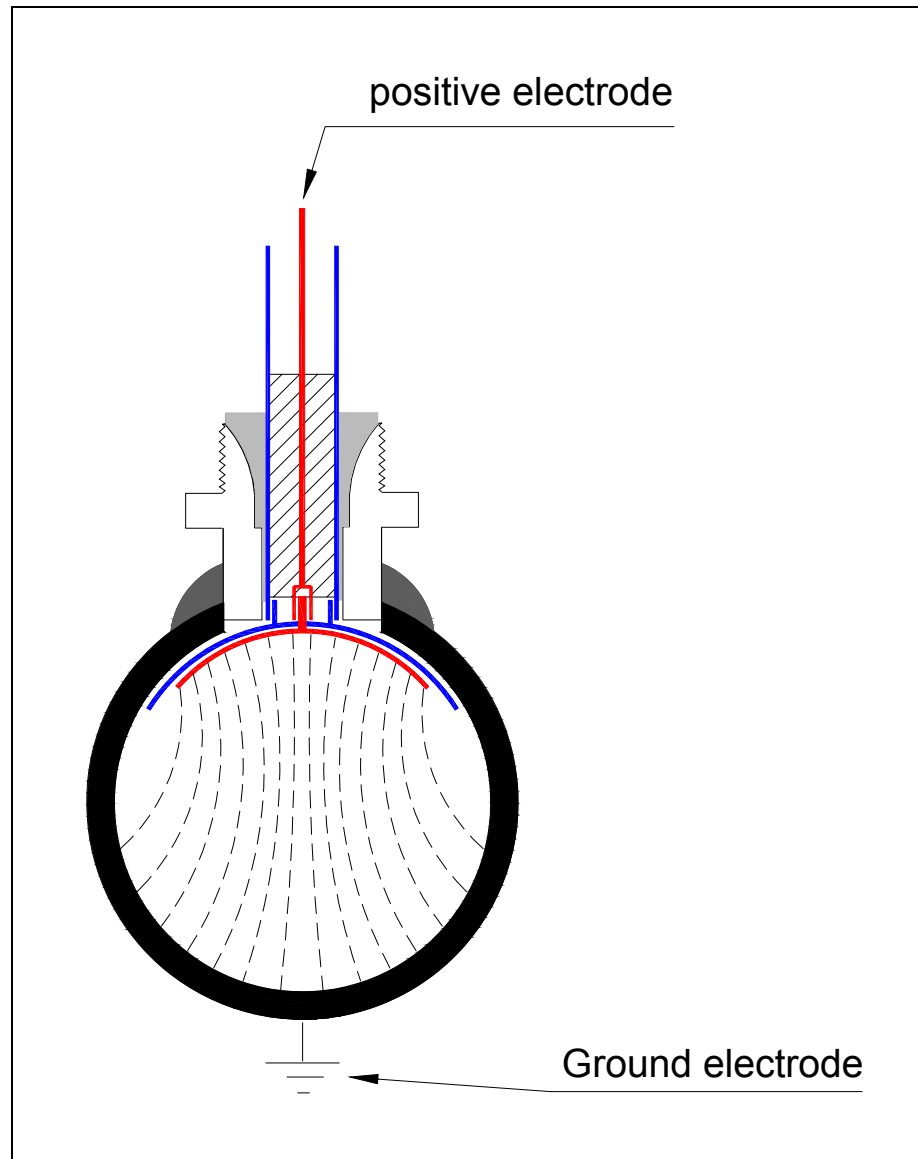


Figure 3.23: Cross-Section of Capacitance Setup Showing Electrical Field.

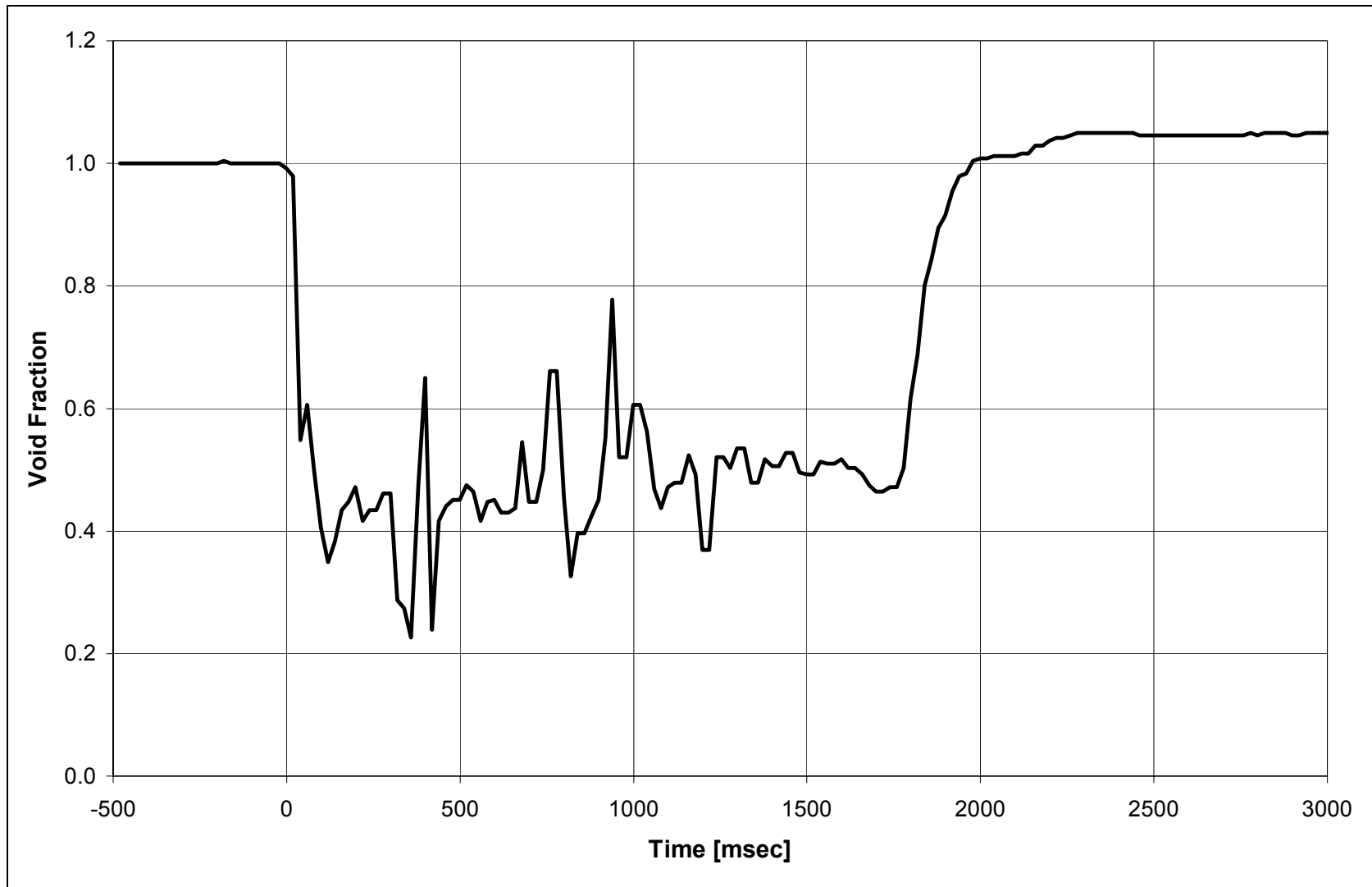


Figure 3.24: Void Fraction Histogram of Run #5.

4. CODE DEVELOPMENT WORK

4.1 INTRODUCTION

4.1.1 SCOPE OF PROGRAM

This computer program (or computer code), named FSP, was developed for the analysis of fire-suppressant fluid delivery systems. It was developed because there was a need for a flexible computer program in the public domain that would allow modeling of delivery systems for a variety of suppressant fluids. It was developed as a part of the Next Generation Fire Suppression Program (NGP), managed by the National Institute of Standards and Technology (NIST). The primary objective of the NGP was to develop fire-suppressant fluids to replace Halon-1301. Hence the main focus of this computer program was to be able to model typical delivery systems with several fluids considered as viable alternatives to Halon-1301.

Typical delivery systems in current use consist of a suppressant storage vessel connected via a piping network to one or more delivery locations. The storage vessel is under pressure of an inert cover gas (usually nitrogen). The suppressant fluid is maintained in a liquid state by the pressurization of the storage vessel by the cover gas, usually to several MPa. The piping network is initially empty and exposed to the environment. The system is activated by a quick opening valve or a rupture disc located between the storage vessel and the piping network, in response to an automatic or manual trigger. This causes the gas driver to expel the suppressant fluid through the piping network. The typical delivery time of the suppressant fluid to the delivery location is in the range of 0.1 to 10 seconds.

Since most suppressant fluids are in a vapor state at standard pressure and temperature, as the suppressant is released from the storage vessel, it will flash inside the piping network. At the discharge location, the fluid will be a mixture of superheated vapor and liquid. Thus significant thermodynamic and thermal non-equilibrium can be expected between the phases. Because of the large pressure difference between the upstream source vessel and downstream exit, continuous flashing can be anticipated as the fluid travels down the piping system, and two-phase critical flow (choked flow) can be expected inside the pipe. Depending on the mass flux in the piping system and its geometrical characteristics, the vapor and liquid phases can be traveling at different velocities, under non-homogeneous conditions. Further, since the storage vessel could be maintained under pressure of the cover gas for significant periods of time prior to discharge of the suppressant, the suppressant liquid will be saturated with the cover gas. As the liquid travels down the pipe and depressurizes, this dissolved cover gas will come out of solution and expand. The effect of this on the suppressant flow would need to be accounted for.

Hence, to accurately predict performance of the delivery system, the computer code should be able to predict transient two-phase flows and allow for non-homogeneous, non-equilibrium conditions. The code should be able to predict two-phase choking. It should account for the release of dissolved gas from the liquid phase. The code should allow users to select one of several fluids as the suppressant of choice. Also, it should allow the ability to model various delivery systems, with the user being able to select the geometrical

characteristics. These would typically include the size of the storage vessel, the layout of the piping network, and choice of pipe sizes. And finally, the code should be non-proprietary, available in the public domain. These were the objectives of the computer program described here.

4.1.2 BACKGROUND

There are several available methods for calculating discharge rates of fire-suppressant fluid delivery systems. In a summary of the state-of-the-art, DiNenno and Budnick (1988) indicate that most flow calculations are performed by vendors using proprietary methods. These methods are verified against standard NFPA procedures for calculations and by discharge testing in scaled tests. It is noted that there are significant uncertainties in the calculations and in extrapolating test results to actual configurations.

Pitts et al (1994) describe a mathematical model for calculating the discharge of fire-suppressant fluids from a pressurized discharge tank across an orifice at the exit and showed that the transient pressure history in the discharge vessel calculated by the model compared reasonably well to data from experiments. Elliott et al (1984) developed a computer program called HFLOW for predicting the discharge of Halon-1301 from a discharge vessel through a piping system. The results of the program compared favorably to results of experiments conducted with Halon-1301 in several piping arrangements. The theoretical model was based on a homogeneous model of two-phase flow. Elliott et al (1984) also modified an existing computer program called SOLA-LOOP (Hirt et al, 1979), which was originally written for steam-water flows, to be able to model Halon-1301. This computer program was a non-equilibrium, non-homogeneous model of two-phase flow, using the drift flux approach to calculate slip between the phases. It was shown that this program, modified to account for Halon-1301 properties, was able to capture the physics of the agent discharge more accurately.

The methods described by Pitts et al (1994) and Elliott et al (1984) appear to be the only methods available in the public domain for calculating performance of fire-suppressant fluid delivery systems. One way to develop a general, flexible computer program that would be able to model a variety of piping networks and handle several candidate fluids would be to extend this work by modifying these methods. Another approach is to take advantage of the advances in two-phase flow modeling that have taken place in the nuclear power industry, which have resulted in several computer codes available in the public domain. The development of the computer code described here followed the latter approach.

Based on a survey of computer codes available in the nuclear power industry (Tuzla et al, 1998), the RELAP5/MOD3.2 computer code (RELAP5, 1995) was chosen for further development for modeling fire suppressant fluid systems. This code contains most of the basic models required for modeling fire suppressant fluid systems. It is based on a two-fluid model of two-phase flow and can model non-equilibrium, non-homogeneous conditions. It contains a model for transport of non-condensable gas through the system. It was written originally for water-steam systems, but the code architecture allows for adding alternate fluids. The code has been tested extensively against experiments for its ability to model loss-of-coolant accidents in nuclear power systems and is suitable for modeling rapid two-phase

transient flows. The thermal-hydraulic phenomena in the early phase of these postulated accidents are similar to the phenomena expected during fire suppressant fluid discharge from a pressurized tank through a piping network. Further, the code input is modular, allowing the user to choose among several available modules to optimally describe the initial and boundary conditions required for the calculation, and the geometrical characteristics of the system.

This manual provides a summary description of the FSP computer code, which was derived by modifying the RELAP5/MOD3.2 computer code, which is referred to in this manual as the base code or, sometimes, as RELAP5. This manual does not contain a detailed description of the code, particularly the numerical solution method. This is because the base code has been documented extensively (RELAP5, 1995) and most of the documentation applies to the FSP code. Hence users interested in the details of the solution method should refer to that documentation.

The main modifications to the base code in developing the FSP code were:

- 1) Fluid Properties: The base code was based on water-steam systems. This was supplemented in the FSP code by using the REFPROP fluid properties package (Gallagher et al, 1993). The REFPROP package, developed by the National Institute of Standards and Technology (NIST), covers many refrigerant fluids including those that are potential candidates for fire suppressant systems. In this version of FSP, four fluids have been incorporated, Halon-1301, CO₂, HFC-227ea, and HFC-125. Any of these alternate fluids can be selected by the user. Water properties, which were the default option in the base code, have not been removed, and hence water is also one of the fluid options in FSP.
- 2) Constitutive Relationships: The code requires specification of constitutive relationships, such as for the calculation of wall drag and interphase drag, to provide closure for the basic two-phase flow conservation equations used by the two-fluid model. In the base code, several of these relationships were based on experimental data from water-based systems and were uniquely applicable to these systems. These relationships were modified in FSP to be fluid-independent. The specific areas modified were the interphase drag models in vertical flow, and wall heat transfer models for critical heat flux and transition boiling.
- 3) Release of Dissolved Gas: The base code contained transport equations for non-condensable gas in the gas phase and also for a solute (boron) in the liquid phase. In FSP, these transport equations were modified. The noncondensable gas transport equation was modified to include a source term to account for release of dissolved gas. The boron transport equation was altered to reflect transport of dissolved gas as the solute instead of boron. A sink term was added to this equation for conserving the total amount of noncondensable gas in the system. This approach allowed modeling the release of gas anywhere in the system based on local conditions. New constitutive relations were added to represent the gas release rate. This requires specification of two additional parameters, a critical bubble radius for initiating the gas release, and a rate constant. These parameters have been implemented in FSP as user input variables, and are further described in later sections of this manual.

The above modifications were the major modifications made to the base code in developing the FSP code. There were some additional minor modifications, primarily for making the code usable on PC-based computer platforms. This Version of FSP runs on a WINDOWS 95/98 operating system. Installation instructions are shown in a section of this manual.

4.2 CODE THEORY

This computer program, FSP, was developed to predict the transient hydrodynamic behavior of a fire suppressant fluid as it discharges from a storage vessel through a piping network. It was developed from a base code called RELAP5/MOD3.2 (RELAP5, 1995), which was developed primarily for nuclear plant transient and accident analyses, and therefore uses water as the working fluid. It is based on a one-dimensional, two-fluid model of two-phase flow and allows prediction of non-homogeneous, non-equilibrium conditions. It is written in Standard FORTRAN-77, and was originally developed to run on the UNIX Operating System, but has been adapted to other operating environments. The version of RELAP5 chosen for further development is generally considered to be machine-independent and portable to a variety of commonly used operating systems.

To run this program, a user generates an input file. This input file is essentially the description of the problem to be executed. It contains the geometrical description of the system under analysis, the necessary boundary and initial conditions, and other constraints imposed by the user, such as partition of the system into control volumes (nodalization), selection of particular code options and control of the time step used in the numerical solution. The code documentation contains a user manual in Appendix A describing how to generate an input file.

In executing the program, FSP generates two files, an output file that can be read by the user, and a restart file written in binary format. The output file provides information at time intervals requested by the user in the input file. The restart file contains all the information the code needs such that the user can restart the code to run for a longer time period, with or without additional changes to the problem description, and is also used for generating graphical output.

The RELAP5 code also contains many user-convenient features and special models, which were developed primarily for nuclear plant analyses, such as the definition of specific components in nuclear systems, and code models to capture the transient behavior of nuclear fuel rods. Some of these are useful for the intended application to fire suppressant fluids and fluid systems, and some are not. In the development of the FSP code, most of the existing features of RELAP5 were retained, although not necessarily useful in modeling fire suppressant delivery systems.

The description of the code presented here is a brief summary, intended to provide basic information for the user. The base code has been documented in great detail (RELAP5, 1995) and the user is referred to that documentation for additional information, particularly the numerical solution method.

4.2.1 GOVERNING EQUATIONS

The thermal-hydraulic model solves eight field equations for eight primary variables as a function of time (t) and distance (x). The eight primary dependent variables are pressure (P), phasic specific internal energies (U_g, U_f), vapor volume fraction or void fraction (α_g), phasic velocities (v_g, v_f), noncondensable quality (X_n), and solute density (ρ_b). Note that the noncondensable quality is defined as the mass fraction of noncondensables in the gas phase, the remaining fraction being the mass fraction of steam in the gas phase. Of these seven variables, six are state variables ($P, U_g, U_f, \alpha_g, X_n, \rho_b$) and two are velocities (v_g, v_f). The corresponding eight field equations are the conservation equations for mass, momentum and energy for each phase, and the conservation of mass for the noncondensables in the gas and liquid phases. The equations are described in detail in RELAP5-1, 1995. The simple forms of these equations are shown below, as one-dimensional area-averaged equations, on a per unit volume basis.

Conservation of Mass:

Gas Phase:

$$\frac{\partial}{\partial t}(\alpha_g \rho_g) + \frac{1}{A} \frac{\partial}{\partial x}(\alpha_g \rho_g v_g A) = \Gamma_g + \Gamma_N \quad (4.2.1-1)$$

Liquid Phase:

$$\frac{\partial}{\partial t}(\alpha_f \rho_f) + \frac{1}{A} \frac{\partial}{\partial x}(\alpha_f \rho_f v_f A) = \Gamma_f \quad (4.2.1-2)$$

The terms on the right hand side of equation 4.2.1-1 are the interfacial vapor generation per unit volume, and the noncondensable gas released from solution per unit volume. The terms on the right hand side of equation 4.2.1-2 are the corresponding terms for the liquid phase. For continuity across the interface, $\Gamma_g + \Gamma_f = 0$. The source term for noncondensable gas, Γ_N , which is the rate of dissolved gas release per unit volume, is treated similar to an external source term. Thus, there is no corresponding term in the liquid phase mass conservation equation. Essentially, this assumes that the liquid density is not affected by the presence of dissolved gas.

Conservation of Momentum:

Gas Phase:

$$\begin{aligned}
\alpha_g \rho_g A \frac{\partial v_g}{\partial t} + \frac{1}{2} \alpha_g \rho_g A \frac{\partial v_g^2}{\partial x} = & -\alpha_g A \frac{\partial P}{\partial x} + \alpha_g \rho_g B_x A - (\alpha_g \rho_g A) FWG(v_g) \\
& + \Gamma_g A(v_{gl} - v_g) - \Gamma_N A v_g - (\alpha_g \rho_g A) FIG(v_g - v_f) \\
& - C \alpha_g \alpha_f \rho_m A \left[\frac{\partial(v_g - v_f)}{\partial t} + v_f \frac{\partial v_g}{\partial x} - v_g \frac{\partial v_f}{\partial x} \right]
\end{aligned} \tag{4.2.1-3}$$

Liquid Phase:

$$\begin{aligned}
\alpha_f \rho_f A \frac{\partial v_f}{\partial t} + \frac{1}{2} \alpha_f \rho_f A \frac{\partial v_f^2}{\partial x} = & -\alpha_f A \frac{\partial P}{\partial x} + \alpha_f \rho_f B_x A - (\alpha_f \rho_f A) FWF(v_f) \\
& + \Gamma_f A(v_{fl} - v_f) - (\alpha_f \rho_f A) FIF(v_f - v_g) \\
& - C \alpha_f \alpha_g \rho_m A \left[\frac{\partial(v_f - v_g)}{\partial t} + v_g \frac{\partial v_f}{\partial x} - v_f \frac{\partial v_g}{\partial x} \right]
\end{aligned} \tag{4.2.1-4}$$

On the right hand side of equation 4.2.1-3, the second term is the body force and the subsequent terms are the wall friction, momentum transfer due to mass transfer (from vapor generation as well as dissolved gas release), interfacial frictional drag and force due to virtual mass.

Conservation of Thermal Energy:

Gas Phase:

$$\begin{aligned}
\frac{\partial}{\partial t} (\alpha_g \rho_g U_g) + \frac{1}{A} \frac{\partial}{\partial x} (\alpha_g \rho_g U_g v_g A) = & -P \frac{\partial \alpha_g}{\partial t} - \frac{P}{A} \frac{\partial}{\partial x} (\alpha_g v_g A) \\
& Q_{wg} + Q_{ig} + \Gamma_g h_g + \Gamma_N h_N - Q_{gf} + DISS_g
\end{aligned} \tag{4.2.1-5}$$

Liquid Phase:

$$\begin{aligned}
\frac{\partial}{\partial t} (\alpha_f \rho_f U_f) + \frac{1}{A} \frac{\partial}{\partial x} (\alpha_f \rho_f U_f v_f A) = & -P \frac{\partial \alpha_f}{\partial t} - \frac{P}{A} \frac{\partial}{\partial x} (\alpha_f v_f A) \\
& Q_{wf} + Q_{if} + \Gamma_f h_f + Q_{gf} + DISS_f
\end{aligned} \tag{4.2.1-6}$$

On the right hand side of equation 4.2.1-5, the third to last terms are the wall heat transfer, interfacial heat transfer, energy transfer due to mass transfer (vapor generation as well as release of dissolved gas), sensible heat due to presence of noncondensables, and dissipation.

Conservation of Mass for Noncondensables in Gas Phase:

$$\frac{\partial \alpha_g \rho_g X_n}{\partial t} + \frac{1}{A} \frac{\partial}{\partial x} (\alpha_g \rho_g X_n v_g A) = \Gamma_N \quad (4.2.1-7)$$

where

X_n = mass fraction of noncondensable gas in the gaseous phase

Γ_N = noncondensable gas generation rate

This equation essentially conserves mass of noncondensables in the gas phase, and allows transport/distribution of the noncondensables along with the gas phase. It is assumed that the noncondensables are transported at the same velocity as the steam in the gas phase, that they are in thermal equilibrium with the vapor, and that the properties of the gas phase are mixture properties of the vapor/noncondensable mixture. The sensible heat transfer terms due to the presence of noncondensables in the energy equations represent heat transfer at the noncondensable gas-liquid interface. This is necessary because the interfacial terms use saturation temperature based on the local vapor partial pressure.

Conservation of Mass for Noncondensables in liquid phase (dissolved gas):

$$\frac{\partial \rho_s}{\partial t} + \frac{1}{A} \frac{\partial}{\partial x} (\rho_s v_f A) = \Gamma_s \quad (4.2.1-8)$$

where

ρ_s = density of the dissolved nitrogen (solute), i.e., mass of dissolved nitrogen per unit volume

Γ_s = negative of mass rate of nitrogen released per unit volume, or solute generation rate

This equation essentially provides the means to model the release of dissolved gas at any location based on local conditions. The gas release model itself is described in a subsequent section, along with the assumptions used in its implementation in the code.

In the base code, it is assumed that at the gas-liquid interface, there is no storage of mass, momentum or energy. In FSP, the dissolved gas release term is modeled similar to an external source. It is assumed separately that $\Gamma_g + \Gamma_f = 0$ (similar to the base code), and that $\Gamma_N + \Gamma_s = 0$. Summing equations 4.2.1-3 and 4.2.1-4 provides a relationship between the interfacial drag terms FIG and FIF. Summing equations 4.2.1-5 and 4.2.1-6 provides a relationship between the interfacial mass transfer and interfacial heat transfer. These are the essentially the interface jump conditions needed for closure of the conservation equations. Note that in FSP, because of the way in which the dissolved gas release term has been

treated, the conservation of mass, momentum and energy at the gas-liquid interface is only approximately satisfied. This is an inherent assumption in the code. The results of executing the code for typical FSP applications have not shown significant effect due to this approximation. If new applications show significant effect, this assumption would have to be re-visited.

To complete the equation set, several terms on the right hand side of the conservation equations need to be specified, such as FWG , FIG , Q_{wg} and Q_{ig} . These are the constitutive relations, described in a subsequent section. Typically, these are based on mechanistic models and empirical correlations, and are written in terms of velocities, thermodynamic and transport properties, and the temperature of the liquid and gas phases. Thus, additional relationships have to be defined to relate these to the primary dependent variables of the code.

4.2.2 NUMERICAL SOLUTION

To solve the above set of equations, the differential conservation equations are cast into a numerically convenient set of finite difference equations, using a staggered spatial mesh arrangement. In this method, mass and energy are conserved over a control volume while momentum is conserved over a cell bounded by the mass and energy cell centers. A semi-implicit method is followed for time advancement where the implicit terms are formulated to be linear in the dependent variables at the new time. Essentially, this requires specification of the partial derivatives of fluid density with respect to the primary dependent variables. Most of the source terms on the right hand side of the equations are also treated semi-implicitly. The noncondensable dissolved gas release term is treated explicitly.

Figure 4.2.1 shows the staggered mesh concept used in the numerical solution. In the method, scalar variables (pressure, internal energies and void fraction) are defined at the cell centers, at K , L , and so on. Vector quantities (velocities) are defined at the cell boundaries, at the junctions connecting the cells, at j , $j+1$, and so on. In this method, to define the flux terms at the boundaries of the mass and energy conservation cells, the void fraction and fluid properties are 'denoted' from the upstream cells. Similarly, to estimate friction losses needed in the momentum conservation, 'volume velocities' are estimated at cell centers using an averaging procedure of the velocities at the junctions connecting to each cell. The documentation of the base code (RELAP5, 1995) provides a detailed description of the method. Here, it is noted that the user can access 'junction properties' as well as 'volume properties' in developing the input model and examining the output of the code. This is further described in the FSP user manual shown in Appendix A.

The governing equations, together with the interface jump conditions, constitutive relations, thermodynamic and transport properties, and property derivatives, as a function of the primary dependent variables, forms a closed set of equation. The code solves this set for the primary dependent variables as a function of time and spatial location. Details of derivation of the finite difference equations and the numerical solution method are described in the base code documentation (RELAP5, 1995).

4.2.3 STATE RELATIONSHIPS AND FLUID PROPERTIES

As discussed previously, the code uses five primary dependent state variables. These five state variables are

- P: total pressure
- α : gas phase volume fraction
- U_g : gas phase specific internal energy
- U_f : liquid phase specific internal energy
- X_n : mass fraction of noncondensable gas in the gas phase

All thermodynamic variables are expressed in terms of the above five state variables. In addition, several state derivatives are needed for the numerical scheme. The next section presents the detailed requirements of the model fluid property package.

4.2.3.1 Basic Thermodynamic Property Tables

Consider first the case without noncondensables. This is referred to as the Single-Component, Two-Phase Case.

A. Single-Component, Two-Phase Case

Three sets of properties are required for this case.

Liquid Phase

The following are needed in the basic thermodynamic property package:

Temperature:	$T_f = T_f(P, U_f)$
Isobaric Specific Heat	$c_{pf} = c_{pf}(P, U_f)$
Isobaric Thermal Expansion Coefficient:	$\beta_f = \beta_f(P, U_f)$
Isothermal Compressibility:	$\kappa_f = \kappa_f(P, U_f)$
Specific Volume	$v_f = v_f(P, U_f)$
Specific Entropy	$s_f = s_f(P, U_f)$

The definitions for isobaric specific heat, isobaric thermal expansion coefficient and isothermal compressibility can be found from standard thermodynamic text books (e.g., Van Wylen and Sonntag, 1985). From these basic properties, the following derivatives are evaluated in the proposed code: density with respect to internal energy, temperature with respect to internal energy, density with respect to pressure, and temperature with respect to pressure.

Vapor Phase

Similarly, the following are needed in the basic thermodynamic property package:

Temperature:	$T_g = T_g(P, U_g)$
Isobaric Specific Heat	$c_{pg} = c_{pg}(P, U_g)$
Isobaric Thermal Expansion Coefficient:	$\beta_g = \beta_g(P, U_g)$
Isothermal Compressibility:	$\kappa_g = \kappa_g(P, U_g)$
Specific Volume	$v_g = v_g(P, U_g)$
Specific Entropy	$s_g = s_g(P, U_g)$

and the same derivatives for the liquid phase are evaluated for the vapor phase.

Saturation Properties

In addition to the phasic properties and derivatives, the saturation properties are needed for interface evaluation and extrapolation to metastable states (i.e., superheated liquid or subcooled vapor). Two tables are needed, one based on temperature and the other based on pressure, as shown below for the liquid phase,

- a. Give saturation temperature, T^s :

Saturation pressure	$P = P(T^s)$
Isobaric Specific Heat	$c_{pf}^s = c_{pf}^s(T^s)$
Isobaric Thermal Expansion Coefficient:	$\beta_f = \beta_f^s(T^s)$
Isothermal Compressibility:	$\kappa_f = \kappa_f^s(T^s)$
Specific Volume	$v_f = v_f^s(T^s)$
Specific Entropy	$s_f = s_f^s(T^s)$

where the superscript s denotes saturation state.

- b. Give saturation pressure, P:

Saturation Temperature	$T^s = T^s(P)$
Isobaric Specific Heat	$c_{pf}^s = c_{pf}^s(P)$
Isobaric Thermal Expansion Coefficient:	$\beta_f = \beta_f^s(P)$
Isothermal Compressibility:	$\kappa_f = \kappa_f^s(P)$
Specific Volume	$v_f = v_f^s(P)$
Specific Entropy	$s_f = s_f^s(P)$

In addition, the derivative of the saturation temperature with respect to pressure is required. This is evaluated using the Clapeyron equation (Van Wylen and Sonntag, 1985). Similar saturation properties are needed for the vapor phase.

B. Two-Component, Two-Phase Case

In the presence of noncondensable gases, the gaseous phase (mixture of vapor and noncondensable gases) is assumed to be a Gibbs-Dalton mixture of vapor (either treated as an ideal gas or from property tables) and ideal gases.

An additional variable is calculated in the code for this case. It is the noncondensable quality, X_n , and is defined as the mass fraction of the noncondensable gases in the gaseous mixture, i.e.,

$$X_n = \text{Mass of Noncondensable Gases} / \text{Mass of Gaseous Phase} = M_n / (M_n + M_v)$$

where M_v is the mass of the vapor phase. The gaseous phase pressure is the sum of the partial pressure of each gaseous component, as usual. The equation of state for each noncondensable component is simply the perfect gas equation of state.

The liquid properties and derivatives are calculated in the same manner as described in Part A above. For the gaseous phase, the independent state properties are taken as P , U_g and X_n . All properties of the gaseous phase are expressed in terms of these three variables. Note that U_g is the specific internal energy of the gaseous phase, not just the vapor phase. The derivatives required are vapor temperature with respect to pressure, internal energy, and noncondensable quality, as well as interface temperature with respect to pressure, internal energy and noncondensable quality. The interface temperature, T_i , is based on the partial pressure of the vapor,

$$T_i = T_i(P_s)$$

The evaluation procedure for the required derivatives is somewhat involved. A detailed discussion is given in the base code documentation (RELAP5, 1995) and not described further here.

4.2.3.2 Generation of Thermodynamic Property Tables

As presented in Section 4.2.3.1 above, data are required for single phase properties as well as saturation properties in the solution method of the code. These data need to be in tabular form and need to be generated for the fluid specified by the user. Once generated, these property tables (in binary format) are used to compute properties at any given pressure and internal energy through iteration, interpolation or both. The code contains the necessary coding to perform the required interpolation calculations for a variety of options needed by the user.

4.2.3.3 Implementation Of Thermodynamic Property Tables

Various fluids have previously been implemented into the base code, RELAP5. Examples are blood, ammonia, liquid sodium and lithium. As a result, RELAP5 was structured to facilitate the implementation of a new fluid. The procedure for incorporating a new fluid is summarized as follows:

1. RELAP5 contains a property generation program. A set of pressure and temperature data points that will be used for the property tables can be supplied to this program following a prescribed format.

2. The required tables are generated via the program, which contains the necessary formulae, empirical correlations, canonical functions, etc. The output from this program contains:
 - a. saturation properties as a function of pressure
 - b. saturation properties as a function of temperature
 - c. single phase properties as a function of pressure and temperature

For light water substance, for instance, this particular program calls other subroutines that calculates the Gibbs and Helmholtz functions as given in the 1967 ASME steam tables (Meyer et al, 1997). For a new fluid, all information can be included in the generating program and hence avoiding the need for additional subroutines.

3. The output from the generating program are the required property tables. The format of the output file is as follows:
 - a. Echo back the user input temperature and pressure points.
 - b. Tabulate the statistics of the table including number of temperature points, number of pressure points, number of saturation temperature points, number of saturation pressure points, and number of words in the binary file.
 - c. Saturation properties versus temperature.
 - d. Saturation properties versus pressure.
 - e. Thermodynamic properties versus pressure and temperature. For each pressure in the user supplied pressure range, the properties for each temperature.

The above information is written to a binary file. Once this binary file is available and linked to the code executable, the code is able to calculate properties as called for by the various interpolation subroutines. Following this procedure, for the new fluids implemented into the FSP code, a generation program was written which would directly access the REFPROP code (Gallagher et al, 1993) which contains methods for calculating thermodynamic properties of the fluids. The generation program's output binary file is then linked to the FSP code. The built-in interpolation subroutines in FSP then take care of generating the required properties by using the information in this binary file. This procedure is transparent to the user of FSP and is being described here for information for users who may want to implement other fluids into the code in the future.

4.2.3.4 Sample Binary Data File Generation for Halon 1301

As an example, this section presents a sample generation program for Halon 1301. The property relations are accessed from the REFPROP V. 4.0 software package (Gallagher et al, 1993). REFPROP is a calculation package for a wide variety of refrigerants including Halon 1301 and the other fluids included in the FSP code. Halon 1301 was the test case for checking out the implementation procedure because there was significant experimental data readily available at the time the development of FSP was initiated.

The major undertaking was to interface the appropriate subroutines in REFPROP with the coding in the generation program. FSP expects three property tables: (i) saturation properties given temperature, (ii) saturation properties given pressure, and (iii) single phase properties versus temperature at a given pressure value (i.e., isobar). The values of pressure and temperature are supplied by the user and are input to the generation program. The needed properties include specific volume (m^3/kg), internal energy (J/kg), thermal expansion coefficient ($1/\text{K}$), isothermal compressibility coefficient ($1/\text{Pa}$), constant pressure specific heat ($\text{J}/\text{kg}\cdot\text{K}$) and entropy ($\text{J}/\text{kg}\cdot\text{K}$).

Figure 4.2.2 shows the flow chart of the generation program. The major steps of the program are described below:

1. The critical states (pressure, temperature and specific volume) as well as the minimum and maximum allowable values were supplied via data statements.
2. The user supplied temperature and pressure values are read. The input data are examined to ensure that they are within the minimum and maximum limits specified in Step 1 and are in ascending order.
3. Various pointers and table statistics are calculated.
4. Call Subroutine *table3* to generate the saturation table as a function of temperatures.
5. Call Subroutine *table4* to generate the saturation table as a function of pressures.
6. Call Subroutine *table5* to generate the single phase tables as a function of temperature for a given pressure.
7. Write output to an ASCII file and a binary file.

The interface with REFPROP are accomplished with the following steps:

1. In the main program, initialize the REFPROP subroutines.
2. In Subroutine *table3*:
 - a. Calculates the saturation pressure, specific volume, enthalpy, constant pressure specific heat, and specific entropy of each phase, by calling appropriate subroutines in the REFPROP package. The internal energy is then calculated from $(h - pv)$, where h is the enthalpy, p is the pressure and v is the specific volume. Finally, the thermal expansion and isothermal compressibility coefficients are estimated by numerical differentiation. Thus, for the thermal expansion coefficient, the following are calculated

$$\beta_f = (1/v_f) [v_f - v_f(T-dT, p)]/dT \text{ along an isobar, and}$$

$$\beta_g = (1/v_g) [v_g(T+dT, p) - v_g]/dT \text{ along an isobar.}$$

For the isothermal compressibility coefficient, the following are calculated

$$\kappa_f = -(1/v_f) [v_f(T, p+dp) - v_f]/dp \text{ along an isotherm, and}$$

$$\kappa_g = -(1/v_g) [v_g - v_g(T, p-dp)]/dp \text{ along an isotherm}$$

Currently, dT and dp are set at 1 °K and 1 kPa respectively. The single phase specific volumes: $v_f(T-dT, p)$, $v_g(T+dT, p)$, $v_f(T, p+dp)$ and $v_g(T, p-dp)$ are also calculated by calling appropriate subroutines in the REFPROP package.

3. In Subroutine *table4*:

The process described in Subroutine *table3* above is repeated here, except that the saturation temperature is calculated given the pressure value.

4. In Subroutine *table5*:

In this subroutine, the fluid state is first determined by comparing the given temperature to the saturation temperature to determine the fluid state. The corresponding single phase properties (the specific volume, enthalpy and hence internal energy, constant pressure specific heat, and entropy) are then calculated by calling appropriate subroutines in the REFPROP package. Finally, the thermal expansion and isothermal compressibility coefficients are estimated using the procedure as discussed in Item 2 above.

The exact calling sequence of each of the REFPROP subroutines is described in the Users Manual of REFPROP.

In addition to generating the binary property data file, several modifications are needed to enable RELAP5 to execute on a fluid different than water. These modifications include:

1. Increasing the number of fluid types
2. Adding the name of the fluid (e.g., “halon”) to the fluid type information
3. Modifying the thermal and transport property subroutines

With the above modifications, and the data file, the code could be used to simulate systems containing Halon 1301. To validate the modifications and to ensure the data file is interfaced properly with FSP, the following validation steps were taken:

1. Verify that the code modifications perform as designed and do not affect the code inadvertently. This was accomplished by running a test case with Halon 1301 as the fluid type and comparing the code calculated results with the property data file. To verify that the new coding did not affect other parts of the code, a test case with water as the fluid type was simulated. The results are compared to those of the same case simulated with the unmodified base code version. The two sets of results were identical as they should be.
2. Verify the correctness of the interpolation subroutines for fluid types other than water. This is partially accomplished in Part 1 above. A comprehensive assessment of these interpolation subroutines was performed by developing a driver program to execute each of the interpolation subroutines interactively, and comparing the results to the results obtained by running the FSP code.

3. Verify the correctness of the property data file. This was accomplished by comparing the results in the ASCII output data file with the results directly from REFPROP.

This validation was conducted using Halon 1301 as the test case. The results of the validation have confirmed that the modifications and data file were correctly implemented, and that the various interpolation subroutines in the code performed as designed. This procedure was repeated for the other fluids. The property generation program is included in the code transmittal package for the FSP code.

4.2.3.5 Critical Region Properties

The REFPROP package imposes certain limits on pressure and temperature in the calculation of saturation properties. In particular, the temperature cannot be more than 0.97 times the critical temperature, and pressure cannot be more than 0.9 times the critical pressure. These limits are set in subroutines BUBLT and BUBLP respectively. Attempt to remove these limits in REFPROP can produce inconsistent trends in the vicinity of the critical region. For instance, if subroutines BUBLT and BUBLP are executed at the critical point, the resulting liquid and vapor values do not equal to each other, as they should be at the critical point. Attempt to interpolate from these inconsistent property tables can lead to hard failure (e.g., IEEE overflow or underflow) in the subsequent FSP calculation using these tables. Hence special consideration must be given in the critical region and at the critical point.

The following observations can be made, regarding the critical region, which have been utilized in getting around the problems encountered with the use of REFPROP:

1. At the critical point, both β and κ are infinity (inflexion point). For computation, some arbitrary values are assigned.
2. At the critical point, both the vapor and liquid specific volume are equal to the critical volume, v_{crit} , which is known.
3. For all other properties (u , s , c_p), the critical values are estimated by visually extrapolating the liquid and vapor values below the critical region.
4. The input values for pressure and temperature satisfy the REFPROP internal limits of $0.97 T_{\text{crit}}$ and $0.9 P_{\text{crit}}$ as discussed above.

Using the above as guidelines, the following critical properties are developed for the candidate fluids of interest: halon-1301, carbon dioxide, HFC-227ea and HFC-125.

Halon 1301

$$v_{\text{crit}} = 1.34309 \text{ e-3 m}^3$$

$$\beta_{\text{crit}} = 0.03 \text{ K}^{-1}$$

$$\kappa_{\text{crit}} = 6.0 \text{ e-8 Pa}^{-1}$$

$$u_{\text{crit}} = 2.6\text{e5 J/kg}$$

$$c_{p,\text{crit}} = 1200 \text{ J/kg-K}$$

$$S_{\text{crit}} = 1.2 \text{ J/kg-K}$$

Carbon Dioxide

$$v_{\text{crit}} = 2.17451 \text{ e-3 m}^3$$

$$\beta_{\text{crit}} = 0.023 \text{ K}^{-1}$$

$$\kappa_{\text{crit}} = 6.0 \text{ e-8 Pa}^{-1}$$

$$u_{\text{crit}} = 3.0\text{e5 J/kg}$$

$$c_{p,\text{crit}} = 5000.0 \text{ J/kg-K}$$

$$S_{\text{crit}} = 1.5 \text{ J/kg-K}$$

HFC-227ea

$$v_{\text{crit}} = 1.68783 \text{ e-3 m}^3$$

$$\beta_{\text{crit}} = 0.03 \text{ K}^{-1}$$

$$\kappa_{\text{crit}} = 6.0 \text{ e-8 Pa}^{-1}$$

$$u_{\text{crit}} = 3.5\text{e5 J/kg}$$

Test 146 of Elliott et al was chosen for study of how this model performs in the code. This experiment was a discharge test of Halon-301 from a supply bottle fitted at the bottom with a nozzle. The test measured the bottle pressure as a function of time when the flow was suddenly discharged from the bottle through the exit nozzle. There was no piping network connected to the bottle in this test.

$$c_{p,\text{crit}} = 1400 \text{ J/kg-K}$$

$$S_{\text{crit}} = 1.3 \text{ J/kg-K}$$

R125

$$v_{\text{crit}} = 1.74843 \text{ e-3 m}^3$$

$$\beta_{\text{crit}} = 50.0 \text{ K}^{-1}$$

$$\kappa_{\text{crit}} = 1.0\text{e-6 Pa}^{-1}$$

$$u_{\text{crit}} = 3.1\text{e5 J/kg}$$

$$c_{p,\text{crit}} = 8000 \text{ J/kg-K}$$

4.2.3.6 Transport Properties

Besides thermodynamic properties, a number of transport properties are needed of the candidate fluid. These include:

- | | |
|-------------------------|--|
| 1. Dynamic viscosity | $\mu_{f \text{ or } g} = \mu_{f \text{ or } g}(T,P)$ |
| 2. Thermal Conductivity | $k_{f \text{ or } g} = k_{f \text{ or } g}(T,P)$ |
| 3. Surface Tension | $\sigma = \sigma(T,P)$ |

These are implemented in the code as functions.

These properties are available from various sources, including REFPROP. In generating the functions needed, REFPROP was used to generate a table of data points and the data fitted with correlations.

An example for HFC-125 is provided below.

This is R125 in the REFPROP package. Its chemical name is Pentafluoroethane (C_2HF_5). The following information are from REFPROP.

$$T_{crit} = 66.18^\circ C$$

$$P_{crit} = 3629 \text{ kPa}$$

$$v_{crit} = 1.74843e-3 \text{ m}^3$$

$$\text{Mol. Wt.} = 120.03 \text{ kg/kg-mol}$$

From REFPROP, the following correlations were developed. For liquid properties, the effect of pressure is minimal and both viscosity and conductivity are mainly functions of temperatures.

Liquid viscosity:

$$\mu_f = 2051.0 - 23.45 T + 0.2873 T^2 - 0.003754 T^3$$

where μ_f is in micropoise, and T in $^\circ C$.

Liquid conductivity

$$k_f = 0.0678 - 0.0004564 T$$

where k_f is in W/m-K and T in $^\circ C$.

For vapor properties, viscosity and thermal conductivity are dependent on temperature and pressure. At atmospheric pressure,

Vapor viscosity:

$$\mu_g = 120.52 + 0.4144 T \text{ at atmospheric pressure}$$

Vapor conductivity

$$k_g = 0.0123 + 7.93e-5 T \text{ at atmospheric pressure}$$

The surface tension data are as follows:

T ($^\circ C$)	Surface Tension (mJ/m^2)
-80	18.67
-40	12.48
0.0	6.88
40	2.14

66.18 0.0

This was correlated as

$$\sigma = 6.867 - 0.123 T + 0.000293 T^2$$

where σ is in mJ/m^2 and T in $^{\circ}\text{C}$., and the second coefficient was adjusted slightly (from 0.125 to 0.123) to give zero value for σ at the critical temperature.

4.2.4 CONSTITUTIVE MODELS

The constitutive relations include models for defining two-phase flow regimes and flow-regime-related models for interphase drag and shear, the coefficient of virtual mass, wall friction, wall heat transfer, and interphase heat and mass transfer. Heat transfer regimes are defined and used for wall heat transfer. For the virtual mass, a formula based on the void fraction is used.

Note that while the FSP code contains models for wall heat transfer, these models have not been exercised or assessed with the various new fluids that have been implemented into the code. Also, wall heat transfer is not expected to play a significant role in the analysis of typical suppressant delivery systems because of the short time period of the expected transient. Hence, the user input manual described in Appendix A does not contain the information needed to model wall heat transfer. If a user encounters a special application of FSP where wall heat transfer may need to be included in the model, the base code documentation (RELAP5, 1995) contains the needed information.

The constitutive relations needed are for the terms shown in equations 4.2.1-1 through 4.2.1-8: Γ_g , Γ_f , Γ_N , FWG, FWF, FIG, FIF, C, Q_{wg} , Q_{wf} , Q_{ig} , Q_{if} , Q_{gf} , DISS_g and DISS_f . In general, these relationships are dependent on the thermodynamic state, void fraction, fluid properties and velocities. As shown in Figure 4.2.1, the thermodynamic state, void fraction and fluid properties are defined at volume centers, while the velocities are defined at the junctions. Fluid properties and the void fraction are ‘donored’ to junctions and volume velocities are estimated by momentum flux weighting of the velocities at the junctions that connect to each volume. It is convenient to use flow regimes to characterize the two-phase flow. This allows specifying a more mechanistic form to the various constitutive relations, which is desirable since the code is structured to handle various different fluids.

Four flow regime maps are included in the base code, but only two of these are relevant for applications of FSP. The other flow regime maps will not be encountered by the user and not discussed here. The flow regime maps in FSP address flow regimes and transitions between flow regimes for horizontal flow and vertical flow.

The flow regime maps are based on the work of Taitel et al, 1980, and Mishima and Ishii, 1984, who have developed flow regime classifications and mechanistic models to describe flow regime transitions. However, some of their transition criteria are quite complex, and further simplification has been carried out to efficiently apply these criteria in the code. When wall heat transfer is not modeled, the flow regimes and the transition criteria are dependent on hydrodynamic conditions only. When wall heat transfer is modeled, there is

a possibility that the wall may encounter the condition of critical heat flux (CHF). In post-CHF condition, the wall will mostly be not wetted by the liquid. This alters the flow regime. To capture this effect, the code recognizes the effect of wall heat transfer explicitly, and if post-CHF conditions are indicated, a separate flow regime map is used to characterize the two-phase flow patterns. Again, note that the post-CHF regimes would be invoked only if the user models wall heat transfer, and the local fluid and wall conditions indicate post-CHF conditions. As discussed above, wall heat transfer is not expected to be modeled in most applications of the FSP code. Hence, these flow regimes are not described here. The base code documentation (RELAP5, 1995) contains a detailed description, if needed.

The vertical flow regime map (for both up and down flow) is for volumes whose elevation angle ϕ is such that $45 < |\phi| < 90$ degrees. This map is modeled as nine regimes--four for pre-CHF heat transfer, four for post-CHF heat transfer, and one for vertical stratification. As noted previously the post-CHF regimes will not be encountered if wall heat transfer is not modeled by the user. The pre-CHF regimes are the same flow regimes as would exist if there was no wall heat transfer. For pre-CHF heat transfer, the regimes modeled are the bubbly, slug, annular mist, and mist-pre-CHF regimes.

The horizontal flow regime map is for volumes whose elevation angle ϕ is such that $0 < |\phi| < 45$ degrees. This map does not distinguish between pre- and post-CHF regimes. Otherwise it is similar to the vertical flow regime map. The horizontal flow regime map consists of horizontally stratified, bubbly, slug, annular and mist-pre-CHF regimes.

In reviewing the base code, RELAP5/MOD3.2, it was found that most of the constitutive relations were structured to be reasonable for the fluids included in FSP. The only areas where correlations specific to water were used were in the computation of interphase drag in vertical flow, and in wall heat transfer. Thus only these were modified. In the description presented below, the emphasis is on providing the user with basic information on what is contained in FSP. Details of the various models can be found in the base code documentation (RELAP5, 1995). Additional information is provided below in the specific areas where the base code was modified. The dissolved gas release model was developed for FSP, and so it is described in more detail than the other models.

4.2.4.1 Wall Friction

The relevant wall friction terms are FWG and FWF in the phasic momentum equations. Note that the wall friction force terms include only wall shear effects. Losses due to abrupt area change are calculated using mechanistic form loss models. Other losses due to elbows or complicated flow passage geometry are modeled using energy loss coefficients supplied by the user in the input, as shown in Appendix A, under the cards for junction information. These terms are also directly used in computing the energy dissipation terms, $DISS_g$ and $DISS_f$ in the phasic thermal energy equations.

The method is to first calculate an overall two-phase frictional pressure drop. This is done by a standard two-phase multiplier method (as shown in Wallis, 1972). The two-phase friction is then partitioned between the phases (Chisolm, 1967) to get the phasic wall friction components. A further adjustment is made to incorporate flow regime effects, using a wetted wall fraction. This provides a more physical representation for certain regimes where it is

clear that one phase would be more influenced by wall friction than the other, as in annular flow, where the wall is fully wetted by the liquid phase.

The model uses the hydraulic diameter and surface roughness data provided by the user for each volume. There is an option for the user to turn off wall friction altogether, as shown in Appendix A, but this is not recommended unless as a sensitivity study to debug results from a specific analysis.

4.2.4.2 Interphase Friction

The interphase friction (or drag) per unit volume in the phasic momentum equations is expressed in terms of a phasic interphase friction coefficient as:

$$F_{ig} = \alpha_g \rho_g \text{FIG} (v_g - v_f)$$

and

$$F_{if} = \alpha_f \rho_f \text{FIF} (v_g - v_f)$$

The magnitude of the interphase drag force per unit volume on the liquid is assumed to be equal to that on the gas phase. This provides a relationship between FIG and FIF,

$$\alpha_g \rho_g \text{FIG} = \alpha_f \rho_f \text{FIF}$$

The interphase drag force per unit volume represents the interphase momentum transfer rate and is due to the difference between the phasic velocities. Thus, analogous to the transfer of heat or mass, it can be expressed as:

$$F_{i,gf} = F_i (v_g - v_f)$$

Where, F_i is a momentum conductance term, and can be expressed as:

$$F_i = A_{gf} B_{gf}$$

Where A_{gf} is the interfacial area per unit volume, and B_{gf} is a momentum transfer coefficient.

The code uses the flow regime characterization to derive relationships for A_{gf} and B_{gf} in terms of fluid properties, flow geometry, phasic velocities and the void fraction. These are then related back to the terms FIG and FIF needed in the phasic momentum equations.

The base code, RELAP5/MOD3.2, uses mechanistic models for the above calculations, except for vertical flow in the pre-CHF regimes. In this case, the base code uses a correlation developed empirically from water data. In FSP, to make this independent of the fluid type, the empirical correlation (called the Drift Flux correlation or the EPRI correlation) has been replaced with the mechanistic models. The models are similar to what exists in the base code for the various flow regimes and therefore are not further described here. It is noted that for the calculation of interphase drag in vertical flow, in FSP, the vertically

stratified regime is not explicitly used. Vertical stratification is recognized primarily for the calculation of interphase heat and mass transfer.

In building the input file, under the volume control flag information, there is a parameter, b , that allows the user to select an optional interphase drag modeling approach for rod bundles. In FSP, in addition to replacing the interphase drag models for vertical flow, this option has been essentially de-activated. Thus choosing a value of 0 or 1 for this parameter will not have an effect. It is recommended that the user choose the default value, which is zero.

4.2.4.3 Interphase Heat and Mass Transfer

The interphase heat and mass transfer rates are related by the assumption that energy is not stored at the interface. It should be noted that the code separately recognizes interphase mass transfer in the bulk fluid and at an interface near the wall. This allows the code to mechanistically treat some special cases, such as subcooled boiling. In this case, there is a radial temperature gradient within the liquid, and boiling occurs near the wall while there is condensation in the bulk fluid. Thus, the general treatment is:

$$\Gamma_g = \Gamma_{ig} + \Gamma_w$$

where Γ_w is computed by the wall heat transfer models. When wall heat transfer is not modeled by the user, this term is zero. Γ_{ig} is computed from the heat transfer at the bulk interface. The interface is assumed to be at the saturation temperature. The heat transfer at the bulk interface is then:

$$Q_{ig} = H_{ig} (T^s - T_g)$$

$$Q_{if} = H_{if} (T^s - T_f)$$

$$Q_{ig} + Q_{if} + \Gamma_{ig}(h_g - h_f) = 0$$

Where h_g and h_f can be at saturation or at the value corresponding to the local pressure and temperature, depending on whether the process is one of boiling or condensation.

The terms H_{ig} and H_{if} are the interphase heat conductance terms, and are conveniently modeled as a product of the interphase area per unit volume and the interphase heat transfer coefficient. These are in turn determined as a function of the flow regime, and modeled as a function of fluid properties, flow geometry, velocities and the void fraction.

4.2.4.4 Wall Heat Transfer

The total wall heat flux, q'' , is modeled as a sum of heat fluxes to the vapor and liquid phases:

$$q'' = h_g (T_w - T_{ref,g}) + h_f (T_w - T_{ref,f})$$

where h_g and h_f are heat transfer coefficients to the gas and liquid phases respectively (per unit wall surface area), and $T_{ref,g}$ and $T_{ref,f}$ are gas and liquid reference temperatures. The reference temperatures can be the local gas or liquid temperature or the saturation temperature, depending on the correlation being used for the heat transfer coefficient.

A heat transfer surface concept is used, based on the heat flux, wall temperature and saturation temperature, to decide the mode of heat transfer (such as convection to single phase liquid, bulk nucleate boiling, condensation). Correlations are used for the heat transfer coefficients in the various heat transfer regimes to compute the heat flux. The total heat flux is ensured to be continuous over the heat transfer-wall temperature surface, to avoid numerical difficulties as the heat transfer regimes go through transitions.

Also calculated is the portion of the wall heat flux (Q_{ig}^w and Q_{if}^w) that contributes directly to mass transfer. Then the interphase mass transfer due to wall heat transfer is calculated from:

$$Q_{ig}^w + Q_{if}^w + \Gamma_w(h_g - h_f) = 0$$

where, as before, h_g and h_f can be either at saturation conditions or at the local pressure and temperature, depending on whether the process is boiling or condensation.

The base code, RELAP5/MOD3.2 contains generic models for the heat transfer coefficients in most of the heat transfer regimes, that can be considered to be reasonably fluid-independent. In two areas, the correlations are more empirical and also based solely on water data. Hence, these have been modified in the FSP code. One area is the critical heat flux (CHF). The base code uses a table look-up procedure for calculating CHF, using data obtained for water at a variety of conditions. This was replaced in FSP by a simpler model, based on a modification to the Zuber correlation (Zuber, 1961).

$$q_{CHF} = 1.31 (0.96 - \alpha_g) \rho_g h_{fg} [\sigma g (\rho_f - \rho_g) / \rho_g^2]^{1/4}$$

Zuber's correlation has been shown to match CHF data for a variety of fluids under pool boiling conditions. The modification to Zuber's correlation is the term $(0.96 - \alpha_g)$ and has shown to match flow data with water and Freon. Note that this condition of CHF is normally one that is associated with hydrodynamic dryout of a heated surface. This is the type of CHF one may expect when wall heat transfer is modeled with only passive heat structures, such as typical pipe walls in fire-suppressant delivery systems. In implementing the above model in FSP, a lower limit of 1000 W/m^2 was imposed to prevent negative values, at high void fractions.

The other area modified is in the correlation for wetted area fraction used for computing post-CHF heat transfer. This correlation utilizes an exponential decay form to capture the decrease of wetted area fraction as the wall temperature increases. The decay constant was derived as a function of flow rate and void fraction, from water data. In FSP, the decay constant has been set to a fixed value. This is considered reasonable because this heat transfer regime is rarely encountered, and will provide continuity for the heat transfer surface if encountered.

Wall heat transfer is not expected to be significant for most FSP applications, because of the very short transient times expected. Hence, the wall heat transfer models were not tested for the various fluids implemented in FSP. The input manual, shown in Appendix A, does not describe how the user can model wall heat transfer. Nevertheless, the models do exist in the code. To access this feature, the user is currently directed to the base code documentation (RELAP5, 1995).

4.2.4.5 Coefficient of Virtual Mass

The last term in the phasic momentum equations is the dynamic drag term due to virtual mass effects, also called the inertial drag force per unit volume. In the base code, in the numerical solution procedure, the spatial dependence of the velocities in this term were neglected. Thus the term only includes the time-dependent portion. This was a compromise, because the spatial terms were dependent on the nodalization selected by the user to represent a particular system, and there was some user experience that suggested that this led to numerical errors. The main intent of this term is to capture sudden accelerating flows, and the time-dependent term provides that capability. The coefficient, C , in this term is called the coefficient of virtual mass. It is given as:

$$C = 0.5 (1 + 2\alpha_g) / (1 - \alpha_g) \text{ for } 0 \leq \alpha_g \leq 0.5$$

and,

$$C = 0.5 (3 - 2\alpha_g) / \alpha_g \text{ for } 0.5 \leq \alpha_g \leq 1$$

4.2.4.6 Release of Dissolved Gas

The liquid agent in the storage vessel is stored under pressure of a noncondensable gas (nitrogen). It is assumed that the agent has been stored for a long enough period for the liquid to be saturated with nitrogen (equilibrium condition). At equilibrium, the concentration of dissolved nitrogen in the liquid medium is proportional to the partial pressure of nitrogen in the gaseous space above the liquid. This is Henry's law:

$$x_N^* = H P_N$$

where x_N^* is the equilibrium concentration (mole fraction of solute in solution), H is Henry's constant and P_N is the partial pressure of nitrogen above the liquid. H is usually a function of temperature and the liquid type.

As the system is depressurized, nitrogen will come out of solution since the partial pressure decreases. According to Henry's law, the corresponding concentration of nitrogen in the solution must also decrease. Hence the excess must be released. In a fast depressurization transient, the excess can still be in solution due to surface tension. Considering a micro-bubble of dissolved gas with radius r_c , the difference between the pressure inside and outside the bubble is given by

$$\Delta P_{\text{NUC}} = 2\sigma/r_c$$

where σ is the surface tension. As the pressure outside decreases, the pressure difference builds up, and until the point where surface tension can no longer hold the bubble together, and the excess nitrogen will then be released. This initiation mechanism is similar to nucleate boiling, in which the liquid is superheated before boiling can occur. The radius of the micro-bubble can be empirically determined by observing the point at which nitrogen release occurs. In this model, this radius is assumed known (user input). The release pressure is then given by

$$P_{\text{rel}} = P_i - \Delta P_{\text{NUC}} = P_i - 2\sigma/r_c$$

where P_i is the initial system pressure.

The above determines the initiation of release. The rate of release is determined as follows. Henry's law determines the equilibrium concentration at given conditions. As the system is depressurized, the corresponding partial pressure decreases. The corresponding equilibrium concentration will be less. The solution is therefore at a state of non-equilibrium. The release is a means to achieve the new equilibrium again. Thus, the release rate is postulated to be proportional to the difference between the actual concentration and the equilibrium concentration (dictated by Henry's law) as follows:

$$\Gamma_{\text{rel}} = \Gamma_0 (x_N - x_N^*)$$

where Γ_0 is some release coefficient, x_N is the actual concentration, and x_N^* is the equilibrium concentration as given by Henry's law. Thus

$$\Gamma_{\text{rel}} = \Gamma_0 (x_N - H P_N)$$

The release will be zero when the actual concentration approaches the equilibrium concentration, as it should be. The release model is similar to other transfer phenomena, such as heat transfer and mass transfer.

The model requires that user specify, as input, the parameters r_c and Γ_0 , and the initial pressure P_i and temperature T_i .

The numerical implementation of the release rate model poses a problem, since the partial pressure is not the local value, but the value above the liquid-gas interface. A compromise is made by using the local total pressure in place of the partial pressure in calculating the equilibrium concentration using Henry's law. This over-predicts the equilibrium concentration, and hence under-predicts the release rate. It may be compensated for by using a larger release coefficient. Thus, the release rate is numerically implemented as, for the k^{th} volume:

$$\Gamma_{\text{rel}, k} = \Gamma_0 (x_{N,k} - H P_k)$$

Note that HP_k is the mole fraction of nitrogen in solution. To convert to mass of nitrogen per unit mass of solvent, one gets

$$\text{Mass fraction} = HP_k W_N / (1-HP_k)W_f$$

where W_N is the molecular weight of nitrogen (28.0) and W_f is the molecular weight of the fluid type. The actual concentration is related to the solute density as

$$x_{N,k} = (\rho_s / \alpha_f \rho_f)_k$$

The solute generation rate is therefore the negative of the release rate:

$$\Gamma_{s,k} = -\Gamma_{N,k} = -\Gamma_0 \{ (\rho_s / \alpha_f \rho_f)_k - H P_k W_N / (1-H P_k)W_f \}$$

The above is only valid if the local concentration is greater than the equilibrium concentration. Otherwise the release rate should be zero. Hence

$$\Gamma_{s,k} = \min (\Gamma_{s,k}, 0.0)$$

Also, the amount of release in one time step should not be more than the total amount dissolved in the volume. Thus the maximum release rate is given by

$$\Gamma_{rel,k, max} = \rho_s / \Delta t$$

where Δt is the current time step. Hence the final expression for the solute generation term is

$$\Gamma_{s,k} = \max \{ \min (\Gamma_{s,k}, 0.0), -\rho_s / \Delta t \}$$

The Henry's constant is estimated from the PROFISSY Code (see Yang et. Al., 1997) as follows. Assuming Henry's law to be valid, the equilibrium concentration is given by

$$x_N = HP_N$$

In PROFISSY, the concentration of nitrogen in the agent liquid (x_N , mole fraction) is calculated given the system pressure (P), temperature (T), total volume (V), and total agent mass (m_a). The partial pressure of nitrogen can be determined from

$$P_N = P - P_v$$

where P_v is the saturation pressure of the agent fluid at T. Table 4.2.1 lists the output from PROFISSY, and the calculation of H as described above. Three fluid systems are considered: HFC-227ea, HFC-125 and Halon 1301. As can be seen, the solubility of nitrogen in all three agents is very similar. Assuming only temperature dependence, the Henry's constant can be correlated as a quadratic, as shown in Figure 4.2.3. The analytical form of the correlation is given by

$$H = H_0 + C_1 T + C_2 T^2$$

where H is in mol/Pa, and T in K.

and,

$$H_0 = 2.347767 \times 10^{-7}$$

$$C_1 = -1.55063 \times 10^{-9}$$

$$C_2 = 2.957799 \times 10^{-12}$$

Figure 4.4 shows the calculated bottle pressure for various release coefficients. The critical radius was specified at 7.5×10^{-9} m. The initial concentration was estimated as 0.02916 kg N₂/kg liquid phase. This value is comparable to the reported initial concentration of Test 146. At about 0.1 seconds, as the pressure decreases to a value of about 4 MPa, there is a noticeable change in the rate of pressure decrease. This is the pressure at which gas begins to be released, and experimental results generally indicate that this would happen at about the same pressure for a given fluid type and system configuration. As discussed earlier, this pressure is controlled by the value of the critical gas bubble radius, r_c , chosen by the user. The lower the value of r_c specified, the lower the pressure at which gas release would be initiated.

The value of Γ_0 controls the rate of gas release. At low values of Γ_0 , the rate of release is small, and the pressure continues to decrease monotonically below the pressure at which gas release was initiated. As the value of Γ_0 is increased, there is a noticeable decrease in the depressurization rate at the gas release pressure (at about 0.1 seconds). This is the expected trend. Test runs of the code indicate that this method of modeling the gas release works relatively smoothly, and the code appears to handle a wide range of release coefficients without numerical difficulty.

One of these sensitivity case, corresponding to Γ_0 of 10,000 kg/m³-s and an initial concentration of 0.02196 kg N₂/kg Liquid, was used to further check out the model. Figure 4.2.5 shows the calculated pressure profile as compared to data. Figure 4.2.6 shows the void fraction responses for the various cells used to model the supply bottle. Volume 203-01, shown in the figure, is at the top of the bottle, and Volume 203-10 is at the bottom. The figure shows a relatively smooth emptying of the bottle, with the void fractions in the lower cells increasing to 1.0 subsequent to the void fractions in the cells above them. The void fraction in the last cell, Volume 203-10, increases to 1.0 after all the other cells, at about 1.0 second. This represents the time in the calculation when the bottle is emptied.

This calculation was also used to check out other parameters. The solute concentration profiles showed smooth changes, following expected trends. A mass balance was carried out to ensure that the code conserved the mass of nitrogen, between the initial amount and the additional amount released from the liquid. Essentially, these checks ensured that the gas release model was implemented in the code as intended, and the mechanistic gas release model produced the expected trends. There is of course some uncertainty in how to specify the correct values for the parameters r_c and Γ_0 . However, as shown in other sections of this report, comparisons to experiments with different fluids and system configurations indicate reasonably good agreement between code calculations and experimental data, with these parameters varying over a relatively narrow range. This has been useful in arriving at a range of recommended values for these parameters. Further, from a design perspective, while

variation of these parameters causes a noticeable variation in the initial pressure history, there is not much variation in the time required to empty the supply bottle. Hence it is believed that this gas release model, used with the range of recommended values for r_c and Γ_0 , would adequately serve the needs of a design engineer evaluating the performance of a suppressant delivery system.

4.2.5 SPECIAL PROCESS MODELS

This section describes certain models in the code that simulate special processes. The user can select many of these processes via input. A detailed description of these process models can be found in the base code documentation (RELAP5, 1995). The information below is a brief summary, to provide some basic information and where appropriate, some user guidelines on the use of these models.

4.2.5.1 Choked Flow

Choking is defined as the condition where the mass flow rate becomes independent of the downstream conditions. Choking occurs because acoustic signals can no longer propagate upstream as the fluid velocity equals or exceeds the propagation velocity. In typical FSP applications, choking can occur at the bottle exit, as soon as the discharge begins, and also at the discharge location from the system. The choked flow model in FSP is by Trapp and Ransom(1982) and is used to calculate the mass discharge from the system. The model can also be used to predict the existence of and calculate choked flow at interior points in the system.

The user can select the choking model as a part of the junction control flag information in the input file. The user can select this option at all junctions. In fact, the default option will select the choked flow model. It is recommended, however, that the user only select this model at the system exit location(s) and at the junction representing the exit of the supply vessel. The model should be turned off at all other internal junctions. This is because the sonic velocity (propagation velocity) in two-phase flow can be a strong function of the void fraction, and the choked flow model imposes an external criterion on the code's normal numerical solution method. This can lead to difficulties in code execution and a drastic reduction in the computational time step.

Also note that the input for junctions allows the use of discharge coefficients for subcooled liquid, saturated fluid and single phase vapor. Current assessment of the code against experiments suggests that best results are obtained by using a subcooled discharge coefficient of 1.0, a two-phase discharge coefficient of 0.8 to 0.9, and a single phase vapor discharge coefficient equal to the two-phase discharge coefficient.

4.2.5.2 Horizontal Stratification and Entrainment

Flow at low velocity in a horizontal pipe can be stratified due to buoyancy forces. The horizontal flow regime map in the code contains a mechanistic model to predict when stratification would occur. When the flow is stratified, the area average pressures are affected by nonuniform transverse distribution of the phases. The normal code equations are based on assuming uniform transverse pressure distribution. To account for the nonuniform pressure

distribution, adjustments are made to the momentum equations to consider area average pressures for the vapor and liquid phases, and the interfacial pressure between them. This model is always active in the code, but becomes significant only when the code's stratification criterion is met. The code then calculates a liquid level in the channel (circular pipe geometry is assumed) and uses this information to estimate the hydrostatic pressure in the transverse direction.

Also, when the flow is stratified, the void fraction flowing in a junction may be different than the upstream volume void fraction. A typical example would be when there is an area contraction. With stratified conditions in the upstream volume, if the level is below the pipe centerline, the void fraction in the junction would be significantly higher than the upstream volume. And if the level is above the pipe centerline, the junction void fraction would be lower than the upstream volume. Also, in addition to the formation of a level and its effect, the vapor can entrain liquid through the junction, and similarly, the liquid can pull through some gas. The code considers these possibilities, and adjusts the junction void fraction to be different than the upstream volume void fraction when the upstream volume is calculated to be stratified.

The user does not actively engage these models. It is part of the code's internal structure and will automatically be invoked as needed.

4.2.5.3 Abrupt Area Change

A general piping network system can contain sudden area changes and orifices. The code contains built-in models for the user to access in simulating these geometries. The basic hydrodynamic model in the code is formulated for slowly varying flow area variations. Hence, special models are needed when the flow area undergoes an abrupt change, such as at an orifice.

Basically, the user can select the abrupt area change option at any junction in the model, as a part of the junction control flag input information. The code will calculate the energy loss coefficients associated with the abrupt area change internally. In a case where the flow is going through a sudden contraction, the code will also internally compute the losses associated with the formation of a vena contracta. Along with selecting the abrupt area change option, if the user also enters form loss coefficients, these will be added to the internally calculated form losses.

4.2.5.4 User-Specified Form Losses

In the junction control flag information card, the user can specify a junction to be a smooth or abrupt area change junction. The user can also specify form loss coefficients at the junction. For standard geometries, and configurations such as elbows and tees, these form loss coefficients can be obtained from standard handbooks. If the user has frictional pressure drop data for a particular system at known flow rates, that can be used to back out form loss coefficients.

The user can also enter flow dependent form loss coefficients. Typically, the form losses would be a function of the Reynolds Number. The code input allows a standard form and the user has to enter the desired constants for the Reynolds Number dependence. This is shown in the code input manual, in Appendix A.

4.2.5.5 Cross Flow Junction

The code's numerical method is generally formulated using one-dimensional elements. However, there are applications where an approximate treatment of transverse flow can provide an improved physical simulation. The crossflow junction component provides this feature.

A typical place to use the crossflow junction would be in modeling a standard 90° Tee. The crossflow junction would be used to model the connection to the branch line, as shown in Figure 4.2.7a. In this case, the momentum flux in the side branch is assumed to be perpendicular to the main flow stream. Thus the main stream momentum flux does not contribute to the crossflow momentum formulation. Essentially, in the crossflow junction formulation, there is no transport of axial direction momentum due to the flow in the transverse direction.

The user selects the crossflow junction option by specifying the appropriate connection code when describing the 'From' and 'To' volumes for a junction. This is described in the input manual in Appendix A.

4.2.6 COMPONENT MODELS AND SYSTEMS

The code contains a variety of generic components that are used to build system models. These include components such as Single Volume, Time-Dependent Volume, Single Junction, Pipe, Valve, etc. Most of these are self-explanatory. This section provides some additional information on building a system model and the use of some of the components and features.

4.2.6.1 Branch

There are several ways to simulate branching flows. Several single junctions can be connected to the exit of a single volume to simulate flow splits. A BRANCH component is also provided in the code. Essentially, this functions no different than a single volume to which more than two junctions are connected. Primarily, it is a user-convenience, which allows all the junction information to be entered along with the volume information in one component instead of using several separate components. A crossflow junction can be used to connect a Branch component to another component. Two typical uses are in modeling branching flows in a one-dimensional branch, and a Tee branch.

A one-dimensional branch is one where more than two normal junctions connect to a volume, and where it is assumed that multidimensional effects are small compared to system interaction effects. Typically, this would be used in branched flows that occur in headers or

plena. Fluid entering a header and then splitting into several parallel paths would be modeled as a one-dimensional branch.

A Tee branch is formed by the arrangement shown in Figure 4.2.7a, where the crossflow junction was used. In this case, the Volume V_2 may be specified as a Branch component, and the crossflow junction connecting to it could be defined by the appropriate connection code, described in the input manual in Appendix A. The Tee connection could also be modeled without a crossflow junction, by using a Branch component with normal junctions, as shown in Figure 4.2.7b. This approach has the advantage that fewer volumes are used. The disadvantage is that if the Tee is really a Standard 90° Tee, then it may not be the best representation of the physical process. In typical FSP applications, very little difference has been observed between the two approaches. Hence, either approach seems acceptable.

Note that a volume with more than two junctions connected to it is treated by the code as a Branch component, even if it has not been defined as such in the input. What this really means is that the volume velocity in this volume is determined as a momentum flux weighted average of the flows in the junctions connecting to it. Also, the volume cross-sectional area is apportioned between the various streams in proportion to the volumetric flow in these streams. The consequence is that, if one stream has a very high velocity, there would be excess error in conserving momentum (and mechanical energy) around this volume. One place where this has an impact is if one of the junctions connecting to the Branch is the exit junction for the system and it is choked at a high velocity. To avoid this situation, it is recommended that the user allow some straight pipe length connected to all the junctions of a Branch. It is also recommended that when the BRANCH component is used, the junctions of the component use the abrupt area change option.

4.2.6.2 Valves

Valves are quasi-steady models that are used to either specify an option in a system model or to simulate control mechanisms. They are essentially treated as single junctions and the input required to describe them is similar. There are two categories of valves, those that open and close instantly or those that open and close gradually. The base code contains several types of valves. Only two types are envisioned to be useful in modeling typical fire suppressant delivery systems, and these are described here.

A Trip valve is one that is fully open or fully closed based on a trip setting. The opening or closing will occur in one time step following the trip signal. The trip signal can be structured to latch the valve in an open or closed position, if desired, as described in the input manual in Appendix A.

A Motor Valve has the ability to control the junction flow area as a function of time. The operation of this valve is controlled by two trips, one to open and one to close. A user-specified rate parameter controls the rate at which the valve area changes. The abrupt area change option is normally used with this component to allow the code to automatically compute the form loss coefficient as a function of the valve area.

Typical use of this component in FSP applications would be to describe the junction that connects the suppressant supply vessel to the piping system. The valve could be opened as fast as desired by the user to simulate the initiation of the discharge transient.

4.2.6.3 Trip Systems

The Trip system consists of the evaluation of logical statements. Each trip statement has a true or false result, and an associated variable, TIMEOF. This variable is the time in the transient at which the trip became true and has a value of -1.0 when the trip is false. This variable can be used to set time delays based on events during the transient. Within the code structure, the trip system only evaluates the logical statements (such as , is transient time greater than 2.0 seconds?) The decision of what action is needed based on the trip status resides within other models. In the above example, the trip system would assign a true or false value to a particular trip number depending on whether the transient time was less or greater than 2.0 seconds. If this trip number is invoked by a valve component, the valve models would decide whether to close or open the valve, at what rate, etc.

Using the trip system is fairly self-explanatory, and directions are provided in the input manual in Appendix A.

4.2.6.4 Control Systems

The control system provides the capability to evaluate simultaneous algebraic and differential equations. This allows simulation of control systems typically used in hydrodynamic systems. Another use is to define auxiliary output quantities, which can then be extracted from the output or restart files as tables or plots.

In typical FSP applications, there are no complicated trip and control logic required. Hence, control systems are primarily used to define auxiliary output variables. For example, enthalpy is not a normal code variable, and if it is needed for some reason, it can be computed using several control systems (such as the SUM and MULTIPLIER components) to calculate it from the internal energy, pressure and specific volume, which are all normal code variables. Another example would be if a user wanted to know the Froude Number at the system exit, for evaluating mixing characteristics in the discharge area. Similarly, the INTEGRAL component could be used to keep track of suppressant mass delivered. A variety of control systems are provided in the input manual in Appendix A, with directions on how to enter the needed cards in the input file.

Table 4.1: PROFISSY Results

	HFC-227ea/N2	Halon/N2	R125/N2
T(K)	H (mol/Pa)	H(mol/Pa)	H(mol/Pa)
190	n/a	4.70357E-08	n/a
200	n/a	4.20328E-08	n/a
210	n/s	3.87112E-08	3.64965E-08
220	3.76614E-08	3.67283E-08	3.79995E-08

230	3.61976E-08	3.58968E-08	3.36686E-08
240	3.52156E-08	3.29835E-08	3.36637E-08
250	3.47006E-08	3.44772E-08	3.46937E-08
260	3.3033E-08	3.1454E-08	3.41243E-08
270	3.34344E-08	3.26477E-08	3.24578E-08
280	3.28759E-08	3.2787E-08	3.47492E-08
290	3.28942E-08	3.21827E-08	3.39495E-08
300	3.35448E-08	3.35049E-08	3.76173E-08
310	3.48921E-08	3.74043E-08	3.90425E-08
320	3.57496E-08	3.96115E-08	4.44921E-08
330	3.78611E-08	4.87664E-08	5.39104E-08
340	4.14481E-08	n/a	n/a
350	4.59199E-08	n/a	n/a
360	5.41519E-08	n/a	n/a

n/a: outside PROFISSY data range for the fluid

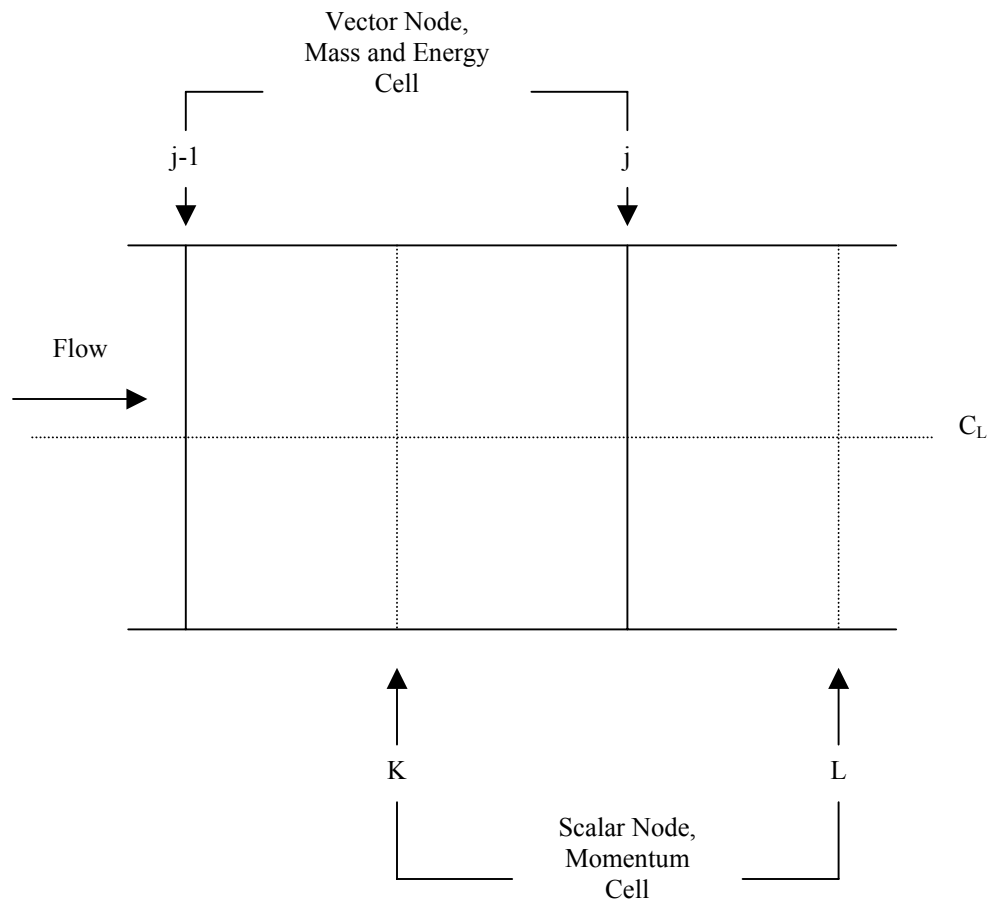
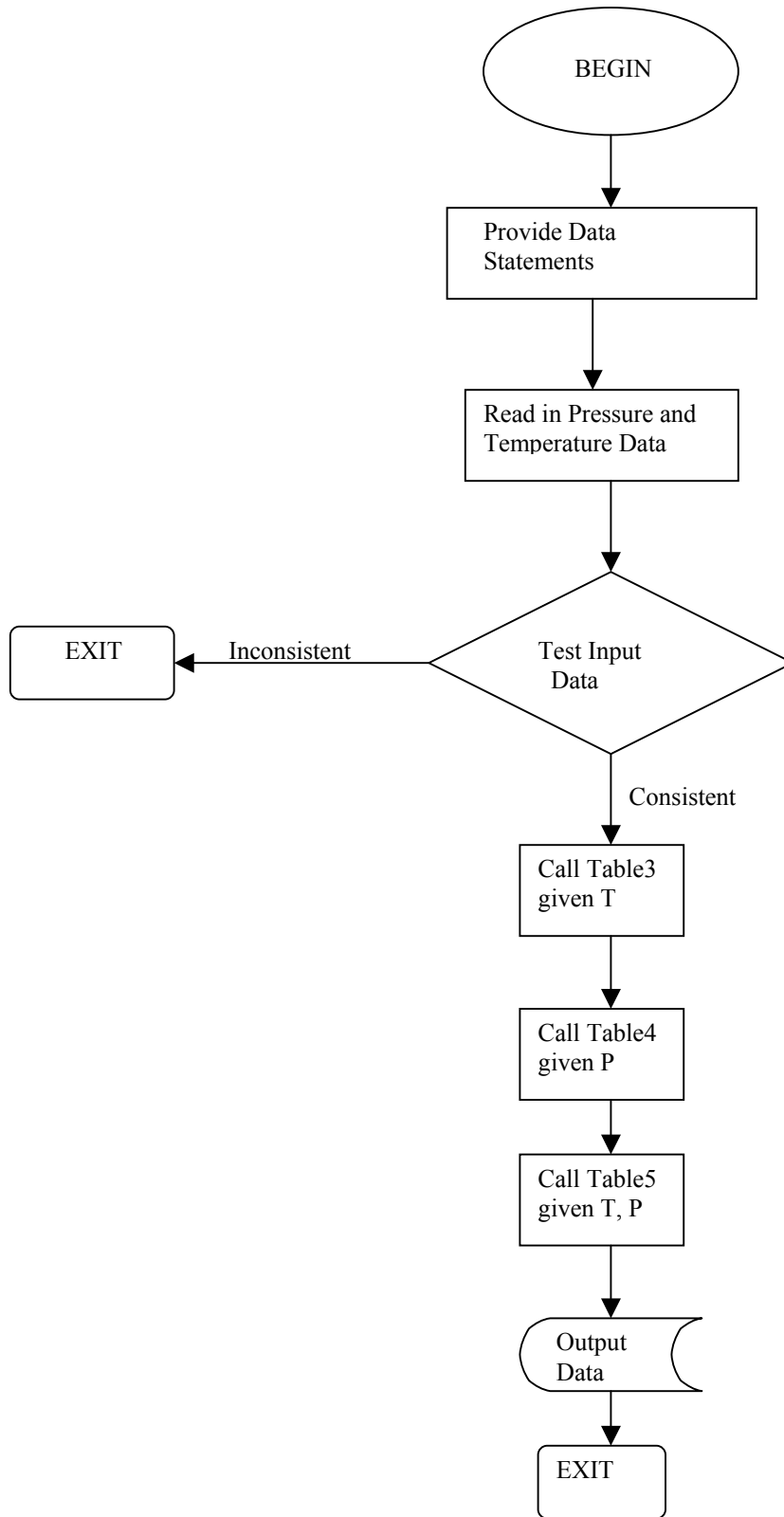


Figure 4.2.1: Staggered mesh numerical method

Figure 4.2.2: Flow Chart of Generation Program



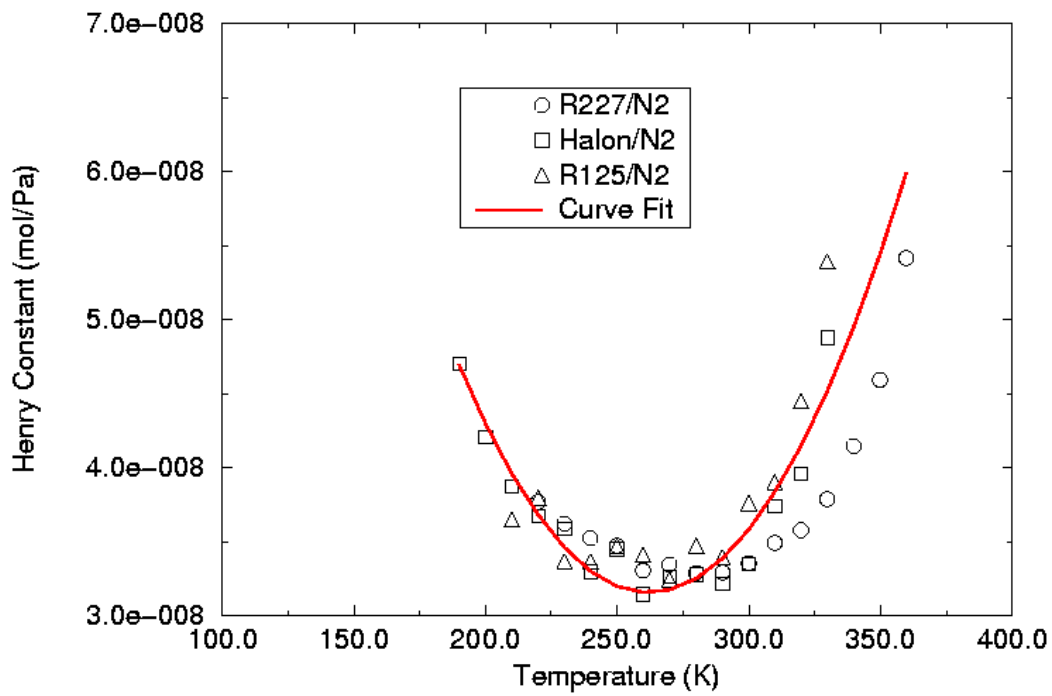


Figure 4.2.3: Curve Fit for Henry Constant

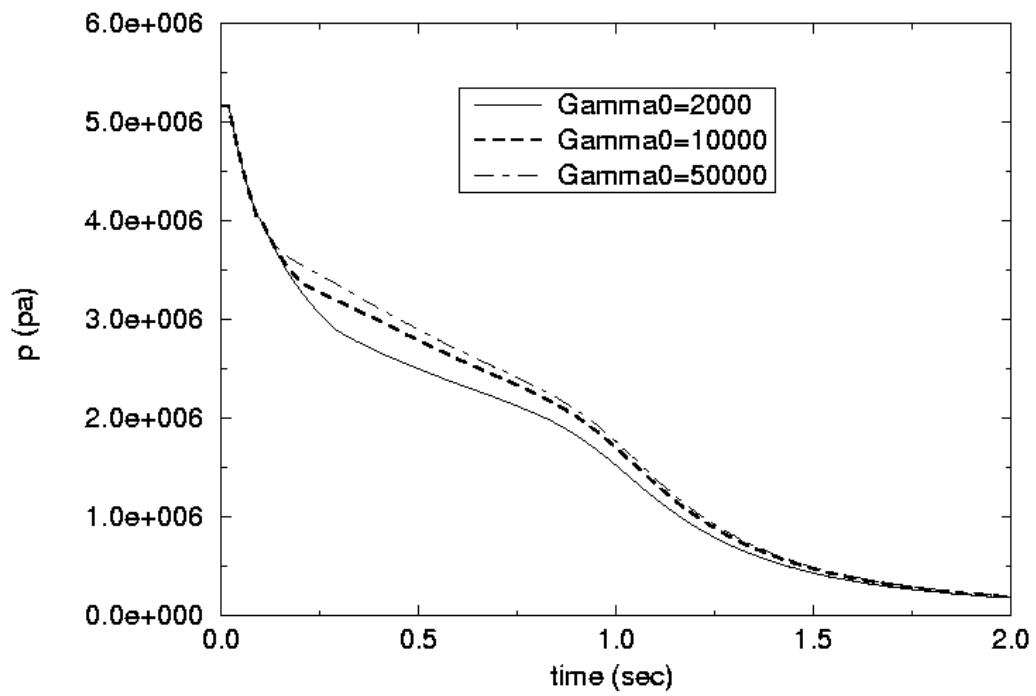


Figure 4.2.4: Effect of Release Coefficient on Calculated Pressure Response

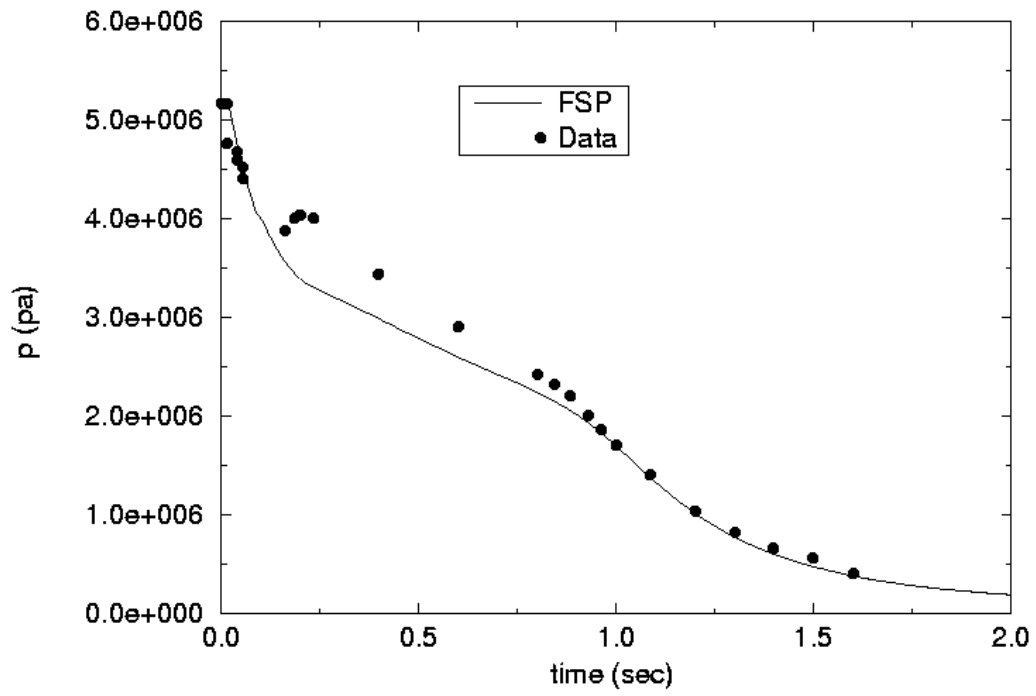


Figure 4.2.5: Comparison of Calculated and Measured Bottle Pressure for Test 146

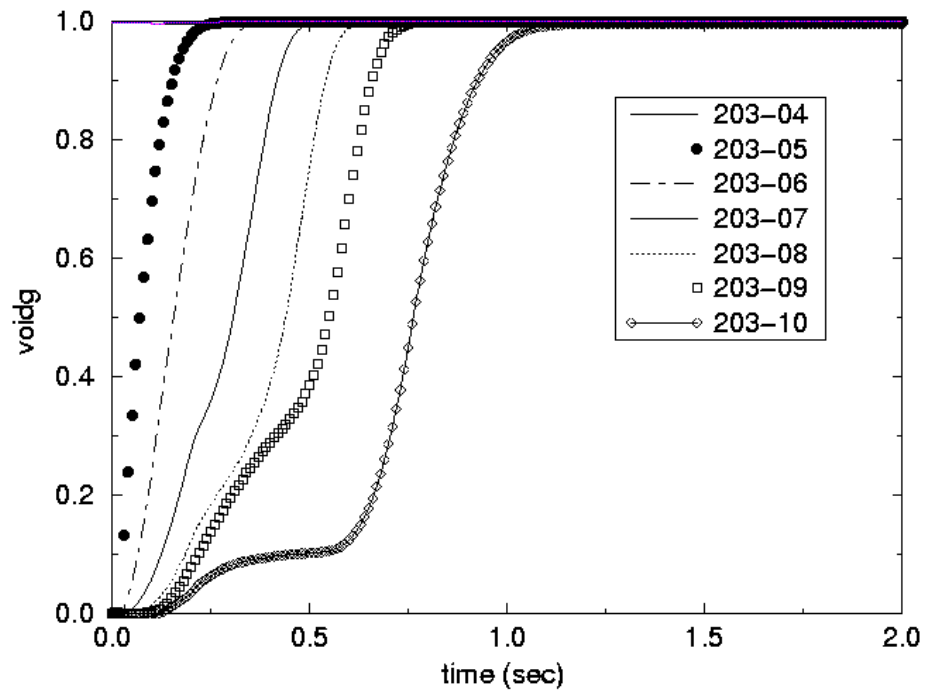


Figure 4.2.6: Void Fraction Responses in Lower Portion of Bottle

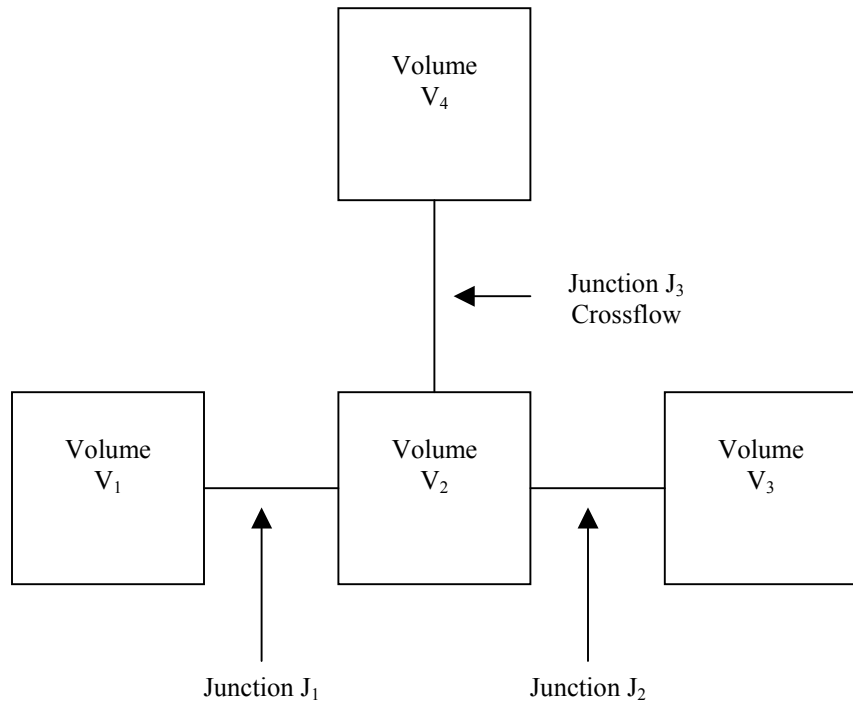


Figure 4.2.7a: 90-degree Tee model with crossflow junction

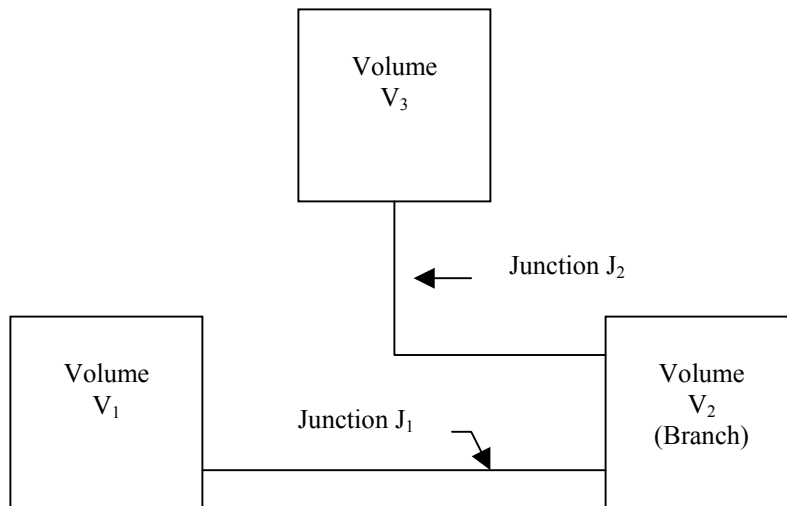


Figure 4.2.7b: Tee model with normal junctions

4.3 CODE ARCHITECTURE

This section provides an overview of the code architecture and briefly summarizes computer adaptability, code organization, input processing, and transient operation.

4.3.1 COMPUTER ADAPTIBILITY

The FSP code was developed from the base code RELAP5/MOD3.2, which was written in FORTRAN 77 for a variety of 64-bit and 32-bit computers. Here, a 64-bit computer is one in which floating point, integer, and logical quantities use 64-bit words; a 32-bit machine uses 32-bit words for those same quantities but also allows 64-bit floating point operations. Examples of 64-bit computers are Cray, Cyber-NOS-VE, and DEC/Alpha machines. Examples of 32-bit computers include IBM mainframes, such as a 3090, workstations, including those from DEC, HP, IBM, SGI, and Sun, and many personal computers.

In developing FSP from the base code, RELAP5/MOD3.2, the source code was obtained from the Idaho Engineering National Laboratory. This code was adaptable to other computing environments. The code was configured to work on a PC with WINDOWS 95 operating system and tested to ensure that the code options would function properly. The hardware chosen for installation was a laptop PC with a Pentium 233 MHz processor, 64 MB RAM and 3.2 GB hard disk drive. The compiler used was the DigitalTM Visual FORTRAN compiler (Standard Edition, Version 5.1) for WINDOWS 95 operating system.

4.3.2 TOP LEVEL ORGANIZATION

The coding is modular, using top-down structuring. The various models and procedures are isolated in separate subroutines. The top level structure is shown in Figure 4.3.1 and consists of input (INPUT), transient/steady-state (TRNCTL), and stripping (STRIP) blocks. The input block (INPUT) processes input, checks input data, and prepares required data blocks for all program options and is discussed in more detail in Section 4.3.3. The transient/steady-state block (TRNCTL) handles both transient and the steady-state options. The steady-state option determines the steady-state conditions if a properly posed steady-state problem is presented. Steady state is obtained by running an accelerated transient until the time derivatives approach zero. Thus, the steady-state option is very similar to the transient option but contains convergence testing algorithms to determine satisfactory steady state, divergence from steady state, or cyclic operation. If the transient technique alone were used, approach to steady state from an initial condition would be identical to a physical transient from that initial condition. Pressures, densities, and flow distributions would adjust quickly, but thermal effects would occur more slowly. To reduce the transient time required to reach steady-state, the steady-state option artificially accelerates heat conduction by reducing the thermal capacity of the conductors. The transient/steady-state block is discussed in more detail in Section 3.4. Note that in running typical FSP problems, the user will not be using wall heat conductors and will typically choose the transient option, allowing a 'null transient' time for steady-state initialization.

The strip block (STRIP) extracts simulation data from a restart plot file for convenient passing of simulation results to other computer programs, for plotting or for examining the results in some other fashion.

4.3.3 INPUT PROCESSING

The code provides detailed input checking for all system models using three input processing phases. The first phase reads all input data, checks for punctuation and typing errors (such as multiple decimal points and letters in numerical fields), and stores the data keyed by card number such that the data are easily retrieved. A list of the input data is provided, and punctuation errors are noted.

During the second phase, all input data are processed. Some processed input is stored in fixed common blocks, but the majority of the data are stored in dynamic data blocks that are created only if needed by a problem and sized to the particular problem. In a NEW-type problem, which is the typical problem for users of FSP, dynamic blocks must be created. Also during this phase, restart data from a previous simulation are read if the problem is a RESTART type. Most FSP problems will not use this feature. In any case, in RESTART problems, dynamic blocks may be created, deleted, added to, partially deleted, or modified as modeling features and components within models are added, deleted, or modified. Extensive input checking is done, but at this level, checking is limited to new data from the cards being processed. Relationships with other data cannot be checked because the latter may not yet be processed. As an illustration of this level of checking, junction data are checked to determine if they are within the appropriate range (such as positive, nonzero, or between zero and one) and volume connection codes are checked for proper format. No attempt is made at this point to check whether or not referenced volumes exist in the problem until all input data are processed.

The third phase of processing begins after all input data have been processed. Since all data have been placed in common or dynamic data blocks during the second phase, complete checking of interrelationships can proceed. Examples of cross-checking are existence of hydrodynamic volumes referenced in junctions and heat structure boundary conditions; entry or existence of material property data specified in heat structures; and validity of variables selected for minor edits, plotting, or used in trips and control systems. As the cross-checking proceeds, cross-linking of the data blocks is done so that it need not be repeated at every time step. The initialization required to prepare the model for the start of the transient advancement is done at this level.

Input data editing and diagnostic messages can be generated during the second and/or third phases. Input processing for most models generates output and diagnostic messages during both phases. Thus, input editing for these models appears in two sections. As errors are detected, various recovery procedures are used so that input processing can be continued and a maximum amount of diagnostic information can be furnished. Recovery procedures include supplying default or benign data, marking the data as erroneous so that other models do not attempt use of the data, or deleting the bad data. The recovery procedures sometimes generate additional diagnostic messages. Often after attempted correction of input, different diagnostic messages appear. These can be due to continued incorrect preparation of data, but

the diagnostics may result from the more extensive testing permitted as previous errors are eliminated.

The results of the input processing appear in the output file. If errors are found that cannot be recovered from, the code stops, with a message stating errors were found during input processing. More specific information on the type of error found and its possible location is also provided in the output file. If no input errors are found, the code prints a message in the output file stating that the input processing was successful. This information is the first part of the output file. Hence, when using the code, even if the code execution appears to have been completed, before proceeding to extract output variables for plotting, it is a good idea for users to check the output file to verify that the input processing was successful.

4.3.4 TRANSIENT PROCESSING

Figure 4.3.2 shows the functional modular structure for the transient calculations, while Figure 4.3.3 shows the second-level structures for the transient/steady-state blocks or subroutines. The subroutine TRNCTL shown in Figure 4.3.1 consists only of the logic to call the next lower level routines. Subroutine TRNSET performs final cross-linking of information between data blocks, sets up arrays to control the sparse matrix solution, establishes scratch work space, and returns unneeded computer memory. Subroutine TRAN, the driver, controls the transient advancement of the solution. Nearly all the execution time is spent in this block, and this block is the most demanding of memory. Nearly all the dynamic data blocks must be in the central memory, and the memory required for instruction storage is high, since coding to advance all models resides in this block. When transient advances are terminated, the subroutine TRNFIN releases space for the dynamic data blocks that are no longer needed.

A description is next presented of the functions of all of the modules (subroutines) driven by TRAN (see Figure 4.3.3). The time step control module (DTSTEP) determines the time step size, controls output editing, and determines whether the transient advancements should be terminated. During program execution, this module displays such information as CPU time, problem time, time step size, and advancement number on the standard output, usually a terminal screen.

The trip system module (TRIP) evaluates logical statements. Each trip statement is a simple logical statement that has a true or false result. The decision of what action is needed resides within the components in other modules. For example, valve components are provided that open or close the valve based on trip values.

The equation of state boundary volume model (TSTATE) calculates the thermodynamic state of the fluid in each hydrodynamic boundary volume (time-dependent volume). This subroutine also computes velocities for the time-dependent junctions.

The heat structure model (HTADV) advances heat conduction/transfer solutions. It calculates heat transferred across solid boundaries of hydrodynamic volumes. This module

will not be used if the user does not enter information in the input file regarding the presence of wall heat structures. Most FSP users will not use heat structures.

The hydrodynamics module (HYDRO) advances the hydrodynamic solution.

The reactor kinetics module (RKIN) will not be activated by FSP users. It is a part of the base code meant for the calculation of nuclear reactor kinetics.

The control system module (CONVAR) provides the capability of simulating control systems typically used in hydrodynamic systems. It consists of several types of control components. Each component defines a control variable as a specific function of time advanced quantities. These control variables are described in the code input manual in Appendix A.

The time-advanced quantities include quantities from hydrodynamic volumes, junctions, valves, heat structures, trip quantities, and the control variables themselves. This permits control variables to be developed from components that perform simple, basic operations.

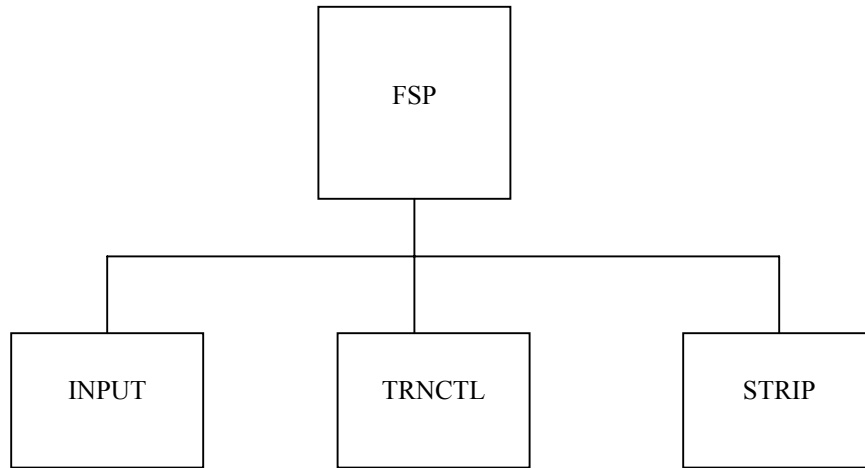


Figure 4.3.1 Top Level Structure

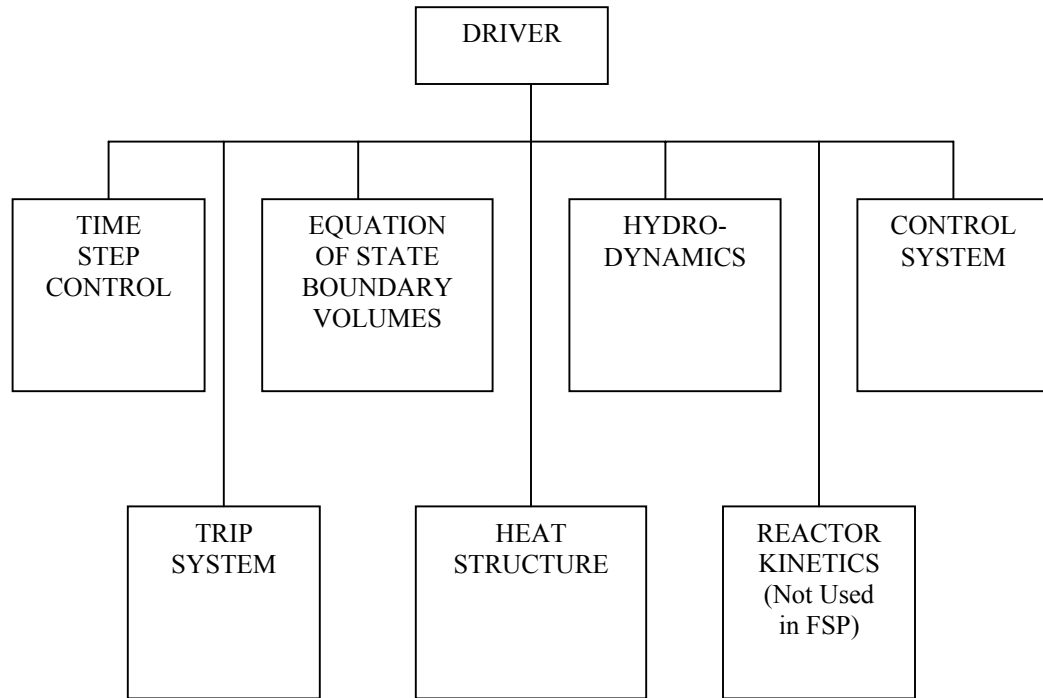


Figure 4.3.2 Modular Structure of Transient Calculations

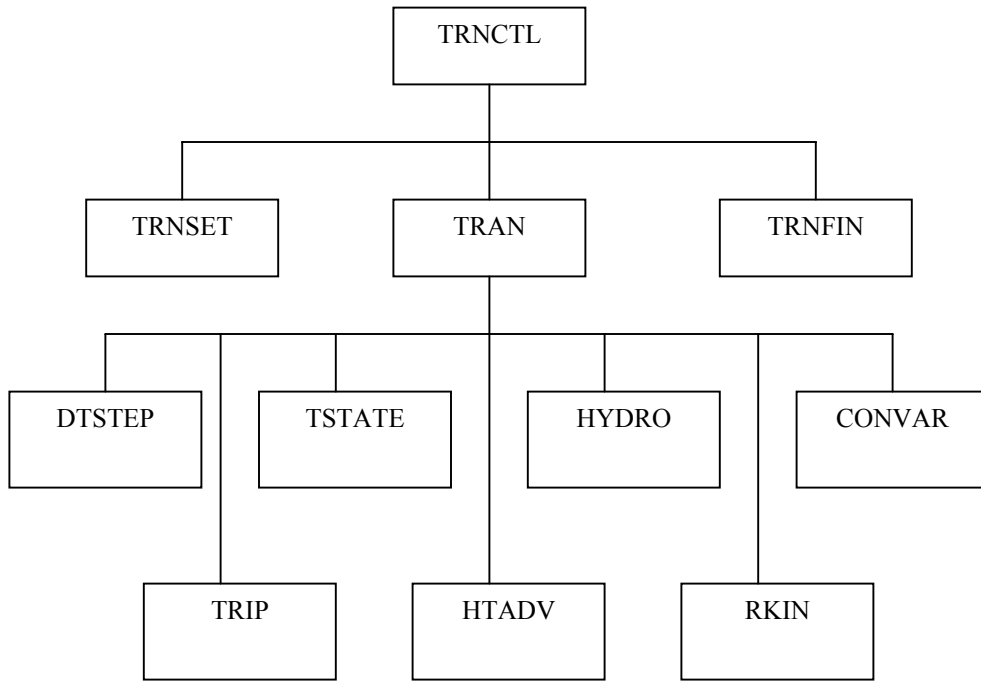


Figure 4.3.3 Transient (Steady-State) Block Structure

4.4 CODE INSTALLATION AND EXECUTION

This section describes how to install the FSP code on a personal computer with a WINDOWS 95 or 98 operating system, and how to execute the code. The code is transmitted on a CD-ROM with several files and folders in it. This section also describes what is on the CD-ROM.

In order to run a problem, the user needs to build an input file and name it with an extension '.i'. Instructions on how to build this file are provided in the code input manual, shown in Appendix A. A sample problem is shown in Section 5 and can be used as a guide to building the input file. This file would be *filename.i*. The user can use as many characters as needed to adequately name this file, but generally keeping this to 8 characters is convenient, making sure to not include any blank spaces in the filename. A sample input file is contained on the CD-ROM and can be located by searching for the file with the '.i' extension. The procedure for editing this file or for running the FSP code with this input file is described in sections 4.4.1 and 4.4.2 below.

When the code is executed with the input file, *filename.i*, the code will create two files. One file is the output file, called *filename.o*. The user can examine this file by choosing the Edit option described in Section 4.4.1. A sample output file is contained in the CD-ROM.

The second file is the restart file, called *filename.r*. This file cannot be examined on the screen because it is a binary file. However, it is the file needed for the user to extract information for plotting any of the code output variables. This file can also be used to restart the problem and run it for a longer transient time, but most problems are expected to be fairly small. Hence, it is recommended that the user not attempt to restart a problem, but simply rerun the problem from the beginning, to a longer transient time, as needed.

To extract output variables for plotting, the user needs to build a file with the extension, '.inp', called *filename.inp*. This file is simply a listing of the variables that the user wants to plot. The first line of this file is a title card, followed by one line for each variable desired. For example, if the user wanted to extract the pressure in component number 203 as a function of time, one line of this file will read 'p 203010000'. A sample is contained in the CD-ROM, and it is recommended that the user modify this file as needed. Note that when this is done, the user should save the file with the same filename as used for the input file, but with the extension '.inp'. The procedure for editing this file is the same as for editing any of the other files, as shown in Section 4.4.1. The procedure for extracting (or stripping) the output variables is shown in Section 4.4.3. When this stripping procedure is executed, the code will create a folder with the extension '.ace', called *filename.ace*. Inside this folder, the code will place a set of files, each file containing a set of X-Y pairs. Each of these files will be named with the name of the output variable requested. For example, the file *p.203010000*, will contain a set of time and pressure values for component number 203 which the user defined in the input file.

To create a plot of any of the output variables chosen, the user may use any convenient software that the user is familiar with. The ACE graphics package, provided on the CD-ROM, offers one convenient method. The procedure for using this graphics software

package is shown in Section 4.4.3. The user manual for this graphics package is contained on the CD-ROM.

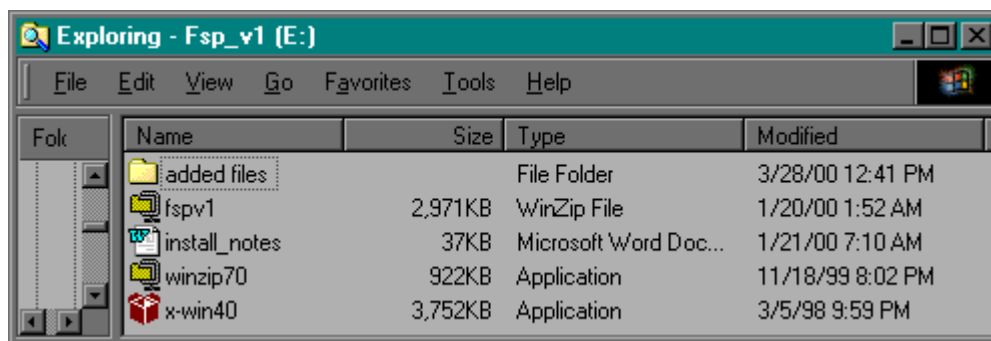
4.4.1 SYSTEM REQUIREMENTS

- Display settings should be at least 256 colors, 800x600 pixels (needed for graphics program Ace (aka xmgr))
- TCP/IP networking protocol must be installed for the Starnet X-Server software required for the graphics program Ace (aka xmgr). See Start Menu – Settings – Control Panel – Network.
- WinZip is required for installation. (WinZip 7.0 Evaluation Copy is available as winzip70.exe.) WinZip is available from www.winzip.com.
- The installation files require approximately 15 Mb on Drive C. This estimate includes 2.5 Mb for WinZip and 5.5 Mb for the Starnet X-Server.
- Pentium II or III and Windows 95, 98 or NT Version 4.

4.4.2 INSTALLATION

Steps 1 through 5 create a scratch directory, load the necessary software, and unpack the FSP Version 1.0 archive in C:\fspv1.

1. Check that the CDROM contains the following files. In the figure below, Windows Explorer was used to check the contents of the CD-ROM, which was loaded on Drive E.



2. Create the C:\tmp directory required for execution (fsp, rstrip.) If input files will reside on another drive, then a \tmp directory must also be created on that drive. The \tmp directory is used for scratch files.

3. ***This step can be skipped if X-Server software such as Hummingbird Exceed is already resident.*** Install the evaluation copy the Starnet x-win32 X-Server software (needed for graphics program Ace (aka xmgr). Execute x-win40.exe from the CDROM. Choose a typical installation and the default location. Enter “demo” (without the “ ”) as the serial number when requested. X-win32 is available from www.starnet.com.
4. ***This step can be skipped if WINZIP or a WINZIP compatible file utility program is already resident.*** Install the evaluation copy the WinZip file utility software (needed to decompress and load the fspv1.zip archive file). Execute winzip70.exe from the CDROM. Choose a typical installation and the default location. Choose to have WinZip start with the “Classic interface” when asked. Note that WinZip is only needed for the next step in the installation. Once the installation has been satisfactorily completed, WinZip can be removed from the system via the Control Panel Add/Remove Programs dialog if desired.
5. Use WinZip to extract all the files **from** fspv1.zip **to** C:\ using the path names in the WinZip archive (**be sure to select the radio button for “All files” and check the checkbox for “Use folder names”**).

Steps 6 through 10 create actions for specific file types (file extensions) in Windows Explorer. These actions are then available on the pop-up menu that is launched by right clicking on a file. These actions can then be used to execute FSP and related programs against the selected file.

Notes:

When browsing for Wordpad in the subsequent steps, the Wordpad.exe is usually located in C:\Program Files\Accessories.

In the steps below, when adding the “%1” in the subsequent steps, there should be a space after the .bat or .exe and before the “%1”. Also, the “ ” around the %1 are to be included because they protect pathnames that may include blank characters.

6. Use Windows Explorer View Menu - Folder Options – File Types tab to setup actions for the new file type *.i files.

<u>File Description</u>	<u>Action</u>	<u>Command</u>
FSP Input “%1”	Edit	Browse and select Wordpad then add
	Run FSP	C:\fspv1\fsp.bat “%1”

7. Use Windows Explorer View Menu - Folder Options – File Types tab to setup an action for the new file type *.o files.

<u>File Description</u>	<u>Action</u>	<u>Command</u>
-------------------------	---------------	----------------

FSP Output	Edit	Browse and select Wordpad then add
“%1”		

- Use Windows Explorer View Menu - Folder Options – File Types tab to setup actions for the new file type **.inp* files.

<u>File Description</u>	<u>Action</u>	<u>Command</u>
Rstrip Input	Edit	Browse and select Wordpad then add
“%1”		
	Run Rstrip	C:\fspv1\fsp.bat “%1”

- Use Windows Explorer View Menu - Folder Options – File Types tab to setup an action for the new file type **.out* files.

<u>File Description</u>	<u>Action</u>	<u>Command</u>
Rstrip Output	Edit	Browse and select Wordpad then add
“%1”		

- Use Windows Explorer View Menu - Folder Options – File Types tab to add the Run Ace action for the existing file type **Folder**.

<u>File Description</u>	<u>Action</u>	<u>Command</u>
Folder	Run Ace	C:\fspv1\ace.bat “%1”

4.4.3 FSP VERSION 1.0 FILES

Table 4.1 lists the files in the WinZip archive including the date and time last modified, file size and pathname for installation. Installation Step 5 (above) uses this pathname to load these files in the proper directory structure.

The .bat files supplied with FSP depend upon the directory structure created under C:\fspv1 by Installation Step 5.

The directories C:\fspv1\fsp\test files\ and C:\fspv1\fsp\test files\r5mbg146.ace contain example inputs and outputs. These files are not necessary for FSP Version 1.0 execution and may be deleted if so desired. All other files are needed for execution of FSP Version 1.0, Rstrip and the graphics program Ace (aka xmgr).

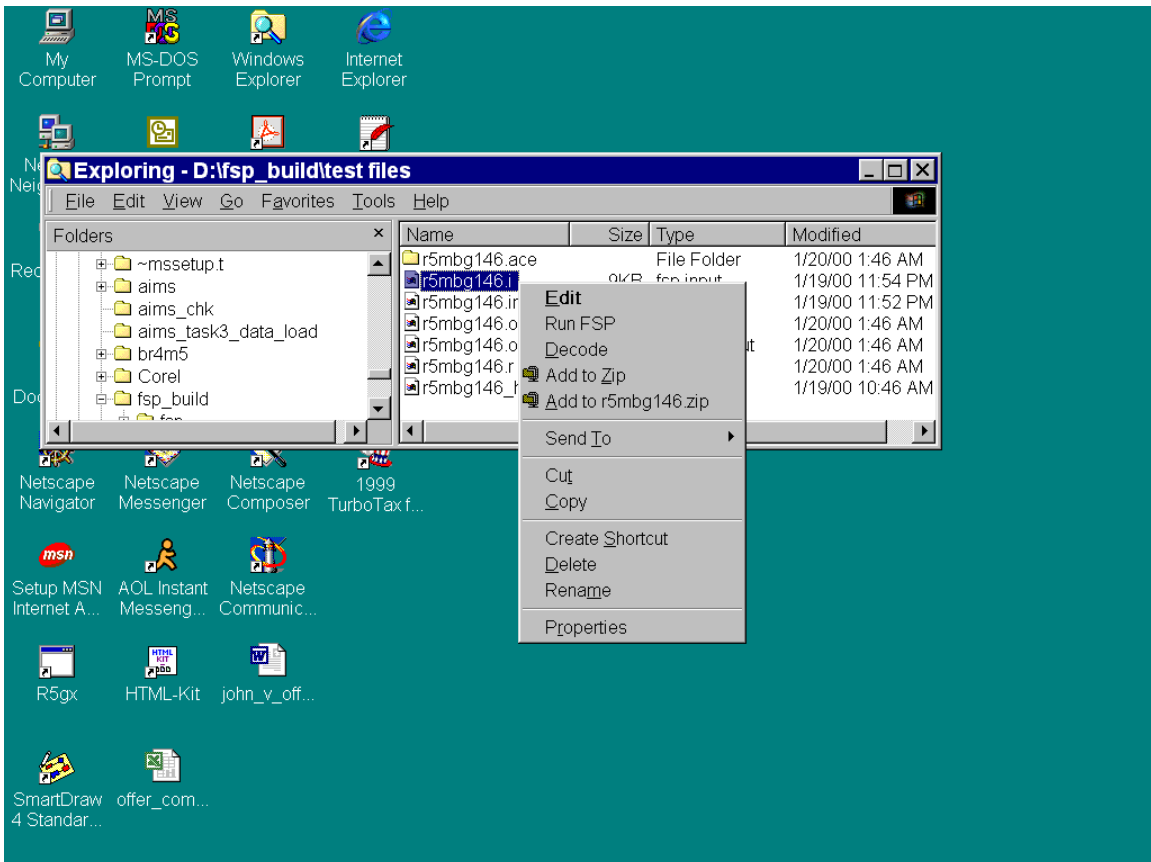
4.4.4 CODE EXECUTION

4.4.4.1 Editing a File

The following file types may be viewed or edited with Wordpad:

<u>File Type</u>	<u>Extension</u>
FSP Input	.i
FSP Output	.o
Rstrip Input	.inp
Rstrip Output	.out

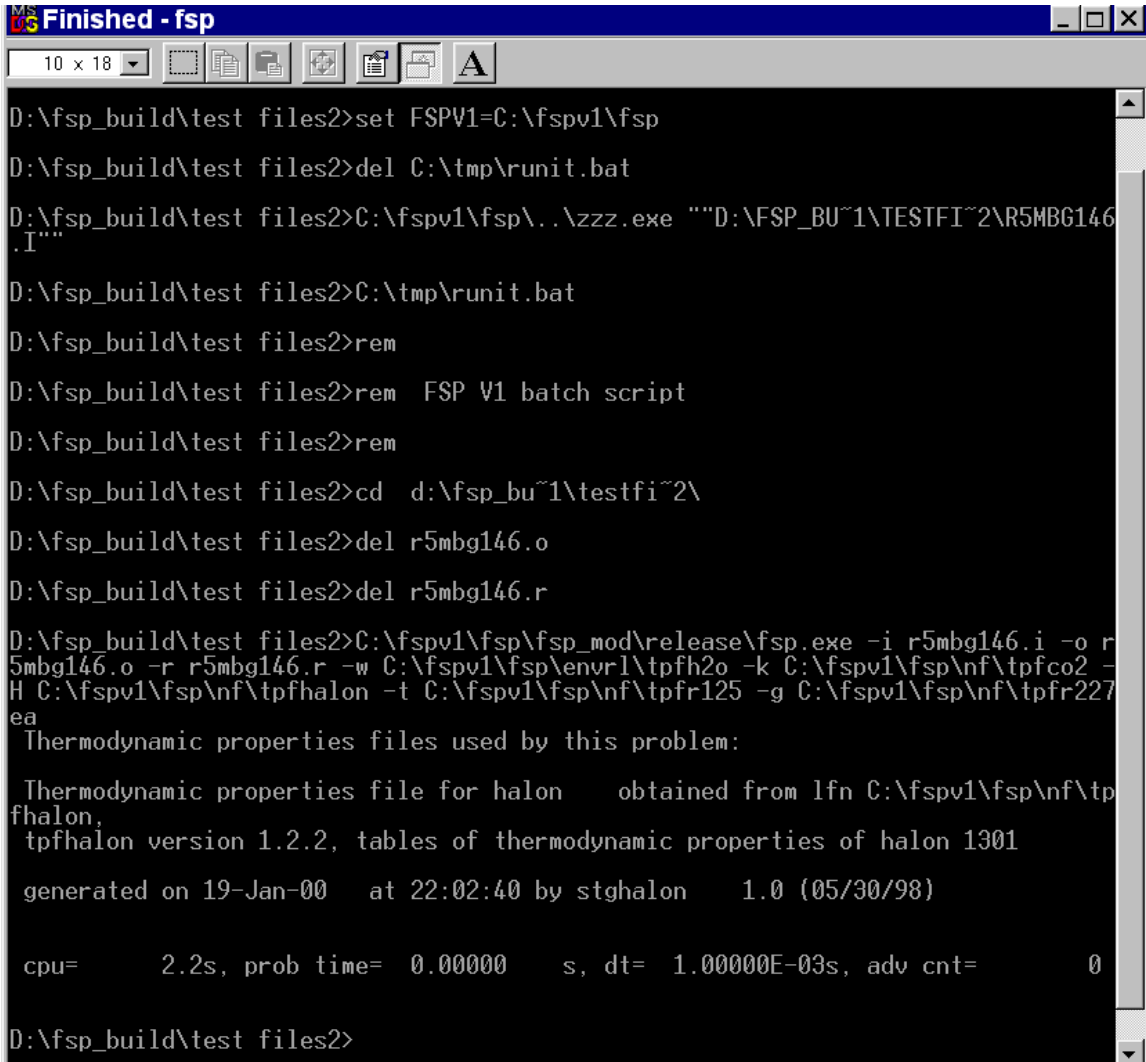
For example, view the test directory C:\fspv1\fsp\test files with Windows Explorer. Then select an input file such as R5mbg146.i with **one left click of the mouse**. Then, **right click the selected file with the mouse**. A pop-up menu will appear as shown below. This menu will include the actions created for *.i files in Installation Step 6.



Selecting the **E**dit action will launch Wordpad to view or edit the file.

4.4.4.2 FSP Execution

To execute FSP bring up the pop-up menu for a FSP Input file (*.i) as described above and select the **Run FSP** action. A MSDOS Window will open and messages will be displayed as the \tmp\runit.bat file executes the FSP application as shown below. For long runs this Window may be minimized. After the run is completed, the Window name will indicate “Finished”. Then, the Window may be closed.

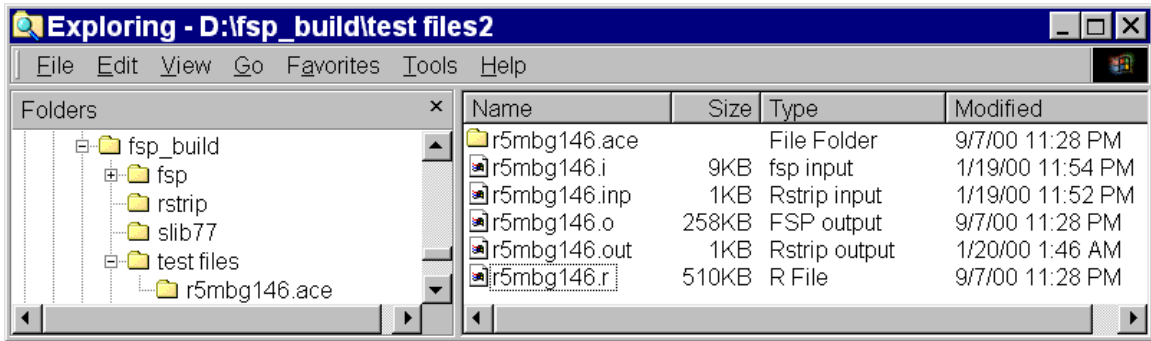


```
D:\fsp_build\test files2>set FSPV1=C:\fspv1\fsp
D:\fsp_build\test files2>del C:\tmp\runit.bat
D:\fsp_build\test files2>C:\fspv1\fsp\..\zzz.exe ""D:\FSP_BU~1\TESTFI~2\R5MBG146
.I""
D:\fsp_build\test files2>C:\tmp\runit.bat
D:\fsp_build\test files2>rem
D:\fsp_build\test files2>rem FSP V1 batch script
D:\fsp_build\test files2>rem
D:\fsp_build\test files2>cd d:\fsp_bu~1\testfi~2\
D:\fsp_build\test files2>del r5mbg146.o
D:\fsp_build\test files2>del r5mbg146.r
D:\fsp_build\test files2>C:\fspv1\fsp\fsp_mod\release\fsp.exe -i r5mbg146.i -o r
5mbg146.o -r r5mbg146.r -w C:\fspv1\fsp\envr1\tpfh2o -k C:\fspv1\fsp\nf\tpfco2 -
H C:\fspv1\fsp\nf\tpfhalon -t C:\fspv1\fsp\nf\tpfr125 -g C:\fspv1\fsp\nf\tpfr227
ea
Thermodynamic properties files used by this problem:

Thermodynamic properties file for halon obtained from lfn C:\fspv1\fsp\nf\tp
fhalon,
tpfhalon version 1.2.2, tables of thermodynamic properties of halon 1301
generated on 19-Jan-00 at 22:02:40 by stghalon 1.0 (05/30/98)

cpu= 2.2s, prob time= 0.00000 s, dt= 1.00000E-03s, adv cnt= 0
D:\fsp_build\test files2>
```

Output and restart-plot files will be created in the same directory. These files will have the same base name as the input file. The output file will have a .o extension and the restart-plot file will have a .r extension as shown below.



4.4.4.3 Rstrip Execution

To execute Rstrip bring up the pop-up menu for an Rstrip Input file (**.inp*) as described above and select the **Run Rstrip** action. A MSDOS Window will open and messages will be displayed as the `\tmp\runit.bat` file executes the Rstrip application as shown below.

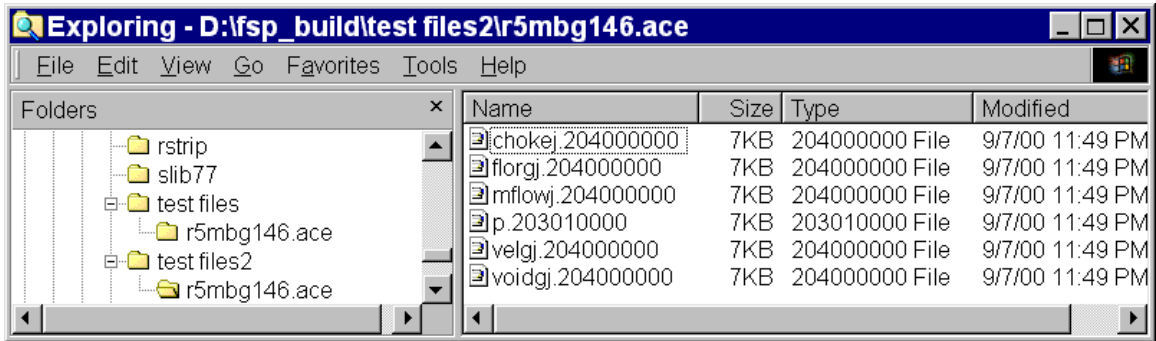
This Window may be minimized; however, the `\tmp\runit.bat` script prompts user before deleting all the files in a directory. If the Window is minimized the prompt will not be seen and the `\tmp\runit.bat` script will remain waiting for a response.

Answer the “Are you sure (Y/N)?” prompt in the MSDOS Window with a **y** or **Y** and **Enter** if the directory name indicated is of the form `\tmp\ace##\`.

After the run is completed, the Window name will indicate “Finished”. Then, the Window may be closed.

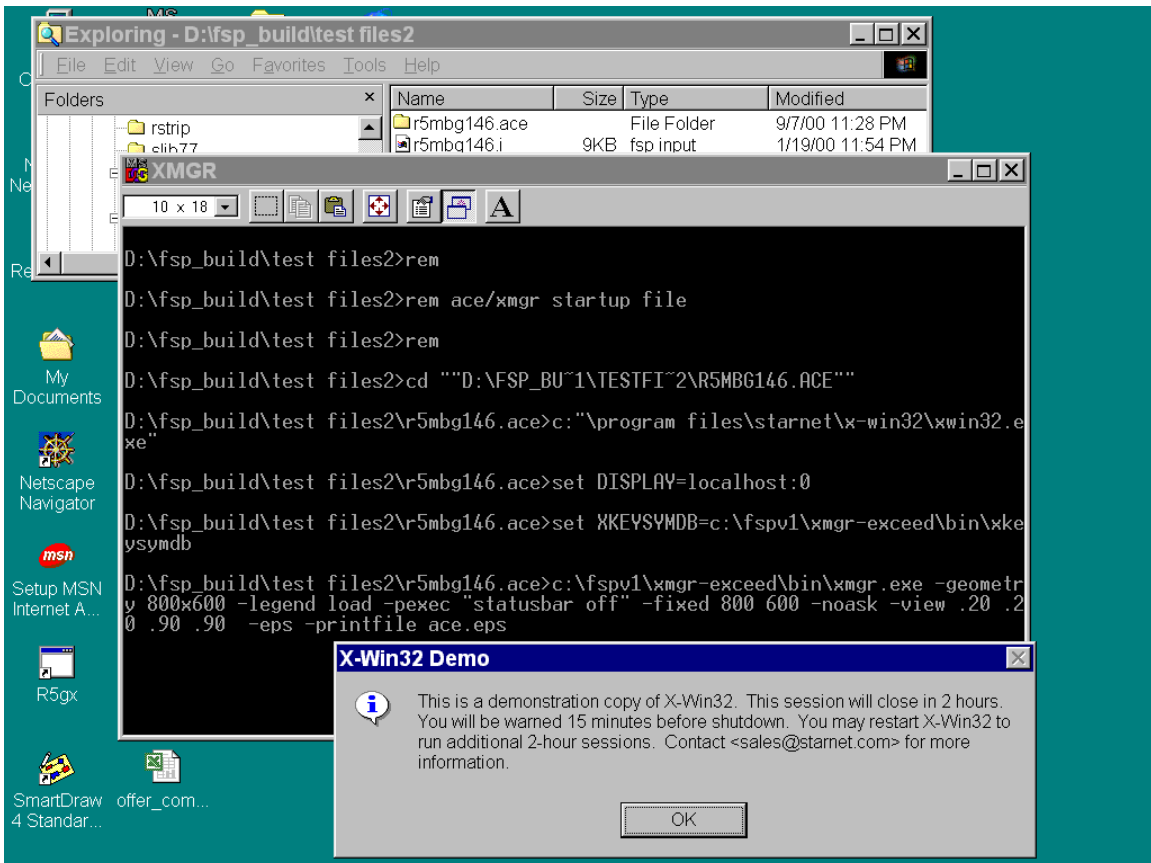
An output with the same base name as the input file will be created in the same directory. The output file will have a **.out** extension.

A sub-directory with the same base name as the input file will be created in the same directory. This sub-directory will have a **.ace** extension. The sub-directory will contain a file for each minor edit variable stripped from the restart-plot file as shown below. The names of the individual files will be formed using the FSP minor edit variable name and the FSP notation for volume, junction or control variable number. For example file `p.203010000` will contain the time and pressure values for volume 20301.



4.4.4.3 Ace (aka xmgr) Execution

To execute the Ace graphics package bring up the pop-up menu for an (**.ace*) directory as described previously and select the **Run Ace** action. A MSDOS Window will open and messages will be displayed as the \fspv1\ace.bat file brings up x-win32 X-Server as shown below.



Dismiss the X-Win32 Demo message by clicking on the OK button.

Ace will then display an empty plot area. Use the File menu and select Read Sets. A Read Sets file selection dialog will then pop-up. Left Click on one of the minor edit data files shown in the Read Sets file selection dialog and then left click on the OK button. A plot of the data will then be created as shown below.

When finished looking at plots of the FSP results, use the File menu and choose Exit to close the Ace graphics program. Also close the X-Win32 X-Server that runs minimized by right clicking on its icon in the taskbar and choosing Close.

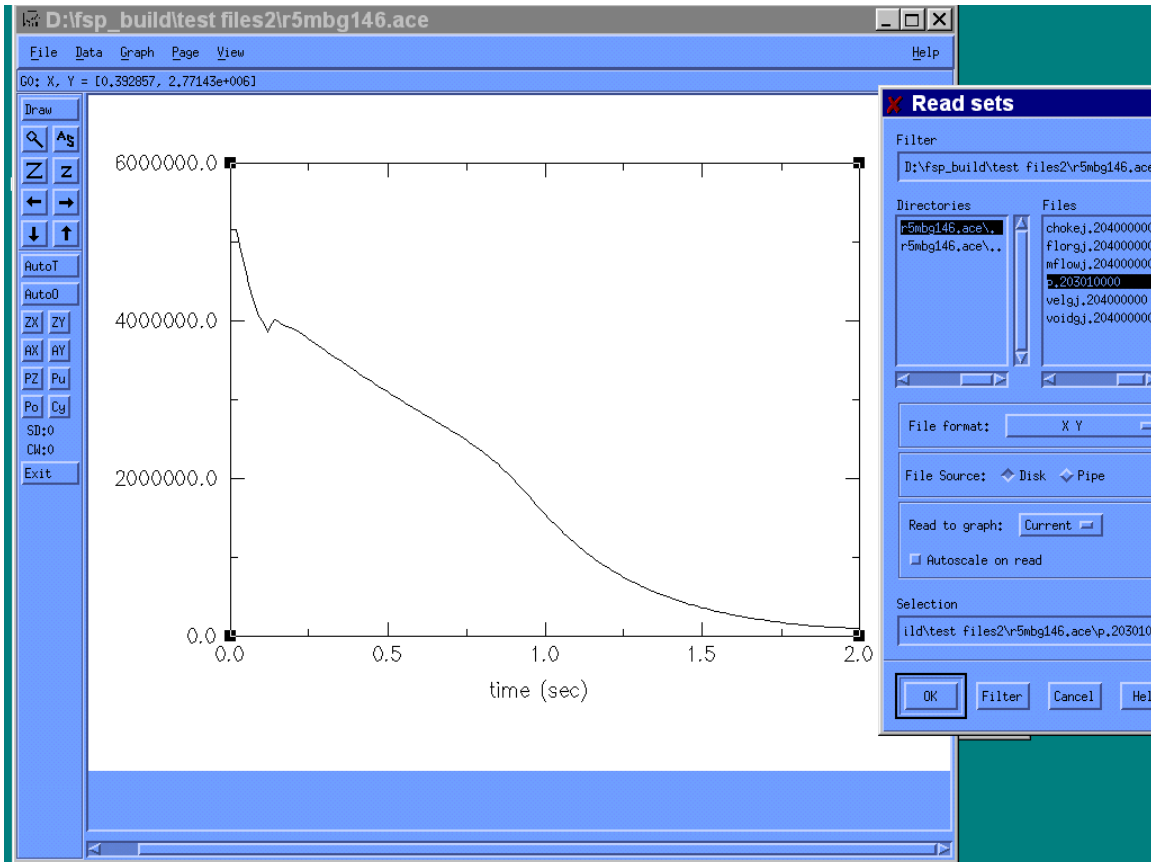


Table 4.4.1 - Contents of the WinZip Archive fspv1.zip

<u>File Name</u>	<u>Modified</u>	<u>Size</u>	<u>Path</u>
Ace.bat	1/19/00 10:50 PM	326 fspv1\	
Ace.pif	1/20/00 01:48 AM	967 fspv1\	
Fsp.bat	1/19/00 11:11 PM	212 fspv1\	
Fsp.PIF	1/20/00 01:46 AM	967 fspv1\	
Zzz.exe	1/19/00 11:06 PM	340,011 fspv1\	
Tpvh2o	1/18/00 11:09 PM	129,440 fspv1\fsp\envr1\	
Fsp.exe	1/20/00 01:35 AM	2,105,344 fspv1\fsp\fsp_mod\Release\	

<u>File Name</u>	<u>Modified</u>	<u>Size</u>	<u>Path</u>
Tpfco2	1/19/00 10:02 PM	62,344	fspv1\fsp\nf\
Tpfhalon	1/19/00 10:02 PM	85,136	fspv1\fsp\nf\
Tpfr125	1/19/00 10:02 PM	117,544	fspv1\fsp\nf\
TpfHFC-227ea	1/19/00 10:03 PM	100,048	fspv1\fsp\nf\
R5mbg146.i	1/19/00 11:54 PM	8,194	fspv1\fsp\test files\
R5mbg146.inp	1/19/00 11:52 PM	164	fspv1\fsp\test files\
R5mbg146.o	1/20/00 1:46 AM	263,305	fspv1\fsp\test files\
R5mbg146.out	1/20/00 1:46 AM	937	fspv1\fsp\test files\
R5mbg146.r	1/20/00 1:46 AM	521,368	fspv1\fsp\test files\
R5mbg146_hp.o	1/19/00 10:46 AM	266,429	fspv1\fsp\test files\
Chokej.204000000	1/20/00 1:46 AM	6,529	fspv1\fsp\test files\r5mbg146.ace\
Florgj.204000000	1/20/00 1:46 AM	6,529	fspv1\fsp\test files\r5mbg146.ace\
Mflowj.204000000	1/20/00 1:46 AM	6,538	fspv1\fsp\test files\r5mbg146.ace\
p.203010000	1/20/00 1:46 AM	6,524	fspv1\fsp\test files\r5mbg146.ace\
Velgj.204000000	1/20/00 1:46 AM	6,535	fspv1\fsp\test files\r5mbg146.ace\
Voidgj.204000000	1/20/00 1:46 AM	6,529	fspv1\fsp\test files\r5mbg146.ace\
Rstrip.exe	1/20/00 12:27 AM	319,488	fspv1\rstrip\
C	9/22/97 11:21 AM	3,184	fspv1\xmgr-exceed\bin\
Hcabout.dll	9/22/97 11:21 AM	153,600	fspv1\xmgr-exceed\bin\
Hcaboutn.nls	9/22/97 11:21 AM	30,208	fspv1\xmgr-exceed\bin\
Hclctl.dll	9/22/97 11:21 AM	18,944	fspv1\xmgr-exceed\bin\
Hclctl3d.dll	9/22/97 11:21 AM	26,112	fspv1\xmgr-exceed\bin\
Hcllocal.dll	9/22/97 11:21 AM	12,288	fspv1\xmgr-exceed\bin\
Hclnls.dll	9/22/97 11:21 AM	8,192	fspv1\xmgr-exceed\bin\
Hclt.dll	9/22/97 11:21 AM	6,656	fspv1\xmgr-exceed\bin\
Hclwprod.dll	9/22/97 11:21 AM	18,944	fspv1\xmgr-exceed\bin\
Hclwutil.dll	9/22/97 11:21 AM	31,232	fspv1\xmgr-exceed\bin\
Hclxpmon.dll	9/22/97 11:21 AM	47,616	fspv1\xmgr-exceed\bin\
Hclxport.dll	9/22/97 11:21 AM	39,424	fspv1\xmgr-exceed\bin\
Nls.dir	9/22/97 11:21 AM	1,788	fspv1\xmgr-exceed\bin\
Pout.dat	3/19/98 09:27 PM	12,216	fspv1\xmgr-exceed\bin\
Xerror.db	9/22/97 11:21 AM	8,604	fspv1\xmgr-exceed\bin\
XkeysymDB	12/21/99 09:35 PM	4,696	fspv1\xmgr-exceed\bin\
Xlib.dll	9/22/97 11:21 AM	279,040	fspv1\xmgr-exceed\bin\
Xmgr.exe	9/21/97 10:14 PM	1,785,856	fspv1\xmgr-exceed\bin\
xt.dll	9/22/97 11:21 AM	185,856	fspv1\xmgr-exceed\bin\

Total
Number of files:43 **Size: 7,035,864Mb**

4.5 INPUT PREPARATION AND SAMPLE PROBLEM

This section describes input preparation and code execution for a typical sample problem. The Lehigh test configuration is chosen for simulation. The information presented here, along with the input manual shown in Appendix A, can be used to understand how to develop an input model of a desired suppressant delivery system using the FSP code. The intent of this section is to describe how the user can set up an input file, and examine relevant output variables to analyze the performance of a suppressant delivery system.

4.5.1 System Configuration

The Lehigh University experimental set up consists of a test section made of a 200-cm long 2" Schedule 80 commercial steel pipe. The test section is considerably longer than typical supply vessels, but the specific geometry is chosen to enable an accurate measurement of the liquid level inside the test section, and subsequent determination of the discharge mass flow rate from the test section. The bottom of the test section is equipped with a Marotta quick-opening valve. The discharged fluid is piped through a 11-ft long ½" Schedule 80 steel pipe to a recovery tank. The recovery tank is about 10" in diameter and has a volume of approximately 28 liters. The pressure in the storage tank is expected to range from 1 to 3 atm at room temperature. Cooling tubes are installed inside the storage tank to achieve the desired downstream pressure and temperature between tests and also to condense vapor and return the liquid agent for subsequent tests. The top of the test section is connected to a nitrogen bottle, for initial pressurization. Figure 4.5.1 shows the schematic of the experimental set-up. Liquid nominally occupies 60% of the test section.

4.5.2 Development of FSP Model

In developing the input model, the physical system is typically discretized into a series of cells or volumes (called SNGLVOL components). These cells or volumes are interconnected via junctions (called SNGLJUN components). The physical dimensions of the system are specified via the geometrical input data associated with these volumes and junctions. Initial fluid thermodynamic conditions are specified for each cell, and initial flow conditions are specified for each junction. Appendix A provides the details of the required input data. To further facilitate the development of an input model, FSP has other built-in special components that can be used to represent typical piping systems. These components include PIPE, VALVE, and BRANCH components. A PIPE component is simply a collection of a number of cells connected by junctions, and is most appropriate to model a physical piping section. This is more convenient to use than specifying a number of SNGLVOL and SNGLJUN components to represent each cell and flow path inside the pipe section.

For the sample problem described here (i.e., the Lehigh apparatus), the vertical test section is represented by a PIPE component 100 with 10 cells. The horizontal discharge pipe is modeled by another PIPE component 300 with 15 cells. A VALVE component (203) is used to model the Marotta valve connecting the bottom of the test section to the discharge

pipe. The collection vessel is modeled by a SNGLVOL component 500. Finally, the connection between the end of the discharge pipe and the collection vessel is represented by a SNGLJUN component 403. Note that the outlet of the system in this case is the storage tank, and it has been modeled using a SNGLVOL component. This is because, in this experiment, the pressure in the storage tank would increase during the experiment, and at some point would have an effect on the system due to its back pressure on the system. This model tries to account for this effect and hence models the storage tank as an 'active' volume. In a design simulation using the FSP code, the outlet would discharge into a large room or the atmosphere, whose pressure would not be affected by the discharge of the agent. To model that situation, the user should use a TMDPVOL component to represent the outlet volume, set at a constant pressure.

The FSP nodalization diagram is shown in Figure 4.5.2. The following presents the details of input data development for the various components used to represent the Lehigh apparatus. The major reference for this section is the Crane Technical Paper No. 410, 24th Printing, (1988). The major components of the experimental set-up are modeled as follows.

Test Section: PIPE component 100

The test section is a 2-m long 2" Schedule 80 commercial steel pipe. In the particular test simulated (Test 3 from Configuration 1), 61.9% of the test section is occupied by liquid agent (i.e., initial liquid level is 1.238 m from test section bottom). From Crane (1988), the ID of the test section is

$$ID = 1.939'' = 0.04925 \text{ m, from Crane, page B-16}$$

Refer to Appendix A, the required input data for this component are as follows (all input are in SI units per Appendix A unless otherwise specified)

Component No.= 100

No. of Volumes = 10

$$\text{Volume Area} = \pi(ID)^2/4 = \pi(0.04925)^2/4 = 1.9050e-3$$

Junction Flow Area = 1.905e-3 or default

Volume Length

In order to model the initial liquid height exactly, the section is discretized such that the top 4 cells have a total length of 0.762 m, and the bottom 6 cells 1.238 m. Hence, the volume length input data are given by: 0.200 for cells 1 to 3; 0.162 for cell 4; 0.238 for cell 5; and 0.200 for cells 6 to 10. Note that the test section is oriented downwards, with cell No. 1 at the top and cell No. 10 at the bottom.

Other Geometrical Input

Volume of Volume = 0.0, default

Vertical Angle = -90°

Elevation Change = Volume Length x sin(Vertical Angle) = negative of the volume lengths

Roughness = 1.5e-4 ft = 4.572e-5 for commercial steel, from Crane, page A-23

Hydraulic Diameter = ID = 0.04925 or default

Forward Loss Coefficient = 0.0, straight pipe

Reverse Loss Coefficient = 0.0, straight pipe
Volume Control Flag = 00000
Junction Control Flag = 000000
Volume Initial Condition Option = 04 for Volumes 1 – 4, and 13 for remaining volumes

Initial Conditions:

As mentioned before, the test section is initially 61.9% agent filled. The test section is subdivided into 10 cells with the bottom 6 cells filled with liquid, and the top 4 cells filled with a mixture of agent vapor and nitrogen. Thus, for Volumes 1-4, the initial condition option No. 4 (see Appendix A) is used to accommodate the presence of noncondensable gas (i.e., nitrogen). The theoretical equilibrium gaseous (vapor + noncondensable) quality is 1.0 (since no liquid is present). For reasons attributed to the numerical solution method of the code, however, it is recommended that a value close to, but less than 1.0 be used. Using a value of 1.0 has led to the code grinding down to small time steps and in some cases, stop running altogether. Experience shows that a value of 0.98 mitigates the problem, without affecting the physics of the model, and is hence used in this sample problem.

For Volumes 5-10, only liquid (with dissolved nitrogen) is present. Hence initial condition option No. 13 is used which allows the user to specify the pressure and temperature, and account for dissolved nitrogen. For this sample problem, the initial filled pressure is 4.180 MPa, and the initial system temperature is 305 K.

Junction Initial Condition Option = 1, specify mass flow
Junction Initial Conditions: zero flow

The initial concentration (based on mass) of dissolved nitrogen is calculated as follows.

Initial Concentration of Dissolved Nitrogen

As discussed in Section 4.2.4.6, FSP uses the total pressure in Henry's law to calculate the mole fraction of the dissolved nitrogen in the liquid solution. Theoretically, the partial pressure of nitrogen should have been used, but it poses difficulty for numerical implementation. To be consistent with this approximation, the initial equilibrium concentration of dissolved nitrogen should also be calculated using the total pressure. Thus, the initial mole fraction of dissolved nitrogen is calculated as

$$x_{N,i} = HP_i$$

where H is the Henry's constant given in Section 4.2.4.6 and P_i is the initial system pressure. The required mass concentration (mass of dissolved nitrogen per unit mass of liquid) for input is:

$$X = x_{N,i} M_N / (1 - x_{N,i}) M_a = HP_i M_N / (1 - HP_i) M_a$$

where M_N and M_a are the molecular weight of nitrogen and liquid agent. The liquid agent in this case is HFC-227ea, which has the formula, C_3HF_7 . So, in the sample problem, this is evaluated as:

$$H = 2.347767 \times 10^{-7} - 1.55063 \times 10^{-9} (305) + 2.957799 \times 10^{-12} (305)^2 = 3.698 \times 10^{-8}$$

$$X = (3.698 \times 10^{-8})(4180000) 28 / [1 - (3.698 \times 10^{-8})(4180000)](170) = 0.03012$$

Since dissolved gas is only present in the liquid, the initial dissolved gas concentration is entered as 0.0 for Volumes 1 through 4, and as 0.03012 for Volumes 5 through 10.

Discharge Valve

The Marotta valve is a quick opening valve (with a stroke time of about 0.05 s). Discharge data for this valve were obtained by experiments at Lehigh University. The data show that the equivalent loss coefficient associated with the valve is about 1.5. Refer to Appendix A, the required input data are as follows:

Component No. = 203

Component Type = valve

From Connection Code = 100010000, outlet of Component 100

To Connection Code = 300000000, inlet of Component 300 (discharge pipe to be discussed later)

Area = default (i.e., minimum of adjacent volume areas)

Forward Loss Coefficient = 1.5, based on test data supplied by Lehigh University.

Reverse Loss Coefficient = 1.5.

Junction Flag = 000000

Discharge Coefficients = 1.0 for subcooled, 0.9 for both two-phase and single-phase vapor.

These values have been determined to be optimum during the data assessment stage.

Initial Condition Option = 0, specify velocity

Initial Conditions = zero velocity

Valve Type = trpvlv, for valve with negligible stroke time

Open Trip No. = 501, where Trip 501 is true when $t > t_1$ where t_1 is the steady state initialization period. A short steady state initialization period is recommended so that the system can adjust itself for hydrostatic pressure balance prior to opening of the valve. In this sample problem, a steady-state initialization period of 0.5 seconds has been allowed.

Discharge Pipe

The discharge pipe is a 11 ft long ½" Schedule 80 commercial steel pipe. Hence, from Crane (1988), the ID is given by

$$ID = 0.546'' = 1.3868 \times 10^{-2} \text{ m. from Crane, Page B-16}$$

Refer to Appendix A, the required input data are as follows:

Component No. = 300

Component Type = pipe

Number of Volumes = 15, to yield approximately 0.2-m grid size

$$\text{Volume Area} = \pi(ID)^2/4 = \pi(0.013868)^2/4 = 1.5105 \times 10^{-4}$$

Junction Flow Area = 1.5105e-4, or default

$$\text{Volume Length} = 3.3528/15 = 0.2235$$

Volume Volume = 0.0, default
Vertical Angle = 0°, horizontal, from Figure 5.1.1
Elevation Change = Volume Length x sin(Vertical Angle) = 0.0
Roughness = 1.5e-4 ft = 4.572e-5 for commercial steel, from Crane, page A-23
Hydraulic Diameter = ID = 0.013868 or default
Forward Loss Coefficient = 0.0, straight pipe
Reverse Loss Coefficient = 0.0, straight pipe
Volume Control Flag = 00000
Junction Control Flag = 000000

Initial Conditions:

Normally, the discharge pipe is predominantly air-filled at the collection vessel pressure, prior to the discharge test. Hence, the initial condition option No. 4 should be used. The quality is theoretically 1.0 (no liquid present). As discussed earlier, 0.98 is used in place of 1.0.

Volume Initial Condition Option = 4
Volume Initial Conditions: P = 7.200e5 Pa, T=305 K, Quality=0.98

In case that the back pressure and initial temperature do not allow the specification of a mixture of vapor and noncondensable, it is recommended that superheated vapor condition be used. For instance, if the back pressure is greater than the saturation pressure at the initial temperature, it would not be feasible to specify a mixture of vapor and noncondensable using Option No. 4. In that case, the given conditions will support the specification of single-phase superheated vapor. The user should then use Option No. 3 and input the given back pressure and temperature.

It should be mentioned that allowing air (or noncondensable) to be present downstream of the discharge valve causes computation difficulties occasionally. By replacing the air-filled condition by superheated vapor at the same pressure and temperature (if possible), the code's performance is decidedly improved. In situations where the specified back pressure and initial temperature do not allow the existence of single phase vapor, the back pressure may be adjusted accordingly to permit the existence of single phase vapor. Since the flow is expected to be choked at the discharge valve, the actual magnitude of the back pressure should have only minimal impact on the discharge transient. The user may need to experiment with both options 3 and 4 when computational difficulties are encountered.

Junction Initial Condition Option = 1, specify mass flow rate
Junction Initial Conditions = zero flow

Inlet to Storage Tank

The other end of the discharge pipe is connected to a storage tank, as shown in Figure 5.1.1. Refer to Appendix A, the required input data are as follows:

Component No. = 403
Component Type = sngljun, for single junction
From Connection Code = 300010000, outlet of Component 300

To Connection Code = 500000000, inlet of Component 500 (storage tank to be discussed later)

Junction Area = $1.5105e-4$, same as discharge pipe area

Forward Loss Coefficient = 1.0, sudden expansion, from Crane, Page A-29

Reverse Loss Coefficient = 0.5, assume sharp-edged, from Crane, Page A-29

Junction Flag = 000000

Discharge Coefficients = 1.0 for subcooled, 0.9 for two-phase and single-phase vapor. These values have been determined during the assessment stage.

Initial Condition Option = 1, specify mass flow rates

Initial Conditions = zero flow

Storage Tank

The storage tank is approximately 10" in diameter and has a volume of about 28 liters (or 0.028 m^3). During a test run, its pressure will increase due to the build up of discharge fluid. Between tests, the tank and its content may be cooled to bring the system back down to a desirable pressure and temperature level. Refer to Appendix A, the required input data are as follows:

Component No. = 500

Component Type = snglvol, for single volume

Volume Flow Area = $\pi/4 (\text{ID})^2 = \pi/4 (0.254)^2 = 0.05067$

Length of Volume = 0.0, default

Volume of Volume = 28 liters = 0.028

Inclination Angle = -90°

Elevation Change = $-(\text{Volume}/\text{Area}) = -(0.028/0.05067) = -0.5525$

Roughness = $1.5e-4 \text{ ft} = 4.572e-5$, assume commercial steel, from Crane, page A-23

Hydraulic Diameter = 0.0, default

Control Flag = 00000

Initial Conditions

The discussion of the initial conditions in the discharge pipe applies here.

Initial Condition Option = 4

Initial Conditions: $P = 7.200e5 \text{ Pa}$, $T=305 \text{ K}$, Quality=0.98

Note that for numerical stability, the user may need to approximate the storage tank conditions as single-phase vapor at the desired pressure and temperature, as discussed before.

Nitrogen Release Model

The nitrogen release model has been discussed in Section 4.2.4.6. It requires four user input data: the release coefficient (Γ_0), critical radius (r_c), initial pressure (P_i) and the initial system temperature (T_i). Note that P_i and T_i are the conditions just prior to discharge. They may be different from the so-called fill pressure and fill temperature. To evaluate P_i and T_i given the fill values, a code such as PROFISSY (Yang et al) could be used. Both the release coefficient and critical radius are semi-empirical. Section 2.4.6 has presented some sensitivity results. For the sample problem here, the following input data are specified:

$\Gamma_0 = 2000$
 $r_c = 10^{-8}$
 $P_i = 4.180 \times 10^6$, same as the initial system pressure
 $T_i = 305$, same as the initial system temperature

Trip Logic

The code allows the user to specify trip logic to perform certain logical operation, such as opening or closing a valve. In this problem, the Marotta valve is modeled as a trip valve with negligible stroke time. The valve is initially close. It opens at 0.5 s (0.5 s is a steady state initialization period). This behavior can be modeled in FSP by specifying one trip that opens at 0.5 s. For time less than 0.5 s, the trip is false, and the valve will remain at its initial specified position (which is close for this application). Refer to Appendix A, the following input data for the trips are used:

Trip 501: $t \geq 0.5$. Open Trip. This trip is true when time is greater than 0.5 s.

Control Variables

Control variables (CV) are used to monitor certain system responses, such as the collapsed liquid level in the test section and the integral discharge flow mass. This section documents the development of these control variables.

Collapsed Liquid Level: CV 010

$CV010 = \sum \text{Vol. Length}_i (\text{voidf})_i$, $i = 100010000$ through 100100000

Integrated Discharge Mass from bottle: CV 020

$CV020 = \int \text{mflowj @ } 203000000 \text{ dt}$

Integrated Discharge Mass from discharge pipe: CV 021

$CV021 = \int \text{mflowj @ } 403000000 \text{ dt}$

4.5.3. Input File Listing

In this sample problem, we have named the input file as *run1-3.i*. A listing of *run1-3.i* is given below.

```

= Lehigh Experiment, Configuration 1, Run 3
*
*****
*
* Test Conditions
  
```

```

*
* Fluid = HFC-227ea
* Initial Pressure = 4180 kPa
* Initial Temperature = 305.0 Deg.K.
* Initial Liquid Volume = 2358 ml
* Initial Liquid Height = 1.238 m
* (Based on x-section area of 1.9053e-03 m2)
* Initial Downstream Pressure = 720.0 kPa
*****
*
* Model Options
*
* CD (two-phase) = 0.9
* Gamma0 = 2000.0
* Crit. Radius = 1.00e-8 m.
*
*****
*
100 new      transnt
101 run
102 si      si
*
* Gamma0  CritRad  Pfill  Tfill
*
106 0.0  1.00e-08  4.180e06  305.0
*
110 nitrogen
*
* RefVol  Elev  Fluid  System
*
120 100010000  0.0  HFC-227ea  testsec
*
* Time Step Control
*
* End      Min      Req      Flags  Minor  Major  Restart
*
201 0.5  1.0e-6  0.001  00003  100   500   500
202 3.5  1.0e-6  0.0001 00003  500  5000  5000
*
* Minor Edit Variables Requested
* None requested, Cards 301-399 not necessary
*
* Trips
*
501 time  0  gt  null  0  0.5  1 *open discharge valve at 0.5
secs.
502 time  0  lt  null  0  0.0  1 *always false
*
*****
* Test Section, Component 100
*****
* Comp.Name Type
1000000 testsec pipe
* nv
1000001 10
* Vol.Area nv
1000101 1.9053e-3 10
* Jun.Area nj
1000201 0.0 9

```

```

*      Vol.Len      nv
1000301  0.200      03
1000302  0.162      04
1000303  0.238      05
1000304  0.200      10
*      Vol.Vol      nv
1000401  0.0         10
*      Vert.Ang     nv
1000601  -90.0       10
*      Elv.Chn      nv
1000701  -0.200     03
1000702  -0.162     04
1000703  -0.238     05
1000704  -0.200     10
*      Rough Dh      nv
1000801  4.57e-5  0.0  10
*      kf          kr      nj
1000901  0.0      0.0  9
*      Vol.Flag    nv
1001001  00000    10
*      Jun.Flag    nj
1001101  001000   9  *no choking option
*      IC          Pres    Temp    Qual    Dummy    nv
1001201  004     4.180e6  305.0  0.98  0.0  0.0  4
1001202  013     4.180e6  305.0  0.0  0.0  0.0  10
*      Vel(0)/Flow(1)
1001300  1
*      Liq Vap Int nj
1001301  0.0  0.0  0.0  9
*
*      Solute Concentration, KgN2/KgLiq
*
1002001  0.0      04
1002002  0.03012  10
*
*****
*      Marotta discharge Valve, Component 203
*****
*      Comp.Name Type
2030000  break  valve
*      From      To      Area    kf    kr      Flag      Cds
*                                          Liq  2p
Vap
2030101  100010000  300000000  1.5105e-4  1.5  1.5  000100  1.00  0.9  0.9
*      IC  Liq  Vap  Int
2030201  0  0.0  0.0  0.0
*      Valve Type
2030300  trpvlv
*      Trip No.
2030301  501
*
*****
*      Discharge Pipe, Component 300
*****
*      Comp.Name Type
3000000  dispipe  pipe
*      nv
3000001  15
*      Vol.Area    nv

```

```

3000101  1.5105e-4  15
*      Jun.Area      nj
3000201  0.0            14
*      Vol.Len       nv
3000301  0.2235         15
*      Vol.Vol       nv
3000401  0.0            15
*      Vert.Ang      nv
3000601  0.0            15
*      Elv.Chn       nv
3000701  0.0            15
*      Rough Dh      nv
3000801  4.57e-5  0.0  15
*      kf      kr      nj
3000901  0.0  0.0  14
*      Vol.Flag      nv
3001001  00000         15
*      Jun.Flag      nj
3001101  001000         14  *no choking option
*      IC      Pres      Temp      Qual      Dummy      Dummy      nv
3001201  004  7.200e5  305.0  0.98  0.0  0.0  15
*      Vel(0)/Flow(1)
3001300  1
*      Liq      Vap      Int      nj
3001301  0.0  0.0  0.0  14
*****
*      Inlet to Storage Tank, Component 403
*****
*      Comp.Name Type
4030000  inlet      sngljun
*      From      To      Area      kf      kr      Flag      Cds
*      Liq 2p Vap
4030101  300010000  500000000  1.5105e-4  1.0  0.5  000000  1.00  0.9  0.9
*      IC      Liq      Vap      Int
4030201  1  0.0  0.0  0.0
*****
*      Storage Tank, Component 500
*****
5000000  storage  snglvol
*      Area      Len      Vol      Azi      Incl      Elev      Rough      Dh
Flag
5000101  0.05067  0.0  0.028  0.0  -90.0  -0.5526  4.572e-5  0.0  00000
*      IC      Pres      Temp      Qual
5000200  4  7.200e5  305.0  0.98
*****
*
** Control Systems
*
*      Collapsed Liquid Level in Test Section (m)
*
20501000  level  sum      1.00  0.0  1
20501001  0.0    0.2      voidf  100010000
20501002  0.2    voidf  100020000
20501003  0.2    voidf  100030000
20501004  0.162  voidf  100040000
20501005  0.238  voidf  100050000
20501006  0.2    voidf  100060000
20501007  0.2    voidf  100070000
20501008  0.2    voidf  100080000

```

```
20501009      0.2      voidf  100090000
20501010      0.2      voidf  100100000
*
*   Integral discharge mass from bottle (kg)
*
20502000  intbrk  integral  1.00  0.0  1
20502001  mflowj  203000000
*
*   Integral discharge mass from pipe (kg)
*
20502100  intpipe  integral  1.00  0.0  1
20502101  mflowj  403000000
*
*
. end of input listing
```

4.5.4 Results & Data Comparison

A new case and keep track of the changes separately

The input file was named *run1-3.i*. The output from FSP consists of an ASCII output file (called *run1-3.o*) and a BINARY restart/plot file (*run1-3.r*). The ASCII output file records the major thermal hydraulic variables at time interval specified by the user through the Major Edit Frequency. The BINARY restart/plot file records most of the calculated variables at time interval specified by the user through the Restart Edit Frequency. Refer to Appendix A for details. The ASCII output file is useful in examining the conditions of the entire system at a given time. The BINARY restart/plot file is useful in examining the transient response of a particular variable. For general data comparisons, the restart/plot file is used. An extraction program has been provided to allow the extraction of any valid variable from the restart file and has been described in Section 4. A list of the valid variables in FSP is given in Appendix A. Once the variable is extracted, it can be plotted with or without the corresponding data for examination.

As discussed in Section 4, the first step is to create an input file containing the list of the variables the user wants to extract from the restart file for plotting. This file should be named *run1-3.inp*. In this example, we have chosen to examine the test section pressure, the collection vessel pressure, and the discharge mass flow rate. The following is the listing of *run1-3.inp*

```
rst01    c:\mydocu~1\fire-s~1\Lehigh~1\run1-3.r  
  
p 100010000  
p 500010000  
mflowj 203000000
```

Note that the first input line (the title card) specifies the full **DOS** path of the restart/plot file, and renames it to a file named “rst01”. The user may not modify the name “rst01”.

Upon execution of the **Rstrip** program (see Section 4.4.4.3), a directory *run1-3.ace* will be created under the current working directory. The following three files will be created by **Rstrip** in the *run1-3.ace* directory: *p.100010000*, *p.500010000*, and *mflowj.203000000*. Each of these files is simply the transient history of each variable (i.e., variable versus time).

If data comparison is desired, the corresponding data as a function of time must be created by the user. The format of any data file should be the same as the FSP data file, i.e., each data line contains time-data pair. There is no restriction to the naming of these user-created data files. In this example, we have created the following test data files: *pbot.dat* (measured test section pressure), and *pcv.dat* (measured collection vessel pressure). It is recommended that the data files be placed in the same directory as the FSP data files. In this example, *pbot.dat* and *pcv.dat* are placed in the *run1-3.ace* directory.

Next, the **Ace** program can be executed to plot any of the FSP data file created by **Rstrip** and any experimental data file created by the user. The execution instruction has been given in Section 4.4.4.4. For instance, to compare the calculated and measured test section pressure, follow Section 4.4.4.4 instruction to open the **Ace** window. Use the File menu and select

Read Sets. A Read Sets file selection dialog window will pop-up. Left Click on *p.100010000* and then left click OK. Left click on the **AS** button on the left menu bar to choose Automatic Scaling. A plot of the calculated pressure in cell 100-01 (i.e, the top of the test section) will appear. Return to the Read Sets file selection dialog window, Left Click on *pbot.dat* and then left click OK. The measured test section pressure will appear in the same plot. At this point, the user can add title and legend, change the line style of each curve, etc. The **Ace** graphic program allows the user to perform many tasks to customize each plot. The user should consult the **Ace** manual for instructions, or experiment with the various action items under the File, Data, Graph, Page and View menus.

When finished looking at the plots, use the File menu and choose Exit to close the Ace graphic program. The user can route the plot to a printer that supports **postscript** printing. Alternatively, the user can write the plot file to a **postscript** file. To generate the **postscript** file, use the File menu and choose Printer setup. A Printer setup window will pop up. Choose Postscript landscape in the “Device” dialog, File in the “Print to” dialog, type in the name of the postscript file to be created in the “Print Control String” box (by convention, this file should have extension ‘.eps’) and depress the “generate EPS” button. Left click the Print button. A file with the specified name will be created. This postscript file can then be imported to a document, or printed out later.

As an example, Figure 4.5.3 shows the comparison of the calculated and measured test section pressure for the sample problem, obtained using the above procedure. Looking at the results of the comparison, the user may want to conduct a sensitivity study by varying an input variable, such as r_c or Γ_0 . In this case, the user would change this parameter in the input file and re-run the case. It would be prudent to rename the input file when running.

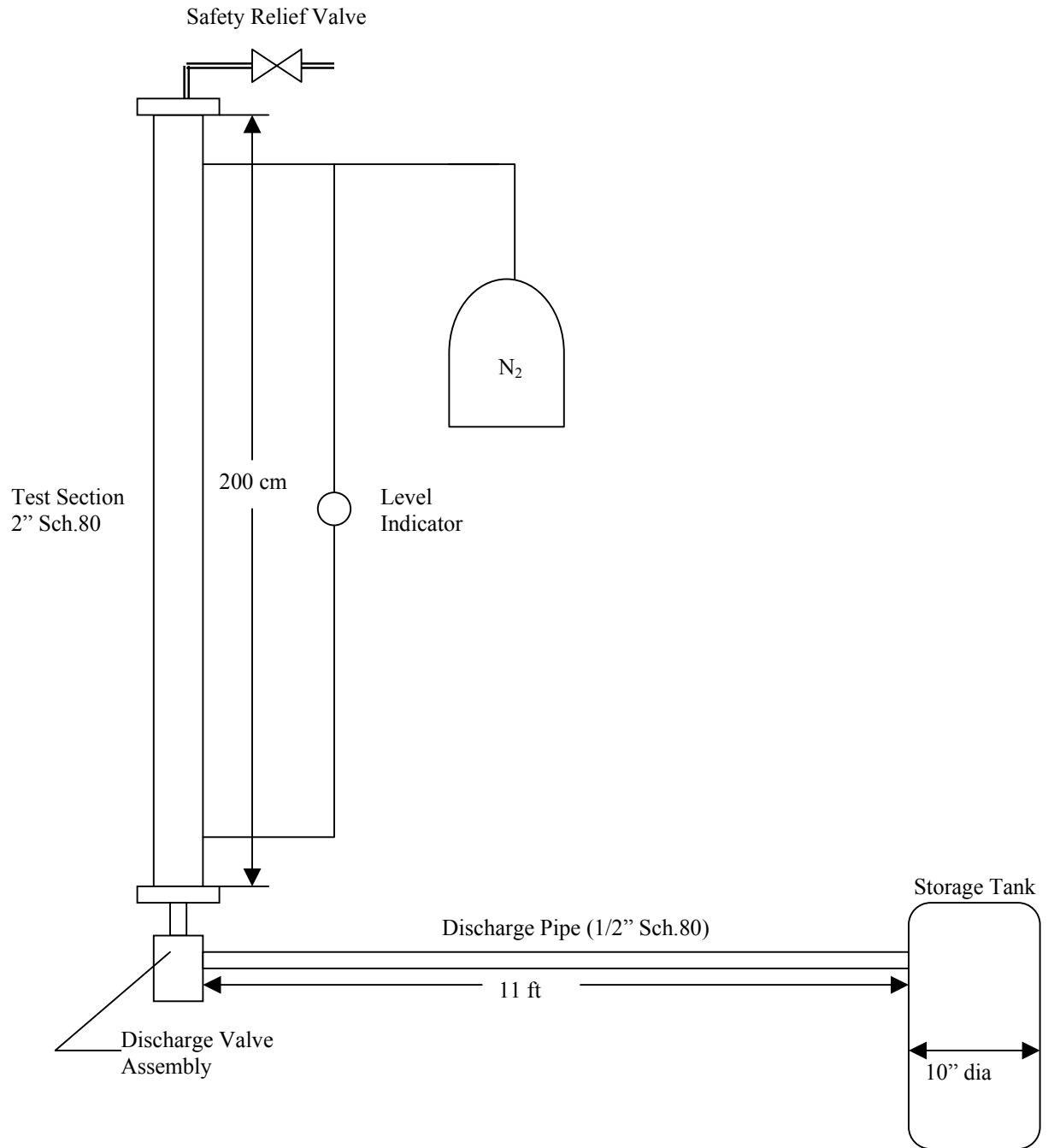


Figure 4.5.1: Schematic of Lehigh Test Apparatus

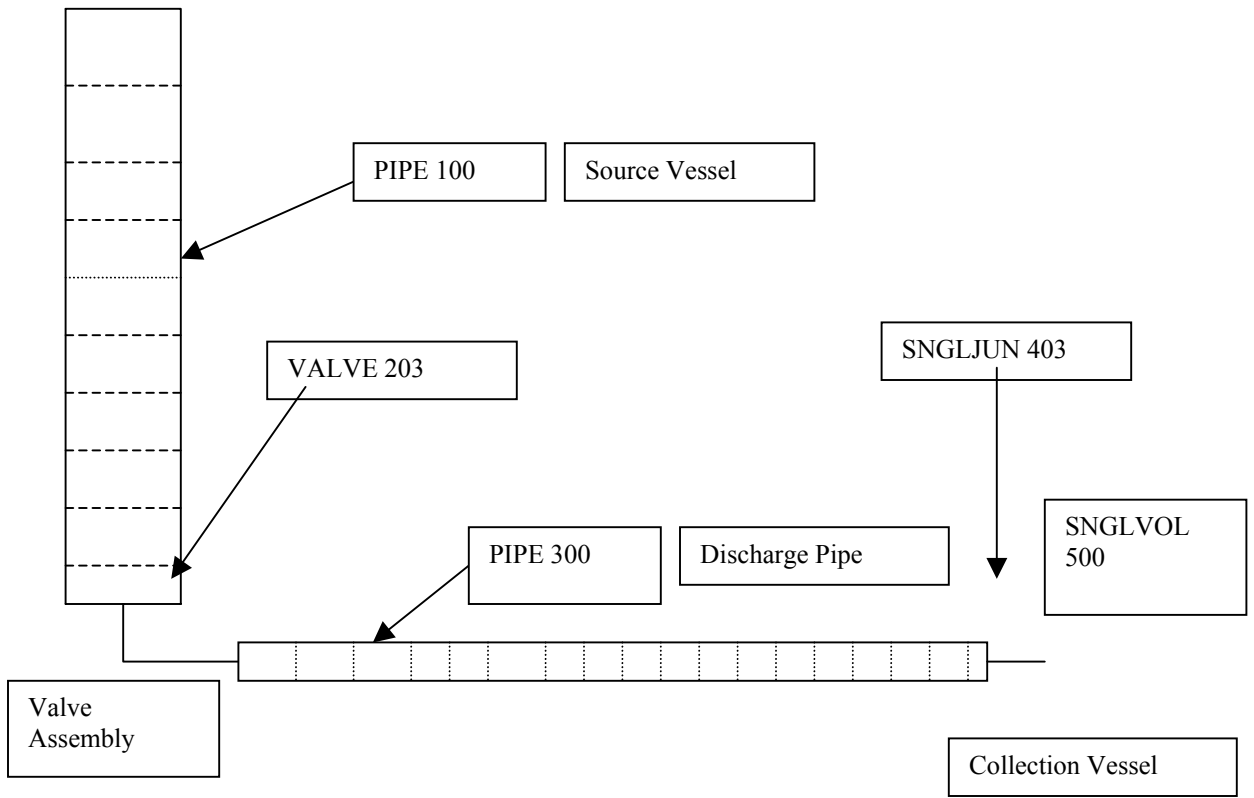


Figure 4.5.2: FSP Nodalization Diagram for Lehigh Tests

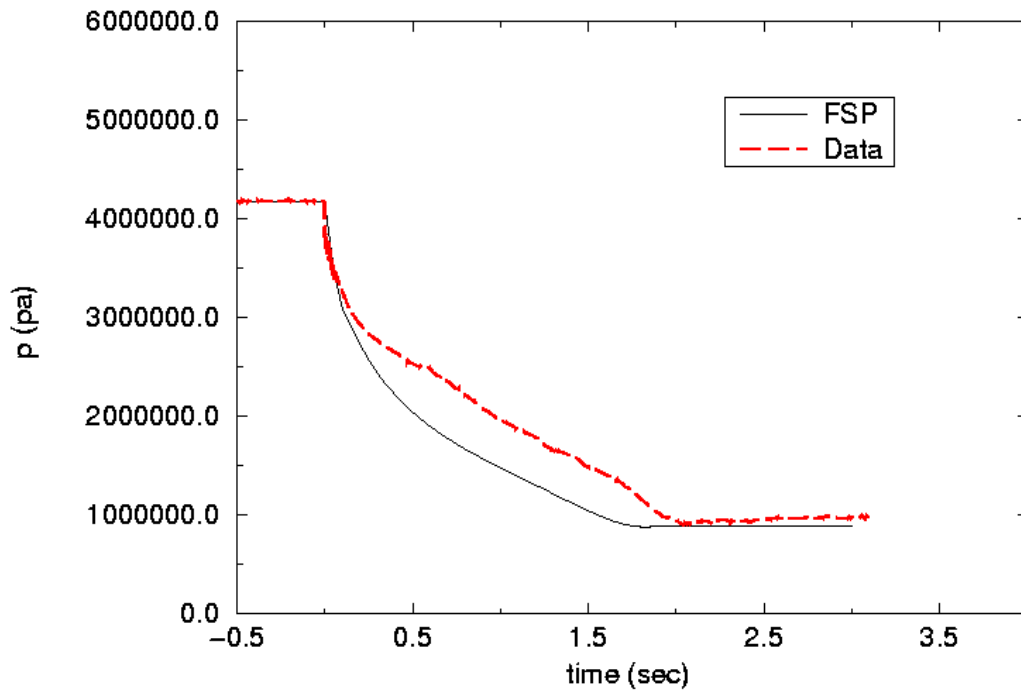


Figure 4.5.3: Comparison of Calculated and Measured Bottle Pressure for Sample Problem

4.6 ASSESSMENT AGAINST EXPERIMENTS

This section discusses some of the code assessments carried out against experiments. Early assessment of the FSP code was against Halon-1301 discharge experiments reported by Elliott et al (1984). These tests were carried out with three different system configurations. These included a bottle-nozzle arrangement, a bottle with straight pipe, and a bottle with a straight pipe branching to two separate exit legs. Test 146 from Elliott et al (1984) was with a bottle-nozzle arrangement. This test was used in early assessment of FSP. The results have been shown in Section 4.2.4.6 of this report, in the discussion of the gas release model. The other configurations tested by Elliott et al (1984) were also simulated during various developmental stages of the code. The results generally showed good agreement between code calculations and experimental data. A re-assessment of the final code version against data from these configurations was not carried out. This was primarily because the tests were conducted with Halon-1301, and the intent of code development was for alternate fluids. The expectation is that the final version of FSP would be able to simulate these tests quite well.

The experiments at Lehigh University, carried out as a part of this code development project, examined several piping configurations, with HFC-227ea and with HFC-125. The code has been assessed against these experiments. These experiments are particularly useful for code assessment because, in addition to the usual measurement of pressure, the experiments were able to estimate the mass flow rate of discharge, and also measured the void fraction near the pipe exit. The results of the assessment are being presented separately, and generally show good agreement against the test data.

Other experimental data on suppressant discharge through typical delivery systems have been compiled and reported by Grosshandler et al, 1994, and by Gann, 1995. This section presents the assessment carried out against some of the experiments reported in Gann, 1995. The experiments were conducted at NIST, and included a series of discharge tests using several agents (including Halon 1301).

4.6.1 FSP ASSESSMENT AGAINST NIST EXPERIMENTS

4.6.1.1 NIST Experimental Apparatus

The basic design of the NIST experimental apparatus consisted of a storage vessel (or pressure vessel), discharge piping, and a recovery tank. A nitrogen make-up tank was connected to the pressure vessel to simulate constant-head discharge if needed. The pressure vessel was fitted with a quick release valve at the bottom. Figure 4.6.1 shows the test apparatus. The data included pressure vessel pressure and pressure at various locations along the discharge piping. Several discharge piping configuration were used. These included: (1) 3.5-m straight discharge; (2) 3.5-m with 90-degree bend; (3) 4.5-m with 90-degree bend; (4) 3.5-m straight with expansion from 9.5-mm ID to 15.9-mm ID; (5) 3.5-m straight with contraction from 15.9-mm ID to 9.5-mm ID; and (6) 4.5-m, 15.9-mm ID Tee configuration. Two pipe sizes were used for all configuration, except otherwise stated, and these were 9.5-mm ID and 15.9-mm ID. The various configurations are shown in Figure 4.6.2.

Four agents were tested in these experiments. These were Halon 1301, HFC-125, HFC-227ea and CF₃I. The assessment presented here is only for the HFC-227ea (or HFC-227ea) experiments. The Table below lists the tests conducted with HFC-227ea. Note that the test identifier in the first column is actually the Figure Number in Appendix II of the NIST Report (Gann, et al, 1995). The various configurations shown in the last column are shown in Figure 4.6.2.

Test Identifier	Pressure (Mpa)	Fill Volume (%)	Configuration
B-54	2.75	56.5	straight pipe, 9.5 mm ID, 3.5 m long
B-56	4.12	60.2	straight pipe, 9.5 mm ID, 3.5 m long
B-58	4.12	49.2	3.5 m, 90-deg bend, 9.5 mm ID
B-59	4.12	49.2	4.5 m, 90-deg bend, 9.5 mm ID
B-60	4.12	49.0	straight pipe with contraction
B-61	4.12	49.0	straight pipe with expansion
B-66	2.75	54.1	straight pipe, 15.9 mm ID, 3.5 m long
B-68	4.12	49.4	straight pipe, 15.9 mm ID, 3.5 m long
B-71	4.12	49.4	3.5m, 90-deg bend, 15.9 mm ID

Of the above tests, four tests were simulated with FSP. These are Tests B-59, B-68, B-61 and B-60. Together they represent a variety of piping configurations. The results of the simulations are presented below.

4.6.1.2 FSP Simulations of NIST Experiments

calculate release rates of dissolved gas. Hence the model was implemented with two user-supplied parameters. These are the critical gas bubble radius, r_c , and the gas

A FSP input model for each discharge piping configuration was developed. The following geometrical information can be obtained from Gann et al, 1995:

Storage Vessel Volume:	4.06 x 10 ⁻³ m ³
Storage Vessel ID:	100 mm
Discharge Valve:	31.8 mm inlet to 44.5 mm exit
Discharge Valve Stroke:	order of 10 ms
Nitrogen Make-up Tank:	88 x 10 ⁻³ m ³
Nitrogen Charge Tubing:	19.1 mm ID
Nitrogen Solenoid Valve:	30 kPa pressure difference opening, stroke 50 ms
Discharge Piping Sizes:	9.5 mm and 15.9 mm ID
Discharge Piping Lengths:	3.5 and 4.5 m
Recovery Tank Volume:	15 x 10 ⁻³ m ³

The above information was used to developed the input models for FSP for each of the tests. The models are not described in detail or presented here. They were very similar, conceptually, to the sample problem described in detail in Section 5 of this report. The supply vessel (called storage tank in these tests) and discharge piping were each modeled with PIPE components, with a VALVE component in between them, simulating the initiation

of the discharge process. In modeling the discharge piping, junctions were located at the physical locations of area changes (contraction or expansion) and bends. Appropriate loss coefficients were entered to simulate the energy losses at these locations. Figure 4.6.3 shows the general FSP model used for these simulations.

These cases were all run with the value of r_c in the range of $7.5e-9$ to $1.0e-8$. The discharge coefficients at the system exit were chosen as 1.0, 0.8 and 0.8 for the subcooled, two-phase, and single phase vapor conditions, respectively. The value of Γ_0 was the same for all the tests, at 10,000. Figures 4.6.4 through 4.6.7 respectively show the calculated and measured pressure responses in the supply vessel, for Test B-59, B-68, B-61 and B-60. Not shown here are the pressure histories at various locations along the discharge piping. Generally, at these locations, the measured pressure would increase sharply as the discharge was initiated, and then decrease gradually as the fluid left the system. This trend was picked up by the code. Overall, the code picks up the qualitative trends in the pressure history. If the time for complete discharge of the agent is taken as the time at which the pressure drops to its lowest value, the code seems to calculate this generally within about 25%. A better agreement between calculation and data could probably be obtained by varying r_c and Γ_0 . This has not been attempted here, primarily because there are inherent uncertainties in these parameters, and a code user would normally vary these parameters in design calculations to get conservative results for design purposes. Generally, a higher value of Γ_0 would release more dissolved gas earlier in the transient. This would generally delay the complete discharge of the bottle slightly. Users can utilize this information to develop conservative designs in applying the FSP code.

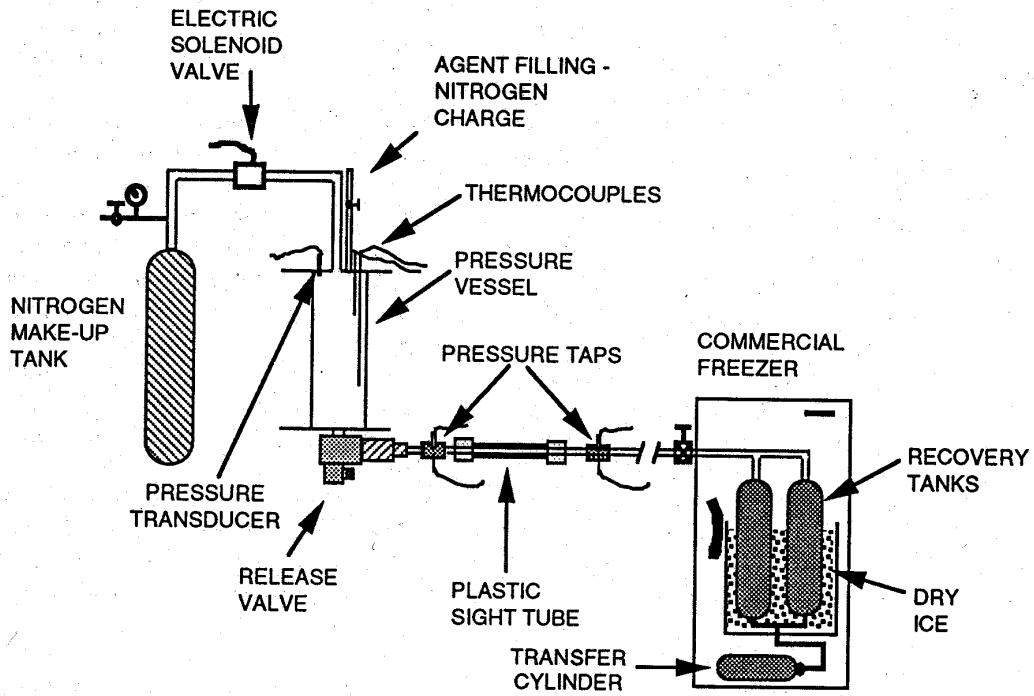


Figure 4.6.1: NIST Test Apparatus (adapted from Gann et al, 1995)

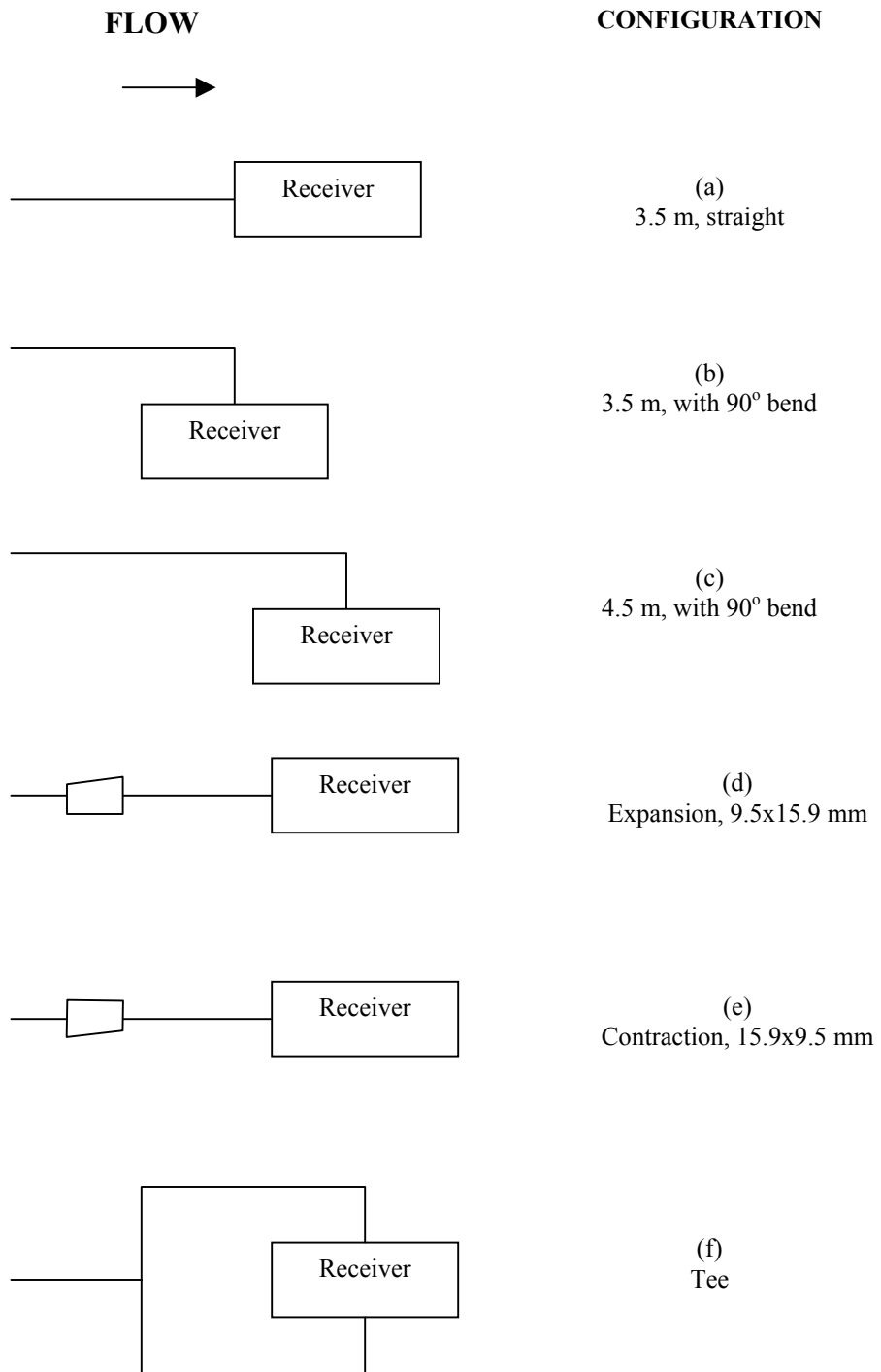


Figure 4.6.2: Piping Configurations for NIST Experiments

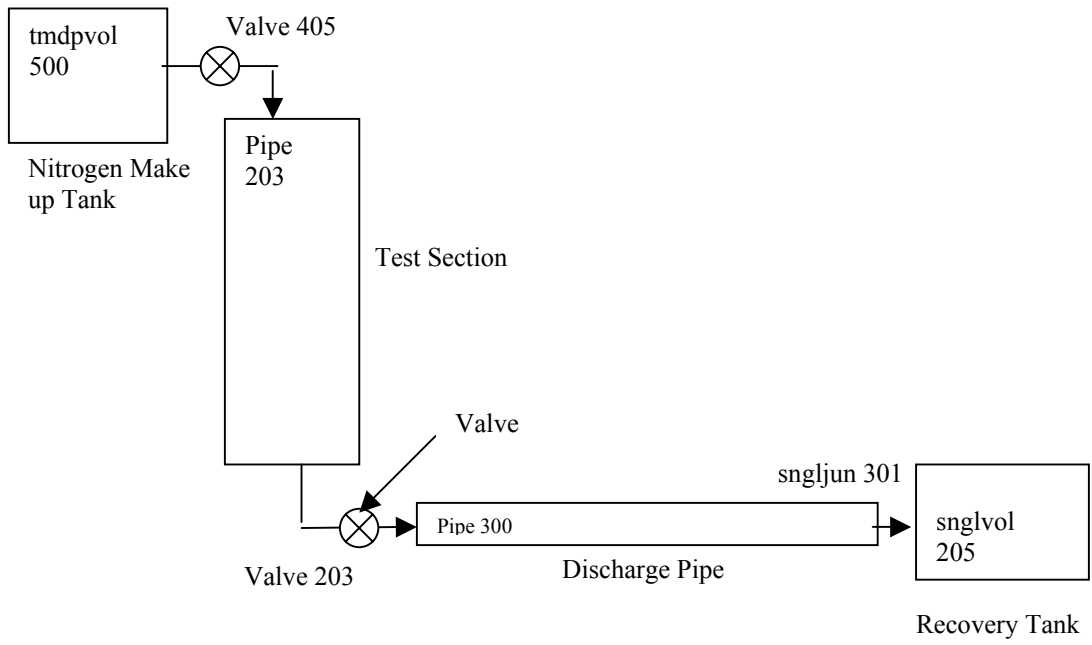


Figure 4.6.3: FSP Input Model

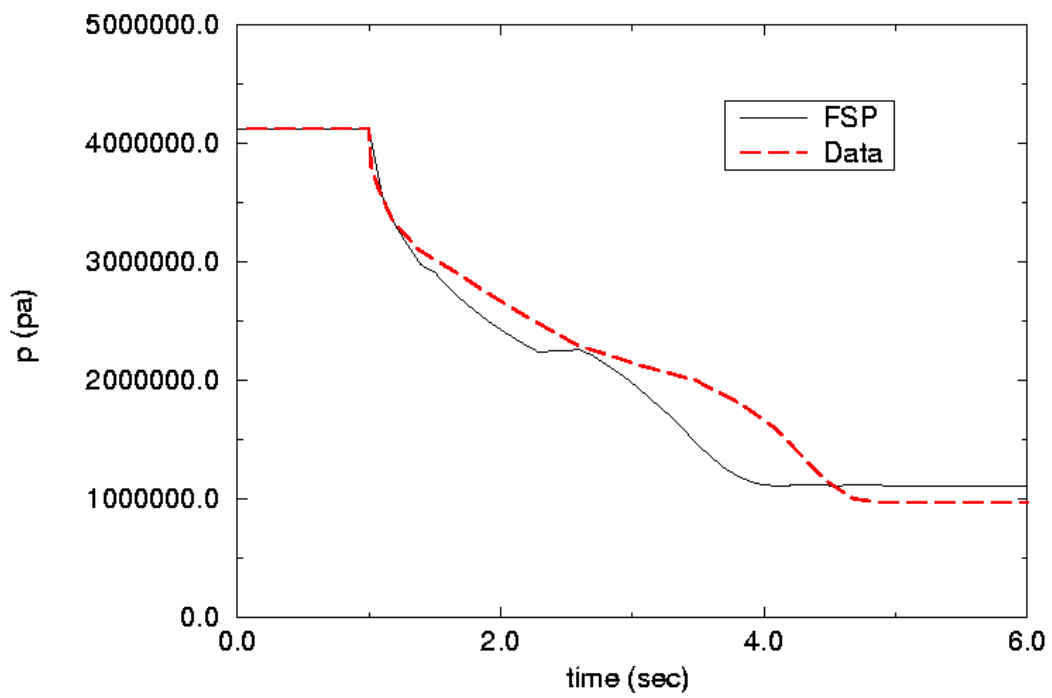


Figure 4.6.4: Comparison of Calculated and Measured Bottle Pressure for B-59

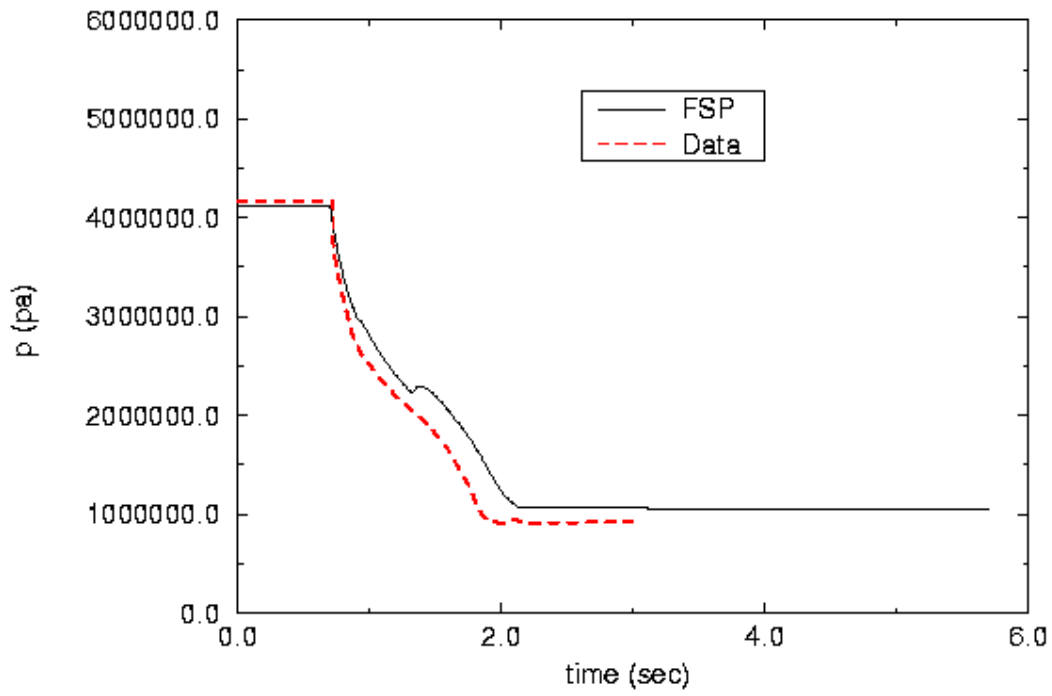


Figure 4.6.5: Comparison of Calculated and Measured Bottle Pressure for B-68

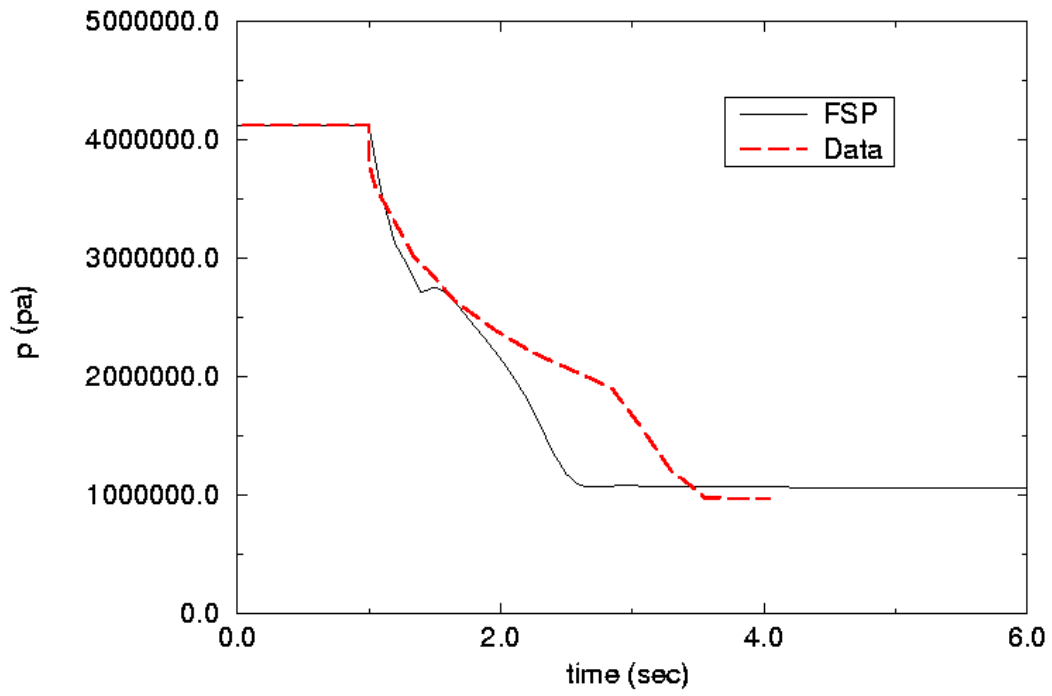


Figure 4.6.6: Comparison of Calculated and Measured Bottle Pressure for B-61

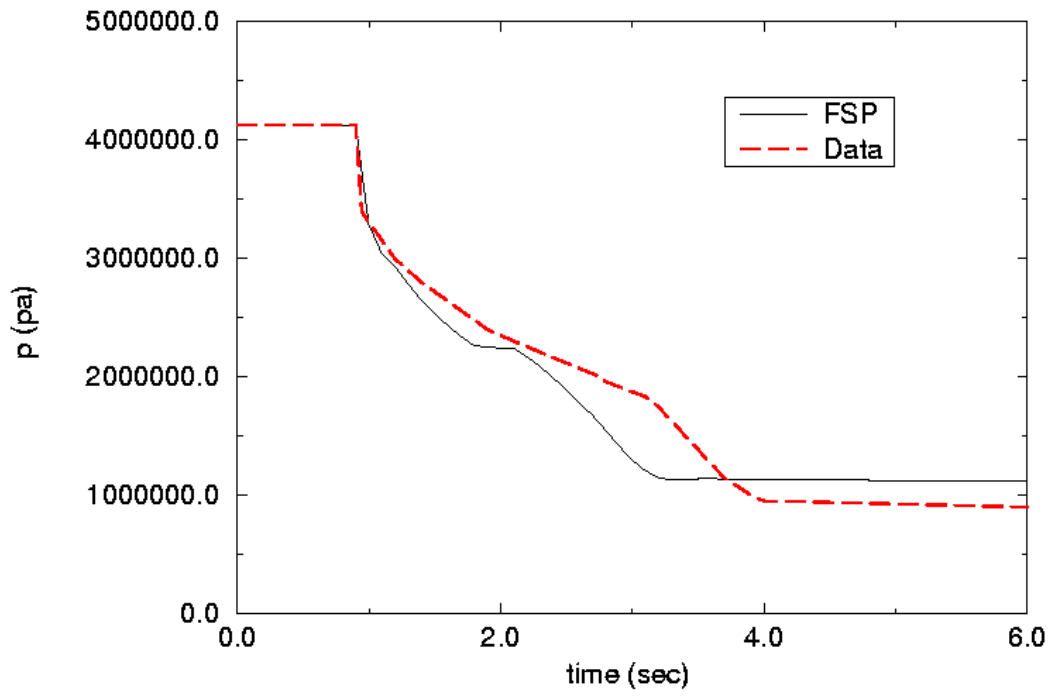


Figure 4.6.7: Comparison of Calculated and Measured Bottle Pressure for B-60

5. Comparison of Code Predictions to Lehigh Experimental Data

5.1 Comparison with Experimental Data Collected at Lehigh Test Facility

In this section a detailed comparison of the computer code predictions and the experimental values for a rapid transient discharge of a suppressant flow will be examined. To fully test the code, all aspects of an actual suppressant discharge must be considered. For this reason we feel the Lehigh experimental data should be the benchmark for comparison since it includes the most extensive experimental data to date. This is due to the fact that we were able to obtain data for local temperatures, void fraction, and mass flow rate which were previously unavailable. In addition, we have extensive data for a number of different flow conditions and piping configurations.

When using the computer code to make predictions, we first had to determine a few operating parameters to represent the operating conditions of a specific run. A detailed list of these parameters are given in the Code Description Section of this report. Some of these parameters are straight-forward and pertinent to the piping configuration, such as diameters, lengths, etc., and operating conditions such as initial pressure, temperature, etc. However, some of these parameters are part of the modeling used in the code. One of these models is the gas dissolution model, which is discussed in the Code Description Section. Dependent on the fluid used during the discharge, the gas dissolution model requires the following constants:

- 1 – The critical bubble radius when nitrogen is released from the fluid,
- 2 – The release rate of nitrogen.

A third parameter, that needs to be defined as input to the code, is the discharge coefficient for choked flow conditions. When using the computer code to make predictions, we first had to determine a few parameters. First off, there is the critical radius, which can be found for a specific run by estimating when the release of nitrogen begins. This is the point near the beginning of the run when the pressure stops dropping rapidly, represented as a change in slope in the pressure histogram. With this pressure and the surface tension of the fluid, a critical radius can be calculated as described in the Section 4.2.4.6. After examining the first set of experimental runs (#1-#7), it was determined that the value was in the range of 5-20 nanometers. As for the second parameter, the rate of degassing, it was found that the range was anywhere from 1000-10,000 depending on the system. Last, the discharge coefficient must be chosen. Since the default is 1.0, we knew that the value must be relatively close to this value. For ease in use and for consistency, it is desirable to choose one value for each of these parameters for use when running the predictive computer code. To determine the appropriate values for these parameters we had to examine the sensitivity of changing their values and the effect they made on the code's output and ultimately, compare them to our experimental data. For the comparison, experimental run #4 was chosen as the test sample.

The first step in our sensitivity study was to examine the effect on the computer code output when changing the critical radius. To isolate the effect of changing this parameter, we kept the values for the gas release rate and the discharge coefficients constant at 1000 and

0.8, respectively. Our findings showed that a lower value for the critical radius caused the slope change in the source vessel pressure trace to occur later. Therefore, this parameter is important for determining when the gas begins to release. By comparing the code outputs for values of 7.5 & 10 nanometers to the experimental results, as seen in Figure 5.1 we chose a final value of 10 nanometer for our critical radius. The resultant trace is the red line in the figure, with the blue line representing the 7.5 nanometer output and the black line showing the experimental data.

The second step in this study was to specify a value for the rate of nitrogen gas release. Once again we kept the parameters that were not being studied constant, the discharge coefficient was 0.8 and the critical radius was 7.5 nanometers. This parameter influences the speed at which the nitrogen gas is released once the process begins, therefore changing the shape of the pressure histogram. This can be seen in Figure 5.2, where the black line is the experimental data, the blue line is a value of 1000, the red line is a value of 2500, and the green line is a value of 5000. It is obvious that at lower values (blue) the pressure trend remains straight and uniform, but at higher values (green) the speed of release of the nitrogen causes a pressure recovery or “bump” in the trace. From this comparison alone, it is hard to determine the best value to use for this parameter, so we made a similar comparison using void fraction. This is shown in Figure 5.3, with an increasing average void fraction as the value for the gas release rate parameter increases. What this figure shows us, that the other did not, is that a value just below the trace for the value of 2500 would seem to work the best. With observations from the above two figures, we chose a gas release value of 2000.

The last step in this procedure was to pick a value for the discharge coefficient. This parameter influences when and where choking will occur in the system. We tried values ranging from 0.75-1.15 and found that there was only a negligible difference in our output. Therefore we decided to go with a value of 0.9 for the discharge coefficient. Now that all of our operating parameters are chosen, a final comparison with the experimental data of Run #4 was conducted. The result shows good agreement and is shown in figures 5.4 & 5.5, with the red lines being the prediction and the black lines being the experimental data. While we have only compared the code output to one experimental run, we feel that it was necessary to chose only one value for each parameter so that in future comparisons we do not have to take into account any effect changing these values might have on the output. Also, this run was chosen over the others because it is one of the repeatability tests and is in the range of typical supersonic discharge applications.

In this next section, the focus will be on comparing the computer code prediction with an entire experimental run. The experimental run used in this comparison is the same run as used earlier in Section 3, run #5. The first quantity we will look at is the cumulative mass in the source vessel as time progresses, shown in figure 5.6. The prediction shows excellent agreement with the experiment. The only noticeable differences being the final mass value and the speed of the discharge represented by the different slope gradients. Even with these differences, the prediction gives an end of liquid flow at approximately 1800 milliseconds compared to a measured time of 1600 milliseconds in the experiment, a very good estimate of discharge time.

The next comparison examined in this study was on the void fraction experienced at the end of the piping system before the discharge reached the collection vessel. Again, the agreement between the prediction and experiment was good as figure 5.7 shows. While the experiment is influenced by the local flow regime giving the output a fluctuating appearance, the prediction has a smooth trace due to the fact that it calculates the void fraction on mass balance terms giving an average void fraction value for how much liquid and vapor are present in the system. A similar trend can be seen in both, a sudden drop as the pipe is filled with liquid and then an increase as nitrogen comes out of solution and raises the average amount of gas in the flow until the run ends and there is no more liquid flowing. The only glaring difference is in the final value reached at the end of the run. The prediction never goes back to an all-vapor reading of 1.0, informing us that in the simulation there is still liquid present in the pipe. In a realistic situation, the liquid would eventually drain into the collection vessel since it is the lowest part of the system, but the prediction is finding this value through a mathematical simulation so it may not account for this. Neglecting this problem, a good representation of the void fraction can be found using the prediction.

The most important comparison for this study would have to be a look at the pressure traces, since this is what drives the discharge and delivers the suppressant to the fire. Figures 5.8-5.12 show the prediction compared to the experiment for the pressures in the source vessel, at pipe position #1, at pipe position #2, at pipe position #3, and in the collection vessel. They all agree very well with the experimental data with the only discrepancy being the final pressure at the end of the run. While the shape of the curves varies slightly, they all show the same trend and a similar slope as the pressure decreases during the discharge. This observation is most exciting since most of the experimental data available is in the form of pressure histograms, allowing for the code to be more widely used in comparisons and in simulating the output of various system configurations.

While these comparisons were available with all of the runs conducted in this study, there were also special measurements made in some cases. For instance, we took experimental measurements of the pressure drop across different pipe fittings. While the prediction used a literature value for the friction loss factor associated with the fittings, we can still compare what the pressure drop would be over these fittings. This gives us an idea of whether the literature values are accurate for a two-phase flow through different pipe configurations. Figures 5.13-5.15 show the experimental data for run #9 compared to the predicted data for the pressure drop across a capped tee, 90° elbow and connecting union, respectively. This run used the more simple of the two alternative piping configurations shown previously in Figure 3.11 of section 3. They all show good agreement, with the prediction claiming that the pressure started to fade earlier than the experiment and gradually fell to zero where the experiment jumped down when the liquid ran out and the vapor/gas flow started. We do not see the sudden drop in pressure at the end of the liquid flow that is evident in the experiment. Although, the prediction shows an end of the run in the same general vicinity as the drop in the experimental trace, proving that this is most likely the end of the liquid flow. Once again, the code predicts the physical results reasonably well even with complicated piping layouts.

The last comparison we examined dealt with the temperature measurements. Unfortunately, the predictive code does not have the fluid to pipe heat transfer turned on, simply meaning that it does not take into account the fact that there is heat transfer with the

metal walls surrounding the flow. This would cause the flow to either heat up or cool down depending on the ambient conditions in the room. It would also be influenced by the heat capacity of the metal walls coming into contact with the flow (i.e. vessels and pipes). Without this included, the only real temperature change will be from the any phase change in the system or any compression or expansion of the contents of the system. In specific, the degassing of the nitrogen and the adiabatic expansion of the nitrogen near the end of the run would be the main contributors. But since the code is not influenced by the ambient temperature of the system, the code predicts a much lower temperature than was found in the experimental runs. The comparisons in this analysis use experimental run #16, which used HFC-125 as a test fluid in which the largest temperature change experience in the experiments. In Figure 5.16, a comparison is made between the experimental measurement of the source vessel temperature with the shielded thermocouple which was at the bottom of the vessel and immersed in the fluid and the fluid temperature predicted by the code. The trend is similar except for the magnitude and speed of the temperature drop, but the fact that the shapes are alike is promising that at least the phenomena behind the temperature drop is correct. Figure 5.17 shows a temperature comparison for the pipe position #1 in the piping system. Once again, the fluid temperatures are being shown and a similar result is obtained. Although, in this case, the differences are more pronounced than in the source vessel comparison. It is clear that the point when the temperatures began to drop is very close, but the magnitude of the drop is very different. As we expected, the heat transfer coefficient in the pipe is greater than anywhere else in the system and therefore the short-comings of not including the fluid to pipe heat transfer in the code are most obvious in this region. The comparison of the gas temperature in the collection vessel is shown in Figure 5.18. The collection vessel shows a slightly different result, a temperature drop at the beginning of the run was experienced due to the fact that the liquid was evaporating to raise the pressure enough to reach its saturation equilibrium. This trend stopped when the pressure rose high enough that there was no longer any need for the liquid to evaporate. Although the magnitude of the drop is different, both the prediction and the experiment show the same insight into whether the measurements were in the right magnitude and trend.

After study of all of the comparisons between the predictions and the experimental runs the general agreement is very good. In most cases, the prediction gives a good estimation of the physical characteristics of a two-phase flow in a model system. The code can even handle two different test fluids with reasonable accuracy. It also predicted three different piping configurations well, showing its versatility in modeling any potential system. While these points support the code's advantage for use with suppressant systems, it must also be noted that there were a few limitations of the code. The most notable being that it will not always work for any initial conditions inputted for a specific test fluid. While this is most likely due to a limitation with the thermodynamics package, it still leaves a small amount of uncertainty when running the code. The user must slightly deviate from the actual run condition in order to fall in a region of the thermodynamics package that will yield an output. For example, in experimental run #5 the initial conditions were entered into the code through the input deck, but an error occurred before the program could complete the simulation. But, it turns out by changing the ambient temperature from 31° Celsius to 30° Celsius the simulation works fine. This is only a minor change, but it still makes operation of the simulation slightly cumbersome.

Another area that caused a problem was when we tried to simulate our low pressure runs (2000-2500 kPa initial source vessel pressure). There were two problems, which arose during these tests. The first was similar to the problem stated previously, something with the thermodynamics package. These experimental runs (#1 & #8), were conducted with low downstream pressures so that flashing could occur in the pipe directly after the start of the run and the actuation of the valve. The code would not allow these conditions to run the simulation due to the fact that it believed that there was non-equilibrium in the downstream areas. The downstream pressure had to be raised to a pressure closer to the saturation conditions of the test fluid in order for the code to operate. The other problem we found with these low pressure test runs was in regard to the high fill level we used in the source vessel. In experimental runs #1, #8, #11, #14, & #18 a fill level of 80%-90% was used to try and cut down on the amount of nitrogen present in the system. The hope was to keep the system pressure low enough to facilitate flashing of the suppressant during discharge. This proved to be a problem with the code's predictive output. While this initial condition would not cause the code to stop running with an error, it did cause an odd result to be predicted. For example, in run #1, a total mass of test fluid (HFC-227ea) filled into the source vessel at the beginning of the run was about 4.9 kilograms. However the code prediction never even got close to that value during its predicted discharge, it reached a final value of about 3.1 kilograms. The only explanation we can add at this time is the possibility that the code was expected to only be predicting discharges that held a fill level of about 60%, instead of the test fill level of about 85%. But, this problem would cause a significant difference in all aspects of the prediction to be encountered.

The last problem that we encountered was with the high pressure runs (4750-5000 kPa initial source vessel pressure). Once again, we believe this had something to do with the properties package. When the initial conditions were fed into the code through the input file an error would occur immediately, causing the program to stop. We found that the only way to get these runs to continue was by lowering the source vessel temperature considerably, while keeping the downstream temperature around the ambient value. Even then we could not always reach the desired operating pressure. For example, in run #6, the source vessel temperature was dropped from 31° Celsius to 2° Celsius and we could only get an initial source vessel pressure of 4860 kPa in place of 4910 kPa to operate. When these runs finally ran, they still only continued for half of the time that the experimental runs were conducted for. It seems that the computer code would finish early in the run (i.e. 1500 milliseconds for run #6) most likely due to the temperature dropping below the range of the thermodynamics package. Even with these observed problems, the code did very good job when predicting most runs in the application area, an initial source vessel pressure between 3000-4500 kPa with a fill level of about 65%. This is the first code that has been able to be compared to void fraction data and instantaneous mass inventory data and it does an excellent job in estimating these values. Plots showing the comparisons between the predicted and experimental data can be found in Appendix C for 18 of the test case runs at the Lehigh University facility.

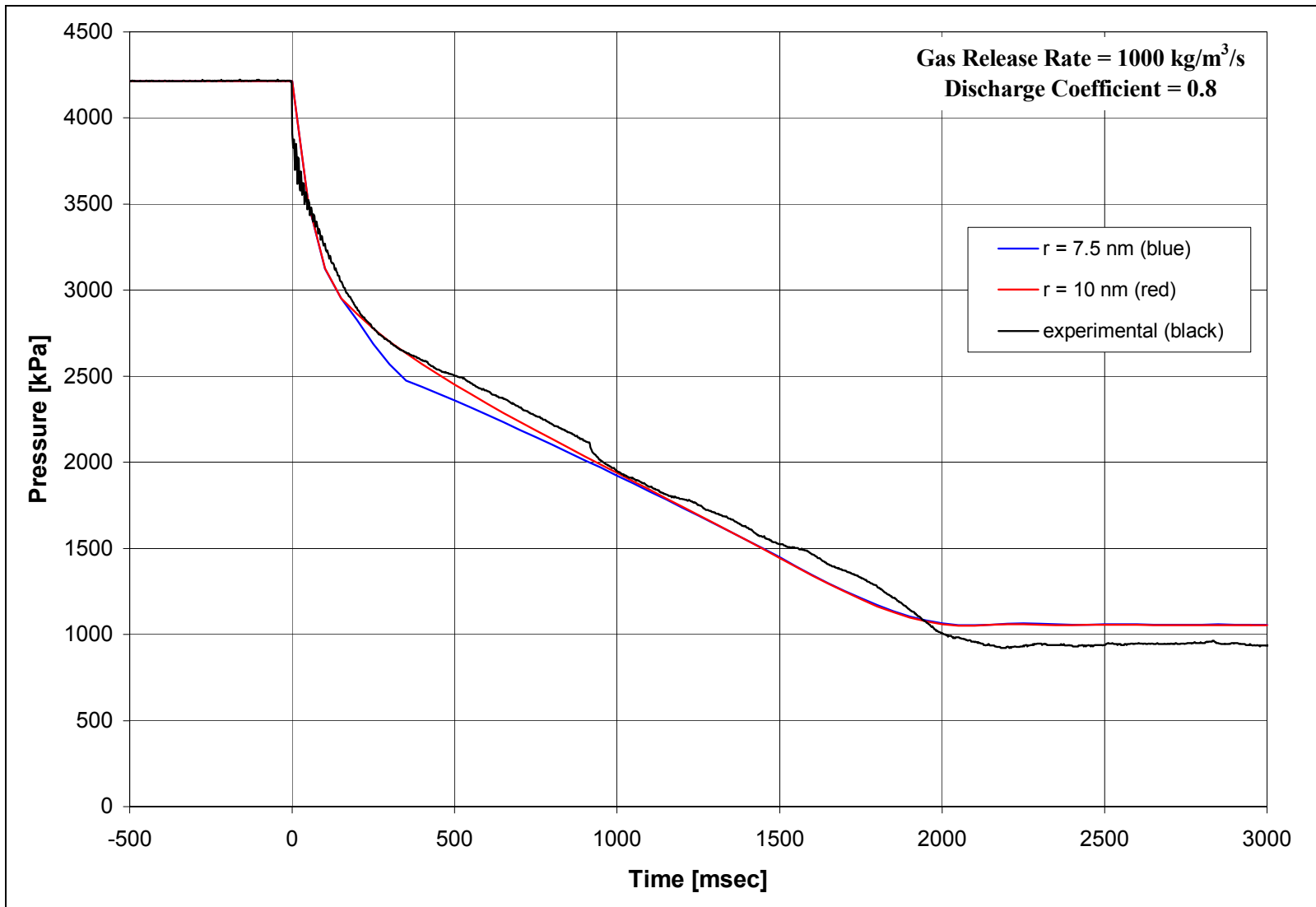


Figure 5.1: Comparison of Experimental and Predictive Source Vessel Pressure Data in Sensitivity Study on Critical Radius Value for Conditions of Run #4.

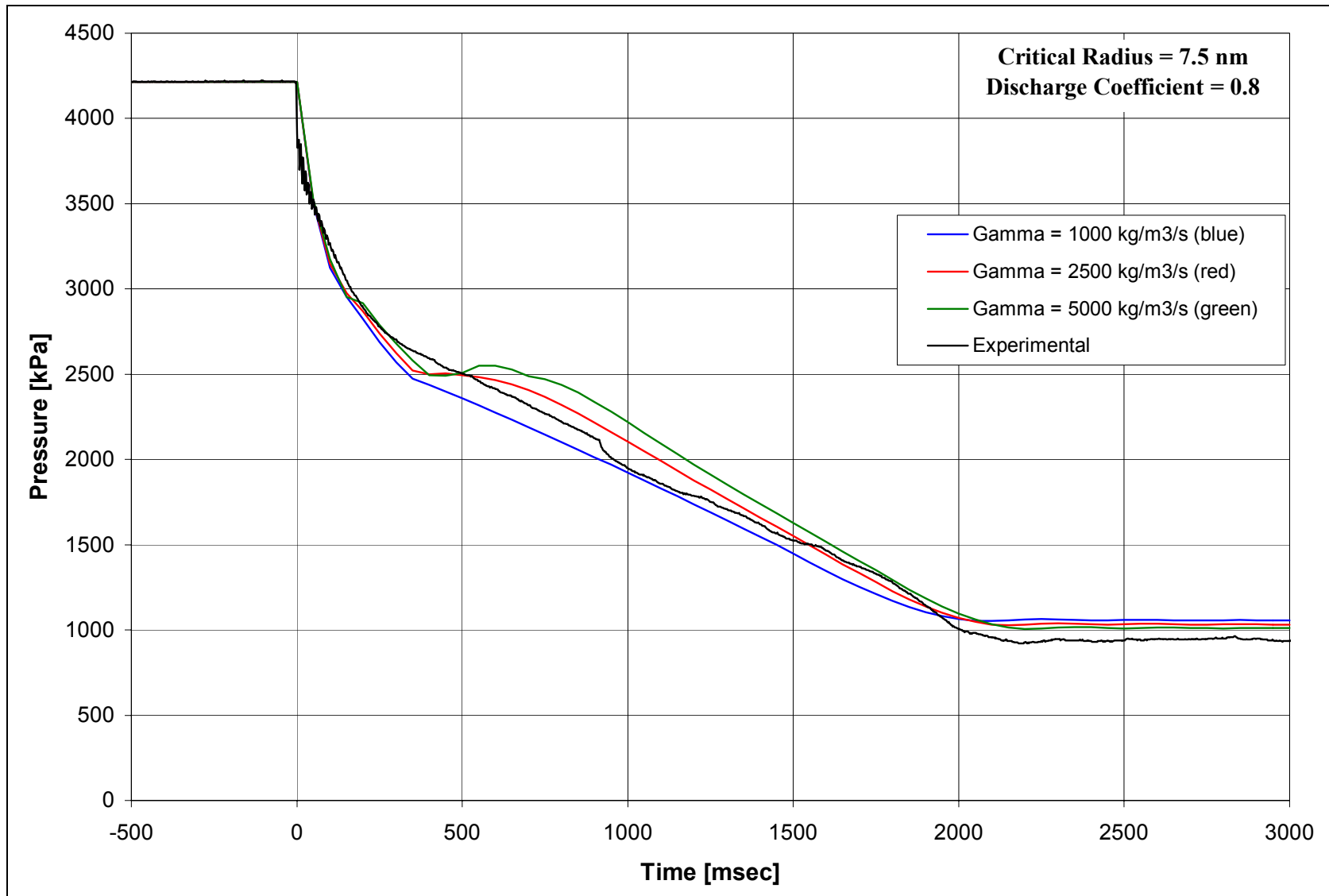


Figure 5.2: Comparison of Experimental and Predictive Source Vessel Pressure Data in Sensitivity Study on Gas Release Rate Value for Conditions of Run #4.

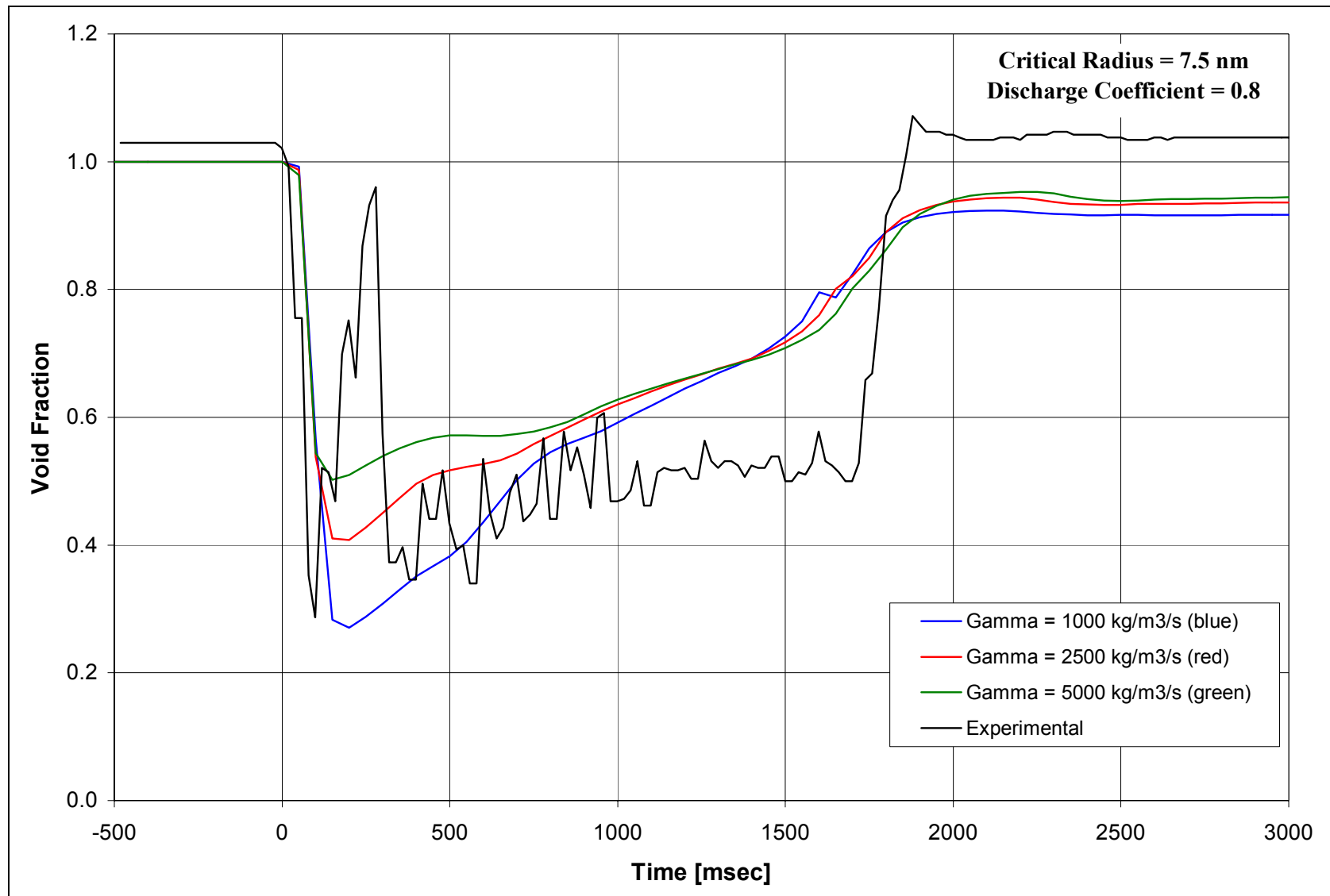


Figure 5.3: Comparison of Experimental and Predictive Void Fraction Data in Sensitivity Study on Gas Release Rate Value for Conditions of Run #4.

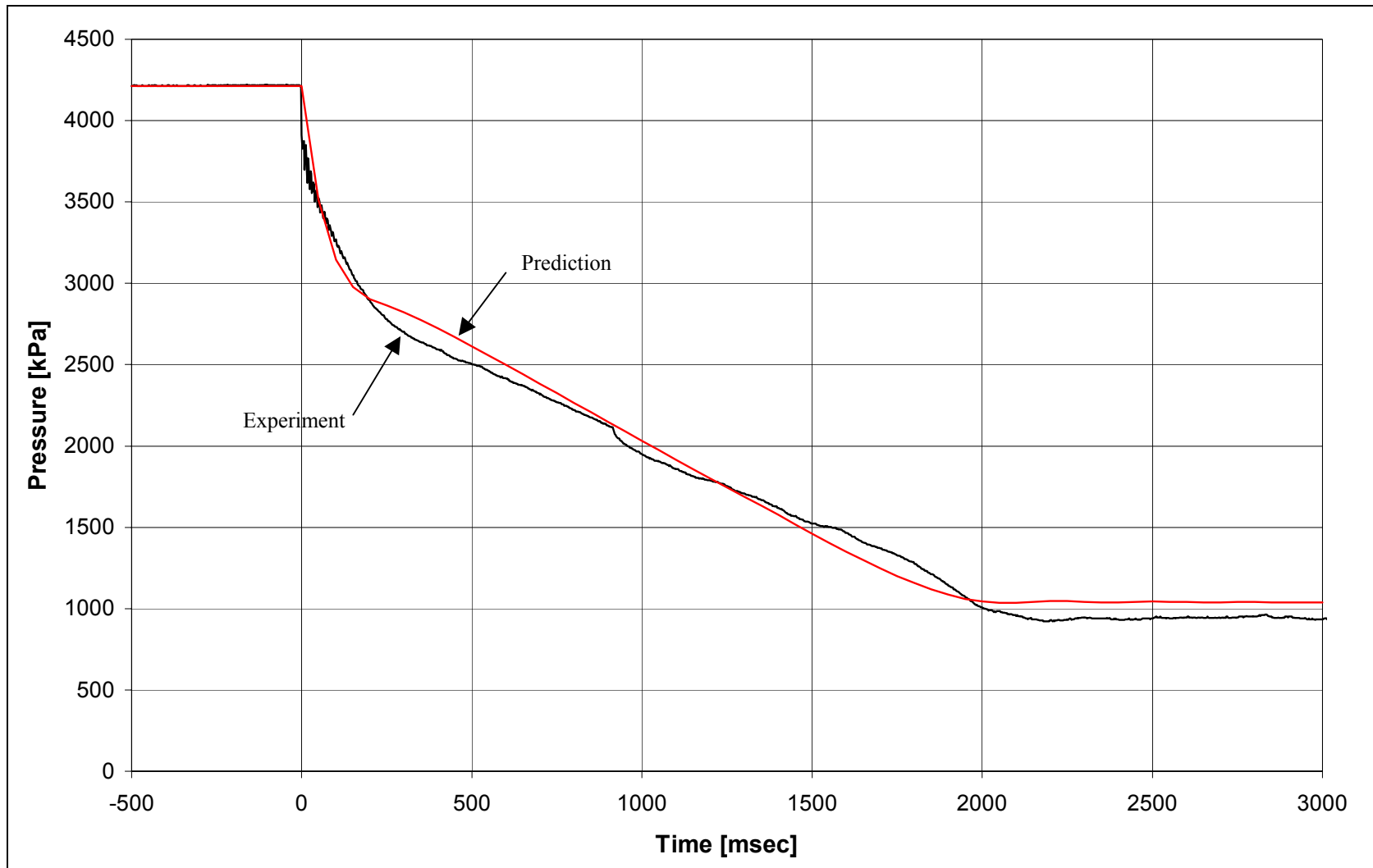


Figure 5.4: Comparison of Experimental and Predictive Pressure Data using Final Values for Code Operating Parameters for Conditions of Run #4.

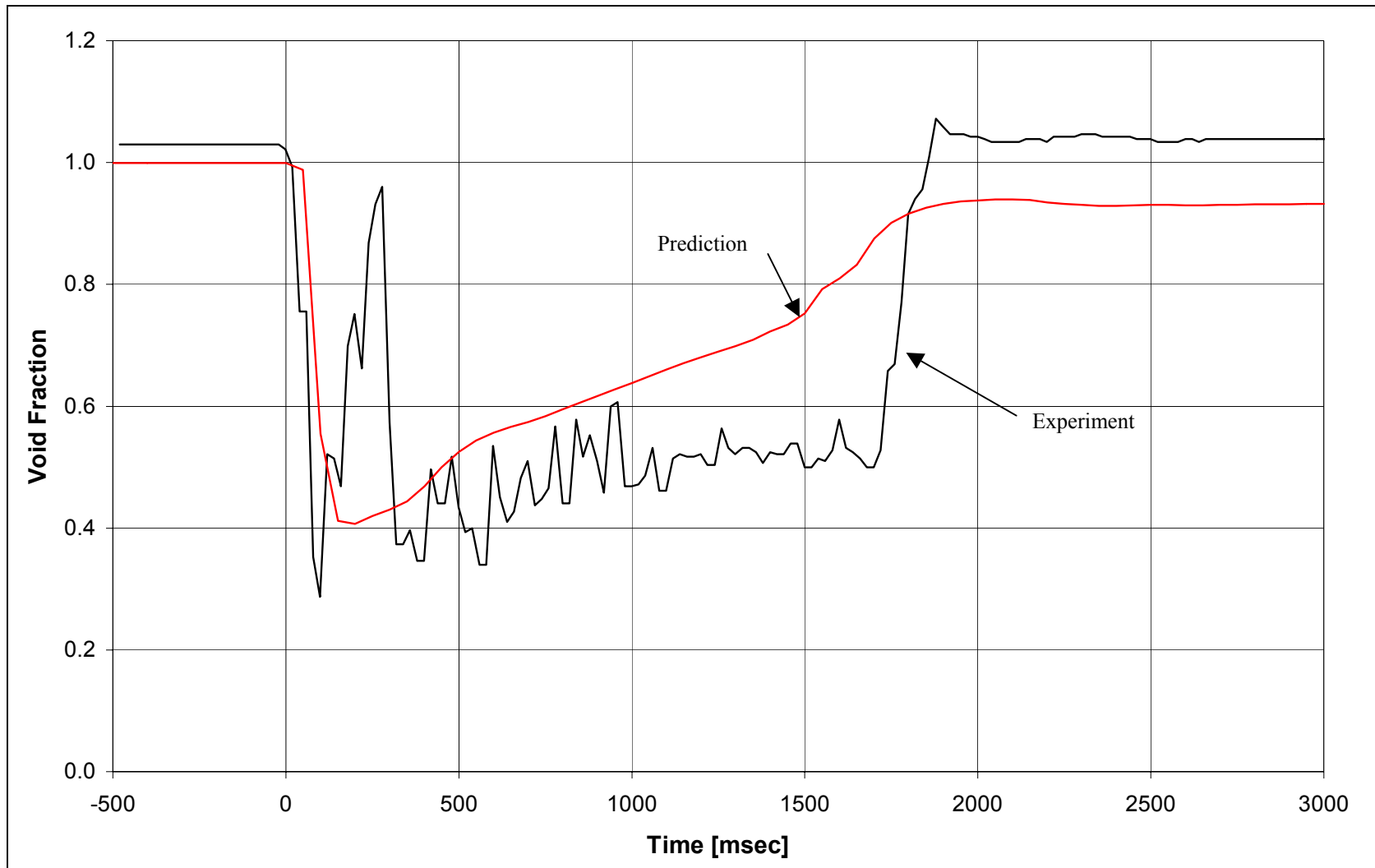


Figure 5.5: Comparison of Experimental and Predictive Void Fraction Data using Final Values for Code Operating Parameters for Conditions of Run #4.

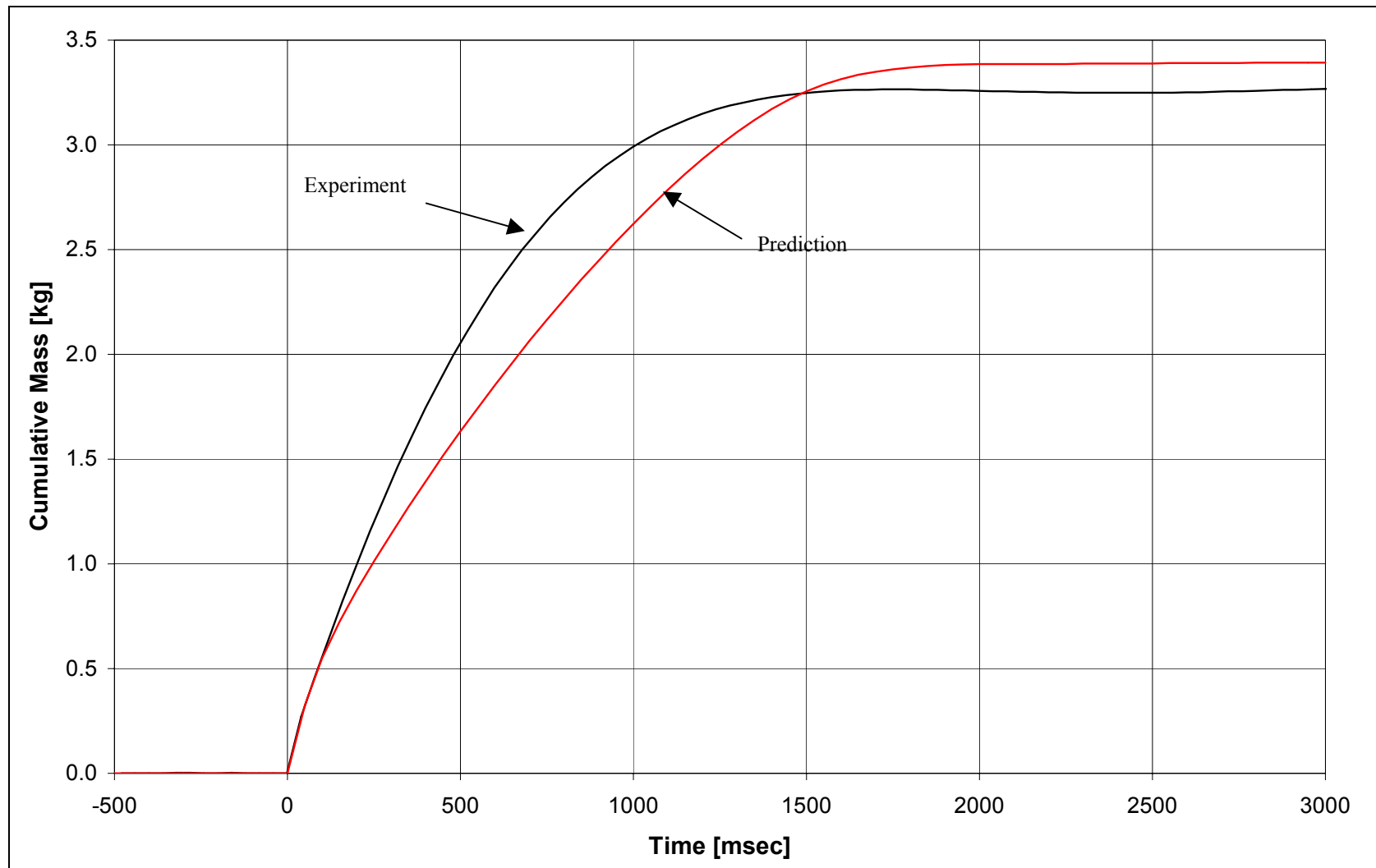


Figure 5.6: Comparison of Cumulative Mass for Experimental Run #5 and Predictive Computer Code Data.

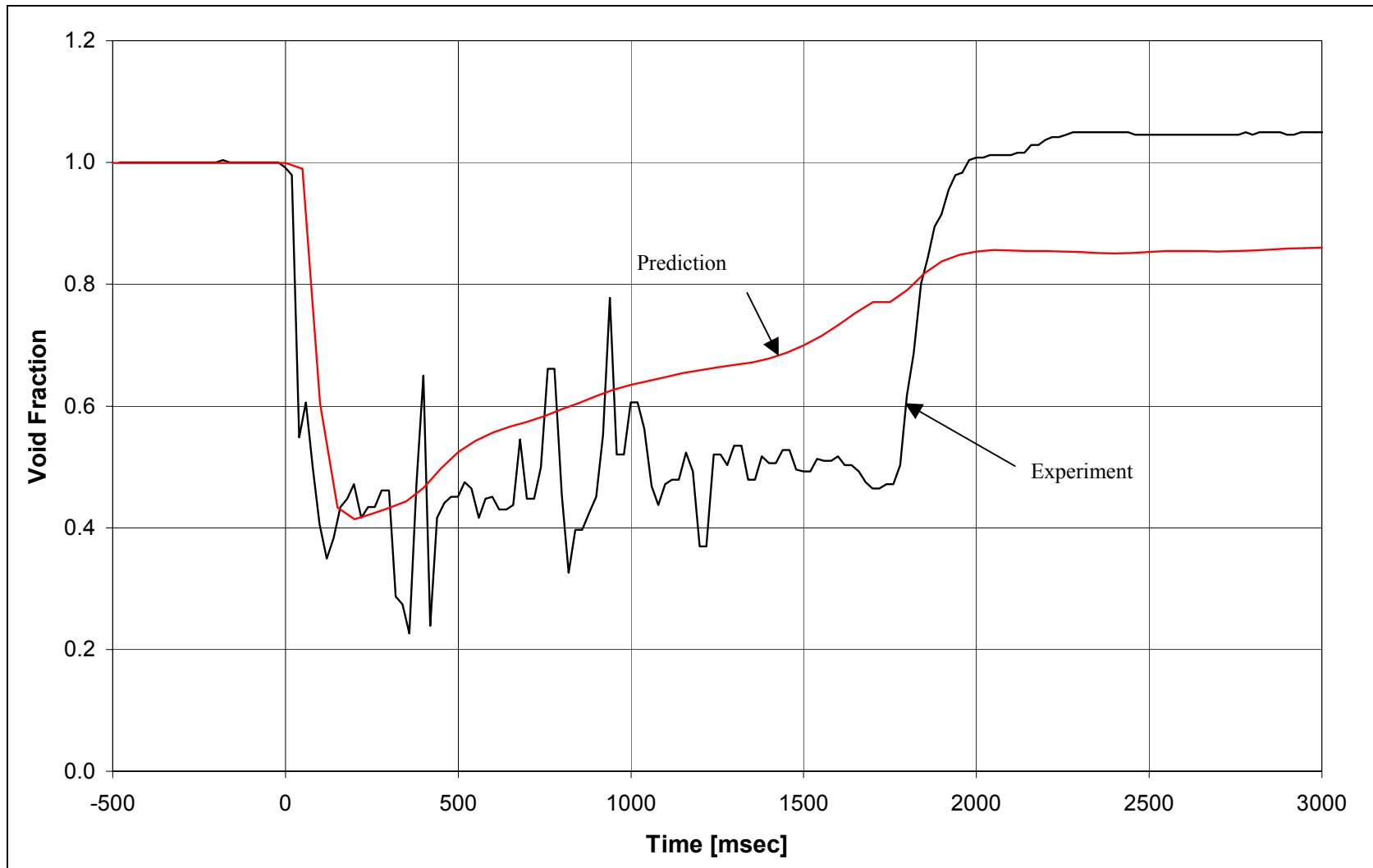


Figure 5.7: Comparison of Void Fraction for Experimental Run #5 and Predictive Computer Code Data.

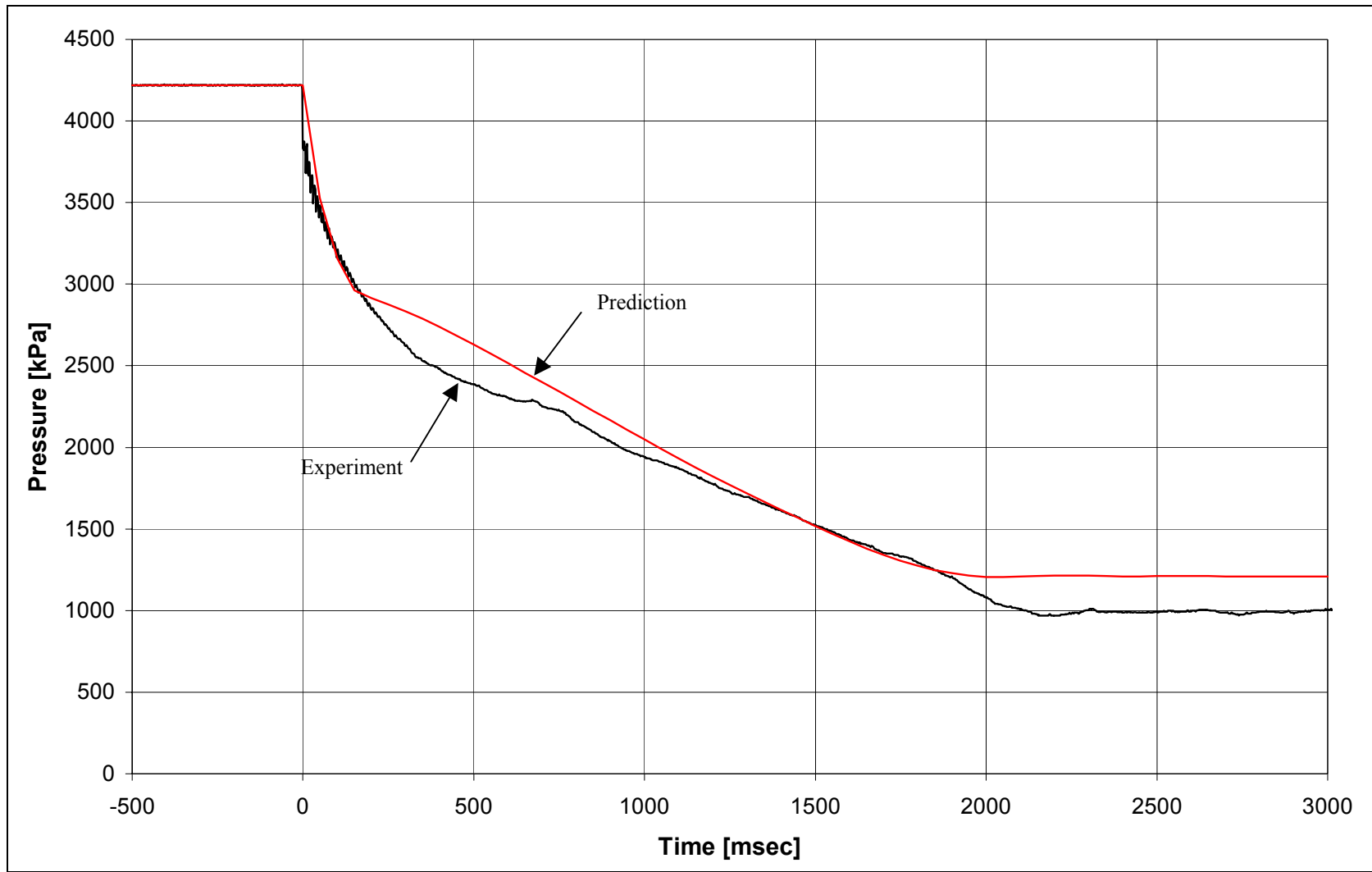


Figure 5.8: Comparison of Source Vessel Pressure for Experimental Run #5 and Predictive Computer Code Data.

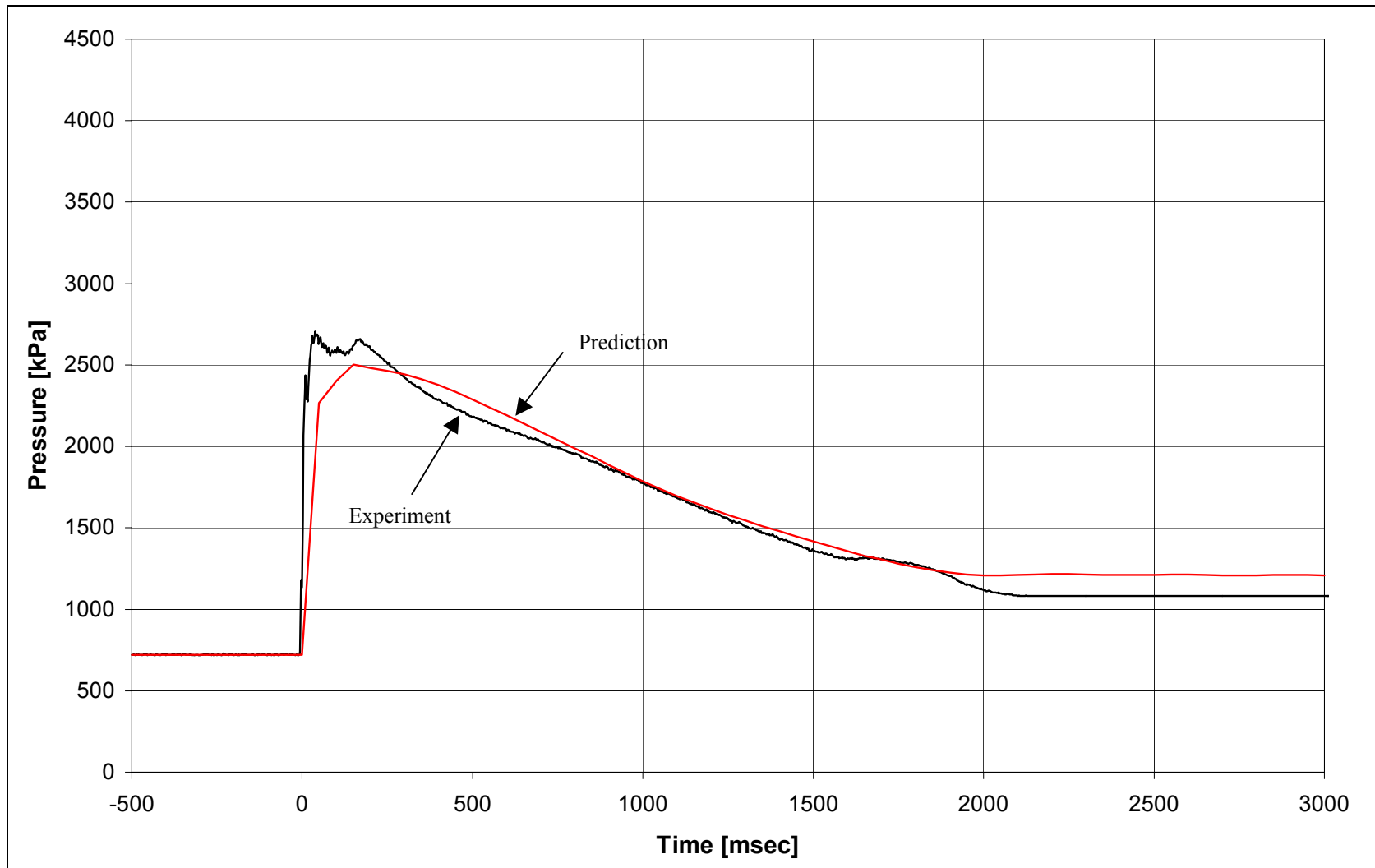


Figure 5.9: Comparison of Pipe Position #1 Pressure for Experimental Run #5 and Predictive Computer Code Data.

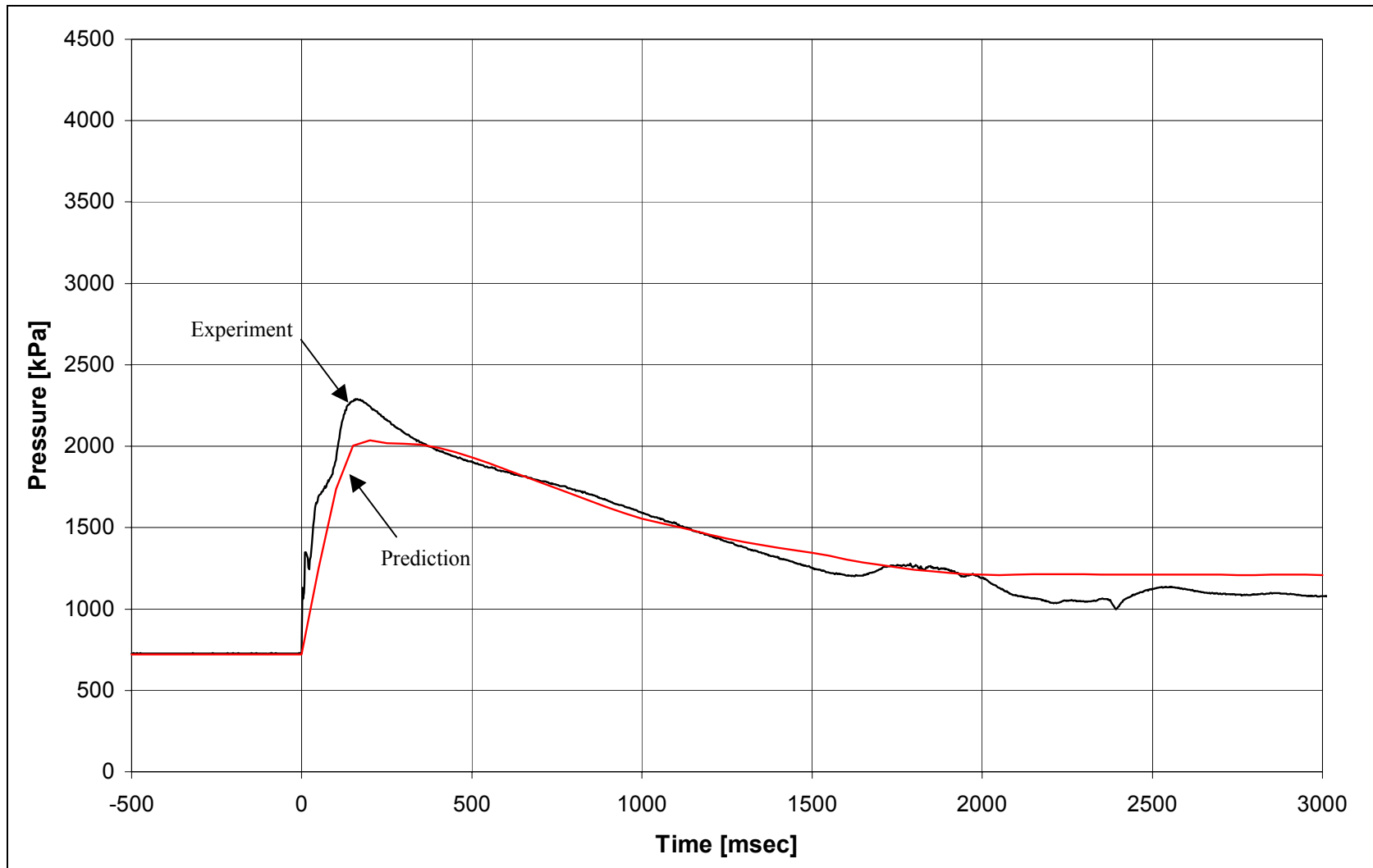


Figure 5.10: Comparison of Pipe Position #2 Pressure for Experimental Run #5 and Predictive Computer Code Data.

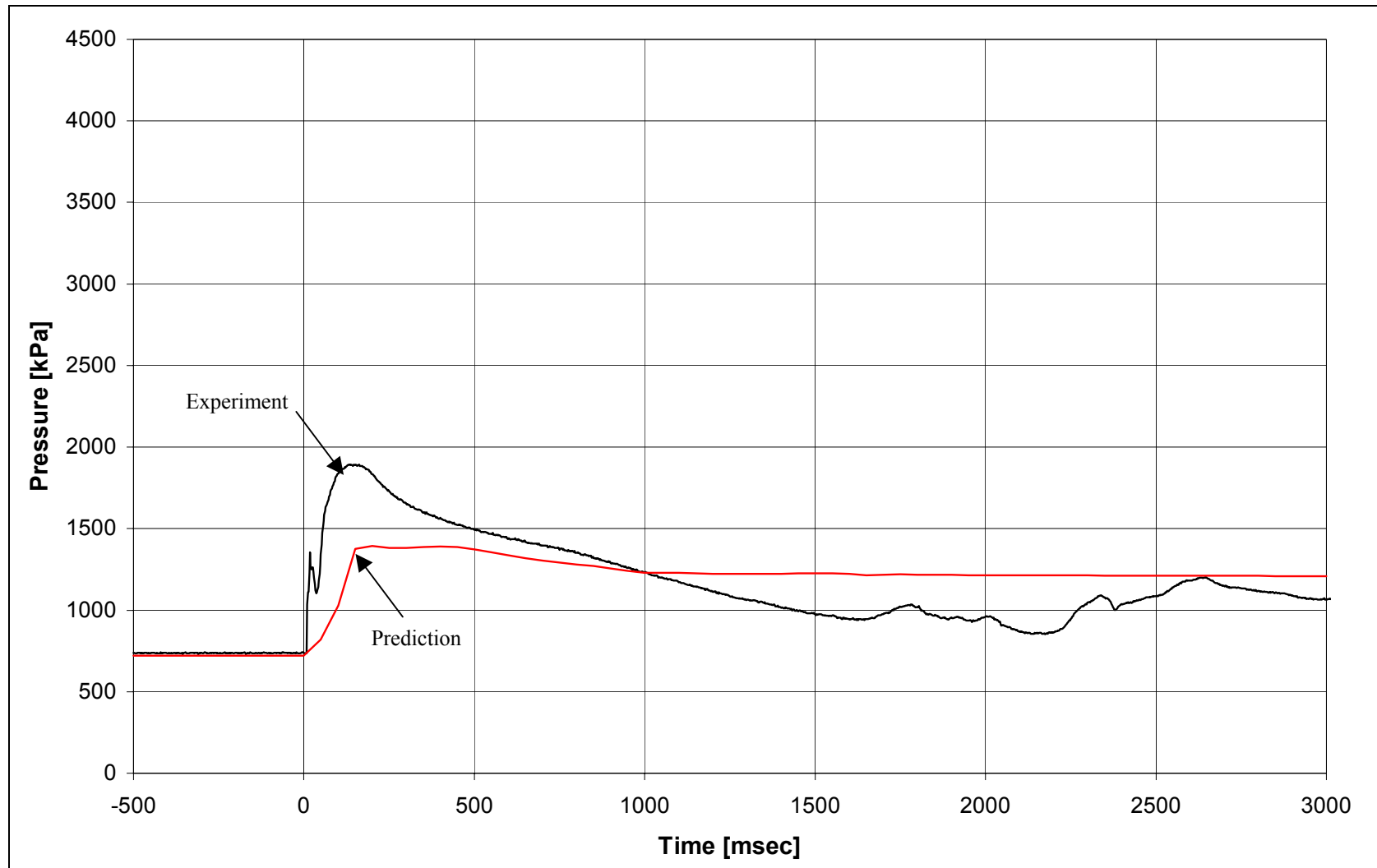


Figure 5.11: Comparison of Pipe Position #3 Pressure for Experimental Run #5 and Predictive Computer Code Data.

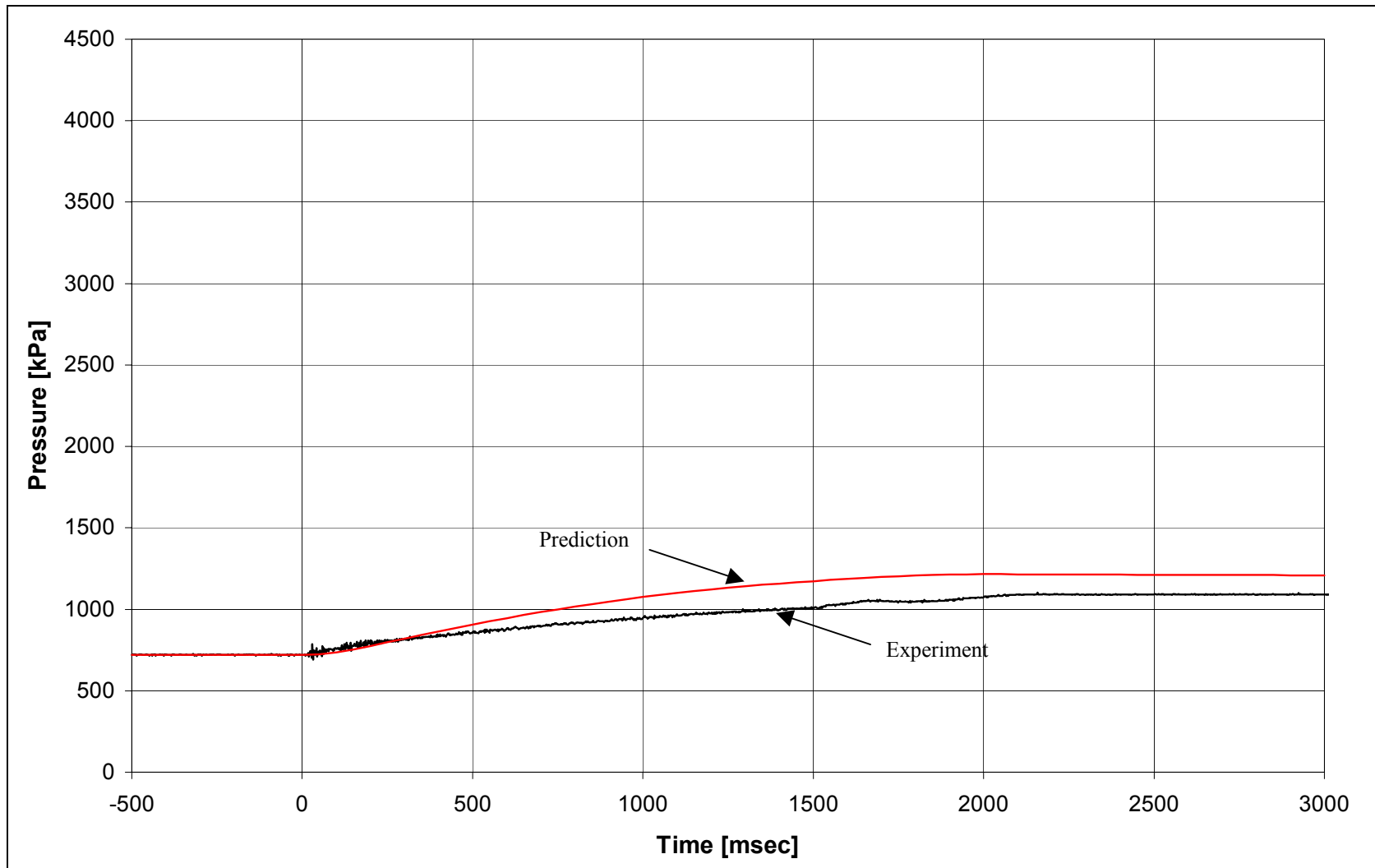


Figure 5.12: Comparison of Collection Vessel Pressure for Experimental Run #5 and Predictive Computer Code Data.

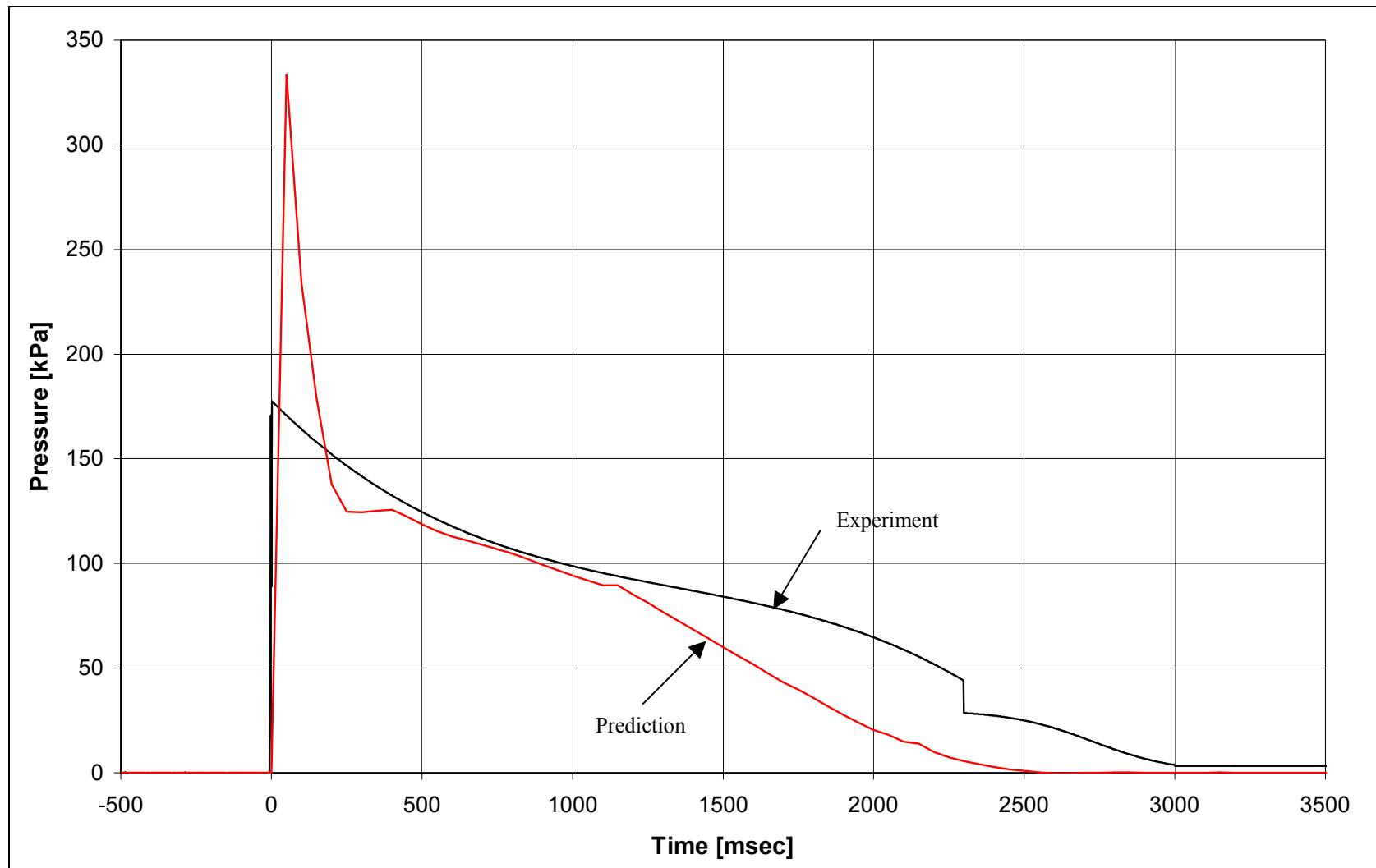


Figure 5.13: Comparison of Pressure Drop Across a Capped Tee for Experimental Run #9 and Predictive Computer Code Data.

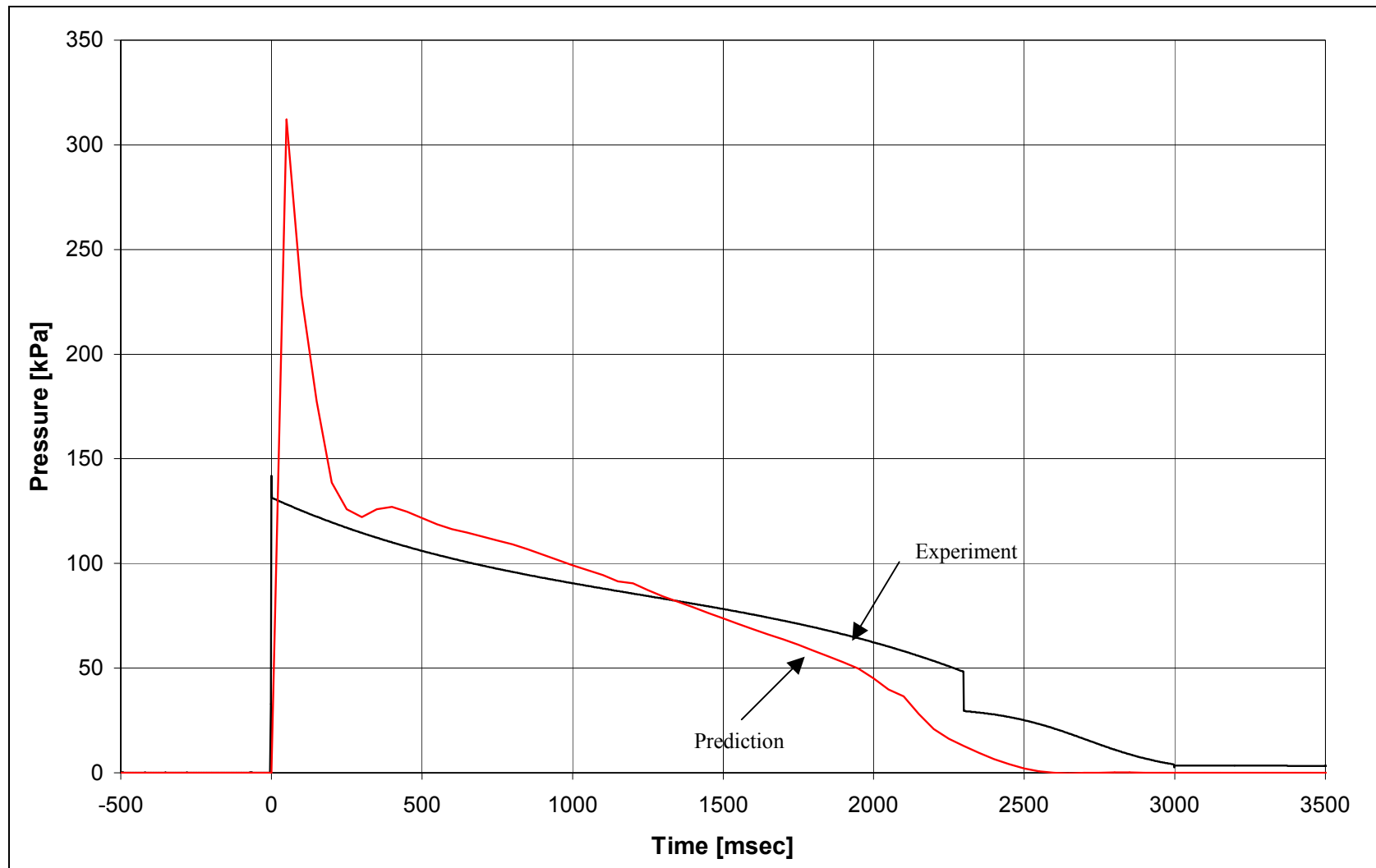


Figure 5.14: Comparison of Pressure Drop Across a 90° Elbow for Experimental Run #9 and Predictive Computer Code Data.

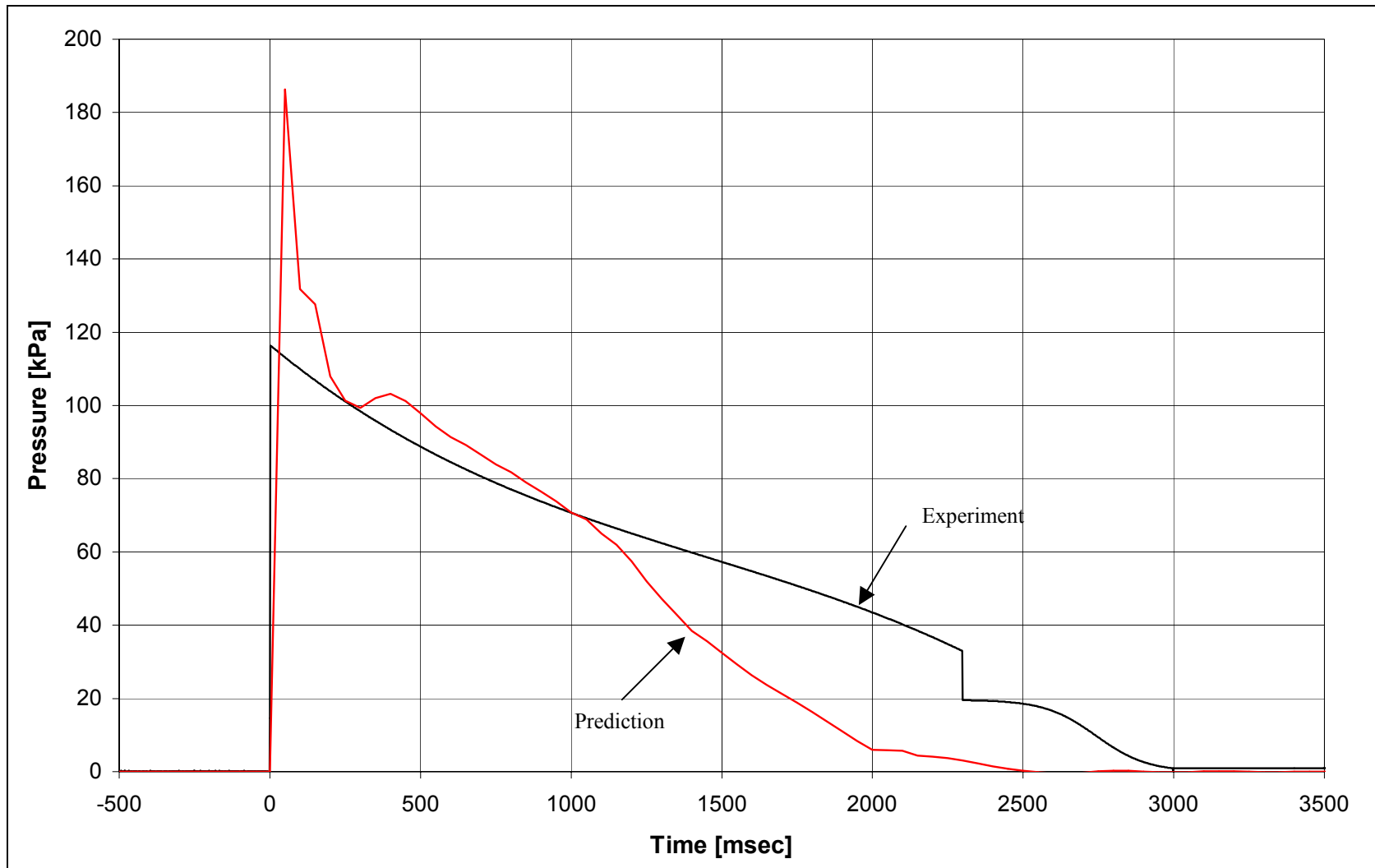


Figure 5.15: Comparison of Pressure Drop Across a Union for Experimental Run #9 and Predictive Computer Code Data.

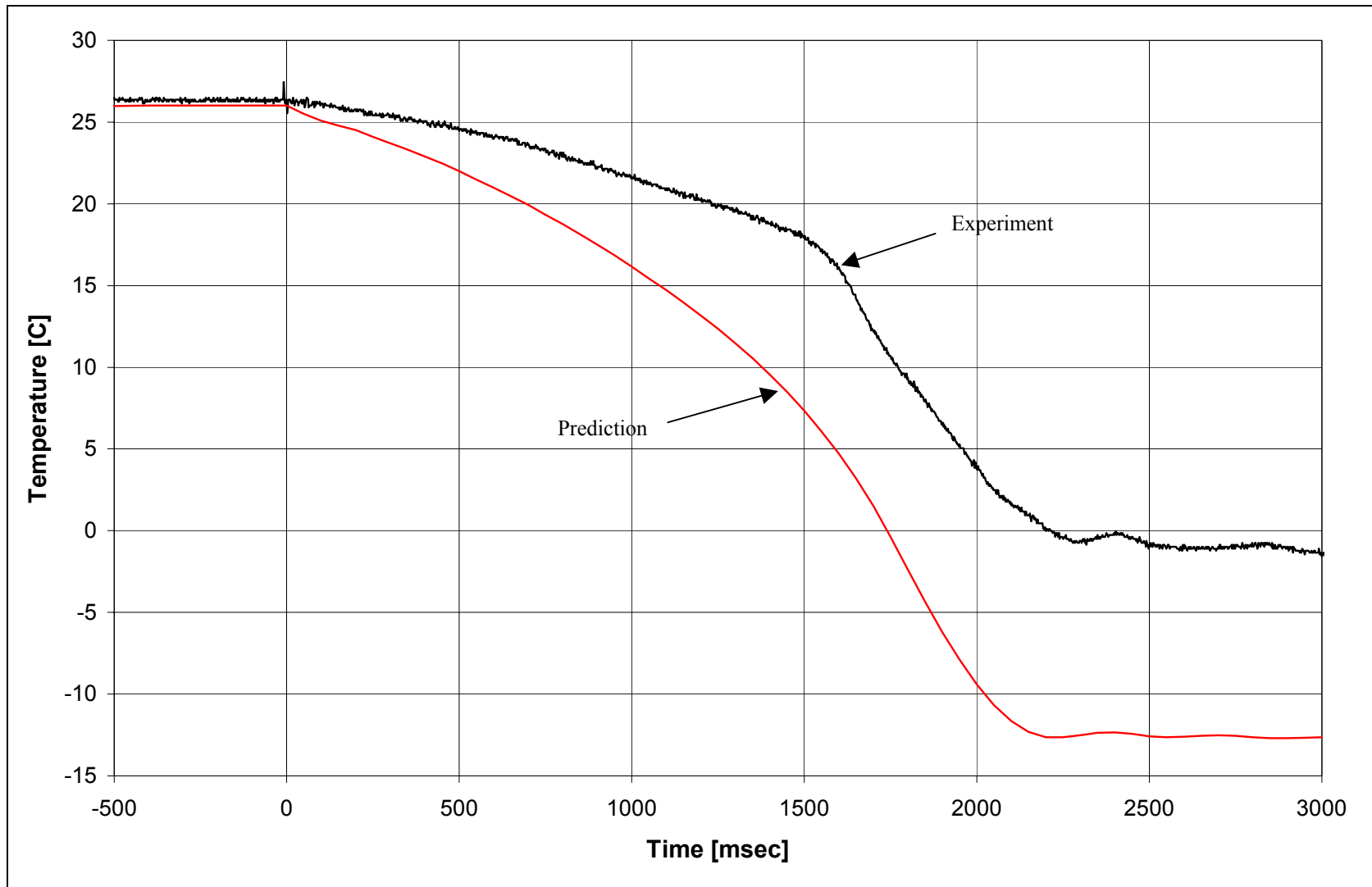


Figure 5.16: Comparison of Source Vessel Fluid Temperature for Experimental Run #16 and Predictive Computer Code Data.

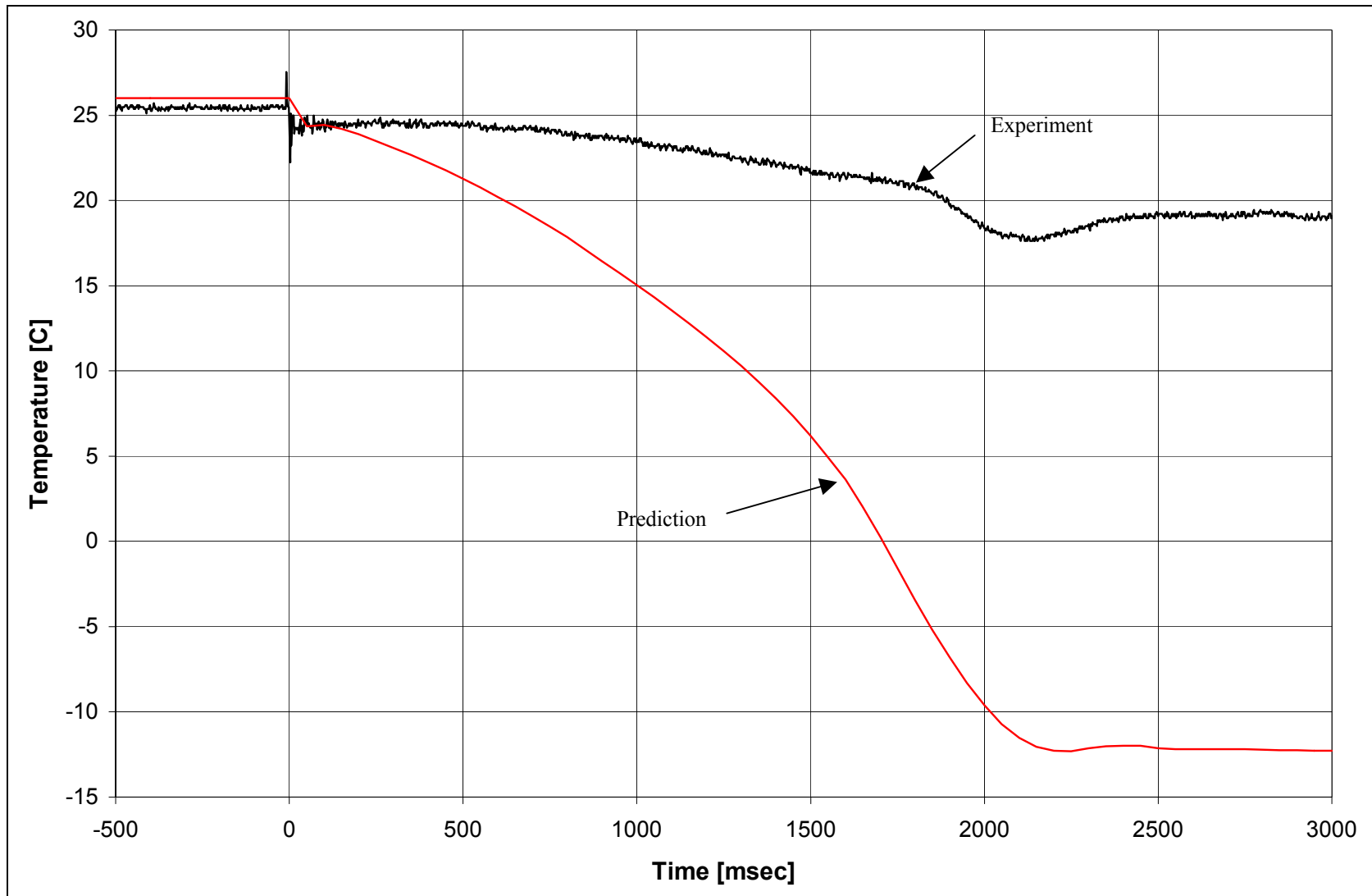


Figure 5.17: Comparison of Pipe Position #1 Fluid Temperature for Experimental Run #16 and Predictive Code Data.

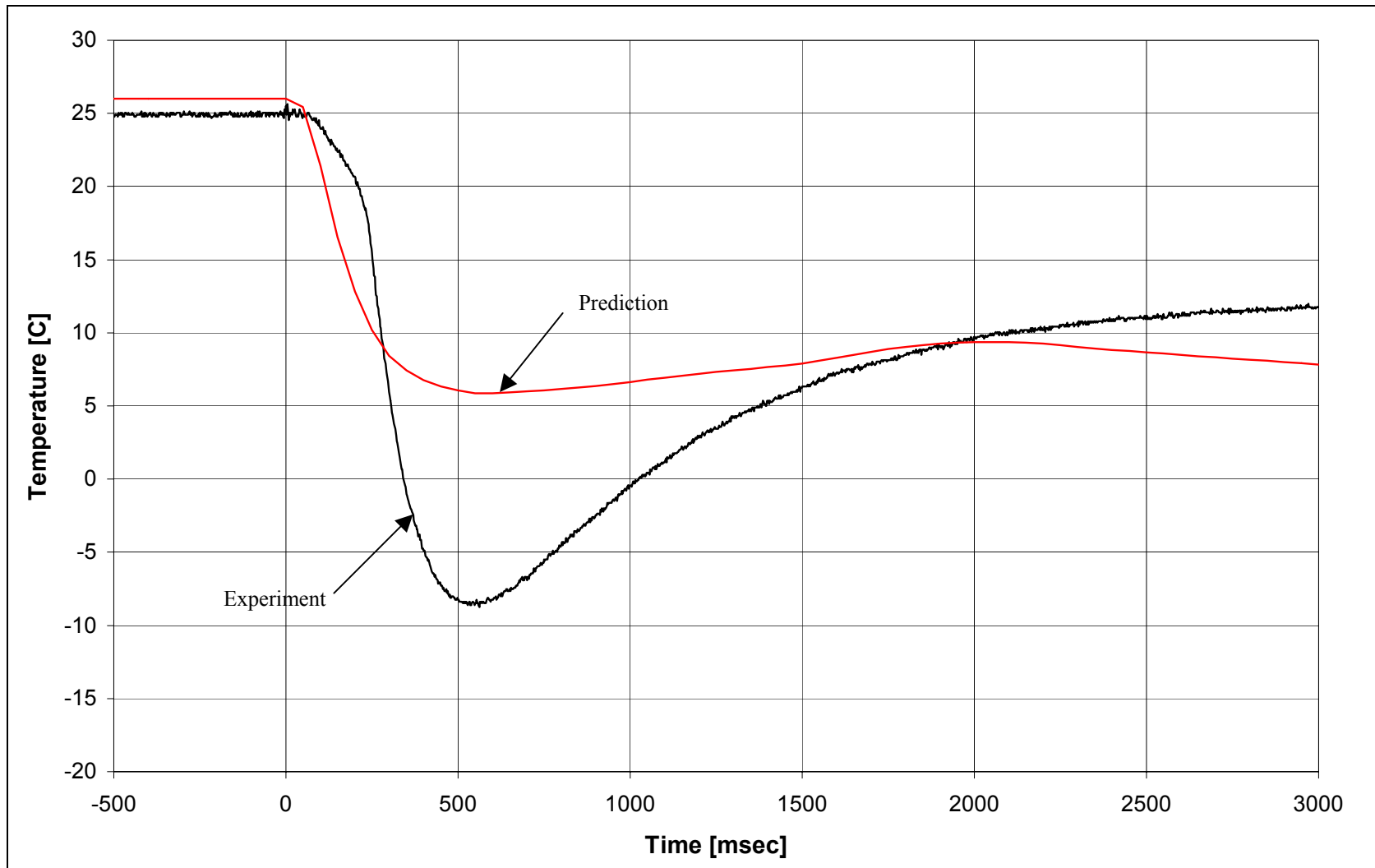


Figure 5.18: Comparison of Collection Vessel Gas Temperature for Experimental Run #16 and Predictive Computer Code Data.

6. SUMMARY

This code development effort was aimed at developing a flexible computer program that would allow prediction of the performance of fire suppressant fluid delivery systems, including a variety of fluids and delivery system piping configurations. The approach taken was to start from an existing transient two-phase flow analysis code, available in the public domain, and modifying it appropriately. In this case, the starting code was RELAP5/MOD3.2 (called the base code in this report), used for analysis of accidents and transients in the nuclear power industry (RELAP5, 1995). It represents the current state-of-the-art for modeling two-phase flows in piping systems, and was written for water-steam systems. It allows flexible modeling of piping systems, with the user being able to control the size of control volumes in the numerical solution procedure, and also control the computational time step.

The major modifications made to the base code consisted of the following:

- 1) Thermodynamic and transport properties were incorporated for Halon-1301, CO₂, HFC-227ea and HFC-125. The intent was to be able to benchmark the code against current systems and methods that operate with Halon-1301, and be able to use the code with other fluids being considered as replacements for Halon-1301. The thermodynamic properties were implemented by using the REFPROP property package, developed by NIST (Gallagher et al, 1993), and incorporating it into the base code. The method by which this was carried out is flexible, and would facilitate incorporation of properties for additional fluids, such as CF₃I, if needed. The modifications were implemented such that the user can select one of the available fluids, as an input option.
- 2) Constitutive relationships were modified as necessary to incorporate fluid-independent models. A review of the base code showed that many of the constitutive relationships in the base code could be directly adapted for fluids other than water. The areas where modifications were made were in the models for the calculation of interphase drag, and wall heat transfer.
- 3) A mechanistic model was implemented for simulating the release of dissolved gas. This required incorporating source and sink terms in appropriate mass conservation equations, and developing a constitutive model for calculating the rate of gas release. There are inherent uncertainties in being able to calculate release rates of dissolved gas. Hence the model was implemented with two user-supplied parameters. These are the critical gas bubble radius, r_c , and the gas release coefficient, Γ_0 . The model calculates the release of dissolved gas as a function of local conditions. This allows prediction of gas release in a continuous fashion as a function of spatial location, as the suppressant fluid is discharged from a supply vessel and flows through a piping system.

The resulting code, FSP, Version 1.0, is a one-dimensional, two-fluid model of two-phase flow, allowing the calculation of nonhomogeneous and nonequilibrium conditions between the phases. It retains all the flexibility of the base code in being to model, via user input, a variety of piping systems. It allows the user to select, via input, one of several fluids being considered currently as viable alternatives to Halon-1301. It was developed from a public domain code, and so was developed as a non-proprietary code. These were the characteristics

required in this code development project. The code has been installed successfully on personal computers with the WINDOWS 95/98 operating system. Some simple procedures were developed for code installation and execution and are shown in Section 4.4 of this report.

An experimental program was also carried out in order to improve the understanding of the discharge process, to determine some related parameters, and to assess the code against the experimental data. The discharge test loop dimensions were selected to be similar to the actual systems used in applications. Special hardware and instrumentation features were included in the loop to allow the study of different operating conditions and to be able to measure parameters that have never been measured before. In the present test loop it was possible to experimentally measure the dynamic discharge flow rate of the suppressant, dynamic void fraction and fluid temperature in the discharge piping. Additional measurements were carried out to determine pressure losses across pipe fittings during this transient two-phase discharge. To the best of our knowledge these are the first successful measurements of above parameters in a fire suppressant discharge loop. Experiments used water, CO₂, HFC-227ea, and HFC-125 as discharge fluids. All of the suppressants, except CO₂, were driven using compressed nitrogen at pressures up to 50 bars.

The total duration of the discharge varied between 1.5 to 6.0 seconds depending on initial pressure and the piping configuration. Experimental tests showed the following characteristics of discharge process:

- During the discharge, first the liquid suppressant is discharged, followed by vapor suppressant mixed with nitrogen gas,
- Nitrogen dissolved in the suppressant comes out of the liquid at small range of pressures, and it takes some time to have all nitrogen come out of the liquid suppressant,
- Void fraction at the end of the piping was found to stay around 0.5,
- The discharge flow rate was found to be highest right after the discharge, and would decrease gradually toward zero at the end of the discharge.
- When using HFC-227ea, the fluid temperatures in the discharge loop were found to be cooling only a few degrees Celsius,
- When using HFC-125, the fluid temperatures in the discharge loop were found to drop from room temperature down to almost zero degrees Celsius.

The code has been assessed against the above-described experiments on suppressant agent discharge, conducted with several fluids, in various piping configurations. The results show that the code is capable of calculating the pressure history and discharge flow rates similar to the measured data. The code is also able to pick up the qualitative behavior associated with the release of dissolved gas as the delivery system undergoes rapid depressurization during the discharge of the suppressant agent. Because of these characteristics, the code appears to be a viable tool for analysis or design of suppressant delivery systems.

Because the code is very flexible in being able to model different piping systems via user input, it offers the user many options in developing an appropriate input model to describe the physical system. The input model essentially provides the initial and boundary conditions

for the equations that the code solves. This can become complicated. A detailed input manual is appended to this report that describes how to build an input model. However, for convenience, a sample problem has been described in Section 4.5 of this report. It is recommended that this sample problem be used, along with the input manual, to develop an understanding of how the user can efficiently develop an input model for a desired application and carry out the code calculation.

Wall heat transfer models are present in the code, and the user can use them to model the metal walls of the supply vessel and piping as passive heat sources. However, typical suppressant discharge calculations examine transient times of the order of a few seconds, which are small compared to the time needed for stored heat in the walls to have an impact on the transient. Hence, the sample problem shown in Section 4.5 and all the code assessments carried out so far have not modeled wall heat transfer. And, in order to keep the input manual reasonably simple to use, the instructions of how to model wall heat transfer have not been included in the input manual. If the user encounters an application where this may be considered important, the documentation of the base code (RELAP5, 1995) provides this information. The user is cautioned that while the expectation is that these models will function as designed, they have not been exercised or assessed during the code development effort.

One code limitation that has been encountered is that the code sometimes appears to have difficulty beginning the computation. A common cause that was found in these cases is the initial thermodynamic state of the fluid specified by the user. The sample problem described in Section 4.5 contains a discussion on this topic and the user is urged to review this discussion.

Once the user builds an input model to describe a delivery system, there are essentially three input parameters that the user can vary to examine analytical uncertainties: a) The discharge coefficient directly affects the magnitude of the discharge flow rate. Note that the code uses this input value as a multiplier on the junction flow area. There are three separate discharge coefficients, for subcooled liquid, two-phase conditions, and single-phase vapor. Based on the assessments carried out, it appears that these should have values of 1.0, 0.8-0.9 and 0.8-0.9 respectively. However, it is recognized that the discharge coefficient depends on the geometry of the exit. A smooth converging-diverging nozzle would have a different discharge coefficient than a sharp-edged orifice plate. The user should be aware of this when specifying the discharge coefficient in the input model. Essentially, the discharge coefficient allows the user to account for uncertainties in the critical flow model of the code and the geometry of the junction. b) The critical gas bubble radius, r_c controls the pressure at which gas release is initiated. The assessments carried out indicate that this parameter should be in the range of $7.5e-9$ to $1.0e-8$ m. The user should examine the assessment cases presented to evaluate whether this is reasonable or whether a value outside this range should be used for this parameter. c) The gas release coefficient, Γ_0 , is directly proportional to the gas release rate. The assessments carried out indicate that this should be in the range of 10^3 to 10^4 Kg/m³-s. However, it is recognized that there is significant uncertainty in this parameter. The user should plan to vary this parameter for a specific application and gain understanding of how this would affect the overall time of suppressant discharge.

Finally, the description of the code theory and structure, in Sections 4.2 and 4.3 of this report, are somewhat brief. This was intentional. The emphasis in these sections is to provide the user with some basic information, and some additional guidelines to successfully build the input model and run the code. A very detailed description of the code theory, code structure, and numerical solution method can be found in the documentation of the base code (RELAP5, 1995). An attempt has been made in this report to identify all the changes made to the base code, and provide sufficient description of the changes.

7. REFERENCES

Chen, J.C., Tuzla, K., and Sundaram, R., Development of Computer Code for Analysis of Fire Suppressant Fluid System, Technical Proposal submitted by Lehigh University, BAA Number 1773-6B, 1997.

Chisholm, D., "A Theoretical Basis for the Lockhart-Martinelli Correlation for Two-Phase Flow", *Journal of Heat and Mass Transfer*, 10, 1967, pp 1767-1778.

Cokmez-Tuzla, A.F., Tuzla, K., and Chen, J.C., "High Speed Thermometry for Detection of Transient Liquid Contact on Superheated Surfaces", Temperature Its Measurement and Control in Science and Industry, 6 (ed. J. Schooley), American Institute of Physics, pp. 1173-1177, 1993.

Crane Handbook, "Flow of Fluids through Valves, Fittings, and Pipe", Technical Paper No. 410, Published by Crane Company, PA, 24th printing, 1988.

DiNenno, Philip J. and Budnick, Edward K. Jr., "Halon 1301 Discharge Testing: A Technical Analysis", National Fire Protection Research Foundation, Quincy, MA, 1988.

Edwards, A.R. and O'Brien, T.P., "Studies of Phenomena Connected with the Depressurization of Water Reactors", *Journal of British Nuclear Energy Society*, Vol. 9, pp. 125-135, 1979.

Elliott, D. G., Garrison, P. W., Klein, G. A., Moran, K. M., and Zydowicz, M. P., "Flow of Nitrogen-Pressurized Halon 1301 in Fire Extinguishing Systems", Jet Propulsion Laboratory Report 84-62, November 1, 1984.

EPRI Report NP-2370, "The Marviken Full-Scale Critical-Flow Tests, Volume 1: Summary Report", Electric Power Research Institute, Palo Alto, CA, 1982.

Gallagher, J., McLinden, M., Morrison, G., and Huber, M., "NIST Thermodynamic Properties of Refrigerants and Refrigerant Mixtures Database (REFPROP)", Version 4.0, November 1993.

Gann, Richard G., Editor, NIST Special Publication SP 890, Volume 1, Section 8.6, September, 1995.

GOTHIC Containment Analysis Package Version 5.0, Numerical Applications, Inc., User Manual (NAI 8907-02 Rev. 6), and Technical Manual (NAI 8907-06 Rev. 5), 1995.

Grosshandler, William L., Gann, Richard G. and Pitts, William M., Editors, "Evaluation of Alternative In-Flight Fire Suppressants for Full-Scale Testing in Simulated Aircraft Engine Nacelles and Dry Bays", NIST Special Publication SP 861, April 1994.

Hirt, C. W., Oliphant, T. A., Rivard, W. C., Romero, N. C., and Torray, M. D., "SOLA-LOOP: A Non-Equilibrium, Drift Flux Code for Two-Phase Flow in Networks", Report No. L-7659, Los Alamos National Laboratory, Los Alamos, NM, 1979.

Ishii, M., "One-Dimensional Drift-Flux Model and Constitutive Equations for Relative Motion between Phases in Various Two-Phase Flow Regimes", Argonne National Laboratory Report ANL-77-47, 1977.

Ishii, M., and Mishima, K., "Study of Two-Phase Fluid Model and Interfacial Area", NUREG/CR-1873, ANL-80-111, 1980.

Marviken Power Station, "The Marviken Full Scale Critical Flow Tests: Volume 1: Summary Report," NUREG/CR-2671, MXC-301, United States Nuclear Regulatory Commission, Washington, D.C., also EPRI NP-2370, 1982

Meyer, C. A., McClintock, R. B., Silvestri, G. J., and Spencer, R. C. Jr., ASME Steam Tables, 1967.

Mishima, K., and Ishii, M., "Flow Regime Transition Criteria Consistent with Two-Fluid Model for Vertical Two-Phase Flow", NUREG/CR-3338, April 1984.

Pitts, W. M., Yang, J. C., Gmurczyk, G. W., Cooper, L. Y., Grosshandler, W. L., and Cleveland, W. G., "Fluid Dynamics of Agent Discharge", Chapter 3 of NIST Special Publication 861, Editors: William L. Groshandler, Richard G. Gann and William M. Pitts, Gaithersburg, MD, April 1994.

RETRAN-03: A Program for Transient Thermal-Hydraulic Analysis of Complex Fluid Flow Systems, EPRI NP-7450, Volume 1, May 1992.

TRAC-PF1/MOD2 Code Manual, Los Alamos National Laboratory, NUREG/CR-5673 or LA-1203-M, Volume 1-3, 1992.

TRAC-BF1/MOD1 Code Manual: An Advanced Best-Estimate Computer Program for BWR Accident Analysis, Idaho National Engineering Laboratory, NUREG/CR-4356 or EGG-2626, Volumes 1-2, 1992.

TRAC-BF1/MOD1 Models and Correlations, INEL, NUREG/CR-4391 or EGG-2680, 1992.

Trapp, J. A., and Ransom, V. H., "A Choked Flow Calculation Criterion for Nonhomogeneous, Nonequilibrium Two-Phase Flows", International Journal of Multiphase Flow, 8, 6, 1982, pp 669-681.

RELAP5 Development Team, "RELAP5/MOD3.2 Code Manuals, Volume 1: Code Structure, Models and Numerical Schemes", U. S. Nuclear Regulatory Commission Report NUREG/CR-5535, 1995.

RELAP5 Development Team, "RELAP5/MOD3.2 Code Manuals, Volume 2: User Manual", U. S. Nuclear Regulatory Commission Report NUREG/CR-5535, 1995.

Taitel, Y.A., Bornea, D., and Dukler, A.E., "Modeling Flow Pattern Transitions for Steady Upward Gas-Liquid Flow in Vertical Tubes", *AIChE Journal*, Vol. 26, No. 3, May 1980, pp 345-354.

Tuzla, K., Palmer, T., Chen, J. C., Sundaram, R. K., and Yeung, W. S., "Development of Computer Program for Fire-Suppressant Fluid Flow", Annual Technical Report to NIST, Lehigh University Institute of Thermo-Fluid Engineering and Science Report ITF 98-2, Lehigh University, Bethlehem, PA, December 1998.

Van Wylen, G.J., and Sonntag, R.E., Classical Thermodynamics, 3rd Edition, John Wiley and Sons, 1985.

Wallis, G.B., One-Dimensional Two-Phase Flow, McGraw Hill, New York, 1972.

Welty, J. R., Wicks, C. E., and Wilson, R. E., Fundamentals of Momentum, Heat, and Mass Transfer, 3rd Edition, John Wiley & Sons, New York, pp. 210-211, 1984.

Yang, J. C., Cleary, T. G., Vazquez, I., Boyer, C. I., King, M. D., Breul, B. D., Womeldorf, C., Grosshandler, W. L., Huber, M. L., Weber, L., and Gmurczyk, G. W., "Optimization of System Discharge", NIST Special Publication 890, Gaithersburg, MD, pp 407-645, November 1995.

Yang, J. C., Vasquez, I., Boyer, C. I., Huber, M. L. and Weber, L., "Measured and Predicted Thermodynamic Properties of Selected Halon Alternative/Nitrogen Mixtures", *Int. J. Refrigeration.*, Vol. 20, No. 2, pp 96-105, 1997.

Zuber, N., Tribus, M., and Westwater, J. W., "The Hydrodynamic Crisis in Pool Boiling of Saturated and Subcooled Liquids", Second International Heat Transfer Conference, Paper 27, Denver, 1961.